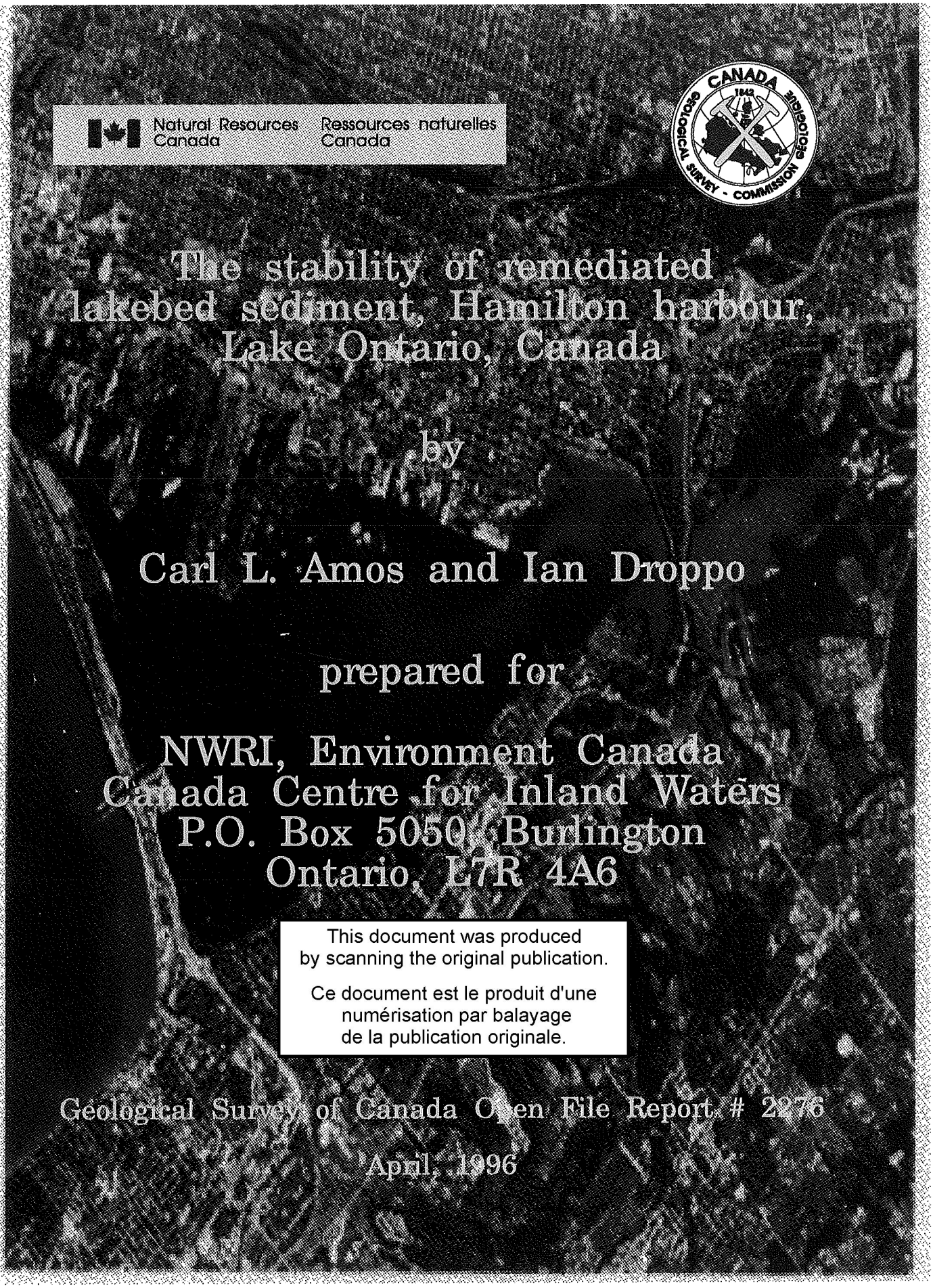

Natural Resources Canada | Ressources naturelles Canada

CANADA GEOLOGICAL SURVEY - COMMISSION GÉOLOGIQUE 1842

The stability of remediated lakebed sediment, Hamilton harbour, Lake Ontario, Canada

by

Carl L. Amos and Ian Droppo

prepared for

NWRI, Environment Canada
Canada Centre for Inland Waters
P.O. Box 5050, Burlington
Ontario, L7R 4A6

Geological Survey of Canada Open File Report # 2276

April, 1996

The stability of remediated lakebed sediment, Hamilton harbour, Lake Ontario, Canada

by

Carl L. Amos
Geological Survey of Canada
Bedford Institute of Canada
P.O. Box 1006, Dartmouth
Nova Scotia, CANADA, B2Y 4A2

and

Ian G. Droppo
National Water Research Institute, Environment Canada
Canada Centre for Inland Waters
P.O. Box 5050, Burlington
Ontario, CANADA, L7R 4A6

Geological Survey of Canada Open File Report # 2276
April, 1996

LIST OF CONTENTS

EXECUTIVE SUMMARY

The erodibility or stability of three test plots have been evaluated in this study. The first plot (C) acted as control, a second plot (W) was used for water injection using the treatment system of Murphy *et al.* (1995), and a third plot (OIP) was fully treated for contamination remediation coupled with physical disturbance. The purpose of the survey was to determine (1) the effects of sediment disruption (if any) of the ploughing action of the remediation method, (2) the effects of the injected medium on bed stability, and (3) the duration of any destabilizing effects.

Six surveys across the control plot provided the "natural" bed stability as well as the spatial variability in this attribute. Three methods were used to define the erosion threshold bed shear stress. These methods yielded mean values of **0.52(±0.11), 0.24(±0.07)** and **0.31(±0.06)** Pa. Erosion rates were best described as a power function of applied bed shear stress of the form: $\mathbf{E = 3.41 \times 10^{-4} \tau^{2.411}}$. Friction angles appeared to vary, being highest near the surface and low beneath; thus two or three layers were evident, the middle layer showing the greatest increase in strength with depth. The topmost layer had a mean friction angle of **14°** and the middle layer an angle of **23°** and the lowermost layer an angle of **2°.** The mean mass settling rate was **0.0013** m/s and the equivalent mean sedimentation diameter was **0.059** mm (i.e. coarse silt).

Four surveys across the water-injected plot provided the bed response to the physical process of lakebed treatment. The erosion thresholds yielded mean values of **0.50(± 0.07), 0.23(± 0.08)**, and **0.33(± 0.12)** Pa. There was no apparent difference in erosion threshold between this site and the control. Erosion rates were best described as a power function of applied bed shear stress of the form: $\mathbf{E = 8.15 \times 10^{-4} \tau^{2.444}}$. The erosion rate of this plot is slightly higher than the control plot indicating a more rapid and greater degree of suspension than at the control plot. Friction angles showed the same structure as the control; that is a high value at the surface (**21°**) and lower values beneath (**2°**). The inference of this is that the bed structure has not been disrupted by the ploughing or it has recovered quickly. The mean mass settling rate was **0.0016** m/s and the equivalent mean sedimentation diameter was **0.085** mm. Both the settling rate and the sedimentation diameter of this plot are higher than the control. This means that settling will be rapid at this site.

Four surveys across the oxidant-injected plot provided the bed response to the physical and chemical process of lakebed treatment. The erosion thresholds yielded mean values of **0.40(± 0.07), 0.19(± 0.04)**, and **0.28(± 0.07)** Pa. This site appeared to have a slightly lower threshold for erosion than the control. Erosion rates were best described as a power function of applied bed shear stress of the form: $\mathbf{E = 7.87 \times 10^{-4} \tau^{2.412}}$. The erosion rate is about the same as the control plot, but slightly lower than the water-injection site. Friction angles showed less structure than at the control and lower overall values (**12°**) than the water-injected site. The inference of this is that the bed structure has been disrupted by the ploughing of the bed and settlement of the bed is less advanced than at the water-injected plot. The mean mass settling rate was **0.0014** m/s and the equivalent mean sedimentation diameter was **0.18** mm. The settling rate is about the same as the control, whereas the sedimentation diameter is the highest of the survey. That is, settling will

be most rapid at this site.

Trends with time are difficult to establish due to the limited period of the study. Nevertheless, there appears to be evidence for bed strengthening throughout the study at all three plots. The strengthening at the control plot may relate to seasonal changes resulting from biostabilization. The trends at the two treated plots appear to be greater and may reflect a rapid return to a natural state. Unfortunately, we were unable to establish the time required by the bed to reach the natural state.

ACKNOWLEDGEMENTS

This project was considered a success due largely to the efforts of several key people. In particular we wish to thank: A. Robertson who helped mobilize and ship the GSCA Sediment Geodynamics container to Burlington; R. Murphy (GSCA) for technical support to CLA throughout the survey period; H. Don (Technical Operations, NWRI) for boat handling a general field logistics while on site in Hamilton harbour; Dr T. Murphy (New Technologies, NWRI) for provision of the treatment equipment; Dr B. Krishnappan (NWRI) for provision of the settling chamber and microscope used in the particle settling analyses; C. Jaskot for analyses of suspended sediments for IGD; and D. Clattenburg (GSCA) for the detailed grain size analyses. The manuscript was reviewed by Drs. M. Z. Li and T.F. Sutherland and was much improved by their comments. This project was funded by Environment Canada,. and by RODAC funds to CLA. This is NWRI contribution number 96-201.

LIST OF FIGURES

erratic nature of the azimuthal current during periods of high applied flow. As a result, we have used the more stable lid rotation as a proxy for flow and bed shear stress.

Figure 4.1.1.4 Time-series plots of the Sea Carousel deployment at control site C4. Variations in ambient S denote losses from Sea Carousel due to leakage.

Figure 4.1.1.5 Time-series plots of the Sea Carousel deployment at control site C5.

Figure 4.1.1.6 Time-series plots of the Sea Carousel deployment at control site C6.

Figure 4.1.1.7 A synthetic core for control site C1, derived from the time-series of S in Sea Carousel and from bulk density determined through Catscan analysis. The solid lines trace the profile of sediment strength with depth that has been traced by eye. The surface intercept of the solid line is interpreted as a measure of the erosion threshold (method 1 herein). The inflection points are interpreted to signify changes in bed structure, while the slope of the lines are proportional to the friction coefficient of the bed. In this case three layers are recognised, the topmost two showing steadily increasing bed strength probably due to biostabilization. The lowest layer shows no consolidation and possibly due to gas production in the sediment.

Figure 4.1.1.8 A synthetic core for control site C2. Two layers are interpreted from this profile, each increasing in strength with depth.

Figure 4.1.1.9 A synthetic core for control site C3. Three layers are interpreted from this profile, each increasing in strength with depth. The higher values of (Φ) in the topmost 4 mm is likely related to biostabilization.

Figure 4.1.1.10 A synthetic core for control site C4. Two layers are interpreted from this profile, each increasing in strength with depth. Notice that the strength profile can be divided into linear segments with reasonable accuracy.

Figure 4.1.1.11 A synthetic core for control site C5. Three layers are interpreted from this profile, the topmost two increasing in strength with depth; the lower layer showing a possible strength reversal.

Figure 4.1.1.12 A synthetic core for control site C6. Notice the rapid strength gain in layer (2) possibly related to biostabilization.

Figure 4.1.1.13 Measured erosion rate (A) and S (B) plotted against applied bed shear stress for control site C1. Mean erosion rate (E_m) and S are expressed as a power functions of stress through least-squares regression analyses. The exponents of the functions are used as indexes of erodibility. Notice that peak erosion (E_p) varies systematically with applied stress. It follows E_m under type Ib erosion; it is constant during transitional erosion; and increases markedly during type II erosion. The base erosion rate (E_o) was defined as 1×10^{-5} kg/m^2/s on the basis of results obtained during the early stages of the experiment (open circles). Ambient S was around 80 mg/L.

Figure 4.1.1.14 Measured erosion rate (A) and S (B) plotted against applied bed shear stress for control site C2. In this case, we identify Type Ia erosion (suspension of surface "fluff" layer). The erosion thresholds are defined by evaluating the stress at E_o (method 2) and evaluating S at ambient concentrations (method 3).

Figure 4.1.1.15 Measured erosion rate (A) and S (B) plotted against applied bed shear stress for control site C3. Notice how well the power function fits the results.

Figure 4.1.1.16 Measured erosion rate (A) and S (B) plotted against applied bed shear stress for control site C4.

Figure 4.1.1.17 Measured erosion rate (A) and S (B) plotted against applied bed shear stress for

control site C5.
Figure 4.1.1.18 Measured erosion rate (A) and S (B) plotted against applied bed shear stress for control site C6.
Figure 4.1.1.19 Time-series of the still-water S derived in the last stages of each experiment: (A) control sites; (B) water-injection sites; and (C) oxidant-injection sites. The trends are adequately explained as logarithmic decaying concentrations, the decay constants (k) being linear functions of the starting value of S.
Figure 4.1.1.20 The decay constants derived from the results shown in Figure 4.1.1.19 plotted against starting S. Notice the strongly linear relationship for all plots, which suggests that settling is unaffected by the means of treatment.
Figure 4.1.1.21 Mean S and incremental mass deposition determined for the time-series of Sea Carousel from control site C1. The equivalent mass settling velocity has been determined from these data, as well as the sedimentation diameter (on the assumption that the particle density is that of the bed at the maximum depth of erosion). Notice that the settling rate diminishes with time as does the diameter diagnostic of segregation on settling and a widely distributed size spectrum of suspended aggregates.
Figure 4.1.1.22 Mean S, incremental mass deposition, mass settling rates, and sedimentation diameter determined for the time-series of Sea Carousel from control site C2. Notice that much of the material in suspension falls into the sand and coarse silt size range.
Figure 4.1.1.23 Mean S, incremental mass deposition, mass settling rates, and sedimentation diameter determined for the time-series of Sea Carousel from control site C3. Notice that settling can be quite irregular in time.
Figure 4.1.1.24 Mean S, incremental mass deposition, mass settling rates, and sedimentation diameter determined for the time-series of Sea Carousel from control site C4.
Figure 4.1.1.25 Mean S, incremental mass deposition, mass settling rates, and sedimentation diameter determined for the time-series of Sea Carousel from control site C5.
Figure 4.1.1.26 Mean S, incremental mass deposition, mass settling rates, and sedimentation diameter determined for the time-series of Sea Carousel from control site C6.
Figure 4.1.2.1 The wet bulk density of a push core taken from an Eckman grab sample from control site C3 determined from Catscan analysis. The core was 10 cm in diameter and 30 cm long. It was frozen slowly upon sampling and has not been corrected for either the effects of freezing or for gas expansion due to removal of hydrostatic pressure. The core depicts three layers: a surface layer of rapidly increasing density; an intermediate layer of transition; and a lower layer of almost constant density (1400 kg/m^3). The horizontal bars denote the scatter in density rather than error in the method.
Figure 4.1.4.1 Conventional optical microscopy micrographs: (A) ambient aggregates/floc remaining in the annulus of the Sea Carousel following the 10 minute initial still-water period; (B) an aggregate eroded from biostabilized surface layer at onset of erosion; and (C) rip-up aggregates eroded from below the biostabilized layer.
Figure 4.1.4.2 Transmission electron microscopy micrographs: (A) an aggregate eroded from biostabilized surface layer at onset of erosion; (B) a rip-up aggregate eroded from below the biostabilized layer; and (C) a virus-like organism eroded from below the biostabilized layer.
Figure 4.1.6.1 The relationship between eroded aggregate size and settling velocity.
Figure 4.1.6.2 The eroded aggregate size as a function of aggregate excess density.

Figure 4.2.1.1 Time-series plots of the Sea Carousel deployment at the water-injection site W1. The brief period of interrupted flow was caused by an overheated power supply. The interruption did not appear to influence the results.
Figure 4.2.1.2 Time-series plots of the Sea Carousel deployment at the water-injection site W2.
Figure 4.2.1.3 Time-series plots of the Sea Carousel deployment at the water-injection site W3.
Figure 4.2.1.4 Time-series plots of the Sea Carousel deployment at the water-injection site W4.
Figure 4.2.1.5 A synthetic core plot of water-injection site W1. The plot shows two layers of increasing strength with depth. The friction coefficients are very low indicating that consolidation is not well advanced. The high surface gradient is suggestive of biostabilization.
Figure 4.2.1.6 A synthetic core plot of water-injection site W2. The surface 3 mm of this site appears distinct from the underlying material and may be related to biological activity.
Figure 4.2.1.7 A synthetic core plot of water-injection site W3.
Figure 4.2.1.8 A synthetic core plot of water-injection site W4.
Figure 4.2.1.9 Measured erosion rate (A) and S (B) plotted against applied bed shear stress for water injection site W1.
Figure 4.2.1.10 Measured erosion rate (A) and S (B) plotted against applied bed shear stress for water injected site W2.
Figure 4.2.1.11 Measured erosion rate (A) and S (B) plotted against applied bed shear stress for water injected site W3.
Figure 4.2.1.12 Measured erosion rate (A) and S (B) plotted against applied bed shear stress for water-injected site W4.
Figure 4.2.1.13 Mean S, incremental mass deposition, mass settling rates, and sedimentation diameter determined for the time-series of Sea Carousel from water-injection site W1. The sedimentation diameter is largely fine sand, though no segregation of size is evident with time.
Figure 4.2.1.14 Mean S, incremental mass deposition, mass settling rates, and sedimentation diameter determined for the time-series of Sea Carousel from water-injection site W2. The sedimentation diameter in this case is largely coarse silt.
Figure 4.2.1.15 Mean S, incremental mass deposition, mass settling rates, and sedimentation diameter determined for the time-series of Sea Carousel from water-injection site W3. A distinct decrease in settling velocity and sedimentation diameter is evident which is diagnostic of sorting.
Figure 4.2.1.16 Mean S, incremental mass deposition, mass settling rates, and sedimentation diameter determined for the time-series of Sea Carousel from water-injection site W4.
Figure 4.2.2.1 A profile of wet bulk density of a push core (10 cm diameter) taken at water-injection site W4. The core shows a surface layer (5 mm thick) of rapidly increasing density and a substrate of constant density (around 1500 kg/m^3).
Figure 4.3.1.1 Time-series plots of the Sea Carousel deployment at oxidant-injection site OIP1: (A) lid rotation, azimuthal current speed, and vertical current speed; (B) ambient S, raw S and S corrected for dispersion; and (C) the erosion rate. The dots in panel B denote measured S determined from samples pumped during the experiment. Notice the erratic nature of the current meter which we put down to interference from the injected oxidant.
Figure 4.3.1.2 Time-series plots of the Sea Carousel deployment at oxidant-injection site OIP2: (A) lid rotation, azimuthal current speed, and vertical current speed; (B) ambient S, raw S and S corrected for dispersion; and (C) the erosion rate. The dots in panel B denote measured S determined from samples pumped during the experiment. The short break in the lid speed was

due to overheating of the power supply.

Figure 4.3.1.3 Time-series plots of the Sea Carousel deployment at oxidant-injection site OIP3: (A) lid rotation, azimuthal current speed, and vertical current speed; (B) ambient S, raw S and S corrected for dispersion; and (C) the erosion rate. Notice the change in erosion from type I at early stages of bed erosion to type II during late stages.

Figure 4.3.1.4 Time-series plots of the Sea Carousel deployment at oxidant-injection site OIP4: (A) lid rotation, azimuthal current speed, and vertical current speed; (B) ambient S, raw S and S corrected for dispersion; and (C) the erosion rate. Notice the erratic behaviour of the flow sensor at high lid speeds.

Figure 4.3.1.5 A synthetic core plot of oxidant-injection site OIP1. The high friction angle in the topmost 10 mm may reflect the effects of the treatment, as they exceed values seen at the other plots..

Figure 4.3.1.6 A synthetic core plot of oxidant-injection site OIP2. No bed structure is evident, which may be the result of physical disturbance by the treatment process.

Figure 4.3.1.7 A synthetic core plot of oxidant-injection site OIP3.

Figure 4.3.1.8 A synthetic core plot of oxidant-injection site OIP4.

Figure 4.3.1.9 Measured erosion rate (A) and S (B) plotted against applied bed shear stress for oxidant-injection site OIP1.

Figure 4.3.1.10 Measured erosion rate (A) and S (B) plotted against applied bed shear stress for oxidant-injection site OIP2.

Figure 4.3.1.11 Measured erosion rate (A) and S (B) plotted against applied bed shear stress for oxidant-injection site OIP3.

Figure 4.3.1.12 Measured erosion rate (A) and S (B) plotted against applied bed shear stress for oxidant-injection site OIP4.

Figure 4.3.1.13 Mean S, incremental mass deposition, mass settling rates, and sedimentation diameter determined for the time-series of Sea Carousel from oxidant-injection site OIP1. Notice the decrease in grain size and settling rate with time through the settling period.

Figure 4.3.1.14 Mean S, incremental mass deposition, mass settling rates, and sedimentation diameter determined for the time-series of Sea Carousel from oxidant-injection site OIP2.

Figure 4.3.1.15 Mean S, incremental mass deposition, mass settling rates, and sedimentation diameter determined for the time-series of Sea Carousel from oxidant-injection site OIP3. The aggregates appear to be up to medium sand in size.

Figure 4.3.1.16 Mean S, incremental mass deposition, mass settling rates, and sedimentation diameter determined for the time-series of Sea Carousel from oxidant-injection site OIP4. Medium/coarse sand was the first to settle out followed by fine sand.

Figure 4.3.2.1 A synthetic core plot of a syringe core (2.5 cm diameter) collected at site OIP4. Notice the presence of a surface layer of rapidly increasing density and the region of constant density beneath.

1. BACKGROUND

1.1 Focus of Collaborative Research

An innovative and effective method for the bioremediation of contaminated sediments has been developed by the National Water Research Institute. The method was developed to decontaminate bottom sediments of lakes or shallow estuaries (Murphy *et al.*, 1995), and involves two processes that influence the physical, chemical and biological characteristics of the sediments in question.

The first process is the injection of an oxidant/nutrient into the sediment. These compounds, often possess high positive cations (Murphy *et al.*, 1995) which can promote significant electrochemical flocculation. The binding of particles together into larger flocs may have the effect of increasing the sediment's stability. This will, however be highly dependent on the floc density. The injection also stimulates metabolic activity of the ambient bacteria. This activity is likely to increase polymeric fibril production which may lead to an enhancement of biostabilization. The biostabilization takes place through adhesion of the polymeric mucilage and through "bio-flocculation". Finally, the injection of an oxidant will result in remoulding of the sediment and possible destabilization.

The secondary process of bioremediation is the mechanical disturbance of the bed brought about by the injection system. This system is made of a large tined rake which is dragged through the sediment to a maximum depth of 30 cm. The resulting remoulding may be associated with collapse of the sediment by the removal of water and gases (Murphy, personal communication, 1994). The resulting compaction may cause an increase in bed stability due to the associated increase in bulk density (Migniot, 1980).

The bioremediation process has been very successful in the treatment of PAHs (coal tar) within Hamilton harbour. However, there remains questions about the bed stability during and subsequent to the bed treatment. As a result of these uncertainties, a collaborative study was undertaken between the Geological Survey of Canada, Atlantic (GSCA) and the National Water Research Institute (NWRI), Environment Canada. This study involved the deployment of the benthic annular flume Sea Carousel (Amos *et al.*, 1992a) on a treatment test site near Dofasco slip, Hamilton harbour, Lake Ontario, Canada. The purpose of the study was to determine changes in lakebed stability consequent to the treatment process at the test site.

1.2 Study Site

Hamilton harbour is an industrial port for the steel manufacturing industry located at the east end of Lake Ontario (Figure 1.2.1). The harbour has an area of 2,150 hectares and is the receiving water body for a watershed of 49,400 hectares. Most of the contamination of the harbour (heavy metals, PCB's, PAH's, oil and grease) is the result of long-term storm water runoff, sewer overflow, sewage treatment plant input, atmospheric input, direct overland flow, and industrial input. Contaminant input to the harbour from the steel mills has been reduced due to advanced

waste treatment (Murphy *et al.*, 1995). The study site is of great interest to the Hamilton Harbour Remedial Action Plan (RAP) because of the potential for contaminated sediment migration to clean areas of the harbour.

The study site is situated approximately 100 m off the Dofasco steel plant slip which is located in 5 to 7 m of water on a gently undulating, featureless lakebed. It is sheltered from strong currents, and large waves and so the site is largely one of deposition. The lakebed at the site is thus composed of gassy, organic-rich muds. These muds, according to diver reports, possess properties of a gel (elastic motion), but are easily fluidised and penetrated.

1.3 Definitions of lakebed erodibility and stability

Erodibility of cohesive bed sediment may be defined as the ablation of that bed due to hydrodynamic forces. By contrast, stability may be defined as the resistance of a bed to hydrodynamic forces. The stability of a cohesive sediment (which is the focus of this study) is often expressed as a single index: the erosion threshold. This index defines the resistance of the bed surface to fluid motion, but does not take into account what takes place once the erosion process has begun, nor does it account for the rate of change in strength with time and the duration over which the erosion event prevails once initiated. Furthermore, bed stability is the time-product of the upward (erosional) and downward (sedimentation) benthic fluxes, and so we must also account for the type of bed erosion (Villaret and Paulic, 1986), the nature (size, shape, and density) of the eroded material, and the associated sedimentation properties (mass settling rate, ballistic momentum flux, and mode of transport). The evolution of a cohesive bed is the sum of the responses to all stabilizing and destabilizing forces applied to that bed. The stabilizing forces impact the sedimentation character of a bed sediment; the destabilizing forces influence the erodibility of that bed. We may describe the erosion character of a bed in terms of the following attributes:

- **the erosion threshold (cohesion)**, $\tau_c(0)$ (in Pa); interpreted as the point at which the surface of the bed begins to erode. There are several criteria by which this threshold is defined. In the past we choose to express it as the intercept of the sediment failure envelop with the sediment surface (Amos *et al.*, 1992b): [method (1)]. In this report we also defined it as the value at which erosion rate approaches 1×10^{-5} kg/m^2/s on a regression plot of erosion rate versus applied bed shear stress: [method (2)]. In method (3), the erosion threshold was defined as the value of bed stress at which the suspended sediment concentration (S) reaches ambient values in a regression plot of S and stress (Sutherland, 1996). As a proxy to erodibility, $\tau_c(0)$ is rather poor because of the large variations in strength just below the surface layer. Indeed, some contend that an erosion threshold doesn't exist;

- **the erosion threshold as a function of sediment depth**, $\tau_c(z)$ (in Pa); interpreted as the sediment failure envelope. It defines the changes in sediment strength (to fluid erosion) throughout the erosion process. It is based on the assumption that, at an applied bed shear stress (τ_o), bed erosion will stop when the bed has eroded to a depth (z) wherein the

strength equals the applied stress: $\tau_c(z) = \tau_o$ (Mehta and Partheniades, 1982). By definition, therefore, it is applicable to type I erosion only; that is, asymptotically decaying erosion with time;

- **the friction coefficient**, ϕ (in degrees); adapted from Terzaghi and Peck (1967) is: $\phi = \tan^{-1}(\tau_c(z)/\sigma')$. Depth is transformed to an effective stress (σ') from a knowledge of sediment bulk density (ρ_b): $\sigma' = \rho_b g z + U'$ where g is the gravitational force and U' is the ambient pore pressure (usually unknown, but assumed to be zero in this study). ϕ is used to define the relative stability of a bed, its consolidation state, and bed sedimentary macro-structure;

- **the peak erosion rate**, E_p (in kg/m^2/s), as a function of applied bed shear stress and eroded depth; erosion rate shows a distinct maximum within the first 60 seconds of an applied eroding stress. This peak then diminishes with time in a fashion that defines the erosion type;

- **the mean erosion rate**, E_m (in kg/m^2/s), as a function of applied bed shear stress and eroded depth; it is defined as a function of the difference in the starting and final S within any velocity increment: $E_m = \delta M/\delta t = (S_{end} - S_{start})V/\Delta t\alpha$, where M is the eroded dry mass, V is the Sea Carousel volume (0.218 m^3), α is the flume bed area (0.87 m^2) and Δt is the duration of the applied eroding bed shear stress;

- **the type of erosion** as a function of time (erosion type) and excess bed shear stress (in kg/m^2/s); it may be either asymptotically diminishing with time (type I) or constant (type II). The two types of erosion results in vastly differing final S's as well as eroded depths. We suppose it is controlled by the change in bed strength with depth, but not enough information is available to accurately predict when either type of erosion will occur;

- **the size spectra and modes of transport** of material eroded from the bed: type I erosion is characterised by the release of flocs and small pellets (surface erosion), and the mode of transport is largely in suspension; whereas type II erosion occurs through the release of rip-up clasts and large (8 mm) aggregates (mass erosion). In this latter case, the mode of transport is largely through saltation and surface creep, with a significant portion of the eroded material moving within 2 cm of the bed. We presume that this bedload fraction has a large impact on the nature of the erosion process itself through the delivery of momentum to the bed. Also, sedimentation of material eroded in type II fashion will be much more rapid than that of material derived from type I erosion; and

- **the effect of consolidation** on the erosion threshold (Pa/s); this is a time-dependent attribute of the sediment which is largely unknown due to its complexity. We may chart its evolution in terms of changes in sediment bulk density with sediment depth and with time. In the present study, it may be a useful index of stability because of anthropogenic bed remoulding.

We define sedimentation character in terms of:

- **the deposition threshold**, τ_d (Pa): that is, the applied stress at which material begins to drop back to the bed. It is dependent on the S (through the influence on water density and viscosity), and the mass settling velocity of the particles in suspension (W_s). We determine it in settling experiments within the *in situ* Lab Carousel using "fresh" sediment and local water. We transform the mass settling equation of Krone (1962) as follows: $\delta M/\delta t = W_s S(1 - \tau_o/\tau_d)$; and $\tau_d = \tau_o/(1 - [\delta M/\delta t.1/S.W_s])$.τ_d cannot be determined using Sea Carousel at present because of the uncertainties resulting from dispersion (leakage). Consequently, it was not measured in this study;

- **the mean mass deposition rate**, D_m (kg/m^2/s); under an applied stress below the critical for deposition, may determine D_m from the rate in change in S: $D_m = \delta M/\delta t = (S_{start} - S_{end})V/\Delta t\alpha$. This can only be determined using Lab Carousel at the present time, and so was not available for this study; and

- **the still water mass settling rate**, W_s (m/s); measured at the end of each Sea Carousel erosion experiment, the still-water mass settling rate may be defined as $D_m = S_t.W_s (1 - \tau_o/\tau_d)$; where $W_s = \delta M/\delta t.\ 1/S_t$, where S_t is the mean suspended sediment concentration for the settling period under consideration.

2. OBJECTIVES

The objectives of this study were two fold: (1) to evaluate the impact of the *in situ* treatment process on the stability of bottom sediments, and (2) to evaluate the duration of the destabilization effect. The first objective was undertaken in a series of sub-tasks that involved (I) the definition of the natural, background stability, and the natural variability of this attribute; (ii) the impact of the mechanical effects of injection (by injecting water instead of the active solution); and (iii) the impact of both mechanical effects and the effects of the active ingredient. This study also provided an opportunity to evaluate the erosion of fresh water sediments; to examine the local factors which influence this process and to compare the results with erosion measurements made in marine environments.

3. MATERIALS AND METHODS

3.1 Field Program

In order to test the impact of the primary and secondary processes of the *in situ* treatment on sediment stability, three adjacent test plots were established just outside the active shipping area of the Dofasco slip, Hamilton harbour, Hamilton, Ontario, Canada (Figure 1.2.1). The treatment system involved towing an injection rake through contaminated sediments while pumping oxidant into the surface layer. The DFO vessel Gander was used to inject the test site. The oxidant used, and the concentration and volume pumped was predetermined and is a function of the degree and type of contamination. A complete description of the *in situ* bioremediation

treatment technology is given in Murphy *et al.* (1995).

The Sea Carousel was deployed from the Goose II which is a flat-decked pontoon barge powered by two 140 horse power outboard motors. The Goose II was equipped with a hiab crane for smooth and safe deployment of the Sea Carousel and box corer. As the Goose II has no significant cover, the Sea Carousel's electronics were installed and operated on a P-class launch (Pintail) which was moored alongside it.

Bathymetry of the site was mapped using a conventional echo sounder (Figure 3.1.1) in order to insure a relatively flat bed with no obvious spatial differences. The site showed a slight slope to the northwest. However, the bed roughness was between 1-2 cm only which was within the tolerances of the Sea Carousel to minimise leakage from the base. The site chosen was about 50 x 50 m in size, and was marked for the duration of the study with four large red corner floats. These floats provided the references for all subsequent positioning. The area was divided into three sub-plots (approximately 17 x 50 m) the corners of which were marked with yellow Grimsby floats. Each sub-plot was designated as follows:

- plot C - the control plot is a natural, undisturbed region adjacent to the test plots. Four replicates of the Sea Carousel analysis were undertaken at points along the centre-line of the plot. Two other deployments (C5 and C6) were made outside the marker region for comparison. The natural stability was thus defined, as well as the spatial variability of this parameter;

- plot W - the water injection plot: here the treatment rake was drawn over the lakebed while ambient water was injected into the sediment at a rate of 17,000 L/hour. Three passes of the plot were made, each in the same direction, to complete the coverage; and

- plot OIP - the oxidant-injection plot: here the treatment rake was drawn over the lakebed, and the active ingredient was injected into the sediment at the same rate and volume as for the water treatment. Again, three passes of the plot were made to ensure full coverage.

3.2 Sea Carousel instrumentation and deployment

Sea Carousel is a benthic annular flume designed for field use in subaqueous settings. The carousel is 1.0 m in radius with an annulus 0.15 m wide and 0.30 m high. It weighs approximately 150 kg in air and 40 kg in water and is made of aluminum (Figure 3.2.1). Flow in the annulus is induced by rotating a movable lid that is driven by a 0.75 HP digital stepping motor that is powered from the surface. Eight small paddles, spaced equidistantly beneath the lid, induce a flow of water in the annulus. The Carousel is equipped with three optical back scatter sensors (OBS's; Downing, 1983). Two of these are located non-intrusively on the inner wall of the annulus at heights of 0.03 and 0.18 m above the skirt (the skirt is a horizontal flange situated around the outer wall of the annulus 0.04 m above the base; it was designed to standardize penetration of the flume into the seabed). The third OBS detects

ambient suspended sediment concentration outside the annulus, or it may be used to detect internal sediment concentration at a height between the other two. A sampling port, through which water samples may be drawn, is situated in the outer wall of the annulus at a height of 0.2 m above the skirt. It is used to calibrate the three sensors under well mixed conditions, and for the collection of biological and chemical samples.

Mean flow within the Carousel is determined from a relationship between azimuthal speed and lid rotation presented in Amos, *et al.* (1992a) and later verified in laboratory measurements made using a Laser-Doppler flow sensor (Fung, 1995). Mean tangential lid rotational speeds are detected through a shaft end-coder resting on the lid. Tangential (U_y) and vertical (U_w) current speeds are also detected by a Marsh-McBirney® EM flow meter (model 513) situated *circa* 0.18 m above the bed. Controller boards for each sensor and necessary power (12 VDC) are derived from an underwater pod located above the annulus. Output voltages from all sensors are digitized and transformed to scientific units on a Campbell Scientific® CR10 data logger and stored on a Campbell Scientific® SM192 storage module (storage capacity of 96,000 data values), also located in the underwater pod. The data logger is interrogated and programmed from the surface using a microcomputer linked to the data logger through an RS232 interface. Maximum sampling rate of all channels is approximately 2 Hz, whereas U_y and U_w may be logged at rates up to 10 Hz. All channels may be monitored and displayed on the surface computer allowing the operator to control experiments interactively. Bed shear stress is varied in time through a series of script commands issued to the digital motor through a surface controller. The data stored from each deployment is downloaded at regular intervals through the RS232 cable throughout each experiment.

A window is located in the inner flume wall for purposes of observing and recording the mechanics of bed failure. Visual observations are made using a Sony® Handycam 8 mm video recorder model CCD-V11 held in an Amphibico®, Amphibian V11 underwater housing. Light is provided by two 100-Watt underwater lights powered from the surface. The housing has a lens that corrects for underwater geometric distortions and so is suitable for accurate image scaling. The camera images 30 frames/s. A co-axial cable connects the camera to a surface monitor for real-time detection. Sequential video images are digitized for particle trajectories at varying heights above the bed. From these, velocity profiles may be constructed. From such profiles, thicknesses of the logarithmic part of the benthic boundary layer may be determined and friction velocities computed. These latter values may then be compared with laboratory measures as a check.

The deployment and operation of the Sea Carousel in this study were held as constant as possible for comparability. The Carousel was lowered to within 1 m of the bed. Thereafter it was lowered at a slow rate of 5-10 cm/s (subsequently found to be below the threshold for erosion). After landing, the Carousel data logger was initialised to log for about 10 minutes under still water conditions. This initial period was used to determine the current meter zero offsets, and to clear the water of any material suspended by the instrument landing. The experiment consisted of subjecting the lakebed to 12 increments of flow, each increment lasting approximately 5 minutes. The mean index azimuthal current speeds (U_y) were: 0.04; 0.09; 0.14; 0.17; 0.25; 0.33; 0.40;

0.48; 0.55; 0.59; 0.66; and 0.72 m/s. The instantaneous azimuthal current speeds were quite variable due to: (1) macro turbulence; (2) variations in lid speed; (3) the influence of magnetic particles which were suspended during the erosion process and which were attracted to the sensor head of the EM meter. (The source of the iron was the adjacent steel mill in Hamilton harbour); and (4) ionic interferences brought about by the high concentrations of the strongly alkaline treatment solution. Finally, the flow was stopped for a 10-minute period and still-water settling of eroded material was monitored. After retrieval of the Carousel, the site was marked with a yellow Grimsby float and fixed with Differential GPS (Magnavox/Leica GPS with differential beacon at CCIW) which was accurate to ± 1 m. This was done to avoid overlap of Sea Carousel "foot prints".

Motor settings (V) were used as the standard input to control flow in the Sea Carousel. These settings show a perfectly linear relationship to lid rotation (rot) of the form: $\mathbf{rot = 0.262(V)}$ m/s, $r^2 = 0.999$, $n = 14$. The index azimuthal velocity is also linearly related to motor setting in the form: $\mathbf{U_y = 0.098(V) + 0.10}$ m/s, $r^2 = 0.96$, $n = 14$. Bed shear stress (τ_o) varies with lid rotation as a power function that approximates the quadratic stress law: $\tau_o = \mathbf{0.43(V^{1.57})}$, $r^2 = 0.99$, $n = 14$ (Figure 3.2.2).

The effect of the suspended sediments on suppression of the bed shear stress is complex. It can cause fluid stress reduction through (1) turbulence dampening due to changes in the Richardson's number (density stratification), (2) consumption of momentum in maintaining material with finite W_s in suspension, and (3) fluid momentum transfer to accelerating saltating aggregates. Nominal experiments on this subject are inconclusive. Nevertheless, a stress reduction algorithm has been applied to our data on the basis of results in Amos *et al.* (1992a) and Li and Gust (unpublished data, 1991). This algorithm is: $\sqrt{(\tau_s/\rho)} = \sqrt{(\tau_o/\rho)} - \mathbf{[0.2267(\log_{10}(S))}.\mathbf{((\sqrt{(\tau_o/\rho)}/6.35))}$ cm/s (evaluated for S in mg/L).

The calculation of mean mass settling rate comes from the transform of the equation: $\mathbf{W_s = \delta M/\delta t.\ 1/S_t}$. By using Gibbs *et al.* (1971), W_s is transformed into an equivalent sedimentation radius (RAD, in cm) as follows: $\mathbf{RAD = (P1 + \sqrt{(P2 + (P5(P3 + P4)))})/P5}$, where $\mathbf{P1 = 0.055804(\rho W_s^2)}$, $\mathbf{P2 = 0.003114(\rho^2 W_s^4)}$, $\mathbf{P3 = 4.5\mu W_s}$, $\mathbf{P4 = 8.704 \times 10^{-3}\ (\rho W_s^2)}$, and $\mathbf{P5 = 981(\rho_b - \rho)}$ (where μ is the viscosity of fresh water at 20°C evaluated as 0.0131 poises, ρ_b is the aggregate bulk density equated with the sediment bulk density at the equivalent eroded depth; all evaluated in cgs units). The fluid density ρ was also corrected for suspended solids as follows: $\rho = (\rho_o(1-V) + \rho_s V)$, where ρ_o is the clear water bulk density (1000 kg/m^3), V is the suspended sediment volume, and ρ_s is the sediment bulk density (2650 kg/m^3).

The raw data from Sea Carousel is processed in order to produce the calibrated plots for interpretation. The processing involves the following:

- define date and time for each record;
- read record and despike the data (± 2 standard deviations);

- time-average the 1Hz data (usually over 10 seconds);
- transform time-averaged OBS output to S (mg/L) and suspended mass (kg);
- transform current meter output to azimuthal and vertical flow (m/s);
- compute the clear water friction velocity (m/s) and bed shear stress (Pa);
- determine stress reduction due to S;
- compute fluid density and flow Reynolds number;
- determine lid rotational speed (m/s);
- compute diffusion rate out of flume (kg/s);
- compute corrected suspended mass (kg) and erosion rate ($kg/m^2/s$);
- compute mean eroded depth (mm);
- compute mass settling rate (m/s) and equivalent particle diameter (m); and
- write output files for plotting results (*.asc; *.dia; *.set).

3.3 Field sampling

3.3.1 Bottom sediment sampling

Bottom sediment samples were collected using a NWRI box corer. The corer was 50 x 50 cm in plan and 0.8 m in length. Two syringe cores (60 cc), a four-inch diameter push core, and a bulk sample were collected from the undisturbed central parts of the corer. The syringe cores were frozen immediately by immersion in liquid nitrogen and kept frozen for the analyses of bulk density and micro fabric using a GE® Hilite Scanner (Amos *et al.*, in press). The push core was frozen slowly and stored in a frozen state. Bulk samples were collected and kept at ambient temperatures for analyses of water content, organic carbon content, chlorophyll content, and grain size.

3.3.2 Water Sampling

Water samples were collected from the sampling port located 0.2 m above the skirt of the Sea Carousel. Samples were collected at each increment of flow about 1 minute into the increment. Known, well mixed volumes (V_{ss}) of the samples were filtered through a Swinnex® system onto pre-weighed, Gelmann® glass-fibre filters to remove the suspended solids. The gravimetric weight of the suspended load (W) in the filtrate was determined by drying the filters (at 60° C for

18 hours) and re-weighing. The suspended sediment concentration was determined from: $\mathbf{S = W/V_{ss}}$. Duplicate samples were collected for particulate organic carbon, major ion and chlorophyll analysis as well as for conventional optical microscopy (COM), transmission electron microscopy (TEM) for observations of particle structure. These samples were also analysed for suspended particle (floc/aggregate) size, settling velocity and aggregate density determinations.

3.3.3 Catscan analysis for bulk density

Bulk density was evaluated using x-ray computed tomography, which offers advantages over standard methods of analysis by being digital (yielding spectra of the Hounsfield Unit), three-dimensional, and able to resolve to a voxel volume of 0.06 mm^3 anywhere within the sample. The Hounsfield Unit (HU) for any voxel is defined as $\mathbf{HU = 1000(\mu_s - \mu_w)/\mu_w}$, where μ_s and μ_w are the x-ray linear attenuation coefficients of sediment and fresh water, respectively. According to Beer's Law, μ_s is a function of sediment bulk density ρ_s. Thus for a constant photoelectric effect, HU should vary in direct proportion to ρ_s. To eliminate negative numbers, and to approximate bulk density, Orsi (1994) transformed HU into a computed tomographic number CT with the expression $\mathbf{CT = 1 + (HU/1000)}$ so that air has CT $\approx$ 0, water has CT $\approx$ 1, and natural, fine-grained sediment has CT between 1 and 3. The transform from CT to fresh-water wet bulk density was: $\rho = \mathbf{390 + 670(CT)}$ kg/m^3; $r^2 = 0.992$; n = 11.

Syringe cores were analysed in a frozen state, wet bulk densities were therefore corrected to equivalent densities at 25 °C (the water temperature at the time of sampling) from the following relationship: $\rho_{s25} = \rho_{s0}\ (\rho_{w25} / \rho_{w0})$, where ρ_{s25} = wet bulk density at 25 °C, ρ_{s0} = wet bulk density at 0 °C, ρ_{w25} = water density at 25 °C (0.997), and ρ_{w0} = water density at 0 °C (0.917).

Sediment volume (V_s) is determined as: $\mathbf{V_s = (\rho_{s25} - \rho_{w25})/(2650- \rho_{w25})}$, that is the wet sediment bulk density minus the water density divided by the sediment buoyant density. Once V_s is known, porosity (η) can be found: $\eta = \mathbf{(1 - V_s)}$, from which the dry weight bulk density (ρ_{bs25}) may be determined: $\rho_{bs25} = \mathbf{(1 - \eta\rho_s)}$ and the water content (W) of the sediment is: $\mathbf{W = \eta\rho_{w25} /(1- \eta\rho_s)}$.

3.3.4 Chlorophyll analysis

A solution of 10 ml of 90% acetone was added to filter pads after filtering between 50 - 100 ml of water from the Sea Carousel. The solution was then placed in a darkened refrigerator for 24 hours, after which time the florescence of the solution was measured using a Turner Model 10 fluorometer. Two drops of 10% HCl were subsequently added and the fluorescence remeasured. Fluorescence was converted to chlorophyll and phaeopigment following the method of Parsons *et al.* (1984).

3.3.5 Particulate organic carbon and major ion analysis

Particulate organic carbon (POC) and major ions (K, Cl, Na, Mg, SO_4, SiO_2) were analysed at

the National Laboratory for Environmental Testing (NLET) of NWRI following the methods of Environment Canada (1979). Control sites only were tested in this fashion.

3.3.6 Particle size analysis

Particle size analyses were made on bulk surface samples. The samples were prepared and analysed at the sediment analysis laboratory, Geological Survey of Canada - Atlantic. The sand fraction was analysed using a settling column while the silt/clay fractions were analysed using a Sedigraph™. Results were processed and plotted using GSCA software READY, which applies the methods of moments to the size distribution in order to derive the mean, the sorting and the skewness of the distribution.

3.3.6.1 Malvern particle size analysis of eroded suspended aggregates

The size spectrum of eroded particles was determined on water samples pumped from Sea Carousel throughout the erosion process of the control plot stations. A Malvern® particle size analyser (Series 2600c) was used to determine the particle size distribution . The Malvern® consists of a 3-mV laser, receiving optics assembly, and electronic circuitry interfaced to a microcomputer. Particle size was derived from measurements of the near-forward Fraunhofer diffraction spectrum that is provided by a particle group randomly distributed in a sample cell mounted in the beam path between the laser source and the detector array. A complete description of the Malvern® particle size analyser can be found in Krishnappan *et al.* (1990).

3.3.6.2 Image analysis of eroded and settled suspended aggregates

Visual representation and characterization of the eroded aggregates was performed for control sites only and followed a modified method of Droppo and Ongley, (1992). Aggregates were analysed by gently pouring the pumped samples directly into settling chambers (the volume used is dependent on sediment concentration) or by subsampling with a large mouth pipette (3.5mm mouth) into a 50 ml plankton chamber filled with distilled water if the natural sediment concentration was too high. Samples were allowed to settled for 24 hours before subsequent imaging. The plankton chambers have four components: (A) a 3 ml reservoir with removable circular microscope slides where the specimen comes to rest after settling, (B) a column available in various volumes (10, 25, 50 and 100 ml), (C) a top cap used to hydrostatically seal the plankton chamber, and (D) a square piece of glass used to cover the reservoir after the column has been removed. The settling column volume used is dependent on the suspended sediment concentration. The higher the concentration the smaller the volume sampled in order to minimize particle-particle interactions and particle overlap during settling. A Zeiss® Axiovert 100 inverted microscope interfaced with an Optomax® V image analysis system and a CCD video camera served as the size analyzing tool for this study. A 2.5X objective with a conventional light source was used. Approximately 20,000 particles/flocs were digitized and sorted into size bands. Grain size distributions were presented as percent by number and volume.

3.3.6.3 Image analysis of bedload aggregates

The SVHS tapes of each erosion experiment were analysed in order to determine the modes and magnitudes of sediment transport. The modes of transport were defined as: no motion; bedload (which includes surface-creep and saltation), and suspension. In particular, the size and number of aggregates in motion were measured and the heights of the bedload and saltation layers documented. The particles in saltation absorb momentum from the flow in the saltation layer thus reducing the mean flow speed. This momentum is then transmitted to the bed when the aggregates bounce back onto the bed, thus transferring momentum to the bed in a ballistic fashion. The forces so transmitted and the equivalent stresses are defined in Amos *et al.* (1995). A detailed report on these results is given in Appendix 1.

3.3.6.4 Suspended sediment settling velocity, density and porosity

A drop of sediment was placed into a 2.5 L capacity settling column (5 x 10 x 50 cm in size) filled with distilled water using a wide mouth pipette. A microscope, situated approximately 35 cm below the top, was used to monitor settling of the particles in the turbid drop. This configuration eliminated any turbulence or settling irregularities resulting from the initial introduction of the sediment and allowed the sediment to reach terminal velocity prior to detection. The particles were video taped and recorded on a VCR as they passed through the field of view of the microscope. Settling velocity was derived by digitally overlaying two video frames (each representing 1/30 s) of a known time interval apart (generally 10 frames or 0.33 s). As the same particle will appear on the newly combined image twice, the distance of settling and the particle size can be determined and from which density and porosity can be derived. The density of a particle is derived using Stoke's law which is based on the settling of single impermeable spherical particles surrounded by a laminar boundary (Reynolds number < 0.5). Nevertheless, it has often been used to determine the wet density of flocs (Li and Ganczarczyk, 1987; Hawley, 1982): $\mathbf{W_s = {}^1/_{18}\, D^2\, (\rho_f - \rho)\, g/\mu}$ where ρ_f is the wet density of the floc and μ = absolute viscosity (kinemetic viscosity . ρ). W_s and D are derived from the image analysis; ρ and μ are constants for a given water temperature, and so the wet density of the floc (ρ_f) can be calculated. For purposes of illustration, the density was expressed as excess density (ρ_f - 1) (Kranck et al., 1992). Following the methods of Li and Ganczarczyk (1987), the floc porosity (η_f) can be expressed by a mass balance equation assuming a typical density of dried silt and clay (ρ_b) of 1650 kg/m^3: $\eta_f = (\rho_b - \rho_f)/(\rho_b - \rho)$.

3.3.7 Transmission electron microscopy

Eroded aggregates pumped to the surface during control deployments were prepared for TEM analysis following the four-fold multi-preparatory method of Liss *et al.* (1996). After sample polymerization in specific resins all samples were sectioned (70 nm thick) with a diamond knife mounted in an ultramicrotome (RMC® Ultramicrotome MT-7). The sections were mounted on formvar-covered copper grids. The ultrathin sections were then observed in transmission mode (TEM) at an accelerating voltage of 80 kV using a JEOL 1200 Ex II TEMSCAN® scanning transmission electron microscope (STEM).

4. RESULTS

Four deployments of the Sea Carousel were completed for each of the study plots (C, W, OIP) over the two week survey. Two further control stations were occupied outside the three plots in order to assess regional variations. Logistical problems were minimal, and excellent data were generally obtained from all. Following the C2 deployment lead weights on the carousel were systematically removed to provide optimum annulus penetration. Stations W1, OIP1 and OIP2 suffered short power losses of between 2 and 4 minutes. These stoppages, although evident in the reduction of suspended solids and bed erosion, did not appear to influence estimates of erodibility. The calibration of the OBS output (O) to S were undertaken from pumped samples. The results showed that a single third-order polynomial equation fitted the data over a range $0 > S > 10{,}000$ mg/L (Figure 4.1). The form of this equation is: $\mathbf{\log_{10}(S) = 1.241 + 0.0127(O) - 3.138 \times 10^{-5}(O^2) + 2.930 \times 10^{-8}(O^3)}$; $r^2 = 0.97$; $n = 73$. The shaft-end coder output (SCO) showed a linear and consistent relationship with lid rotational speed (rot) of the form: $\mathbf{rot = 0.0023(SCO)}$ m/s (Figure 4.2). Mean azimuthal flow was determined from lid speed using the laboratory-derived equation: $\mathbf{U_y = 0.574(rot)}$; $r^2 = 0.92$. This latter relationship is a guide only as the ratio (U_y/rot) decreases with time throughout the experiment. The results from station C1 is plotted in Figure 4.3a. Notice that U_y diminishes as a proportion of rot with increasing S (Figure 4.3b). The inference from this is that S has an influence on eddy viscosity and hence bed shear stress above a value of 1000 mg/L. The increase in S also impacts the freshwater density, which increases from 1000 to 1044 kg/m^3 throughout the erosion process (Figure 4.4). Note that the "gel point" of most fluid muds is around 1090 kg/m^3 (Torfs, 1995).

A summary of the results obtained from all deployments and tentative interpretations are given in Table 4.1

DEPLOYMENT SITE	EROSION THRESHOLD (Pa)			FRICTION COEFFICIENT (ϕ)		
	method (1) eroded[a] depth	method (2) mean[b] erosion	method (3) mean S[c]	Layer 1	Layer 2	Layer 3
C1	0.6	0.29	0.32	7	6	0
*C2	0.3	0.09	0.19	7	14	--
C3	0.5	0.28	0.32	17	37	4
C4	0.5	0.25	0.31	17	6	--
C5	0.6	0.28	0.36	17	18	0
C6	0.6	0.27	0.38	18	57	2
MEAN	**0.52**	**0.24**	**0.31**	**18**	**23**	**2**
W1	0.5	0.13	0.17	18	1	--
W2	0.5	0.36	0.40	21	1	--
W3	0.4	0.19	0.28	22	2	--
W4	0.6	0.26	0.48	25	-4	6
MEAN	**0.5**	**0.23**	**0.33**	**21**	**2**	**--**
OIP1	0.3	0.12	0.17	32	1	--
OIP2	0.4	0.22	0.29	4	--	--
OIP3	0.4	0.21	0.30	5	--	--
OIP4	0.5	0.23	0.38	8	--	--
MEAN	**0.40**	**0.19**	**0.23**	**12**	--	--

a - calculated from synthetic core plots as surface intercept of bed strength
b - calculated with corrected (dispersion) erosion rate
c - calculated from corrected S
* - unreliable due to excessive bed penetration

Table 4.1 Sea Carousel station summary including data on surface erosion thresholds, computed friction coefficients, and the range of wet-weight sediment bulk densities determined from Catscan analysis of syringe cores.

Method (1) yields the highest erosion thresholds of the three methods, method (3) is intermediate

in results and method (2) yields the lowest strengths. Despite slight differences in absolute values methods (2) and (3) show the same trends. That is, the control plot is the strongest, and the water injection and oxidant-injected plots are slightly weaker. Which site is weakest cannot be determined as differences between them are within our experimental errors. Only methods (2) and (3) provide erosion rates. Here results are clear: the control site exhibits the lowest erosion, the oxidant-injection site is intermediate, and the water injection site shows the highest erosion rates. These trends are summarised in Figure 4.5a (method (2)) and Figure 4.5b (method (3)). The mean erosion rate and S follow power functions of applied bed shear stress in almost all cases. These functions are:

control plot - $E = 3.41 \times 10^{-4}\ \tau^{2.411}$; $S = 945\ \tau^{2.124}$

water injection plot - $E = 8.15 \times 10^{-4}\ \tau^{2.444}$; $S = 1542\ \tau^{2.540}$

oxidant-injection plot - $E = 7.87 \times 10^{-4}\ \tau^{2.412}$; $S = 1722\ \tau^{2.234}$

Erosion thresholds for the control sites showed relatively consistent trends with time when measured using method (2) (Figure 4.6a) whereas strengthening with time was apparent when measured using method (3) (Figure 4.6b). The rate of strength increase was greatest for the water and oxidant-injection sites and suggests a rapid recovery from the disturbances of treatment. Nevertheless, an increase in strength was also evident at the control sites perhaps reflecting microphytobenthos activity in the very warm waters (25°C) of the harbour. Overall stability may be evaluated by examination of the critical shear stress (erosion threshold) for each plot versus the erosion rate constant (Figure 4.7a) and the suspension rate constant (Figure 4.7b). Notice that the plots are subdivided into relatively erodible and resistant fields. In both cases, the control sites appear most stable and the water and oxidant-injection sites appear most erodible.

The results on settling show a similar segregation between the three plots. In summary:

control plot - $W_s = 0.0013$ m/s; $D = 0.059$ mm

water injection plot - $W_s = 0.0016$ m/s; $D = 0.085$ mm

oxidant-injection plot - $W_s = 0.0014$ m/s; $D = 0.18$ mm

The greatest settling rate was over the water injection plot (due to higher S resulting from high erosion rates), intermediate settling rates were found over the oxidant-injection plot, and lowest rates were found over the control plot. The inference is that the higher the erosion rate, the greater the settling rate. The oxidant has added stability to the bed when compared against the water-injection plot, but has not overcome the disruptive effects of the ploughing.

4.1 Control plot

4.1.1 Sea Carousel

The calibrated time-series plots from the control sites (C1 to C6) are shown in Figures 4.1.1.1 to 4.1.1.6. Panel A in each figure illustrates lid speed and azimuthal and vertical current speeds at the reference hight (0.18 m). In panel B, the calibrated OBS outputs are plotted together with the dry-weight S's determined from the pumped samples. OBS 1 and 3 are inside the annulus of the Carousel. The sediments of Hamilton harbour were quite soft and so the lower OBS (3) was invariably buried. As such, only OBS 1 was used to define S inside the flume. Results of OBS 1 show synchronized trends of increasing S with the current time-series of panel A. OBS 2, however, shows little change with time as it is outside the annulus and monitors ambient S. Raw S is uncorrected for dispersion (leakage) and agrees reasonably well with the pumped samples (solid dots). OBS 1 has been corrected for dispersion following the methods of Amos *et al.* (1992). Panel C illustrates the erosion rate time-series determined from the changes in corrected S with time. The peaks in erosion (E_p) for lid rotations up to 1.0 m/s clearly correspond to the beginnings of each increment of lid speed and are relatively short-lived events. This exemplifies type I erosion, wherein bed erosion ceases approximately one to two minutes after application of the eroding flow. Above 1.0 m/s, erosion appears to be constant with time and S steadily increases (panel B). This conforms to type II erosion.

The sequence of bed erosion at station C1 was documented from video images. The erosion process was as follows:

BED SHEAR STRESS (Pa)	**OBSERVATION**
0.00	instrument on bottom (small pock mark in field of view) abundant oligochaetes present, significant gas escape
0.01	no bed erosion, but clear bed vibration with gas escaping
0.06	no bed erosion
0.35	type Ia erosion, organic flocs suspended
0.58	surface creep of aggregates begins type Ib erosion, flow separation over roughness elements
0.85	aggregates filling pock mark (3.1×10^{-3} cm^2/s)
1.16	2.5 mm aggregates in surface creep; saltation of shells
1.96	5 mm aggregates in surface creep; infilling depressions
2.66	onset of 5 mm aggregate saltation; largest 10 mm diameter
3.60	saltating aggregates broken down; suspension dominant

The erosion process at station C3 showed similarities to C1 and is described below:

BED SHEAR STRESS (Pa)	**OBSERVATION**
0.00	smooth lakebed, abundant oligochaetes numerous gas bubbles escaping
0.01	no bed erosion; no particle motion

0.35	type Ia erosion, movement of organic-rich flocs and aggregates
0.50	surface creep of organic fragments
0.85	type Ib erosion; floc erosion from bed surface creep of 2 mm aggregates; no saltation
1.16	onset of suspension of fine fraction
1.96	surface creep 3 mm aggregates; no saltation
2.66	surface creep 5 mm aggregates; rapid corrasion
3.60	5 - 10 mm aggregates in saltation; rip-up clasts evident

The erosion process began with movement of the organic rich "fluff" (type Ia) that was present throughout the plot. This gave way to the erosion of bed material (type Ib) which moved partly as surface creep and partly in suspension. Our erosion threshold is based on the onset of type Ib erosion. Surface creep (bedload) was a high proportion of the total load in transport and infilled depressions in the bed to create a smoothed surface and took place below mass erosion of the bed. The size of aggregates moving as bedload increased with mean velocity reaching maximum sizes of 10 mm. In many cases, the larger fragments moved faster than the smaller ones. The finer fraction moved immediately into suspension, but suspension often lagged the onset of traction. Saltation of rip-up clasts was evident in all deployments and was dominant at intermediate speeds. The mean size of saltating aggregates was around 5 mm and the frequency was around 5/s. The saltation height was between 1 and 2 cm.

The erosion threshold ($\tau_c(0)$) was evaluated in three ways: (1) from plots of applied bed shear stress versus eroded depth (herein referred to as synthetic cores; Figure 4.1.1.7 to 4.1.1.12); (2) from applied bed shear stress against mean erosion rate (E_m) (Figures 4.1.1.13 to 4.1.1.18 panels a); and from applied bed shear stress against S (Figures 4.1.1.13 to 4.1.1.18 panels b). The derived threshold values from the three methods for estimating erosion threshold are summarised in Table 4.1. The degree of variability in the data between the six deployments within the control plot for measures (2) and (3) of $\tau_c(0)$ was reasonably small. The mean erosion thresholds for the control sites adopting the three methods are: (1) **0.52 (± 0.11) Pa**; **(2) 0.23=4 (± 0.07) Pa**; and (3) **0.31 (± 0.06) Pa**. Notice that the method (1) has the highest scatter in results and method (3) the lowest. Also note that methods (2) and (3) agree closely, and predict a substantially lower threshold than does method (1). For purposes of comparison, we have chosen method (3) as the standard. The question of whether the "fluff" layer constitutes the bed is debatable. We chose to define the "fluff" layer as part of the water column. A large part of the scatter in methods reflects real differences from site to site which appear to be related to systematic changes with time, possibly due to increasing biostabilization.

The depth plots are interpreted as synthetic cores as the applied shear stress (τ_o) is equated with the erosion threshold when erosion ceases (τ_c) at depth z, and thus is a measure of the sediment strength (τ_d) at that depth. The erosion threshold at any depth, z, may be determined from the Mohr-Coulomb equation: $\tau_c(z)=\sigma.\tan(\Phi) + \tau_c(0)$.

Values of Φ are summarised in Table 4.1. All control site synthetic cores demonstrated two or three layers of increasing sediment strength; a surface layer showing relative little consolidation

and deeper more resistant layers. The range in Φ indicates that the structure of the sediment was complex, variable, and of low consolidation compared to other studies. The transition between the topmost two layers was also observed from the catscan and from microscopy. In general, a positive friction coefficient conforms to a normal-loaded bed; a zero friction coefficient implies no consolidation; and a negative friction coefficient implies the possible presence of a surface biofilm with weaker material beneath (not encountered in the control plot).

Erosion rates may be expressed in two ways: (a) the mean erosion rate (E_m) - that is, the net eroded mass over the duration of the increment of an applied flow; and (b) the peak erosion rate (E_p) - that is, the maximum erosion rate evident over an applied flow (usually associated with the start of the applied speed increment). A summary of the erosion thresholds and mean erosion rates determined using methods (2) and (3) is given below in Table 4.1.1.1. The highly-significant correlation coefficient of method (3) contrasts with that of method (2).

STA.	EROSION RATE METHOD (2)			SUSPENSION RATE METHOD (3)		
	EQUATION	τ_{crit} (Pa)	r^2	EQUATION	τ_{crit} (Pa)	r^2
C1	$E_m = 3.42 \times 10^{-4}\tau^{2.876}$	0.29	0.72	$S = 955\tau^{2.290}$	0.32	0.93
C2	$E_m = 7.53 \times 10^{-4}\tau^{1.959}$	0.09	0.60	$S = 2138\tau^{1.826}$	0.19	0.94
C3	$E_m = 2.62 \times 10^{-4}\tau^{2.567}$	0.28	0.61	$S = 729\tau^{2.035}$	0.32	0.95
C4	$E_m = 2.90 \times 10^{-4}\tau^{2.451}$	0.25	0.53	$S = 771\tau^{2.181}$	0.31	0.93
C5	$E_m = 1.60 \times 10^{-4}\tau^{2.170}$	0.28	0.47	$S = 453\tau^{2.135}$	0.36	0.95
C6	$E_m = 2.38 \times 10^{-4}\tau^{2.444}$	0.27	0.61	$S = 622\tau^{2.275}$	0.38	0.95

Table 4.1.1.1. A summary table of the mean erosion rates and erosion thresholds determined for the control sites using methods (2) and (3).

The mean erosion rates (E_m) and S show positive correlations with applied bed shear stress. The control plot mean power functions are:

$$\mathbf{E_m = 3.41 \times 10^{-4}\ \tau^{2,411}}$$

$$\mathbf{S = 945\ \tau^{2.124}}$$

The above equations will form the basis of comparison with results from the two treatment plots.

The mean still-water mass deposition rate ($\delta M/\delta t$) has been derived from the rate of change in S within Sea Carousel. The settling curves for stations C1 to C6 are shown in Figure 4.1.1.19a. The curves show a logarithmic decay in S with time: $\mathbf{S(t) = m.log_{10}(t) + S(0)}$. The computed mean

values of mass settling rate, W_s, and equivalent sedimentation diameter (D) are presented in Table 4.1.1.2.

DEPLOYMENT SITE	decay constant, m	S(0) (mg/L)	W_s (m/s)	SEDIMENTATION DIAMETER (mm)
C1	-1100	2904	0.00064	0.0 7
C2	-383	1042	0.00111	0.11
C3	-653	1809	0.00094	0.05
C4	-1010	2615	0.00194	0.07
C5	-1029	2742	0.00183	0.30
C6	-661	1887	0.00131	0.37

Table 4.1.1.2. Calculated values of mean settling velocity (W_s) for control plot deployments.

The plot-averaged still-water settling trend is expressed by the equation: $\mathbf{S(t) = -806\log_{10}(t) + 2106}$ mg/L. The mean settling rate (W_s) varies by a factor of three, whereas the sedimentation diameter (D) varies from coarse silt (0.07 mm) to medium sand (0.37 mm). The decay constant in the settling equation varies as a function of the starting S and has the linear form: $\mathbf{k = 0.35S(0) - 14}$ /s (Figure 4.1.1.20). The site-averaged W_s was **0.00129 (± 0.00046)** m/s. The site-averaged sedimentation diameter was **0.162 (± 0.125)** mm.

Both W_s and D varied throughout the settling period. Thus time-series of these attributes as well as S and incremental mass deposition are plotted in Figures 4.1.1.21 to 4.1.1.26. The trends show a decreasing settling rate with time from 0.005 m/s to 0.0006 m/s. The equivalent sedimentation diameters of this changing population of settling sediment varies from medium sand (0.6 mm) at the initial stages to fine sand (0.13 mm). The settling rates are rapid for this fine-grained lakebed material, and reflects strong flocculation of the suspended material and large clast sizes of suspended aggregates.

4.1.2 Catscan bulk density

The bulk density profiles of the surface sediment has been evaluated through Catscan analysis of a syringe core and push core following the sampling and analytical methods described in section 3.3.3. Results for site C3 are plotted in Figure 4.1.2.1. As in the synthetic cores (Fig. 4.1.1.9), two distinct layers were recognized: (1) a surface layer, 8-10 mm thick of relatively low bulk density; and (2) a reasonably uniform sub-stratum of higher density. The low density of the top layer is likely related to an open pore matrix with associated high water content. This is indicative of a recently deposited flocculated material with a large component of active microbial communities (Liss *et al.*, 1996). The reasonably constant density layer (2) suggests that the process of self-weight consolidation has not taken place. The scatter in bulk density values

(horizontal bars around each data point) reflects the heterogeneity of each depth interval, not the error in detection. This scatter is large throughout the cores and may reflect the presence of bioturbation, poorly-sorted material, or trapped gas. The first is most likely the case as significant bioturbation resulting from oligochaetes was observed during direct underwater video analysis (taxonomy identification by T. Reynoldson, personal communication, 1995). The standard deviation of density values (± 500 kg/m^3) is diagnostic of an inhomogeneous sediment, subject to intensive bioturbation.

4.1.3 Chlorophyll and POC

Tables 4.1.3.1 and 4.1.3.2 summarise the chlorophyll (CHLa) and POC concentrations derived from samples pumped from Sea Carousel at the control sites. These data mimic the trends in S shown in Figures 4.1.1.1 to 4.1.1.6. The point of significant increase in chlorophyll and POC corresponds with that of the increase in S. The high ambient values are noted and may reflect resuspension of the fluff layer at the time of deployment of Sea Carousel. The presence of chlorophyll reflects a thriving diatom community which also contributes to bed stabilization.

Sample #	C1 CHLa (μg/L)	C2 CHLa (μg/L)	C3 CHLa (μg/L)	C4 CHLa (μg/L)	C6 CHLa (μg/L)
1	6.9	6.9	8.0	5.3	8.01
2	8.0	4.8	8.0	7.3	10.0
3	8.8	5.9	8.0	6.0	8.0
4	8.0	6.4	24.0*	8.0	9.6±0.8 (n=3)
5	5.6	12.0*	18.0	14.7*	13.4*
6	9.6*	22.9	29.4	28.0	26.0
7	28.0	48.1	48.1	40.1	38.4
8	37.4	64.1	76.1	76.1	69.4
9	40.0	--	181.6	68.1	90.8
10	56.1	--	277.7	128.2	108.7
11	76.1	--	272.3	194.5	181.6
12	218.9	--	--	165.5	--

Table 4.1.3.1. Chlorophyll a concentrations for control plot sites. * increment at which bed failure first occurred.

SAMPLE #	C1	C3	C5
	POC (mg/L)	POC (mg/L)	POC (mg/L)
1	3.24	3.29	3.21
2	1.72	3.84	2.15
3	2.05	3.83	2.75
4	1.54	11.2*	2.34
5	1.32	20.4	6.45*
6	3.0*	25.0	15.4
7	13.3	37.3	30.8
8	27.4	86.3	45.7
9	35.6	125	n/a
10	66.9	310	132.0
11	73.1	124	218.0
12	125	--	--

Table 4.1.3.2. POC concentrations for eroded suspended bed sediment. * increment at which bed failure first occurred. The percentage POC of the total SPM varied between 3 and 6 %.

4.1.4 Microscopy

The existence of a surficial biostabilized layer at the control sites was confirmed by conventional optical microscopy (COM) for control deployment C3 and by transmission electron microscopy (TEM) analysis for control deployment C4 (Figures 4.1.4.1 and 4.1.4.2 respectively). Figure 4.1.4.1a illustrates ambient suspended sediment aggregates/flocs (pumped to the surface following the 10-minute still-water period and prior to lid rotation). The aggregates are relatively small and compact in structure. This sediment, once deposited, becomes incorporated into the sediment structure of the bed through physical compaction and chemical and biological modifications. Figure 4.1.4.1b exemplifies the typical structure of the aggregates during initial bed failure. The very large size and open matrix of these aggregates is typical of high organic content surficial fine-grained sediments (Liss *et al.*, 1996) or biofilms. Figure 4.1.4.1c illustrates a typical rip-up aggregate which has been eroded below the biostabilized layer. These aggregates are generally rounder and more dense in nature due to greater compaction at lower sediment layers. The size of these aggregates varied greatly, however, because of their dense nature they represent a much greater mass of eroded sediment than the larger aggregates from the eroded

biostabilized layer.

Figure 4.1.4.2 represents three TEM micrographs of sediments collected from samples pumped during control deployment C4. Figure 4.1.4.2a was collected during initial bed failure (increment 4, lid speed - 0.5 m/s) and represents the biostabilized layer, while Figure 4.1.4.2b and c was collected from deeper eroded sediment below the biostabilized layer (increment 11, lid speed - 1.8 m/s). Both micrographs reveal an aggregate/floc principally composed of bacteria, polymeric fibrils and inorganic particles (clays) similar to that illustrated by Liss *et al.* (1996) for natural riverine suspended sediments. Fibrils produced by bacteria, act as binding and bridging mechanisms between aggregates/flocs and thus tend to stabilize the bed (Droppo and Ongley, 1994; Liss *et al.*, 1996). Droppo and Ongley, 1992) have suggested that it is these fibrils that give the flocs their pseudo-plastic nature. Because of the very high magnification of TEM, gross differences between aggregate structure can not be observed. Figure 4.1.4.2a does however demonstrate a more closely linked network of fibrils which is common in newly formed biofilms, whereas Figure 4.1.4.2b reveals more convoluted and fragmented fibrils diagnostic of an older structure. It appears from this preliminary work that the main mechanism of aggregate/floc stabilization in the upper biostabilized layer is the bacterial fibrils, whereas in the deeper sediment, compaction combined with relict fibrils appears more important.

4.1.5. Grain size distributions

The surface sediments from the control plot appear to be consistent from site to site. They comprise between 10 and 15% sand, around 43% silt and the remainder is clay. The mean diameter is between 4 and 6 microns which places the desegregated sediment in the clay - very fine silt size range. All sediments are poorly sorted, reflecting a range of sources. The sand fraction is largely made up of anthropogenic fly ash and other stack emissions and so was probably airborne. A summary of the sediment texture is presented in Table 4.1.5.1. Analysis of major elements (EDAX) showed only SiO_2 varied throughout the deployment, systematically increasing . All other major ions K, Cl, Na, Mg and SO_4 remained steady (data in Appendix 2) thus reflecting an association with pore water fluids rather than the siliceous sediment.

STATION	% SAND	% SILT	% CLAY	DIAM (mm)	SORTING (mm)
C1	10.3	43.2	46.3	0.0042	0.141
C2	14.3	42.8	42.8	0.0052	0.128
C3	13.2	42.8	43.9	0.0048	0.130
C4	8.3	43.7	48.0	0.0037	0.151
C6	13.5	42.0	44.4	0.0047	0.133
W4	11.9	44.6	43.4	0.0049	0.136

OIP4	18.1	41.0	40.7	0.0062	0.122

Table 4.1.5.1. A summary of the textural analysis of surface samples.

4.1.5.1. Bedload transport (video interpretation)

A summary of the video analyses for station C1 is given in Table 4.1.5.1.1. This table provides values of bed shear stress, and mode of transport (NM - no motion; BL - bedload, surface creep; SL - saltation; SSL - suspension.

STATION/ SHEAR STRESS (Pa)	**TRANSPORT MODE**	**TRANSPORT RATE (ag/min)**	**AGGREGATE DIAM. (mm)**	**VOLUME TRANSPORT ($m^3/m/s$)**
0.01	NM	--	--	--
0.06	NM	--	--	--
0.11	NM	--	--	--
0.17	NM	--	--	--
0.35	BL	TRACE	--	--
0.58	BL	??	??	??
0.85	BL/SL	35	3	4.94×10^{-8}
1.16	BL/SL SSL	108 306	2 2	4.52×10^{-8} 1.28×10^{-7}
1.96	BL SL SSL	97 41 298	3 2 2	1.37×10^{-7} 1.71×10^{-8} 1.24×10^{-7}
2.66	BL SL SSL	75 44 65	2 2 2	3.12×10^{-8} 1.83×10^{-8} 2.70×10^{-8}

Table 4.1.5.1.1. A summary table of sediment movement observed from SVHS video records collected at site C1.

The results show that there is a clear traction population moving as surface creep once the erosion threshold has been exceeded (0.32 Pa). The mean diameter of the aggregates moving as surface creep is around 2 mm. The aggregates infill depressions in the bed and create small ripples that migrate through the field of view. At around double the erosion threshold (0.85 Pa), saltation of aggregates begins in association with surface creep. The aggregates are about the same size as

the traction population (2-3 mm) and have a saltation height of 1 cm. At around four times the erosion threshold (1.16 Pa) a portion of the aggregates are found at all depths of the flow, and comprise a large volume of the total mass transported. The suspended sediment flux for τ = 1.16 Pa was 0.28 kg/m/s, while the bedload/saltation flux was only 2.6 x 10^{-4} kg/m/s (i.e. 0.1%). Similarly, the suspended flux for τ = 2.66 Pa was 0.72 kg/m/s and the bedload/saltation flux was 1.1 x 10^{-3} kg/m/s (again only 0.1%). Suspended sediment transport thus dominated our experiments.

The size distribution of the aggregates appears to be widespread, and a portion of them are between 6 - 10 mm in diameter. In view of the unit volume of such aggregates (a 10 mm grain has 125 times more volume than a 2 mm grain assuming sphericity), much of the mass in transport is moved intermittently as the largest material that appears to be eroded under the highest (type II) flows. The aggregates show evidence of corrasion which probably results from impacts with the bed. With time over a steady shear stress, the aggregates appear to become smaller in size through the process of corrasion.

4.1.5.2. Suspended sediment transport

Control samples collected from the pump sampler were analyzed for grain-size distributions by two methods; each yielding an aggregate particle size distribution. The first method, using the Malvern Particle Sizer™, is an indirect measure of particle size and can be somewhat destructive of the flocs due to the magnetic stirrer used in the analysis. Nevertheless, the median grain diameter D_{50} is similar to the Sedigraph™/settling column analyses of bulk sediments. The Sedigraph™ provides information on primary particle distributions only, due to the destructive physical and chemical preparation required for this analysis. The similarity in size between the two tests and sediment types is likely due to larger sand size particles being present in the bed sediment sample (for settling column) but not in the pumped sample (for Malvern™).

The second method is through direct observation of individual aggregates with an Optomax V™ image analysis system. This is the least destructive of the methods of particle sizing and yields significantly larger particle size distributions (Table 4.1.5.2.1). It should be realized that the Optomax V™ counts substantially fewer particles than the Malvern™ and as such the D_{50} by volume values can be significantly biased by only a few very large particles. It is interesting to note, however, that D_{50} for the C3 samples generally increase with depth (with the exception of C3-10 and C3-11). This is consistent with the video interpretation of bedload transport which shows that rip-up clasts increase in size with eroded depth (see section 4.1.5.1). This is related to increasing compaction with depth. The data outputs are presented in Appendix 3.

Sample #	C1	C3		C5
	Optomax™ D_{50} (mm)	Malvern™ D_{50} (mm)	Optomax™ D_{50} (mm)	Malvern™ D_{50} (mm)
1	--	0.054	0.23	0.054

2	--	0.044	0.15	0.0555
3	--	0.048	0.27	0.0568
4	--	0.043	0.27	0.0535
5	--	0.04	0.34	0.059
6	--	0.048	0.5	0.0554
7	--	0.054	0.39	0.0486
8	--	0.05	0.37	0.0447
9	--	0.049	0.56	--
10	0.5424	0.048	0.17	0.0489
11	0.4806	0.073	0.24	0.0534
12	0.1988	--	--	--
sonicated (primary particles)	--	0.0100 (C3-10)	--	0.0111 (C5-10)

Table 4.1.5.2.1. Median diameter of eroded aggregates as determined from the Malvern Particle Sizer™ and the direct observation Optomax™ image analysis system.

4.1.6. Settling velocity, density and porosity of suspended eroded aggregates

The settling velocities of individual particles were directly measured using the settling column described in section 3.3.6.4. Density and porosity were calculated based on Stoke's law. As the analyzed sediment is flocculated, Stoke's law is not ideal because of the assumption of single solid spherical particles. These results nevertheless provide us with some initial trends on how aggregate settling velocity, density, and porosity are related to aggregate size. It should be realized that these results are for individual particles and not for bulk settling velocity presented in section 4.1.1. In addition because the samples were pumped from depth, they may not contain the larger aggregates observed on the underwater video due to hydraulic sorting and breakage in the pump tubing. As such, settling velocities are smaller than those presented for bulk sediment sizes (Table 4.1.2.2).

Figure 4.1.6.1 illustrates results from a typical sample collected during the 10th speed increment of station C5 (below biostabilized layer). All samples analyzed (Appendix 4) demonstrated a positive relationship between settling velocity and particle (aggregate) size. W_s (for C5) varied linearly with D_{50} in the form: $\mathbf{W_s = 0.006(D_{50}) + 0.81}$ mm/s, $r^2 = 0.47$, n = 48. Also the excess density varied as a weak power function of D_{50}: $\rho_b = \mathbf{102(D_{50})^{-1.32}}$ gm/cm^3, $r^2 = 0.67$, n = 48 (Fig. 4.1.6.2). The wide scatter (low r^2) in the data is typical as settling velocity can vary greatly

depending on the particle's density, composition, shape, and porosity (Li and Ganczarczyk, 1987). Individual particles ranging in size from approximately 0.15 mm to 1.0 mm on average had settling velocities ranging from 0.001 to 0.004 m/s and from 0.008 to 0.012 m/s respectively. Note that this is well outside of the Stokes settling range, and is equivalent to a quartz sphere of fine sand (demonstrating the considerable influence of flocculation/aggregation). These individual particle settling velocities are substantially larger than those derived for the bulk sediment (Tables 4.1.1.2, 4.2.1.1, and 4.3.1.2). As such, they are likely reflective of the differences in water density (higher in the Sea Carousel due to high S concentration), differences in the methods of physical analysis, as well as the mathematical derivation of settling velocities [mass settling rate based on Gibbs *et al.* (1971); individual particle settling rate based on Li and Ganczarczyk (1987)].

Calculations of individual eroded aggregate density demonstrate an inverse relationship between particle size and density (Figure 4.1.6.2). Conversely particle porosity increases with increasing particle size (Figure 4.1.6.2). For very large aggregates, particle density approaches the density of water and porosity approaches 100%.

4.2. Water injection plot

4.2.1 Sea Carousel

The calibrated time-series plots from the water injection site are shown in Figures 4.2.1.1. to 4.2.1.4. Even with the physical disturbance and fluidization of the sediment by the injection system, the time series plots, at first sight, do not appear significantly different from the control. Well-defined peaks in erosion rate (E_p) are evident at the onset of the first 5 increments of flow (above threshold): type I erosion. Thereafter, constant (type II) erosion prevailed. The transition in erosion type took place at a lid speed of about 1 m/s. The index current showed very large and erratic fluctuations compared to the control site. The reason for this may in part be due to the highly magnetised nature of the anthropogenic material brought in by stack emissions and surface runoff which would influence the EM flow sensor. The mean surface erosion threshold (by eroded depth) using method (1) was similar to the control plot (0.5 ± 0.07 Pa; Figures 4.2.1.5 to 4.2.1.8). However, this threshold is well above those derived using methods (2) and (3) (see later) and indicates that the method is probably insensitive to the onset of erosion. The method is however, responsive to the gross bulk properties of the bed reflected in the friction angle, which is also similar to the control plot. The highly variable results are diagnostic of a spatially variable substrate which may reflect disruption by the injection method. The similar ϕ in layer (1) is surprising given the recent bed reworking.

The erosion thresholds obtained from methods (2) and (3), are indicated in Figures 4.2.1.9 to 4.2.1.12. In all cases, the data were expressed as power functions of bed shear stress. These power functions for the four water injection stations are presented below in Table 4.2.1.1.

STA.	EROSION RATE - METHOD (2)			SUSPENSION RATE - METHOD (3)		
	EQUATION	τ_{crit} (Pa)	r^2	EQUATION	τ_{crit} (Pa)	r^2
W1	$E_m = 2.19 \times 10^{-3}\tau^{2.651}$	0.13	0.77	$S = 3715\tau^{2.135}$	0.17	0.96
W2	$E_m = 3.04 \times 10^{-4}\tau^{2.338}$	0.36	0.57	$S = 883\tau^{2.880}$	0.40	0.96
W3	$E_m = 4.89 \times 10^{-4}\tau^{2.343}$	0.19	0.63	$S = 1168\tau^{2.246}$	0.28	0.97
W4	$E_m = 2.79 \times 10^{-4}\tau^{2.443}$	0.26	0.36	$S = 401\tau^{2.899}$	0.48	0.95

Table 4.2.1.1 A summary of the erosion thresholds and erosion rates for the water injection sites determined using methods (2) and (3).

The mean erosion threshold derived from method (2) is **0.23** (± 0.08) Pa, while that for method (3) is **0.33** (± 0.12) Pa. The differences in the two methods is within the scatter of results and so is not significant. The erosion thresholds of this plot are the same as for the control. The erosion rates are however, slightly higher than for the control. The plot-averaged mean erosion rate (E_m) and S approximate power relationships to bed shear stress in the following forms:

$$\mathbf{E_m = 8.15 \times 10^{-4}\tau^{2.444}}$$

$$\mathbf{S = 1542\tau^{2.540}}$$

At highest stresses, the average erosion rate exceeds that of the control by about 200%. This shows a loss of strength over the control plot, and is likely the result of ploughing. The computed mean values for mass settling rate (W_s) during the 10 minute settling period are given in Table 4.2.1.2.

DEPLOYMENT SITE	decay constant,m	S(0) (mg/L)	W_s (m/s)	SEDIMENTATION DIAMETER (mm)
W1	-910	1304	0.00186	0.11
W2	-769	1733	0.00133	0.07
W3	-745	1373	0.00158	0.08
W4	-704	1128	0.00150	0.08

Table 4.2.1.2. Calculated values of mass settling rate (W_s) for the water injection plot deployments.

The mass settling velocities were approximately 20% higher than at the control site with a plot-averaged value of **0.0016** (± 0.0002) m/s. Mass settling velocities between sites were within the

scatter and therefore trends can not be inferred. It is however known that the higher the initial S at the start of settling (a function of erosion rate), the greater will be the mass settling velocities. As the W plot had consistently greater erosion rates than the C it is not surprising that the mass settling velocities were higher (although not significantly so). The plot-averaged still-water settling rate may be approximated by: $\mathbf{S(t) = -782\log_{10}(t) + 2282.}$ The mean sedimentation diameter was also coarser than the control site and was within the very fine sand size range: **0.085** (± 0.015) mm.

W_s and D_{50} appeared to decrease throughout the period of settling, although a considerable scatter was evident (Figures 4.2.1.13 to 4.2.1.16). The sedimentation diameters varied from medium sand during initial settling to coarse silt during the latter stages. The decay constant m indicates that settling on this plot was at about the same rate as over the control.

4.2.1.1 Bedload transport (video interpretation)

The video analysis reflected the same trends as were apparent at the control. That is, a significant bedload transport took place as both surface creep and in saltation. This took place in association with bed erosion and suspension of finer material. The material in transport was largely 2 - 3 mm in diameter though aggregates up to 10 mm in diameter were present. The mass transported as bedload accounted for only 0.1% of the total transport.

STATION/ SHEAR STRESS (Pa)	TRANSPORT MODE	TRANSPORT RATE (ag/min)	AGGREGATE DIAM. (mm)	VOLUME TRANSPORT ($m^3/m/s$)
0.01	NM	--	--	--
0.06	NM	--	--	--
0.11	NM	--	--	--
0.17	NM	--	--	--
0.35	BL	TRACE	--	--
0.58	BL	??	??	??
0.85	BL/SL	35	3	4.94×10^{-8}
1.16	BL/SL SSL	108 306	2 2	4.52×10^{-8} 1.28×10^{-7}
1.96	BL SL SSL	97 41 298	3 2 2	1.37×10^{-7} 1.71×10^{-8} 1.24×10^{-7}

2.66	BL SL SSL	75 44 65	2 2 2	3.12×10^{-8} 1.83×10^{-8} 2.70×10^{-8}

Table 4.2.1.1.1. A summary table of observed bedload transport from site W2 (BL - surface creep; SL - saltation; SSL - suspension of aggregates).

4.2.2 Catscan bulk density

The bulk density of the syringe core collected at site W4 is shown in Figure 4.2.2.1. Two layers have been interpreted from the profile; (1) a topmost layer of rapidly increasing density with depth to 7 mm; and (2) an underlying layer of slowly increasing density. The surface density is 1130 kg/m^3 rising to 1420 kg/m^3 at the base of layer 1. The maximum density is 1550 kg/m^3. The apparent decreasing density at the base of the core is likely related to disturbance upon sampling. While biostabilization was evident in the control sites, its significance in the W plot is likely significantly reduced due to the disturbance of the injection system. The density profile mimics that of the control site (see Fig. 4.1.2.1). Also, the range of densities is similar to the control suggesting that erodibility is not strongly related to bulk density. The scatter around the mean bulk density values is however, less than those observed for the control plot. This is likely related to the removal of gas bubbles by the physical disturbance of the injection rake. The standard deviation of density values (± 400 kg/m^3) is diagnostic of an inhomogeneous sediment, possibly subject to intensive bioturbation by oligochaetes.

4.2.3 Chlorophyll analysis

The chlorophyll data in Table 4.2.3.1 substantiates the increment in lid speed at which point bed failure occurs as determined in the time-series of the Sea Carousel (Figures 4.2.1.1 to 4.2.1.4). Initial concentrations prior to bed erosion are generally higher than for the C sites. This result is likely related to the disturbance of the biostabilized layer and general sediment structure by the injection rake. As such, the higher ambient values may reflect greater resuspension upon the deployment of the Sea Carousel due to the destabilization and fluidization of the surface layer by the injection equipment. Also, nutrients within the injected water may stimulate diatom productivity and enhance chlorophyll production.

Sample #	**W1 CHLa** (μg/g dry wt.)	**W2 CHLa** (μg/g dry wt.)	**W3 CHLa** (μg/g dry wt.)	**W4 CHLa** (μg/g dry wt.)
1	10.0	7.3	16.7	16.7
2	7.3	6.7	14.7	10.7
3	12.7	6.0	15.4	8.7

4	9.3	6.7	12.8	10.7
5	26.7*	14.7*	28.8*	17.4*
6	40.0	18.3	34.7	29.4
7	48.1	22.4	28.8	48.1
8	74.8	48.1	42.7	26.7
9	117.5	32.0	48.1	53.4
10	165.5	74.8	81.9 ± 3.1 (n=3)	149.5
11	--	128.2	133.5	117.5
12	--	--	--	--

Table 4.2.3.1 Chlorophyll a concentrations for control plot sites. (*) is the increment at which bed failure first occurred.

4.3. Oxidant injection plot

4.3.1. Sea Carousel

The calibrated time-series plots from the oxidant injection plots (OIP1 to OIP4) are illustrated in Figures 4.3.1.1. to 4.3.1.4. These plots are very similar to both the control and water injection plots except for the fluctuations in azimuthal current speed measured by the electro-magnetic current meter at site OIP1. The higher variability was probably due to the increased concentration of major ions in the water/sediment from the injected oxidant. Well-defined peaks in E_p were prominent at the onset of all flow increments: type I erosion. A transition to type II erosion may be evident in the last two increments of flow. A summary of the surface erosion thresholds is given in Table 4.1. The mean erosion thresholds for the three methods are respectively: **0.40 (± 0.07)**, **0.19 (± 0.04)**, and **0.28 (± 0.07) Pa**. Notice that method (1), used in the synthetic plots, yields the highest strengths, and that these strengths are about 20% less than the control plot strengths. By contrast, the thresholds derived from methods (2) and (3) yield much lower values, which are about 30% less than the control plot.

Friction coefficients (Φ) for the OIP were all positive and showed monotonic increases in bed strength with depth (Figures 4.3.1.5 to 4.3.1.8). However, the surface values were much lower than those from either the control or water-injected sites. In general, only one layer was detected suggesting that the sediment column has been remoulded with the loss of the previously-defined macro-structure.

The detailed observation of the erosion process from high-resolution video provided a guide on the mechanism of bed failure. The following describes this mechanism from station OIP3:

BED SHEAR STRESS (Pa)	OBSERVATION
0.03	flat bed, no motion
0.35	suspension of organic flocs; type Ia erosion
0.58	bed erosion of flocs; type Ib erosion
1.16	turbulent rough conditions; surface creep of 1 mm aggregates infilling behind irregularities
1.96	shell fragments (5 mm) in traction, high suspension
2.66	5 mm aggregates in traction; accretion of bed through traction
3.60	ripple formation from traction of eroded aggregates 5 cm ripple advance in 300 s
4.46	5 mm clasts and shells in saltation; rapid corrasion

In this time-series we noticed the presence of shell fragments saltating over the bed. These shells can cause erosion of the bed through the cutting action of the shell edges, and may contribute to the high erosion rates in this plot.

STA.	EROSION RATE METHOD (2)			SUSPENSION RATE METHOD (3)		
	EQUATION	τ_{crit} (Pa)	r^2	EQUATION	τ_{crit} (Pa)	r^2
OIP1	$E_m = 2.03 \times 10^{-3}\tau^{2.521}$	0.12	0.74	$S = 3908\tau^{2.178}$	0.17	0.95
OIP2	$E_m = 4.92 \times 10^{-4}\tau^{2.600}$	0.22	0.70	$S = 1291\tau^{2.187}$	0.29	0.97
OIP3	$E_m = 3.67 \times 10^{-4}\tau^{2.300}$	0.21	0.58	$S = 1119\tau^{2.223}$	0.30	0.98
OIP4	$E_m = 2.61 \times 10^{-4}\tau^{2.239}$	0.23	0.59	$S = 570\tau^{2.349}$	0.38	0.97

Table 4.3.1.1. A summary table of the mean erosion rates and erosion thresholds determined for the control sites using methods (2) and (3).

The erosion thresholds obtained from methods (2) and (3) are illustrated in Figures 4.3.1.9 to 4.3.1.12. The mean erosion threshold derived from method (2) is **0.19(±0.04)** Pa and for method (3) is **0.28 (±0.07)** Pa. Differences between the two methods are not significant, due to the scatter in results. The overall threshold values appear marginally lower than the control and water-injected sites by about 20%.

Mean erosion rates (E_m) and S are power functions of applied bed shear stress (Table 4.3.1.1), and are similar to the control and water injection plots. The plot-averaged relationships for E_m and S are:

$$\mathbf{E_m = 7.87 \times 10^{-4}\ \tau^{2.412}}$$

$$S = 1722\ \tau^{2.234}$$

The erosion rate constants indicate that this site is intermediate between the control and the water injection site.

DEPLOYMENT SITE	decay constant, m	S(0) (mg/L)	W_s (m/s)	SEDIMENTATION DIAMETER (mm)
OIP1	-736	1403	0.00180	0.04
OIP2	-743	1202	0.00121	0.22
OIP3	-779	1255	0.00151	0.26
OIP4	-583	1065	0.00130	0.20

Table 4.3.1.2. Calculated values of mean settling velocity (W_s) for water injection plot deployments.

The computed mean values for mass settling velocities (W_s) during the 10 minute settling period are presented in Table 4.3.1.2 and have an average for the plot of 0.00146 ± 0.00023 m/s. The plot-averaged still-water settling rate may be expressed as: $\mathbf{S(t) = -710\log_{10}(t) + 1993}$ mg/l. The mass settling velocities are on average intermediate to the control and water-injected sites although the differences are insignificant when the standard deviations are accounted for. Nevertheless, this trend makes sense as the mean erosion rates for OIP were also of an intermediate value in relation to the other sites. Mass settling velocity is highly dependent on the initial S prior to settling which is in turn dependent on erosion rate. The sedimentation diameters for this plot are the highest of the survey and may reflect the high cationic strength of the oxidant which enhances flocculation leading to larger sedimentation diameters. Plots of computed S, incremental settled mass, mass settling rates and sedimentation diameter are shown in Figures 4.3.1.13 to 4.3.1.16 for stations OIP1 to OIP4 respectively. All show a general decrease in grain size with time throughout the settling period. Notice, however, the oscillations about this trend which may reflect the passage of discrete turbid fronts.

4.3.2. Catscan bulk density

The wet bulk density profile of the OIP4 syringe core is shown in Figure 4.3.2.1. The core consists of 2 layers: (1) a surface layer of rapidly increasing density with depth to 7mm; and (2) a lower layer of constant density. The decreasing density at the base of layer 2 is likely related to disturbance. The surface bulk density is 1100 kg/m^3 rising to 1500 kg/m^3 at the base of layer 1. The density remains at 1500 kg/m^3 for the 100 mm that was sampled by the syringe core. The standard deviation of density values (± 400 kg/m^3) is diagnostic of an inhomogeneous sediment, possibly subject to intensive bioturbation by oligochaetes. Scatter around the bulk density values was again less than for the control plot, likely indicating a reduction in gas content with the

physical disturbance of the injection rake.

4.3.3. Chlorophyll analysis

The chlorophyll data in Table 4.3.3.1 once again confirms the increment in lid speed at which point the surface threshold for erosion ($\tau_c(0)$) is achieved. The initial concentrations prior to bed erosion are generally higher than for the control sites. This is indicative of greater resuspension during landing of the Sea Carousel due to the destabilization of the surface layer by the treatment.

Sample #	OIP1 CHLa (μg/L)	OIP2 CHLa (μg/L)	OIP3 CHLa (μg/L)	OIP4 CHLa (μg/L)
1	10.2	14.0	9.3	17.4
2	8.7	12.0	10.7	12.7
3	9.3	14.7	9.3	11.3
4	14.7*	10.7	10.4	12.7
5	24.0	16.0*	25.6*	18.7 ± 1.3 (n=3)*
6	35.2	32.0	31.2 ± 3.1 (n=3)	25.2
7	40.0	118.8 ± 2.3 (n=3)	36.0	29.4
8	64.1	--	44.1	48.1
9	53.4	--	74.8	64.1
10	74.8	--	160.2	128.2
11	90.8	--	133.5	165.5
12	128.2	--	--	--

Table 4.3.3.1. Chlorophyll a concentrations for control plot sites. * is the increment at which bed failure first occurred.

5. SUMMARY AND DISCUSSION

The erodibility or stability of three test plots have been evaluated in this study. The first plot (C) acted as control, a second plot (W) was used for water injection using the treatment system of Murphy *et al.* (1995), and a third plot (OIP) was fully treated for contamination remediation. The purpose of the survey was to determine (1) the effects of sediment disruption (if any) of the ploughing action of the remediation method, (2) the effects of the injected medium on bed stability., and (3) the duration of the destabilizing effects (if any).

Six surveys across the control plot provided the "natural" bed stability as well as the spatial variability in this attribute. Three methods were used to define the erosion threshold: the first is based on the development of synthetic cores, and the extrapolation of the interpreted failure envelop to the sediment/water interface; the second method plots erosion rate against bed shear stress and solves the best fit relationship to an erosion rate of 1×10^{-5} kg/m^2/s; and the third method plots suspended sediment concentration against bed shear stress and solves the best fit relationship to ambient (pre-test) concentrations. These methods yielded mean values of **0.52(±0.11), 0.24(±0.07)** and **0.31(± 0.06)** Pa. Erosion rates were best described as a power function of applied bed shear stress of the form: $\mathbf{E = 3.41 \times 10^{-4}\ \tau^{2.411}}$. Friction angles appeared to be greatest near the surface (layer 2) and least below 10 mm; this was reflected in two or three layers, each layer showing an differing rate of increase in strength with depth. The topmost layer had a mean friction angle of **14°**, the underlying layer had an angle of **23°** and the lowermost layer had an extremely low angle of **2°** (little consolidation). The mean mass settling rate was **0.0013** m/s and the equivalent mean sedimentation diameter was **0.059** mm. These results are within those expected from natural beds in estuaries (Black and Paterson, 1996).

Four surveys across the water-injected plot provided the bed response to the physical process of lakebed treatment. The erosion thresholds yielded mean values of **0.50(± 0.07), 0.19(± 0.04)**, and **0.28(± 0.07) Pa.** The results from this site are almost exactly the same as those derived from the control suggesting no effect from water injection. Erosion rates were best described as a power function of applied bed shear stress of the form: $\mathbf{E = 8.15 \times 10^{-4}\ \tau^{2.444}}$. The erosion rate of this plot is higher than the control plot indicating a much more rapid and greater degree of suspension for the same force. Friction angles showed the same structure as the control (**21°** for the near surface) and virtually zero beneath with the elimination of the rapidly strengthening layer of the control plot. Thus bed disruption due to ploughing may have taken place. The mean mass settling rate was **0.0016** m/s and the equivalent mean sedimentation diameter was **0.085** mm. Both the settling rate and the sedimentation diameter of this plot are greater than the control. This means that settling will be more rapid at this site, but only in proportion to the suspended sediment concentration.

Four surveys across the oxidant-injected plot yielded bed response to the physical and chemical process of lakebed treatment. The erosion thresholds yielded mean values of **0.40(± 0.07), 0.19(± 0.04)**, and **0.28(± 0.07) Pa**. This site appeared to have a slightly lower threshold for erosion than the control. Erosion rates were best described as a power function of applied bed shear stress of the form: $\mathbf{E = 7.87 \times 10^{-4}\ \tau^{2.412}}$. The erosion rate is considerably higher than the control plot, but lower than the water-injection site. Friction angles showed less structure than at the control and lower overall values (**12°** for the near surface). The inference of this is that the bed structure has been disrupted by the ploughing and settlement of the bed (at least in the topmost mm) is less advanced than at the water-injected and control plots. The mean mass settling rate was **0.0014** m/s and the equivalent mean sedimentation diameter was **0.18** mm. The settling rate was about the same as the control, whereas the sedimentation diameter was the highest of the survey.

Trends with time are difficult to establish due to the limited period of the study. Nevertheless,

there appears to be evidence for bed strengthening throughout the study at all three plots. The strengthening at the control plot may relate to seasonal changes resulting from biostabilization. The trends at the two treated plots appear to be more rapid and may reflect a return to a natural state. Unfortunately, we were unable to establish the time required by the bed to reach the natural state.

6. CONCLUSIONS AND RECOMMENDATIONS

A two week study of the stability of the lakebed of Hamilton harbour was undertaken during August, 1995. The aim of the study was to determine the effects of treatment of contaminated material of the lakebed through ploughing and oxidant injection. Three plots of the lakebed were set aside. The first was the control, the second was used for water injection and ploughing, and the third was ploughed and injected with oxidant (full treatment). Fourteen deployments of the Sea Carousel were completed: 6 at the control site; 4 at the water-injection site; and 4 at the oxidant-injection site. Water samples were collected from the Carousel during each deployment by pumping. The samples were analysed for: suspended sediment concentration; chlorophyll; organic carbon content; grain size; microscopic observations; and suspended sediment settling and density determination. As well, three syringe cores (2 cm diameter) and one push core (10 cm diameter) were collected at each site for measurements of physical properties. Finally, a bulk sample of the lakebed surface was collected for disaggregated grain size distribution. Excellent results were obtained from the study and several well defined effects of lakebed treatment were found. The following are the major conclusions of the study.

- the effect of treatment had an affect on the stability of lakebed sediments. The effect was to physically disrupt the structure and fabric of the bed leading to erosion rates twice as high as natural beds;

- the erosion thresholds of the water-injected sites were the same as for the controls. Physical disruption of the bed by the injection process seems to be irrelevant to this bed parameter;

- the erosion thresholds of the oxidant-injected sites were slightly lower than the other two plots. The inference of this is that oxidant treatment may reduce bed strength in the topmost few mm;

- the erosion rates of the water-injected sites were the highest recorded. The oxidant-injected site was slightly lower, and the natural sites were the lowest. The inference of this is that the oxidant contributed to stabilizing the bed (compared to water-injection) with respect to erosion rate;

- the mass settling rates were direct and linear functions of suspended sediment concentration. That is, the higher the concentration (such as at the treated sites) the greater the settling rates. No differences in trends were detected between plots. That is, the oxidant has no effect on settling rate;

- the highest sedimentation diameter occurred for the oxidant-injection site. This may reflect the high cationic strength of the oxidant enhancing flocculation and thus sedimentation diameter.

- there appeared to be an increase in bed strength with time throughout the survey period. This was observed at the control sites, and is attributed to the effects of biostabilization due to the high water temperature (25° C). The increase in bed strength with time at the treated sites was also observed and though more erratic appeared to take place at a greater rate than on the natural sites. The inference of this is that bed recovery from treatment is rapid. Unfortunately, we were unable to define the length of time required for full bed recovery due to the limited time-period of the survey.

The time scales for recovery would be expected to vary depending on the response of interest. For example, on the scale of minutes the sediments should dewater and vent gas. On the scale of hours, diatoms and bacteria would recolonise the bed creating a distinct biofilm, and oligochaetes would become re-established. On the scale of days, grazing would occur, worm tubes would develop and bed irrigation would take place. Finally, on the order of weeks, a new biofilm would form stimulated by the injection of nutrients that would lead to the beds ultimate stable state.

This report has reached some interesting conclusions regarding the effects of lakebed treatment on stability and erodibility. These conclusions are worthy of publication in the scientific literature, and attempts will be made to do so in the near future. A shortfall of the work is the short duration of the study. We were thus unable to determine the time over which bed recovery took place. The size and settling rates of resuspended material shows some marked differences between methods. Insofar as the size influences settling rate (and hence stability) a closer examination of these results is warranted. Sampling is likely to break down the larger aggregates in suspension (T. Milligan, personal communication, 1996), and so a better method of size analysis is needed (possibly strobe-light photography). The effect of treatment on bed roughness was noted. A new survey of the region using either sidescan or swath bathymetry may prove useful in defining the physical effects of ploughing. We attempted to take bottom photographs from a height of 1.5 m above the lake bed and observed nothing due to high organic content of the water. Photographs of the bed from perhaps 0.5 m would be valuable in describing the nature of the physical disturbance as well as the variety of benthic organisms. We observed bedload transport to take place during erosion. From a scientific standpoint, this is an important observation as it describes a mode of transport hitherto considered absent from cohesive beds. Insofar as pollutants may be transported this way, it is a mode of transport that should be studied further. No monitoring of S was made *during* the process of treatment. This might help determine the impact of treatment while treatment is taking place. What we have reported in this studies are the effects only *after* the treatment process has taken place.

7.0 ITINERARY

DATE/TIME(GMT)	OPERATION
9 Aug., 1995	Ship container to NWRI
12 Aug.	C. Amos & R. Murphy travel to Hamilton
13 Aug.	Initial meeting at NWRI with I. Droppo
14 Aug.	Mobilizing Sea Carousel
15 Aug.	Mobilizing electronics on Petrel
16 Aug.	Collection of box core samples from C1 - C4
17 Aug.	Sea Carousel station C2
18 Aug.	Sea Carousel stations C1, C3 and C4
21 Aug.	Preparation of injection sites (water and treatment)
	Sea Carousel deployment OIP1 and W1
22 Aug.	Sea Carousel deployments OIP2, W2, and C5
23 Aug.	Sea Carousel deployments OIP3, W3, and C6
24 Aug.	Bottom camera deployments at all stations
25 Aug.	Demobilization of equipment
26 Aug.	Terminate field program

8. REFERENCES

Amos, C.L., Grant, J., Daborn, G., and Black, K. 1992a. Sea Carousel - a benthic annular flume. Estuarine, Coastal and Shelf Sciences 34: 557-577.

Amos, C.L., Daborn, G.R., Christian, H.A., Atkinson, and Robertson, A. 1992b. In situ erosion measurements on fine-grained sediments from the Bay of Fundy. Marine Geology 108: 175-196

Amos, C.L.,Li, M.Z. and Gomez, A.E. 1995. The contribution of ballistic momentum flux to the erosion of cohesive beds by flowing water. American Geophysical Union, Fall Meeting, San Francisco.

Amos, C.L., Sutherland, T.F., Radzijewski, B. and Doucette, M. (in press). A rapid technique to determine bulk density of fine-grained sediments by x-ray computed tomography. Journal of Sedimentary Research.

Black, K. And Paterson, D. 1996. LISP - Littoral Investigation of Sediment Properties. Preliminary Results. Publ. Gatty Marine Labs., St. Andrews: 176p.

Downing, J.P. 1983. An optical instrument for monitoring suspended particulates in ocean and laboratory. Proceedings of Oceans'83: 199-202.

Droppo, I.G. and Ongley, E.D., 1992. The state of suspended sediment in the freshwater fluvial environment: a method of analysis. Water Research 26(1): 65-72.

Droppo, I.G. and Ongley, E.D. 1994. Flocculation of Suspended Sediment in Rivers of Southeastern Canada. Water Research, 28(8): 1799-1809.

Environment Canada. 1979. Analytical Methods Manual; Inland Waters Directorate, Water Quality Branch; Burlington, ON., Canada.

Fung, A. 1995. Accurate calibration measurements of flow in Lab Carousel under varying lid rotations. Unpublished Contract Report 23420-5-M083 to Geological Survey of Canada.

Gibbs, R.J., Matthews, M.D. and Link, D.A. 1971. The relationship between sphere size and settling velocity. Journal of Sedimentary Petrology 41: 7-18.

Hawley, N. 1982. Settling velocity distribution of natural aggregates. Journal of Geophysical Research. **87**(C12): 9489-9498.

Kranck, K., Petticrew, E., Milligan, T.G. and Droppo, I.G. 1992. *In situ* particle size distributions resulting from flocculation of suspended sediment. In: Nearshore and Estuarine Cohesive Sediment Transport, (Ed) A.J. Mehta. Coastal and Estuarine Studies Series (AGU), Vol. 42, Washington, DC.

Krishnappan, B.G., Droppo, I.G., Rao, S.S. and Ongley, E.D. 1990. Evaluation of a filter-fractionation technique for fine sediment; NWRI Contribution 90-11; Canada Centre for Inland Waters, Burlington, ON, Canada.

Krone, R.B. 1962. Flume studies of the transport of sediment in esturial shoaling processes. Final Report Hydraulic Engineering Laboratory and Sanitary Engineering Research Laboratory, University of California, Berkeley.

Li, D.H. and Ganczarczyk, J.J. 1987. Stroboscopic determination of settling velocity, size and porosity of activated sludge flocs. Water Research 21(3):257-262.

Liss, S.N., Droppo, I.G., Flannigan, D., Leppard, G.G. 1996. Floc architecture in wastewater and natural riverine systems. Environmental Science and Technology. 30(2): 680-686.

Mehta, A.J. and Partheniades, E. 1982. Resuspension of deposited cohesive sediment beds. Eighteenth Conference Coastal Engineering: 1569-1588.
Migniot, C. 1980. Dynamique sedimentaire estuarienne - materiaux cohesifs et non cohesifs. Oceanis 6: 359-432.
Murphy, T., Moller, A. and Brouwer, H. 1995. *In situ* treatment of Hamilton Harbour sediment. Journal of Aquatic Ecosystem Health, 4: 195-203.
Murphy, T. 1995. Personal Communication, Environment Canada, National Water Research Institute, Burlington, Ontario, Canada.
Orsi, T. 1994. Computed tomography of macrostructure and physical property variability of seafloor sediments. Unpublished Ph.D. thesis, Texas A & M University: 181p.
Parsons, T.R., Maita, Y., and Lalli, C.M. 1984. A Manual of Chemical and Biological Methods for Seawater Analysis. Publ. Pergamon Press, Oxford: 107-110.
Reynoldson, T. 1995. Personal Communication, Environment Canada, National Water Research Institute, Burlington, Ontario, Canada.
Sutherland, T.F. 1996. Biostabilization of estuarine subtidal sediments. Unpublished Ph.D. thesis. Dalhousie University, Halifax: 179p.
Terzaghi, K. and Peck, R.B. 1967. Soil Mechanics in Engineering Practice. Publ. John Wiley & Sons, New York: 729p.
Torfs, H. 1995. Erosion of mud/sand mixtures. Unpublished Ph.D. thesis, Katholieke Universiteit Leuven: 223p.
Villaret, C. And Paulic, M. 1986. Experiments on the erosion of deposited and placed cohesive sediments in an annular flume. Report to Coastal and Oceanographic Engineering Department, University of Florida, Gainesville

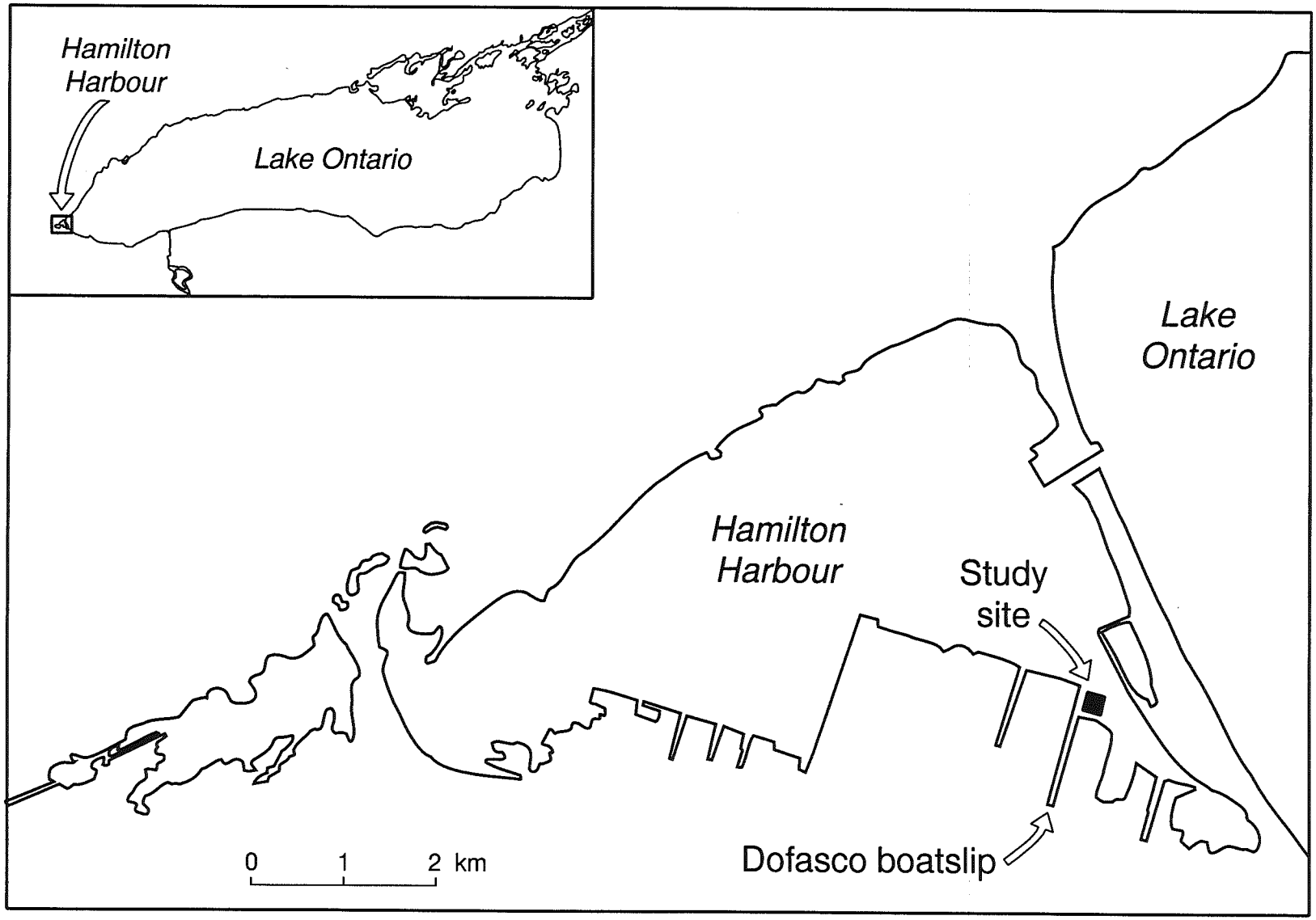

Figure 1.2.1 Hamilton Harbour and study site location

Figure 3.1.1. Bathymetry of the field site. The shaded area represents the approximate 50 m^2 plot which was divided into the three sub-plots (C, W, and OIP). The contour interval is 5 m.

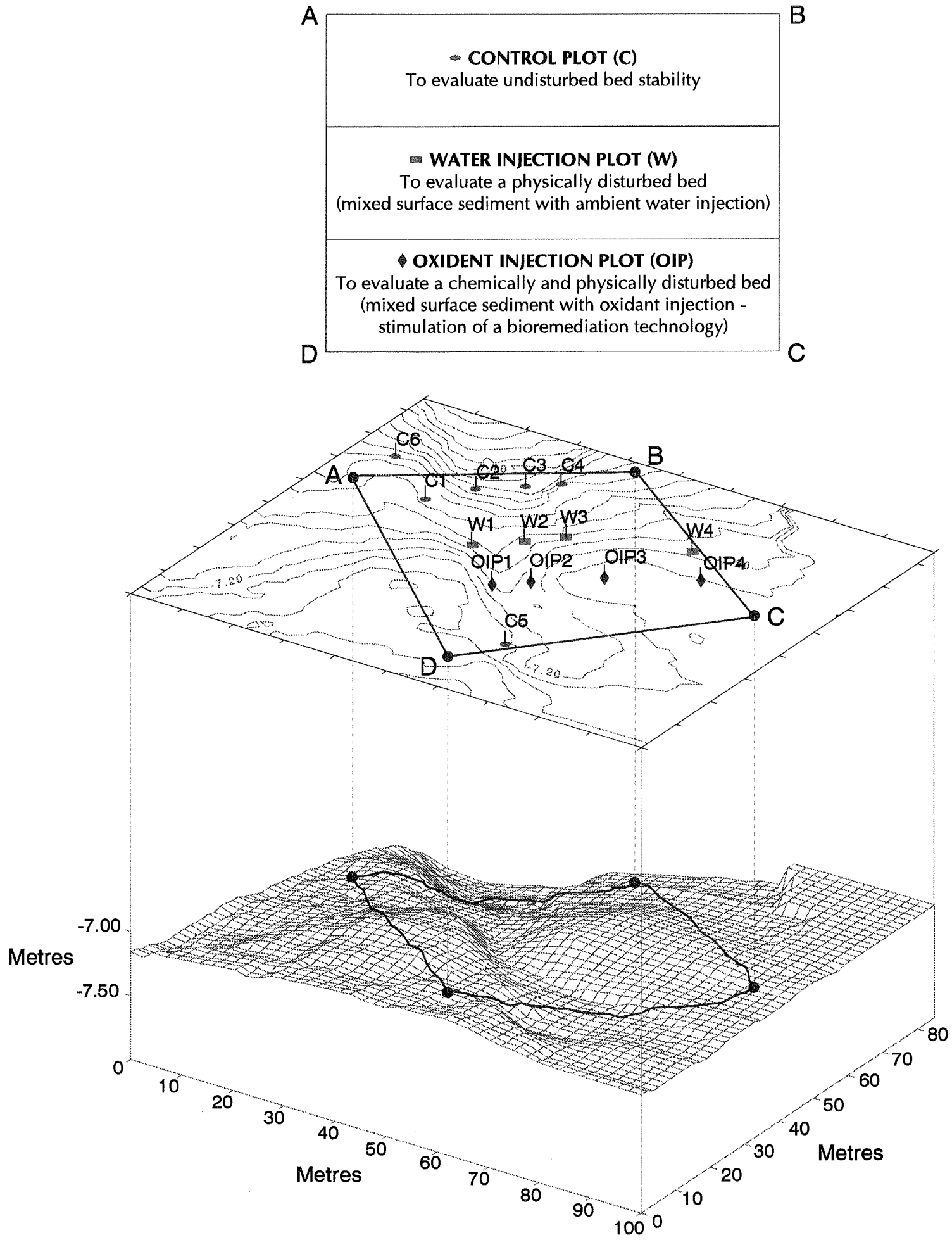
A
B
CONTROL PLOT (C)
To evaluate undisturbed bed stability
WATER INJECTION PLOT (W)
To evaluate a physically disturbed bed
(mixed surface sediment with ambient water injection)
OXIDENT INJECTION PLOT (OIP)
To evaluate a chemically and physically disturbed bed
(mixed surface sediment with oxidant injection -
stimulation of a bioremediation technology)
D
C
C6
C1
C2
C3
C4
W1
W2
W3
W4
OIP1
OIP2
OIP3
OIP4
C5
7.20
-7.00
Metres
-7.50
0
10
20
30
40
50
60
70
80
90
100
Metres
0
10
20
30
40
50
60
70
80
Metres

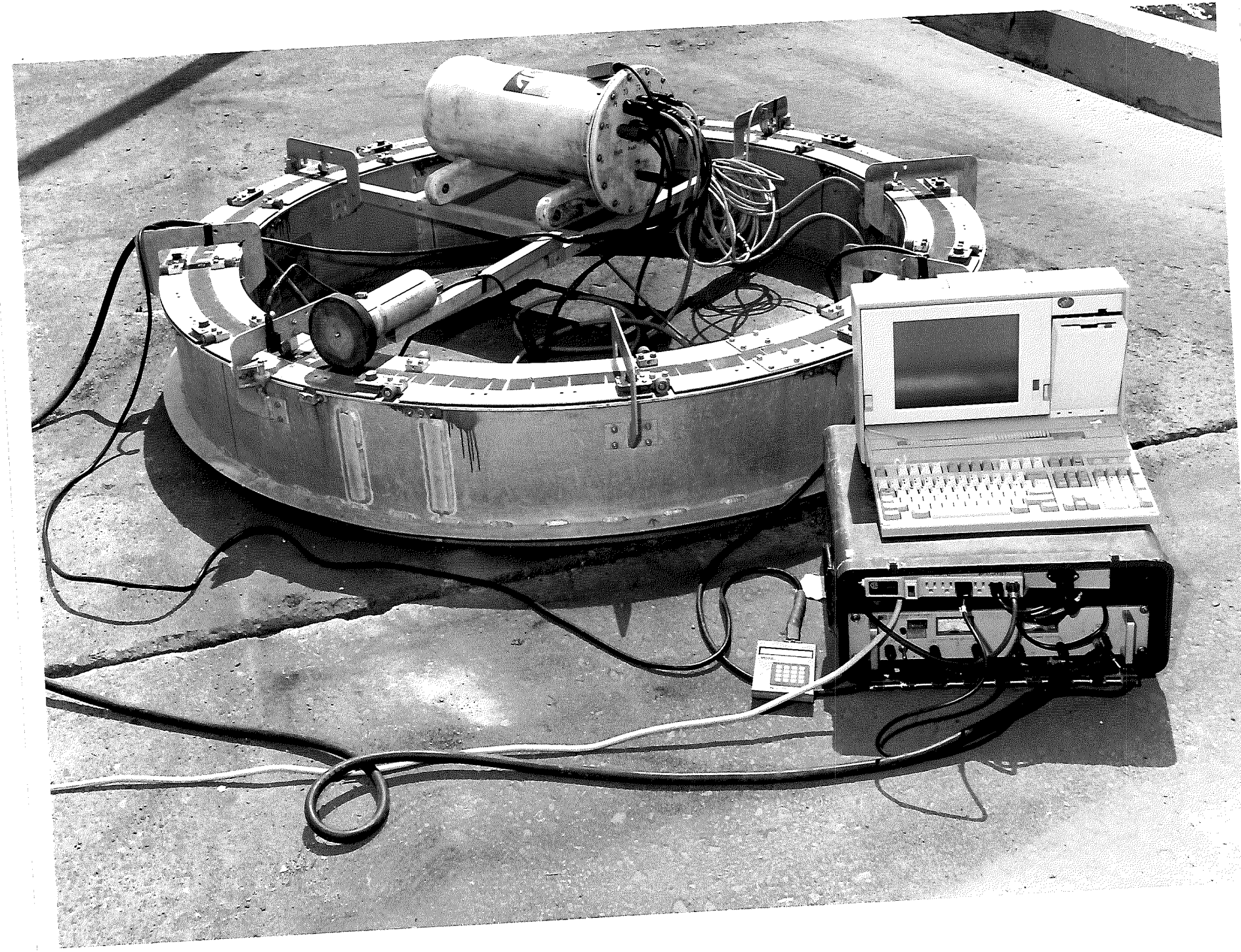

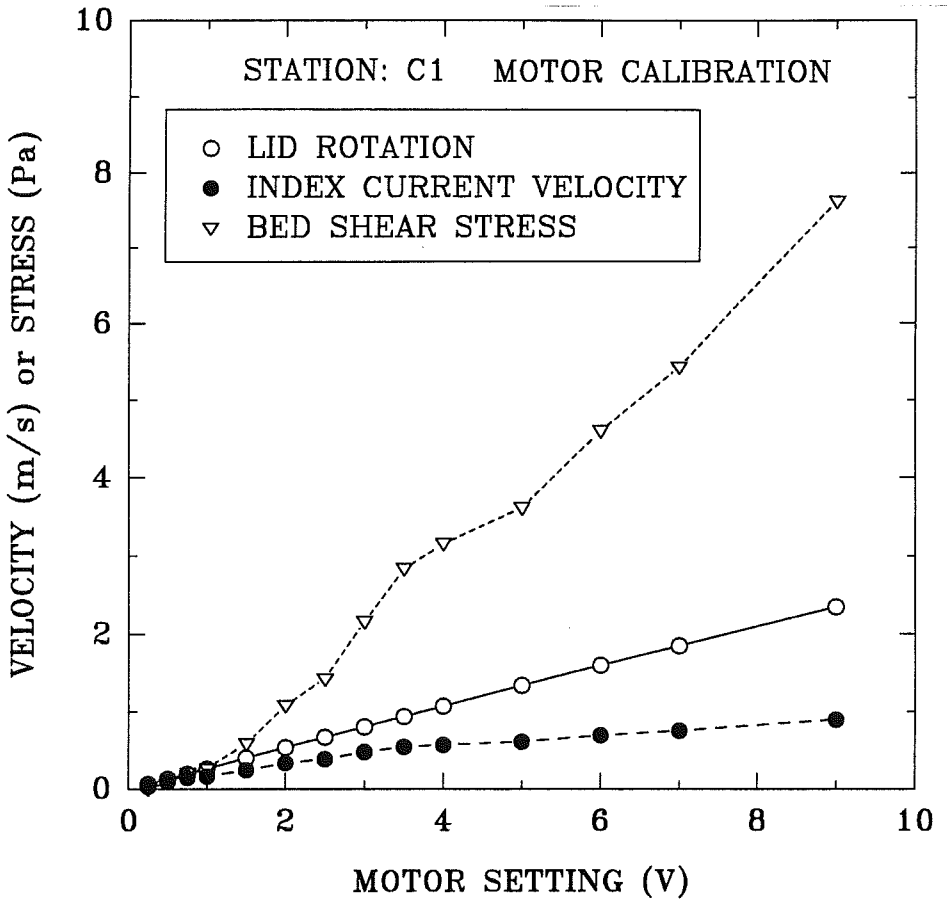

Figure 3.2.2 The relationship between motor settling and resulting lid rotational speed (m/s), index current speed (m/s), and bed shear stress (Pa).

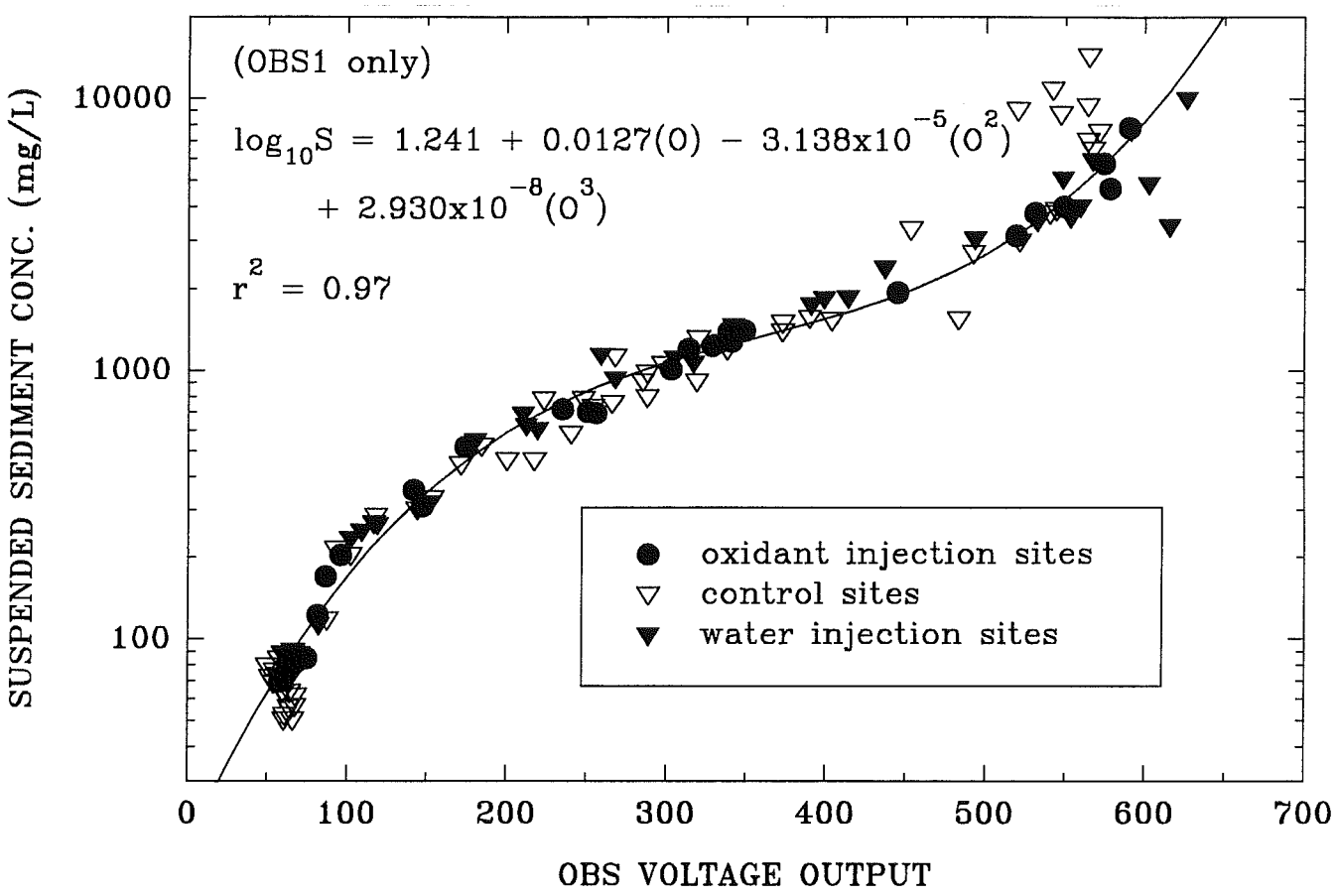

Figure 4.1 The calibration of the optical backscatter sensors used on Sea Carousel to suspended sediment, S. The optical response to S follows a complex third-order function. There is no appreciable differences between the three plots of this study.

a

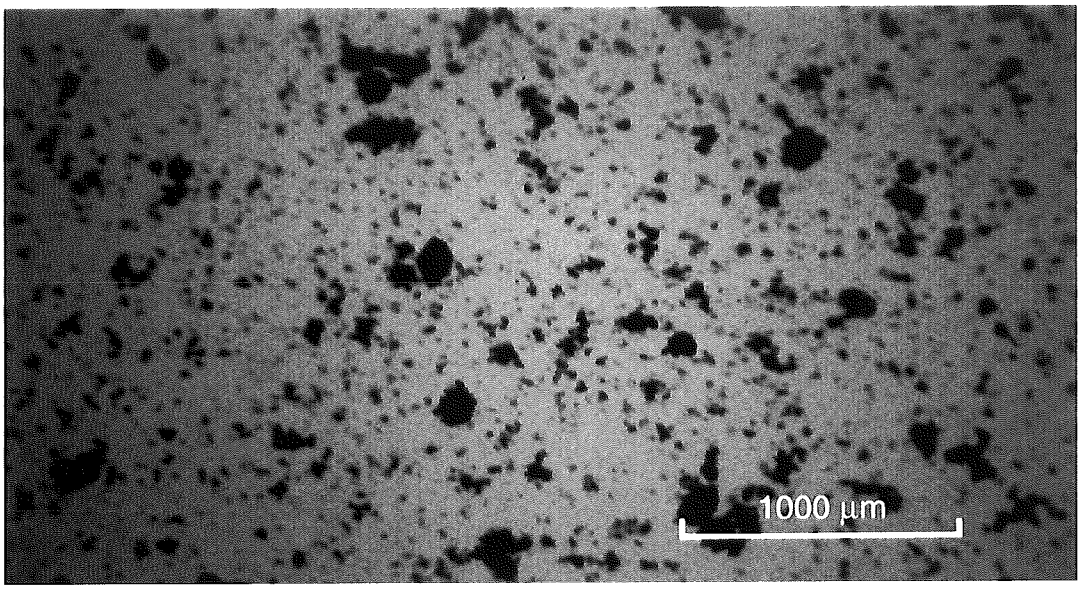

b

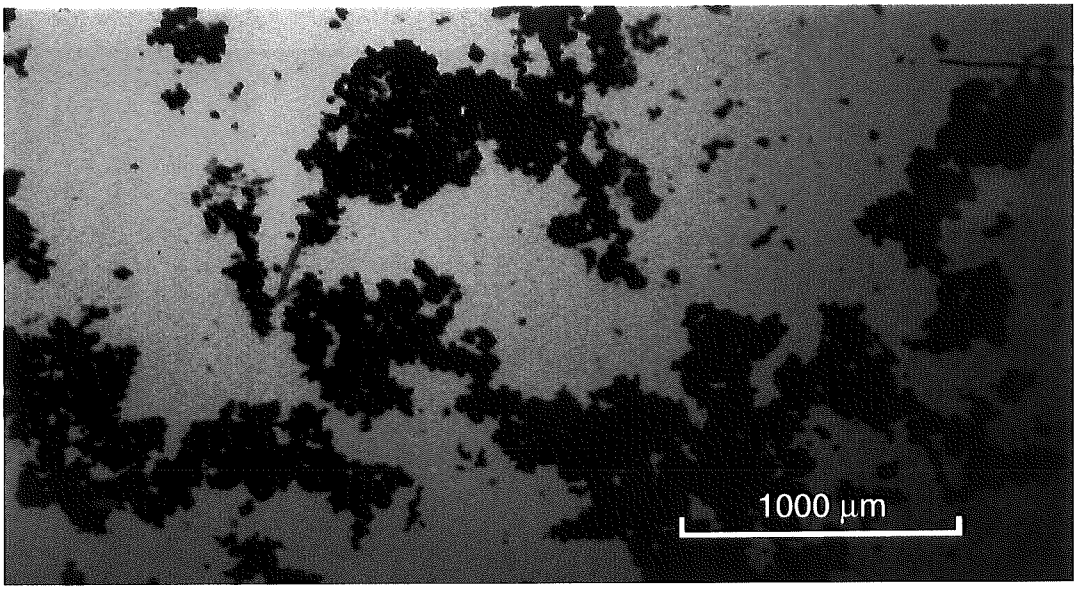

c

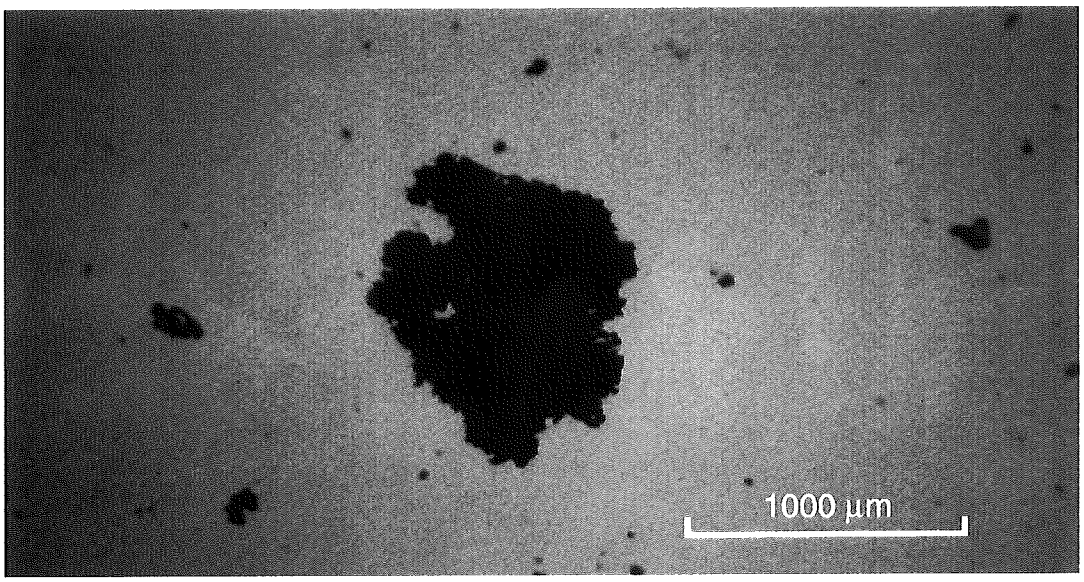

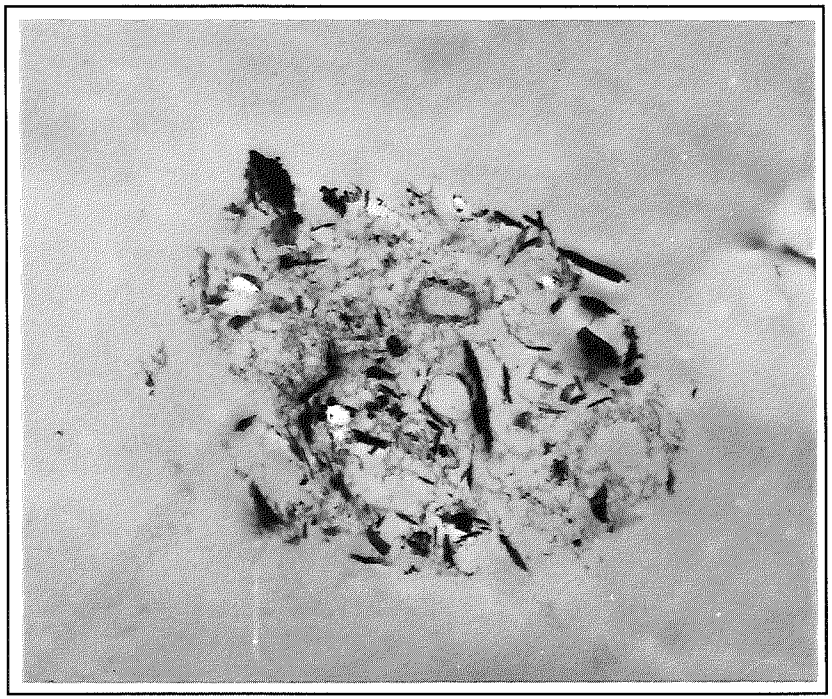
a
0
2 µm


b
0
2 µm

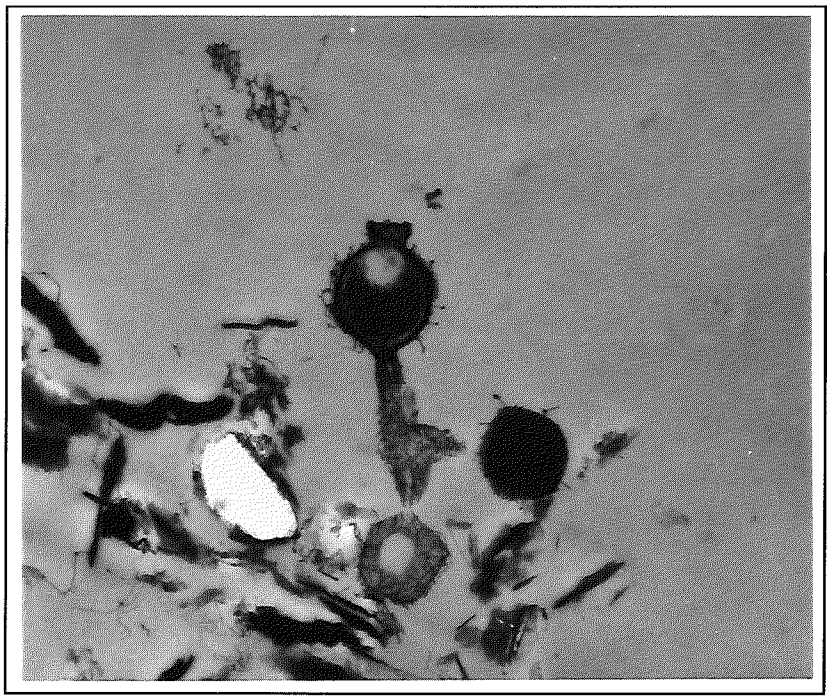
c
0
1 µm

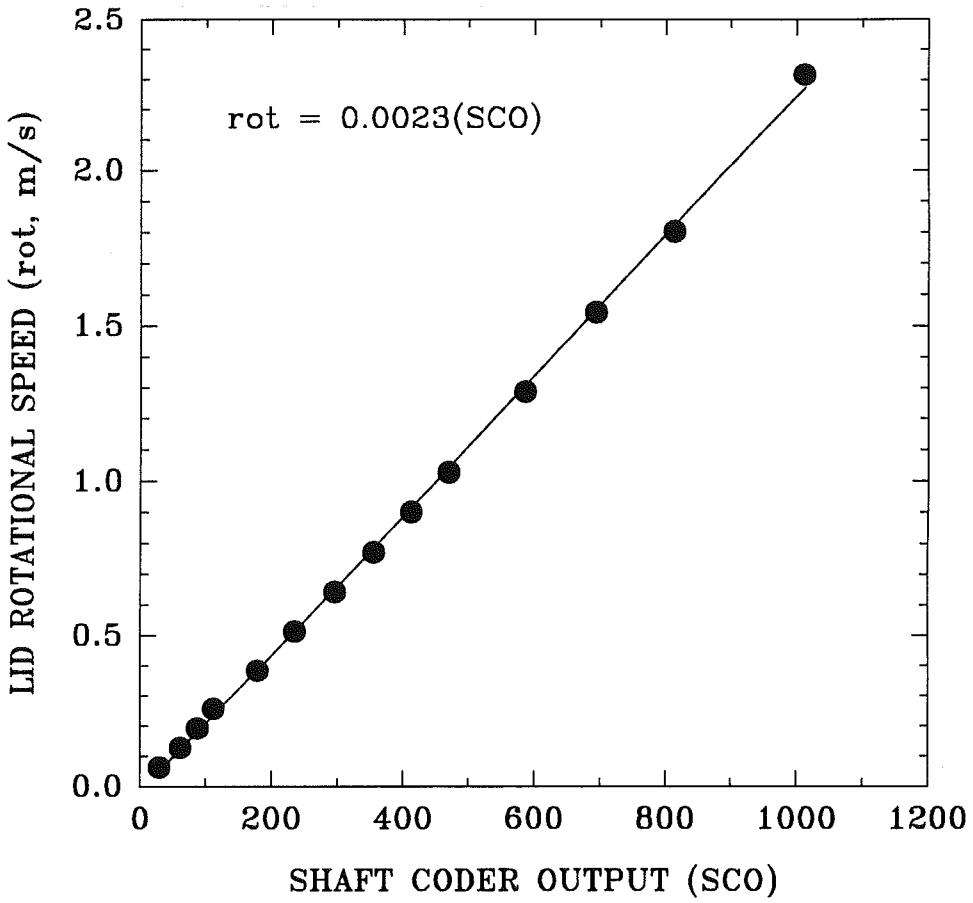

Figure 4.2 The relationship between shaft end-coder output (on Sea Carousel) and the observed lid rotation. An almost perfect linear relationship is apparent.

Figure 4.3 An example of the ratio of the azimuthal index velocity from Sea Carousel (U_y) and lid rotation (rot) for the time-series measured at control site C1. The mean calibration used to transform rot to U_y (0.574) is indicated. Notice that the actual ratio is not constant but decreases as S increases. We interpret this to be due to changes in eddy viscosity due to turbidity. The solution to this problem is beyond the scope of this study.

Hamilton harbour (Dofasco slip)
Station C1

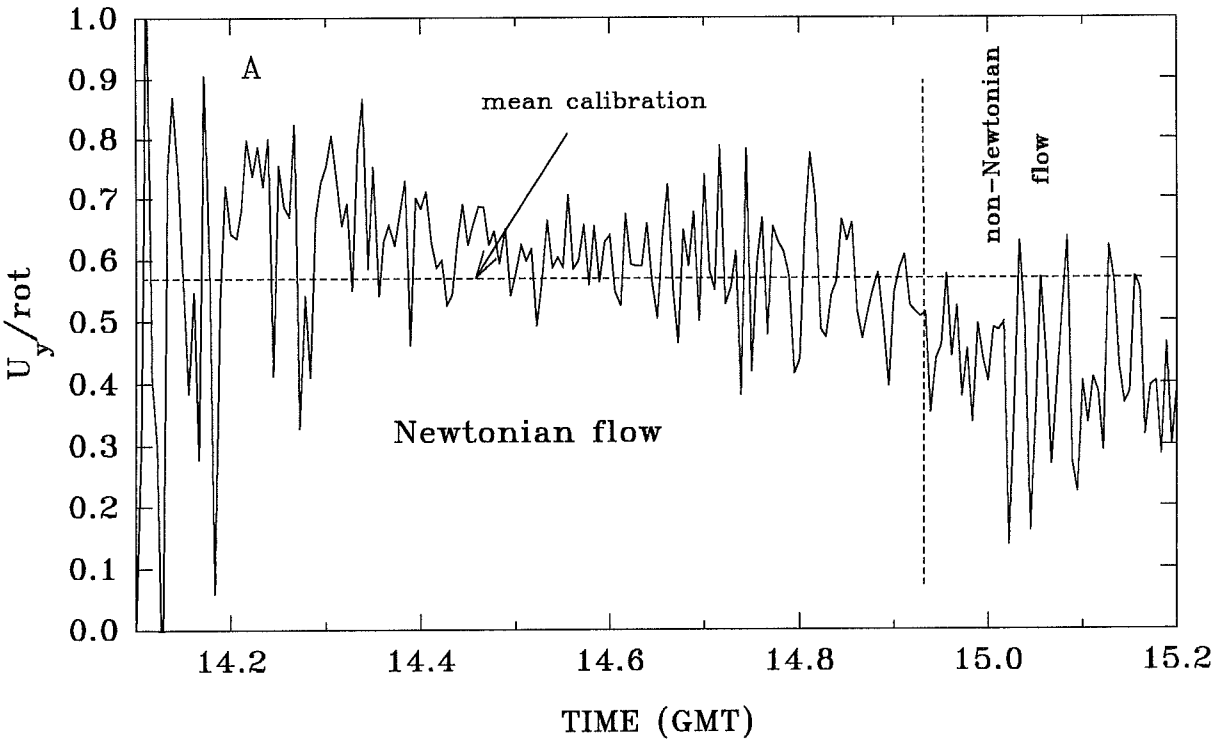

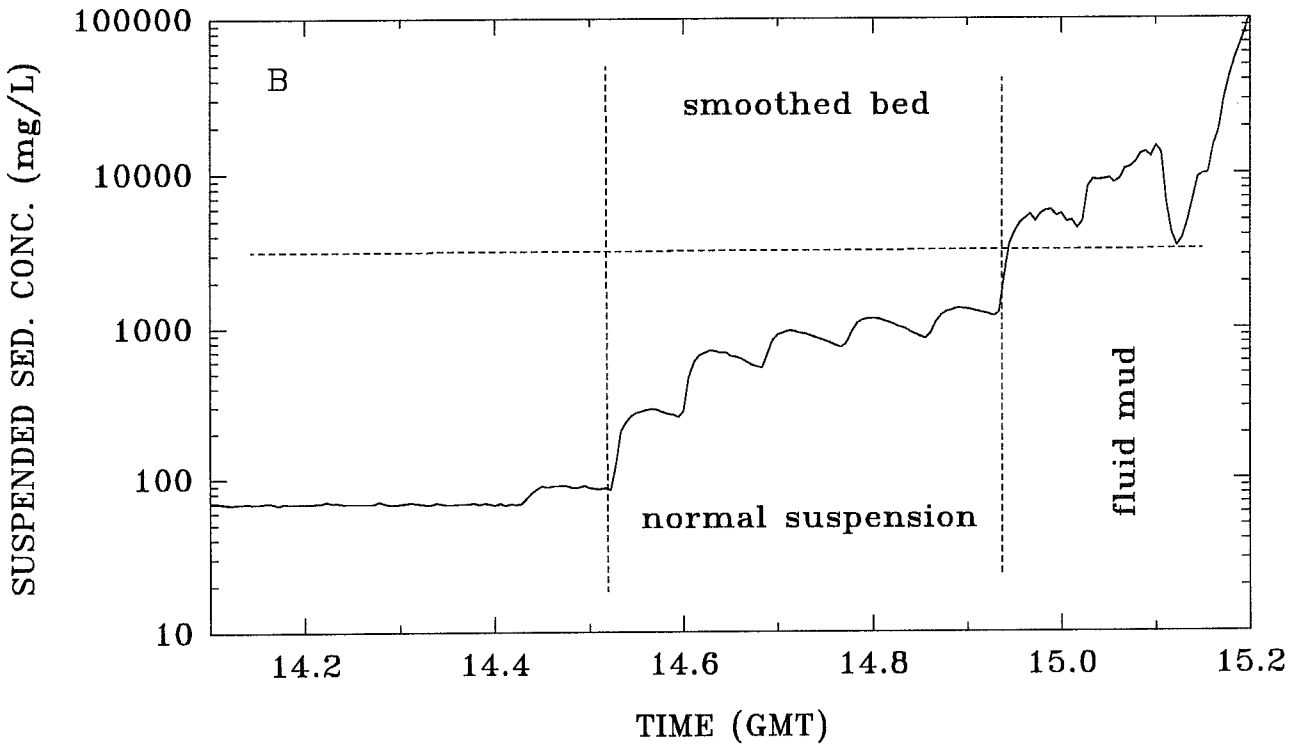

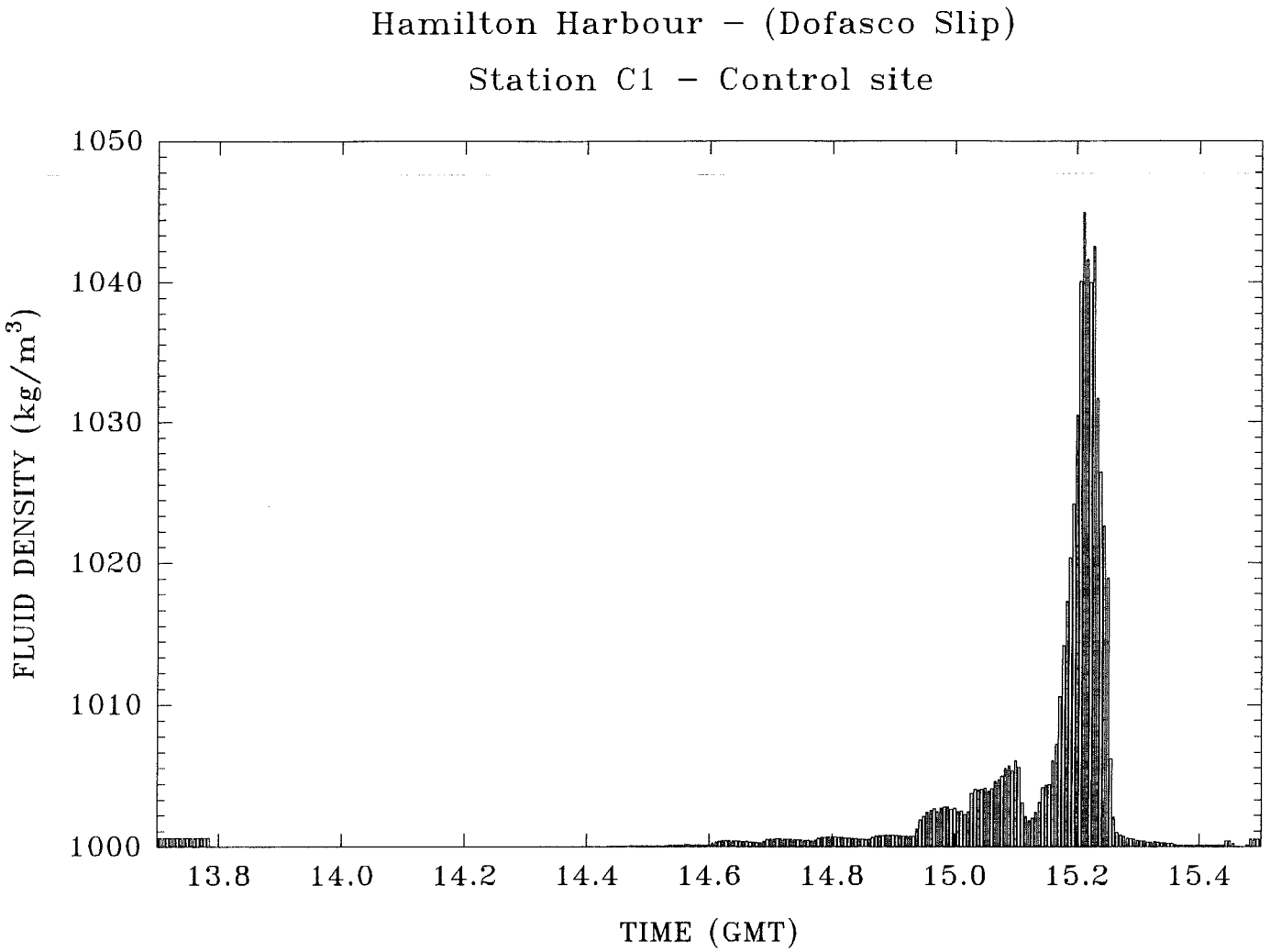

Figure 4.4. An example of the fluid density determined for the time-series collected at control site C1. Notice that during maximum applied flows, there is a significant increase in density in response to increasing S. This change will no doubt influence erosion and settling.

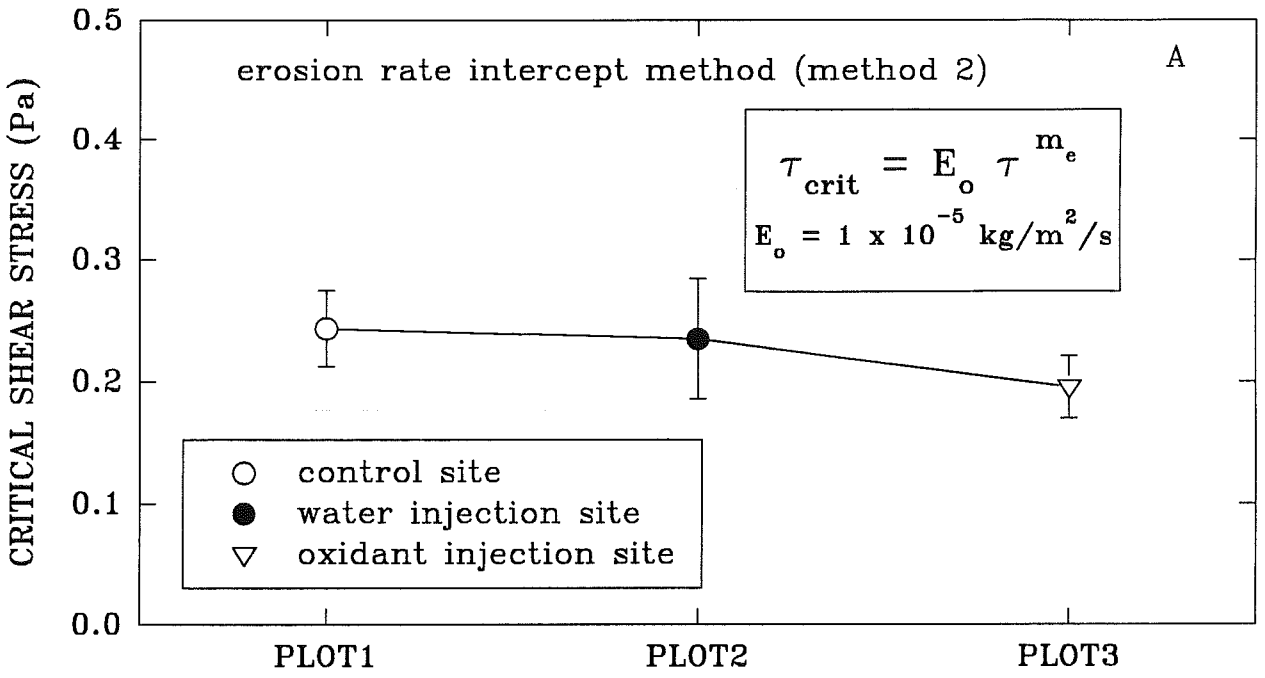

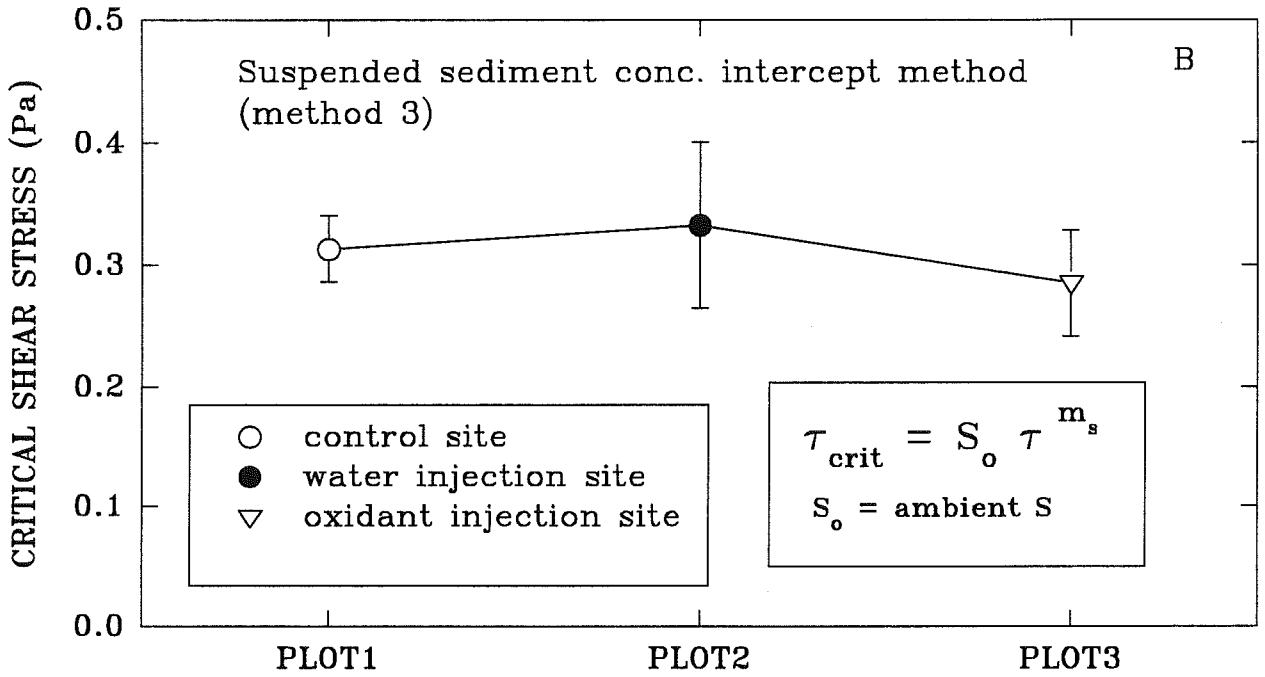

Figure 4.5 The mean erosion thresholds for the three plots of this study derived by method 2 (A) and method 3 (B). Notice that there is a slight reduction in strength in the water- and oxidant-injected plots compared to the control, but no obvious differences exist between the two treated plots.

Figure 4.6 The mean erosion thresholds for the three plots of this study plotted against time, and derived by method 2 (A) and method 3 (B). Notice that there appears to be a strengthening through the survey period at all three plots. The strengthening of the treated plots appears faster than at the control suggesting a greater recovery rate.

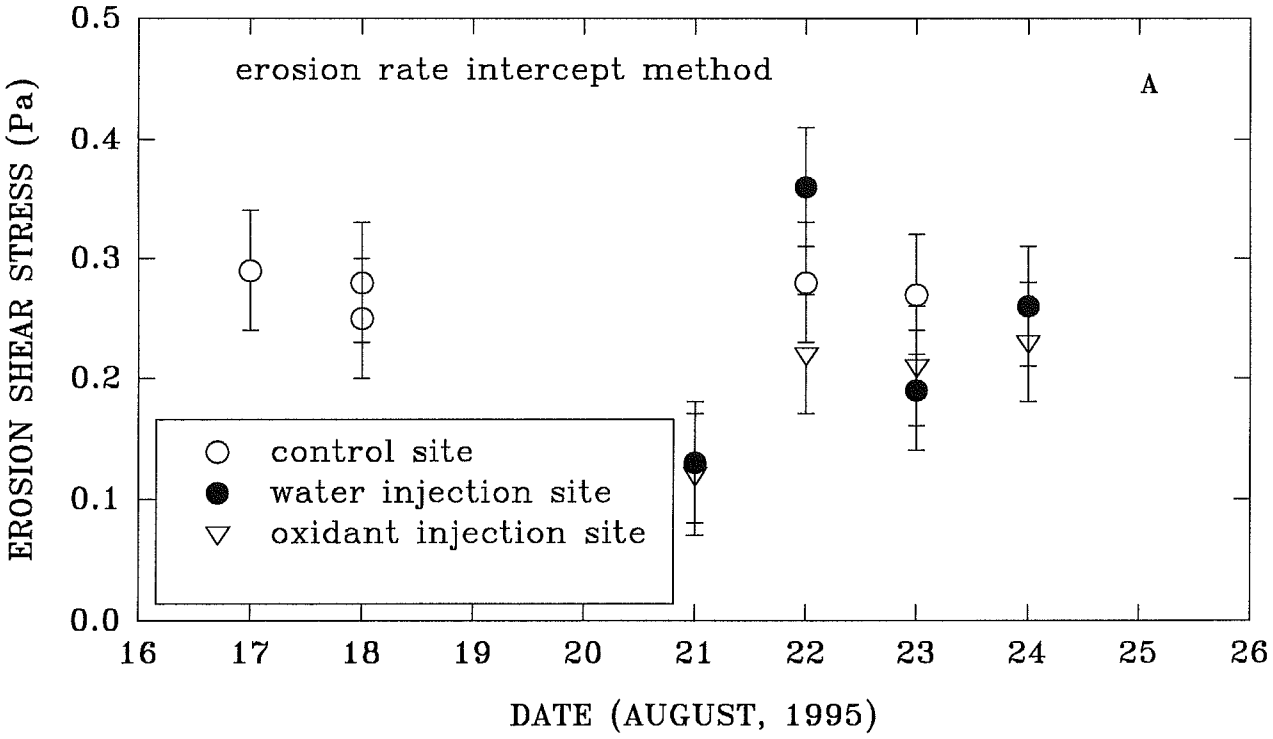
erosion rate intercept method
A
EROSION SHEAR STRESS (Pa)
0.0
0.1
0.2
0.3
0.4
0.5
16
17
18
19
20
21
22
23
24
25
26
DATE (AUGUST, 1995)
control site
water injection site
oxidant injection site

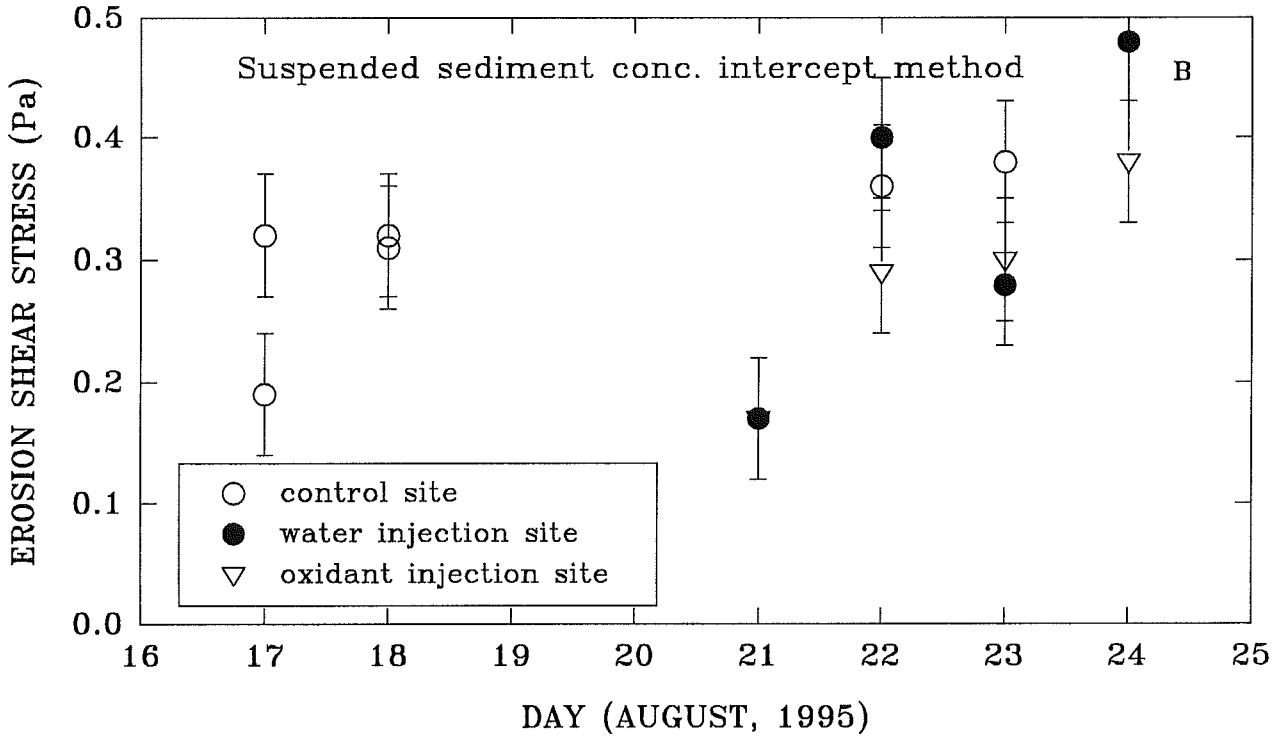
Suspended sediment conc. intercept method
B
EROSION SHEAR STRESS (Pa)
0.0
0.1
0.2
0.3
0.4
0.5
16
17
18
19
20
21
22
23
24
25
DAY (AUGUST, 1995)
control site
water injection site
oxidant injection site

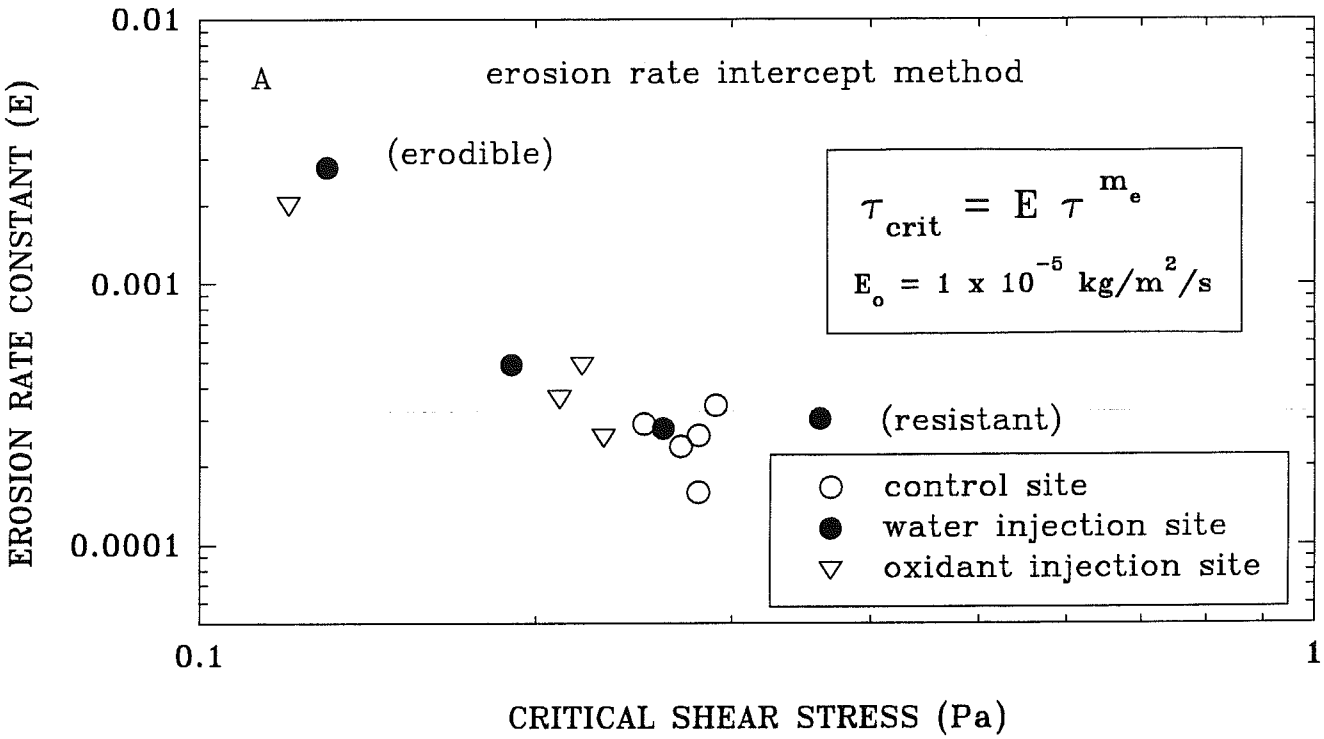

Figure 4.7 The erosion rate constant (E) and suspension rate constant (S) plotted against mean erosion threshold for the three plots using methods 2 (A) and 3 (B). Notice that the control plots generally fall into the "resistant" portion of the diagram in both cases, whereas the early treated plots fall into the erodible portions.

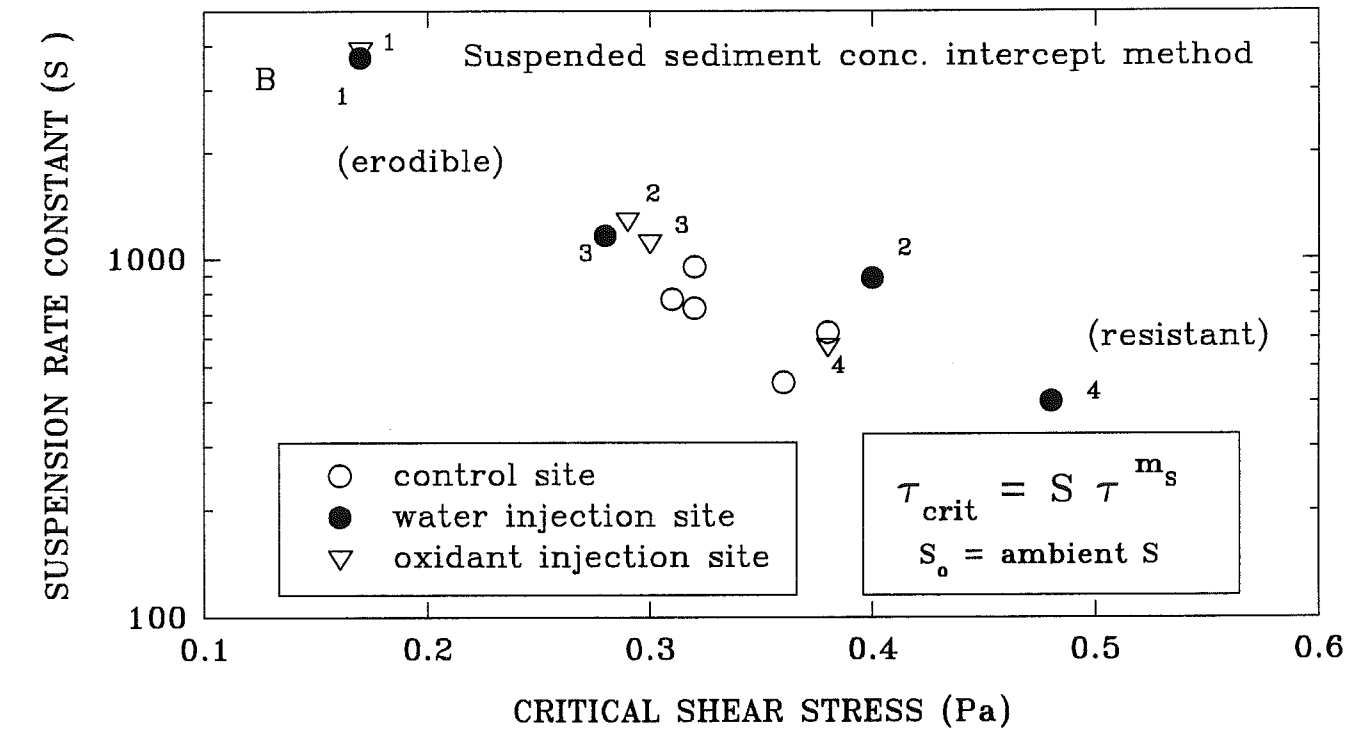

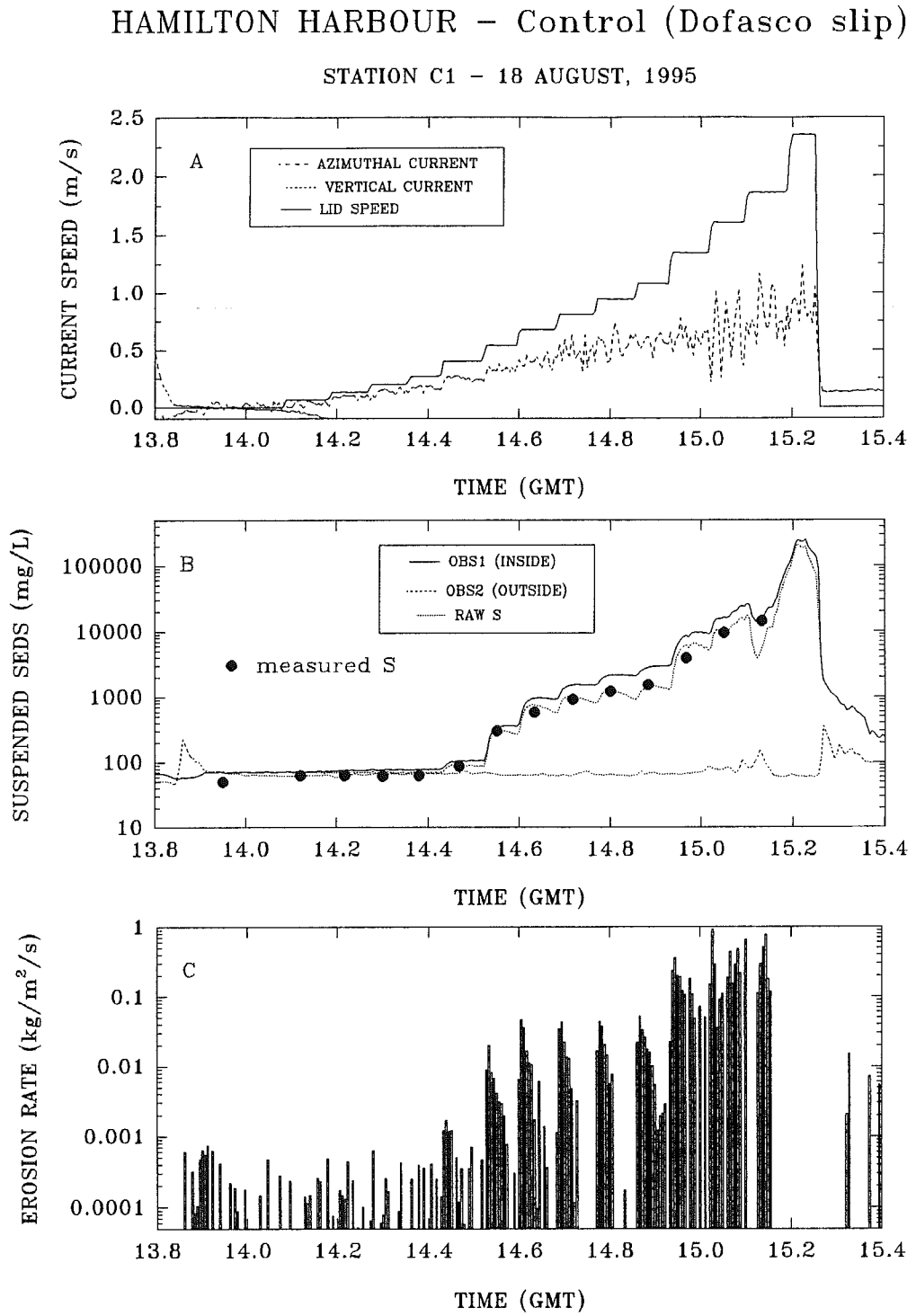

Figure 4.1.1.1 Time-series plots of the Sea Carousel deployment at control site C1: (A) lid rotation, azimuthal current speed, and vertical current speed; (B) ambient S, raw S and S corrected for dispersion; and (C) the erosion rate. The dots in panel B denote measured S determined from samples pumped during the experiment. Notice the prevalence of type I erosion at early stages of erosion and type II erosion during periods of highest applied flow. The latter stages of the time-series were devoted to still-water settling, hence the apparent discontinuity of results when lid rotation returns to zero.

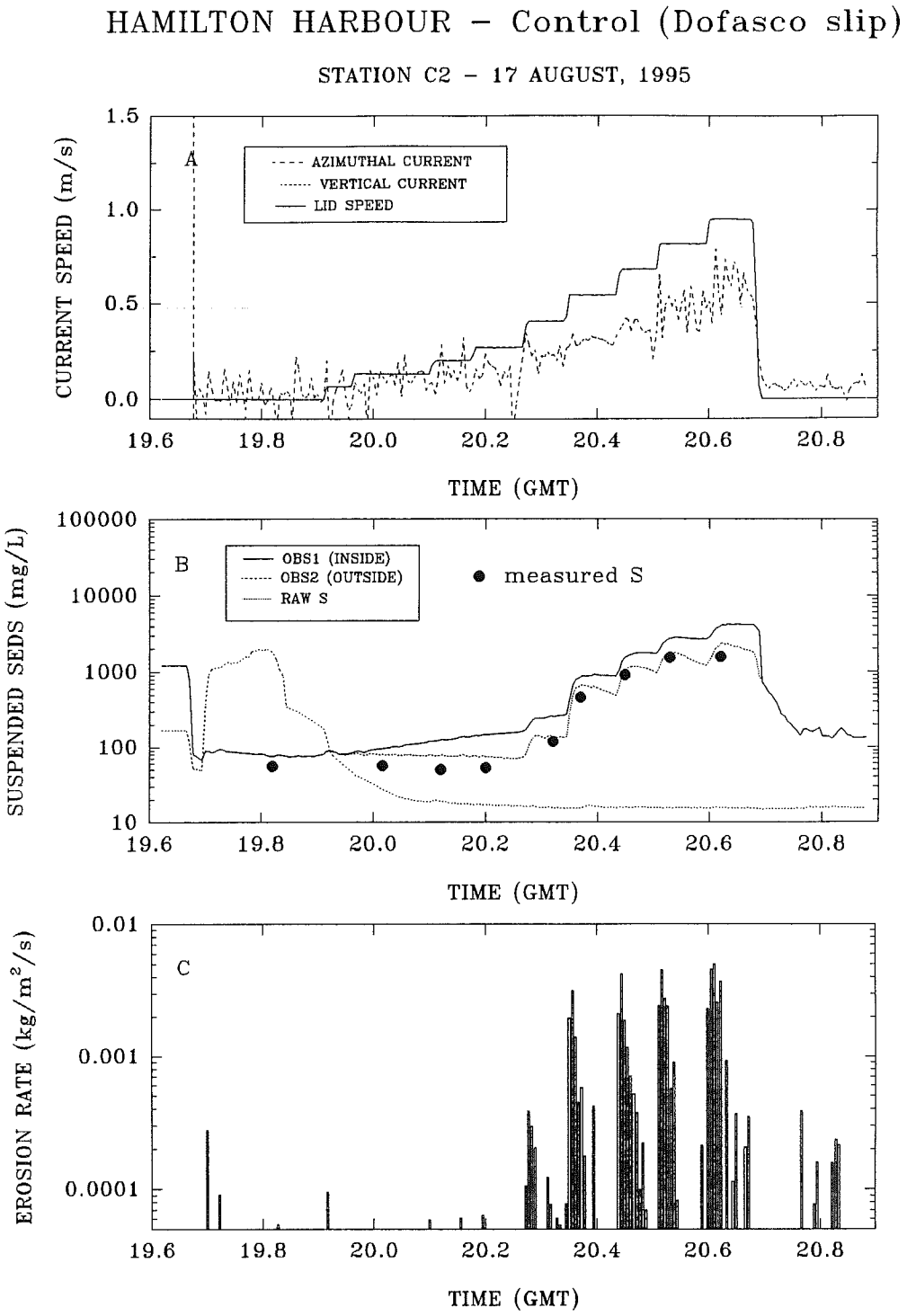

Figure 4.1.1.2 Time-series plots of the Sea Carousel deployment at control site C2. Notice the prevalence of type I erosion at early stages of erosion and the steady decay in ambient S throughout the experiment.

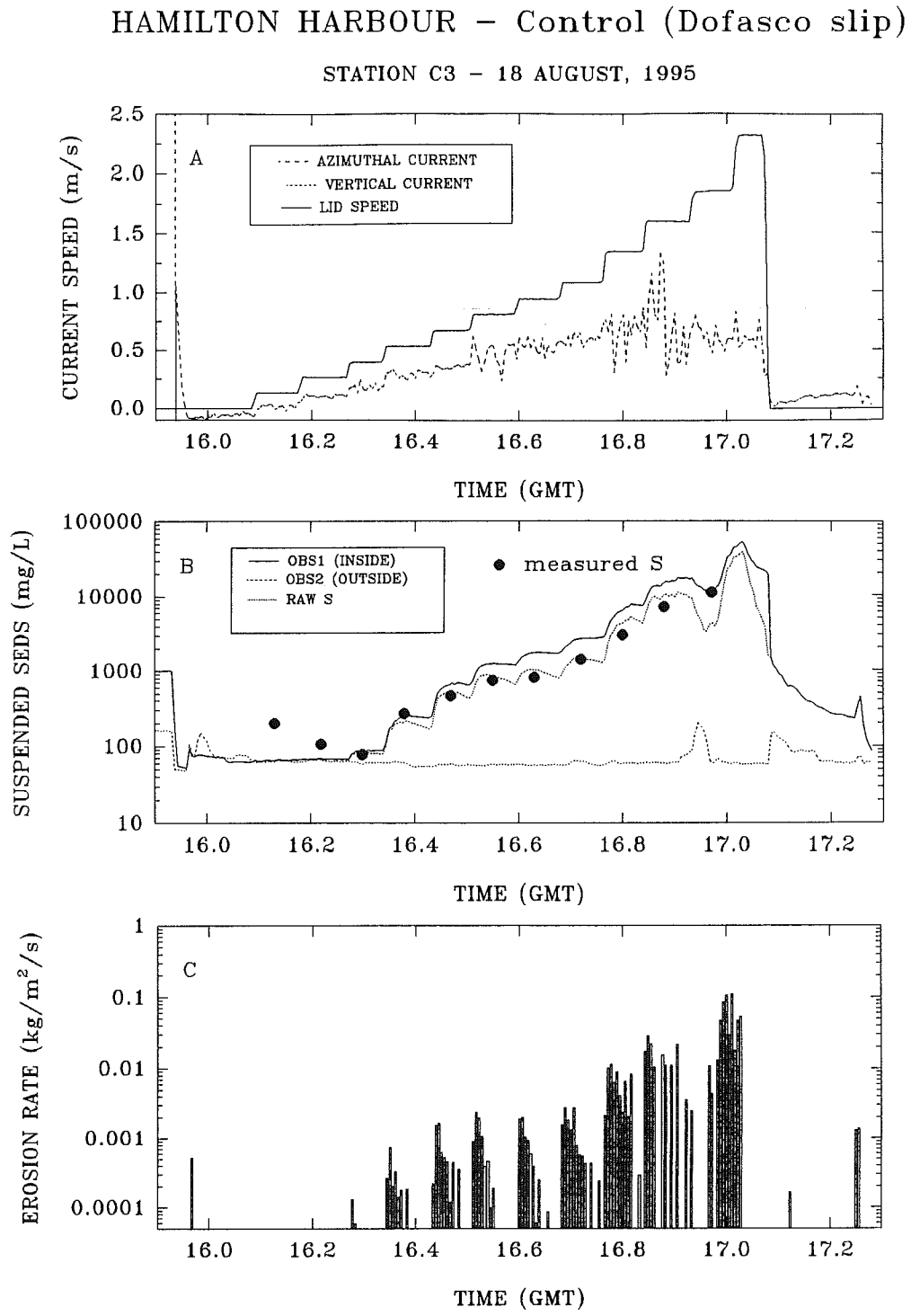

Figure 4.1.1.3 Time-series plots of the Sea Carousel deployment at control site C3. Notice the erratic nature of the azimuthal current during periods of high applied flow. As a result, we have used the more stable lid rotation as a proxy for flow and bed shear stress.

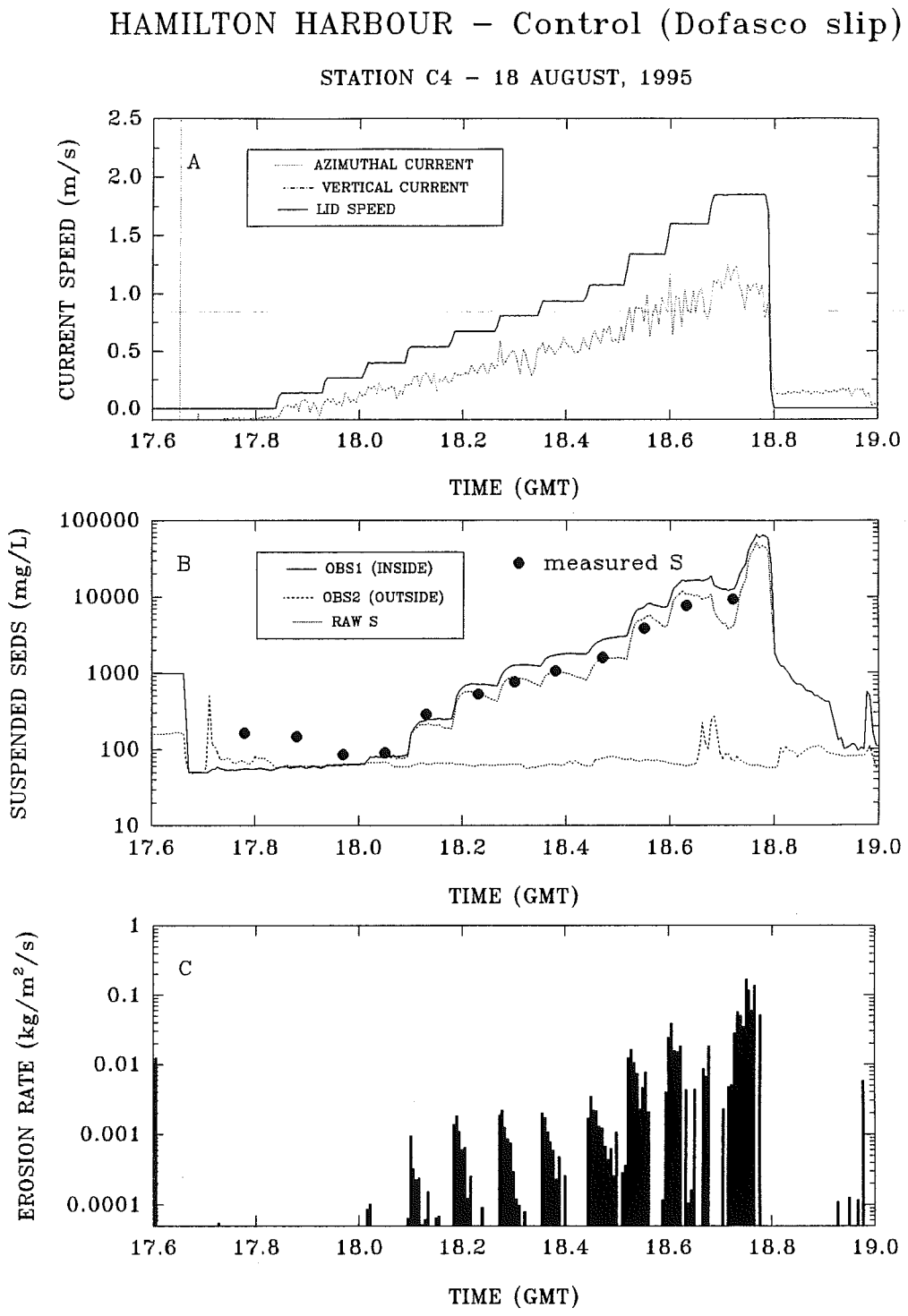

Figure 4.1.1.4 Time-series plots of the Sea Carousel deployment at control site C4. Variations in ambient S denote losses from Sea Carousel due to leakage.

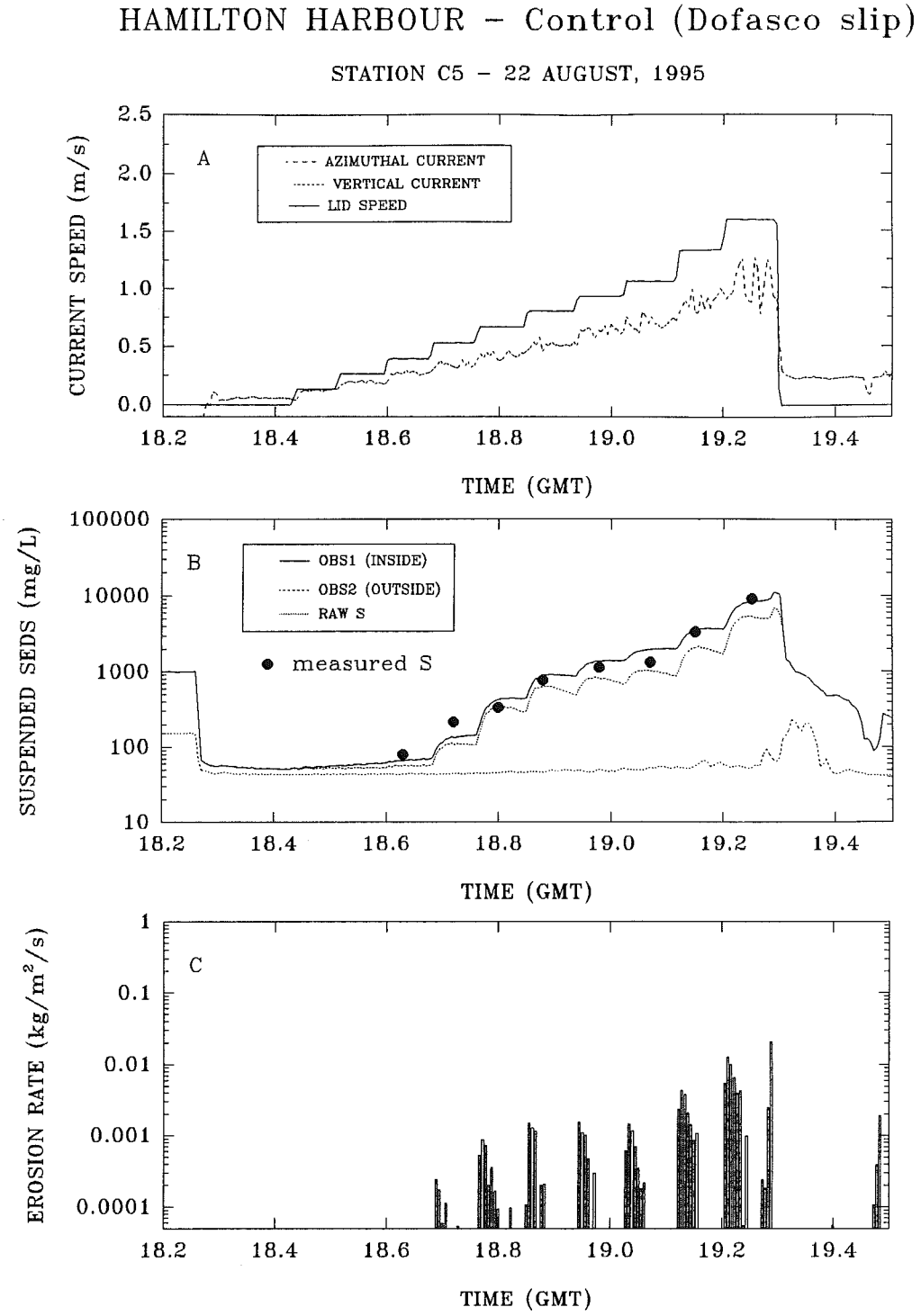

Figure 4.1.1.5 Time-series plots of the Sea Carousel deployment at control site C5.

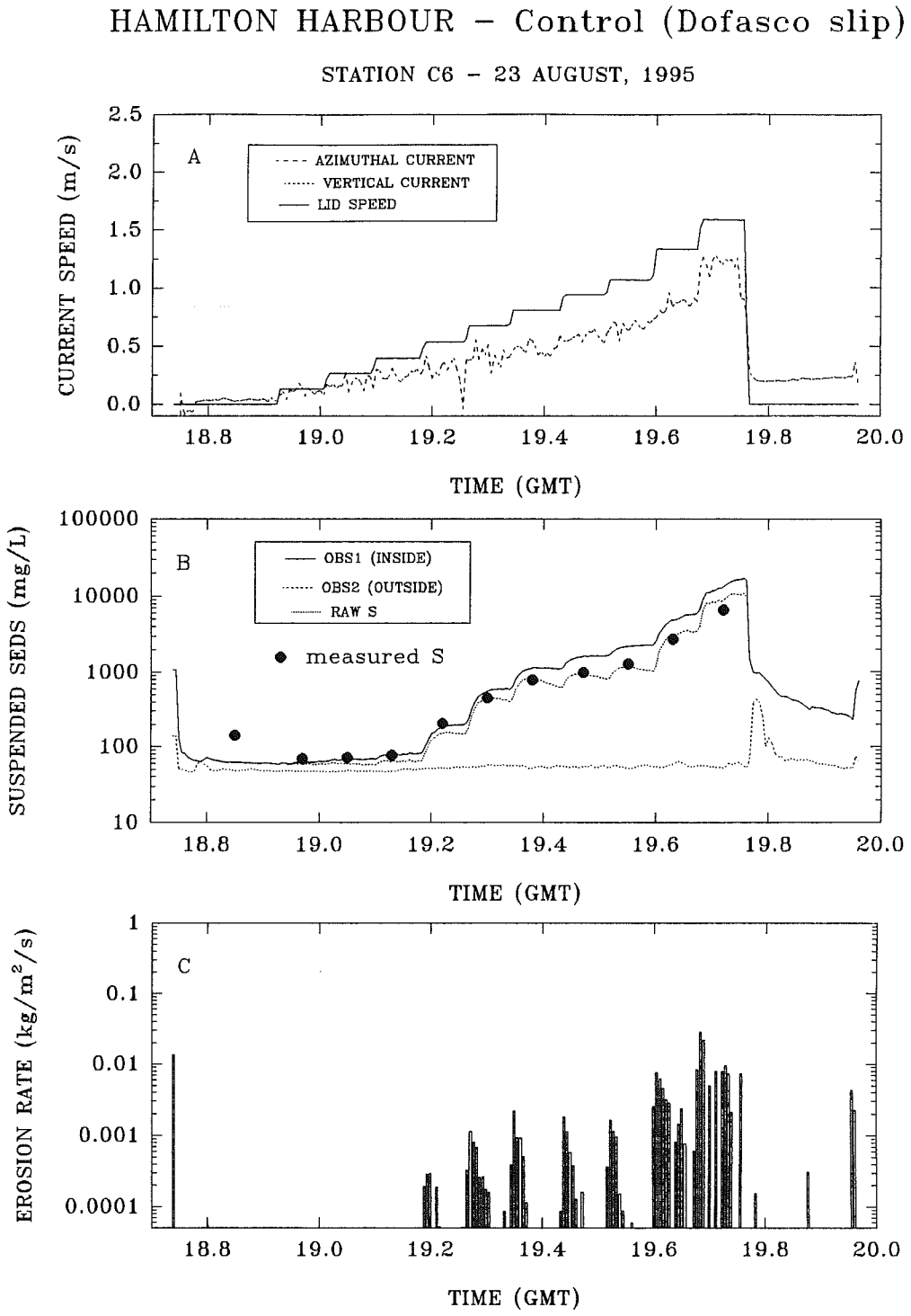

Figure 4.1.1.6 Time-series plots of the Sea Carousel deployment at control site C6.

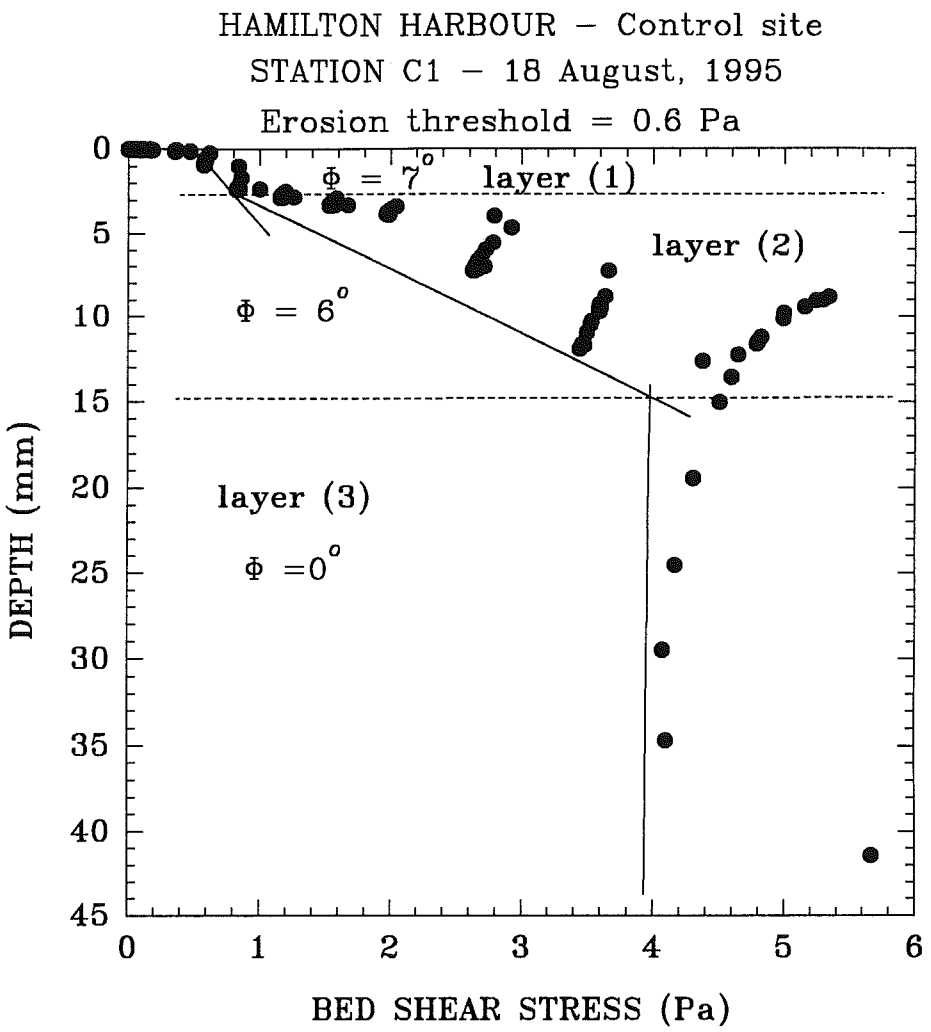

Figure 4.1.1.7 A synthetic core for control site C1, derived from the time-series of S in Sea Carousel and from bulk density determined through Catscan analysis. The solid lines trace the profile of sediment strength with depth that has been traced by eye. The surface intercept of the solid line is interpreted as a measure of the erosion threshold (method 1 herein). The inflection points are interpreted to signify changes in bed structure, while the slope of the lines are proportional to the friction coefficient of the bed. In this case three layers are recognised, the topmost two showing steadily increasing bed strength probably due to biostabilization. The lowest layer shows no consolidation and possibly due to gas production in the sediment.

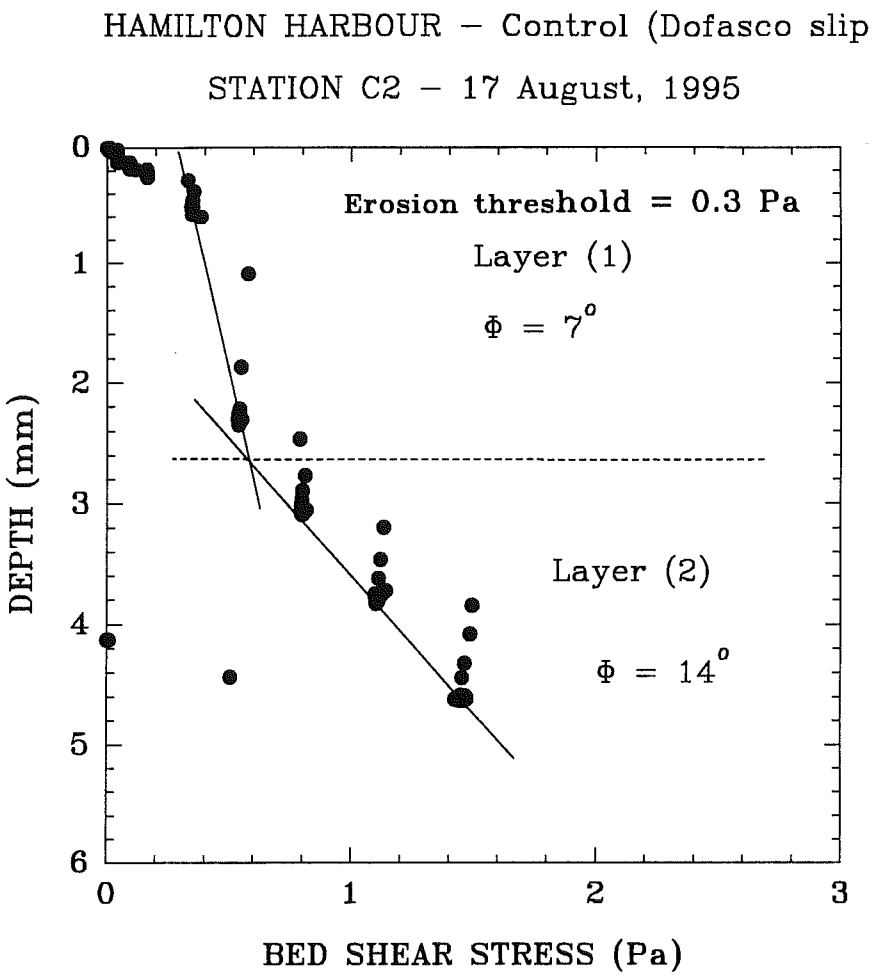

Figure 4.1.1.8 A synthetic core for control site C2. Two layers are interpreted from this profile, each increasing in strength with depth.

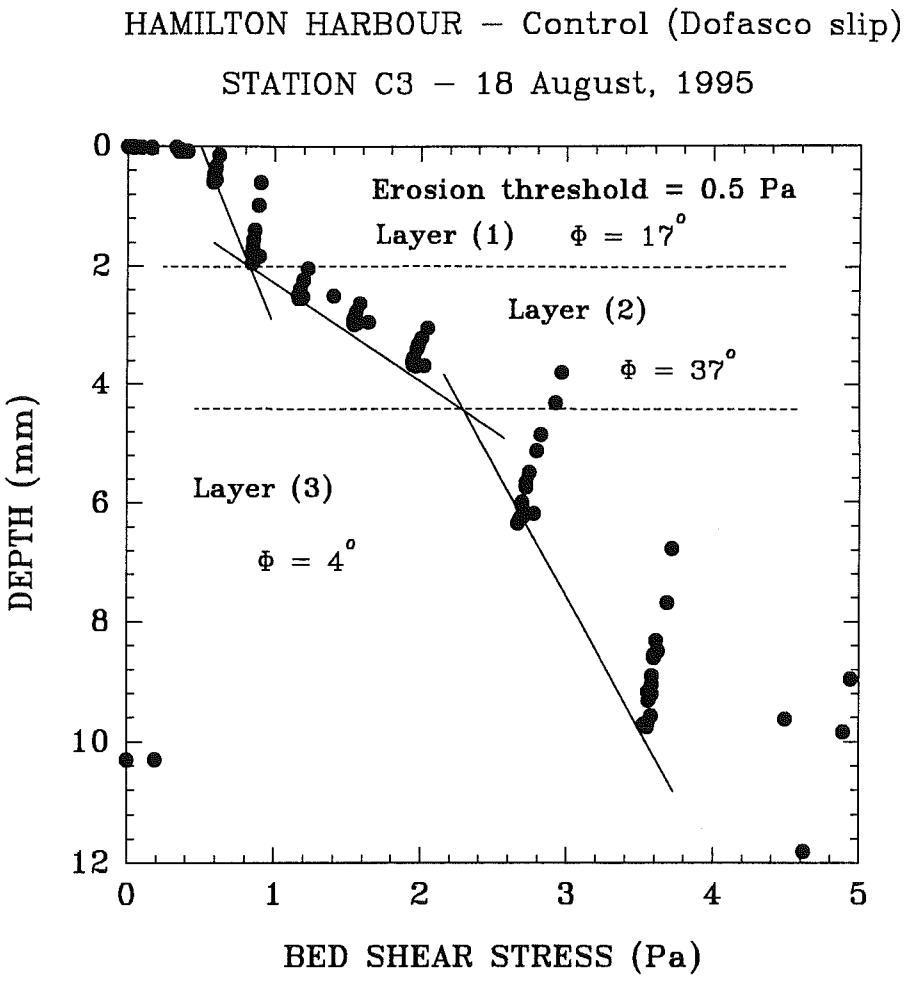

Figure 4.1.1.9 A synthetic core for control site C3. Three layers are interpreted from this profile, each increasing in strength with depth. The higher values of (Φ) in the topmost 4 mm is likely related to biostabilization.

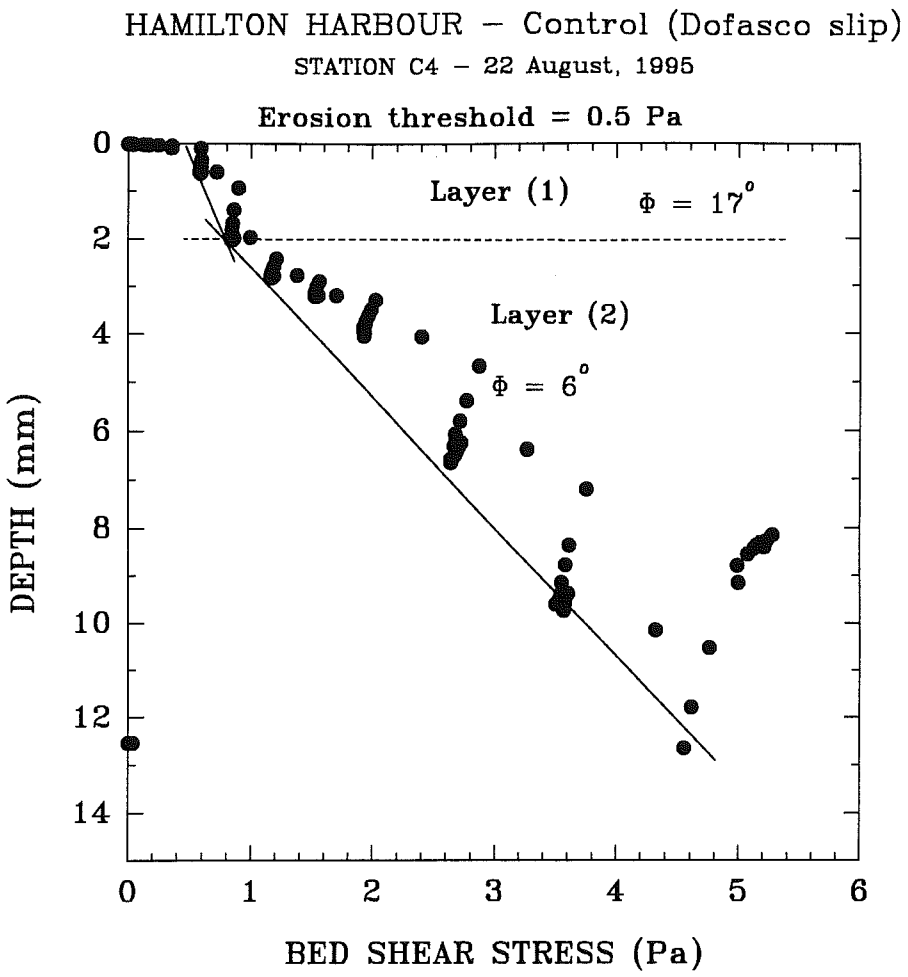

Figure 4.1.1.10 A synthetic core for control site C4. Two layers are interpreted from this profile, each increasing in strength with depth. Notice that the strength profile can be divided into linear segments with reasonable accuracy.

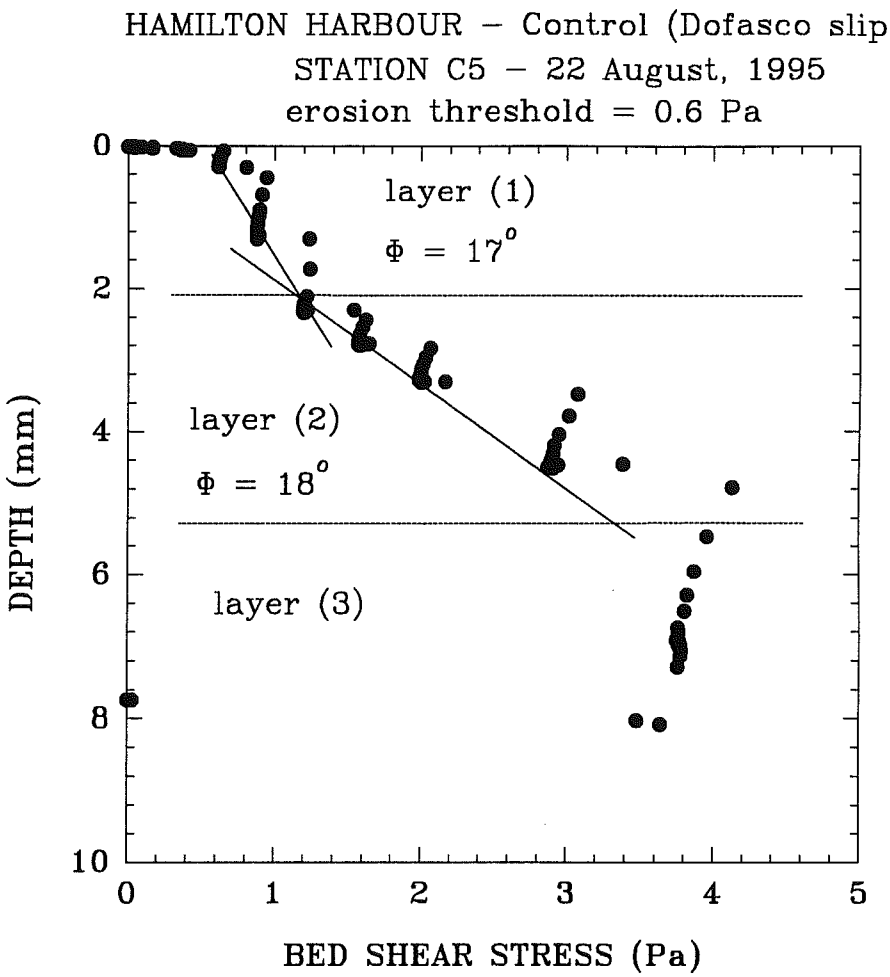

Figure 4.1.1.11 A synthetic core for control site C5. Three layers are interpreted from this profile, the topmost two increasing in strength with depth; the lower layer showing a possible strength reversal.

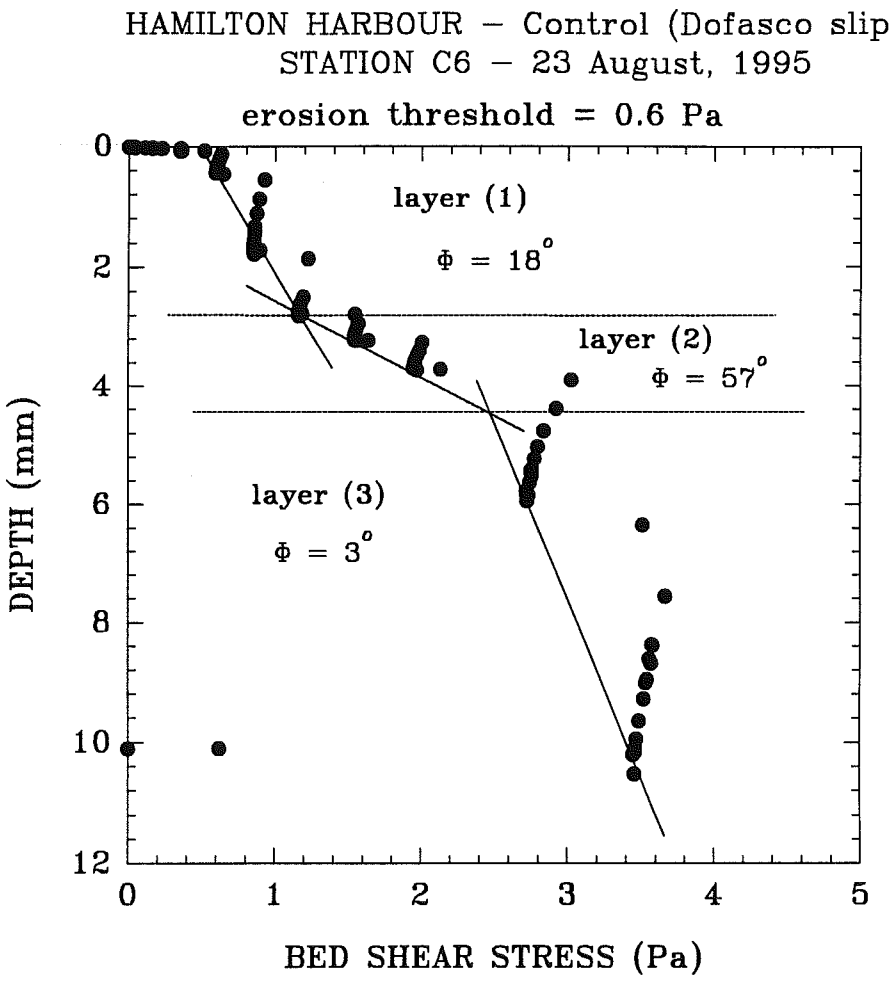

Figure 4.1.1.12 A synthetic core for control site C6. Notice the rapid strength gain in layer (2) possibly related to biostabilization.

Figure 4.1.1.13 Measured erosion rate (A) and S (B) plotted against applied bed shear stress for control site C1. Mean erosion rate (E_m) and S are expressed as a power functions of stress through least-squares regression analyses. The exponents of the functions are used as indexes of erodibility. Notice that peak erosion (E_p) varies systematically with applied stress. It follows E_m under type Ib erosion; it is constant during transitional erosion; and increases markedly during type II erosion. The base erosion rate (E_o) was defined as 1×10^{-5} kg/m^2/s on the basis of results obtained during the early stages of the experiment (open circles). Ambient S was around 80 mg/L.

STATION C1 – 18 AUGUST, 1995

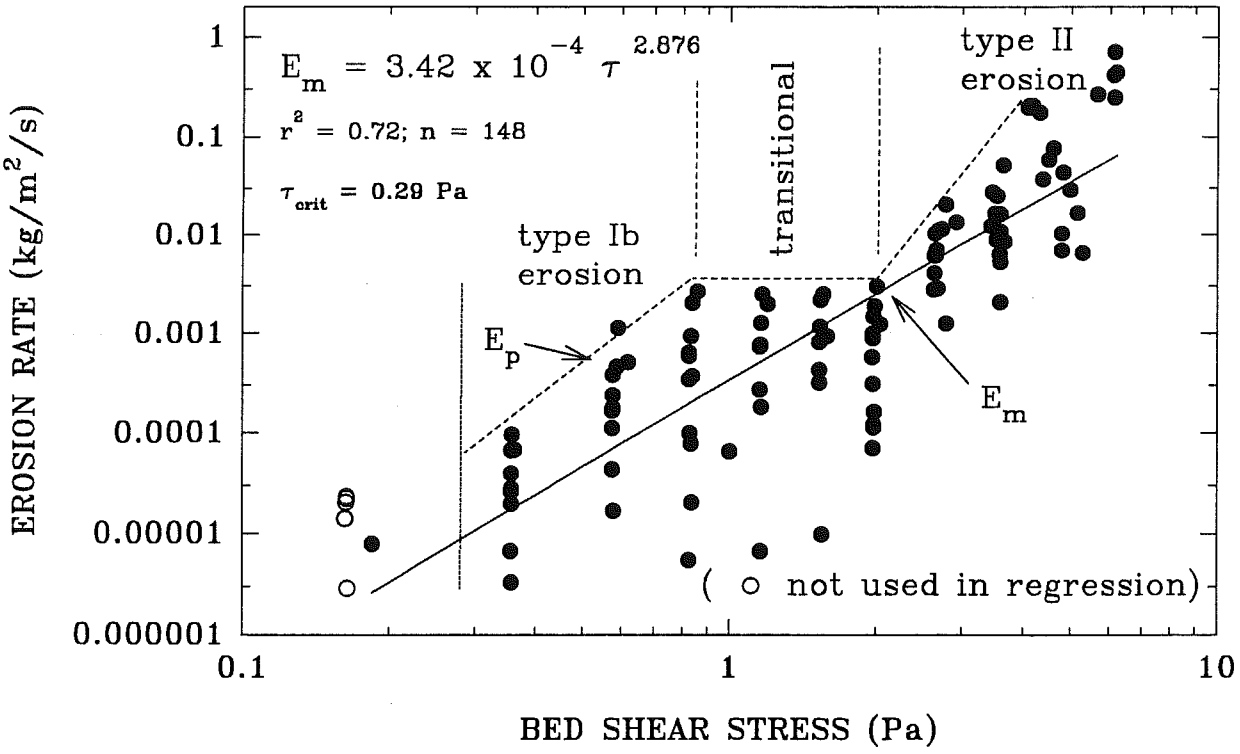

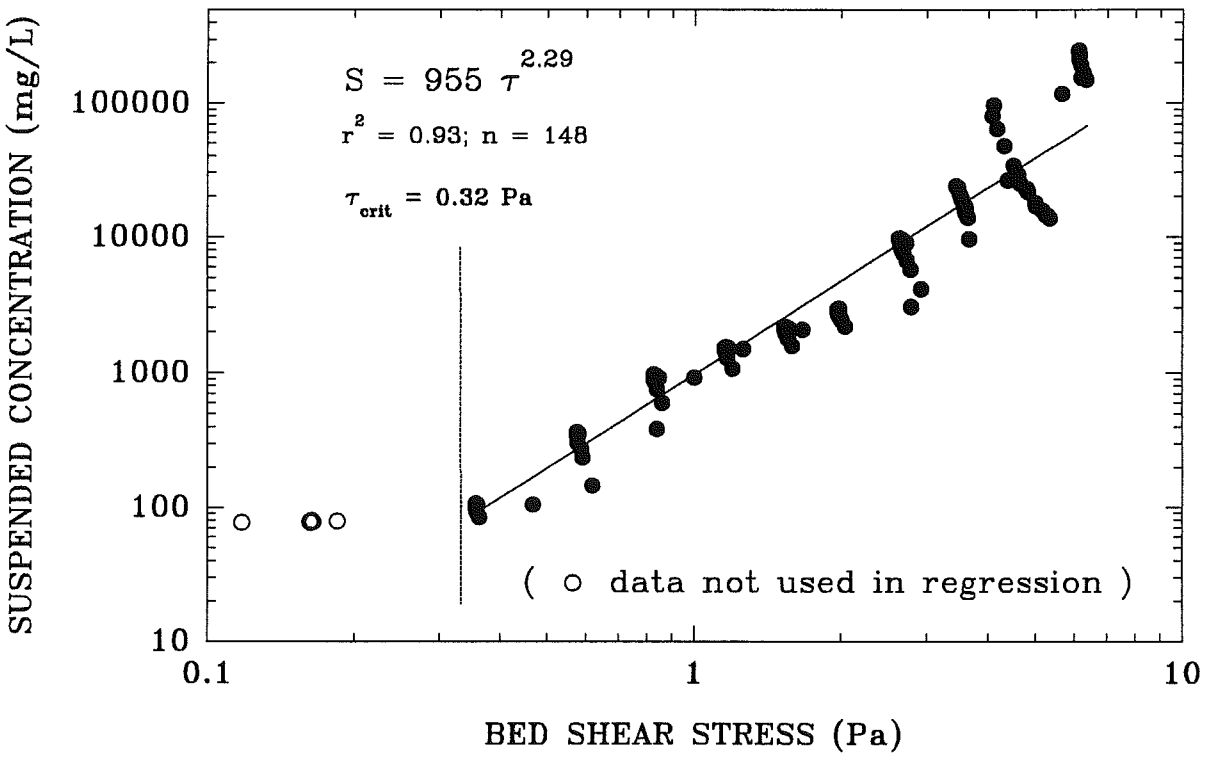

Figure 4.1.1.14 Measured erosion rate (A) and S (B) plotted against applied bed shear stress for control site C2. In this case, we identify Type Ia erosion (suspension of surface "fluff" layer). The erosion thresholds are defined by evaluating the stress at E_o (method 2) and evaluating S at ambient concentrations (method 3).

STATION C2 – 17 AUGUST, 1995

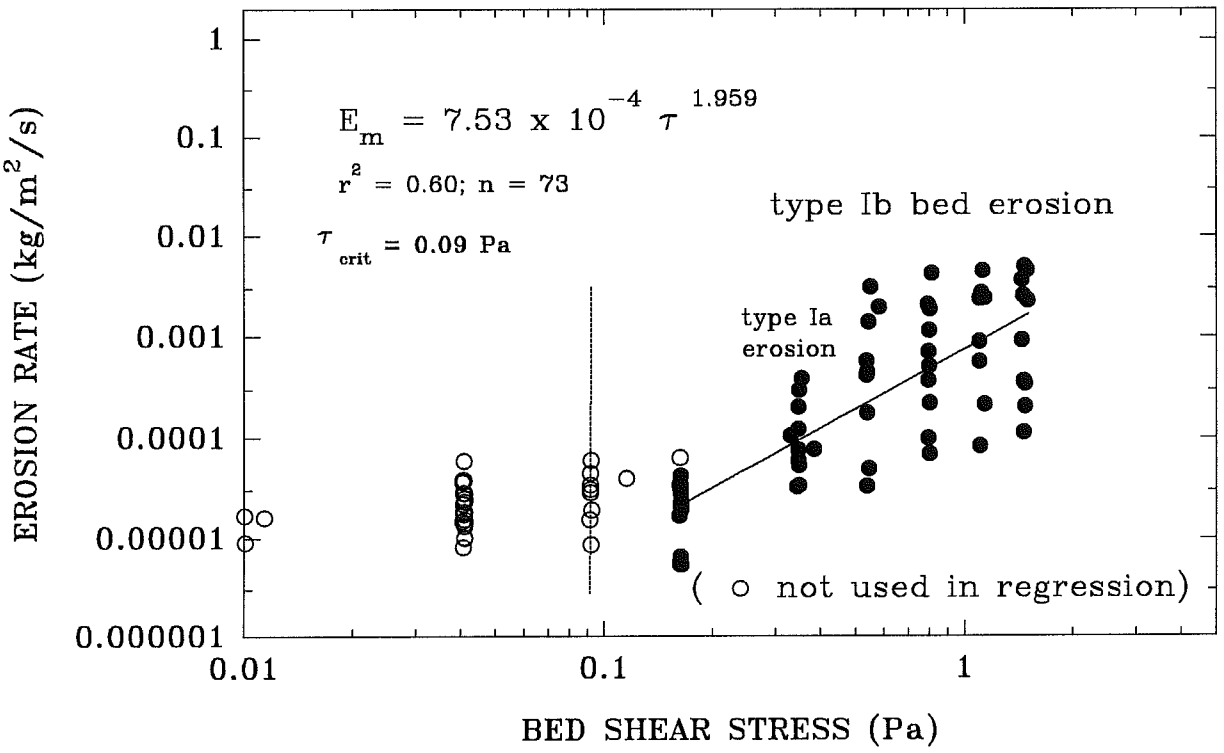

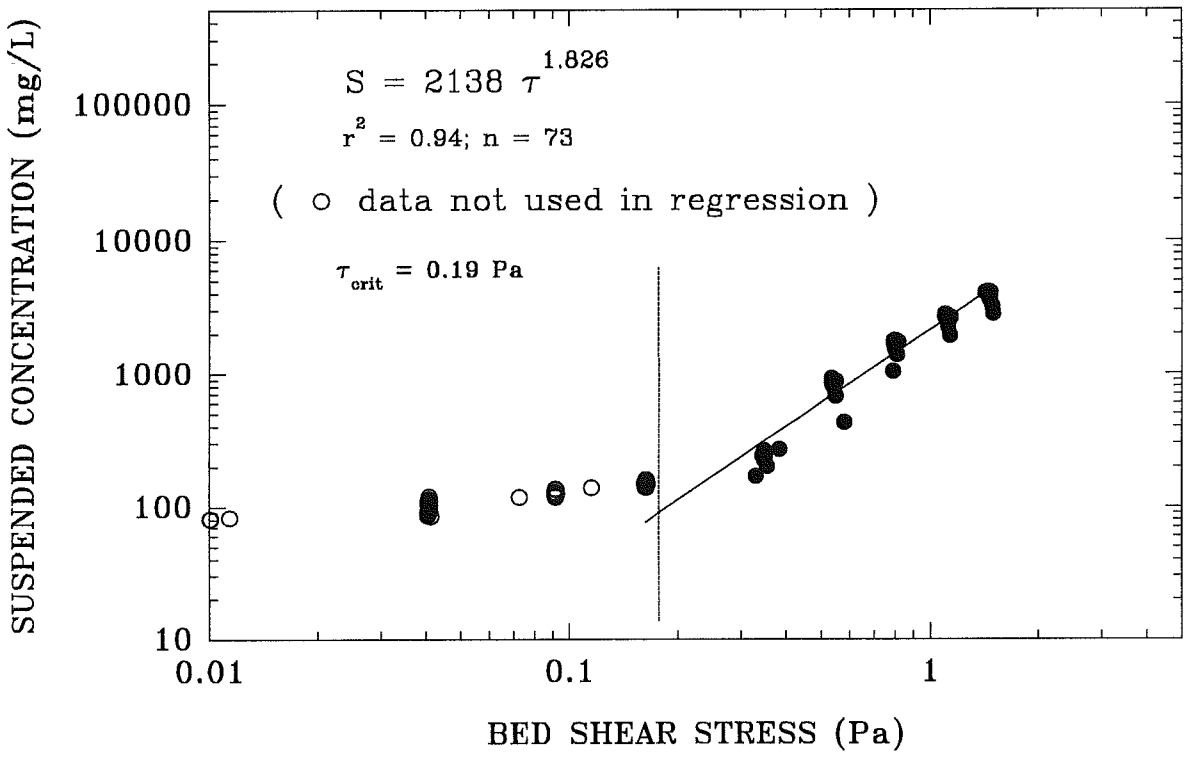

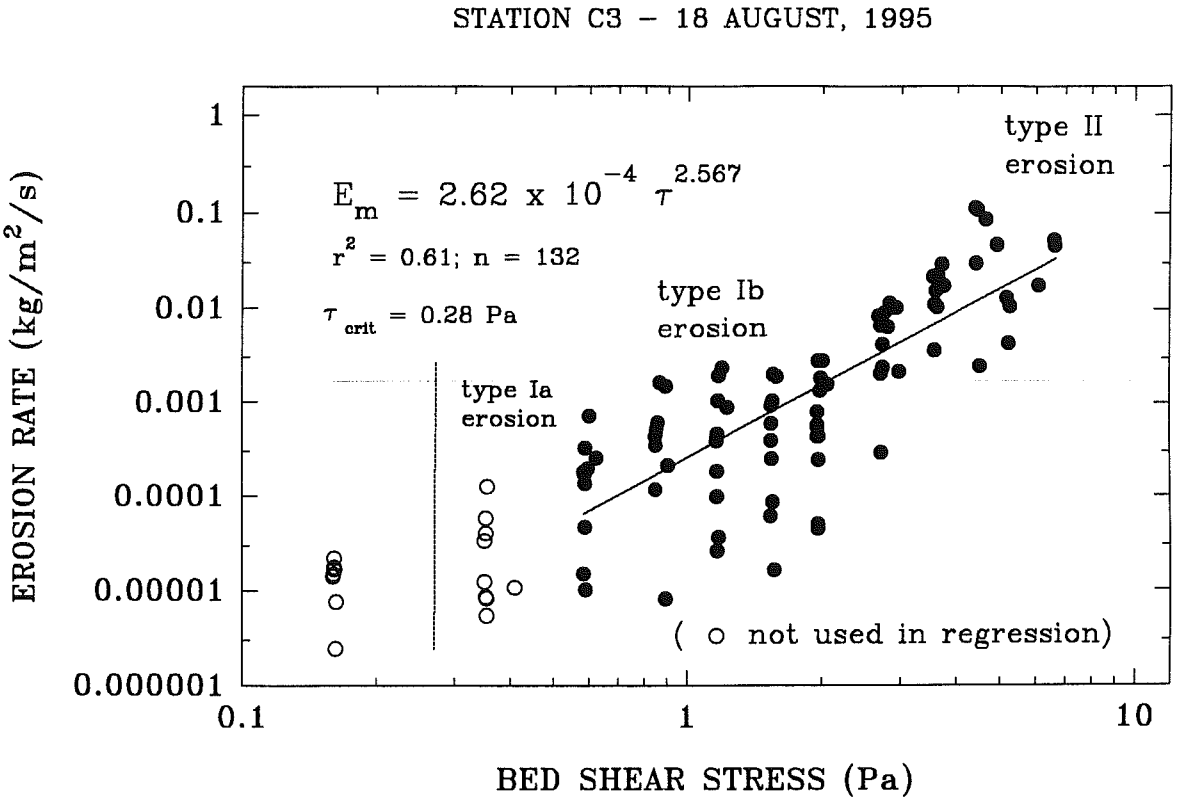

Figure 4.1.1.15 Measured erosion rate (A) and S (B) plotted against applied bed shear stress for control site C3. Notice how well the power function fits the results.

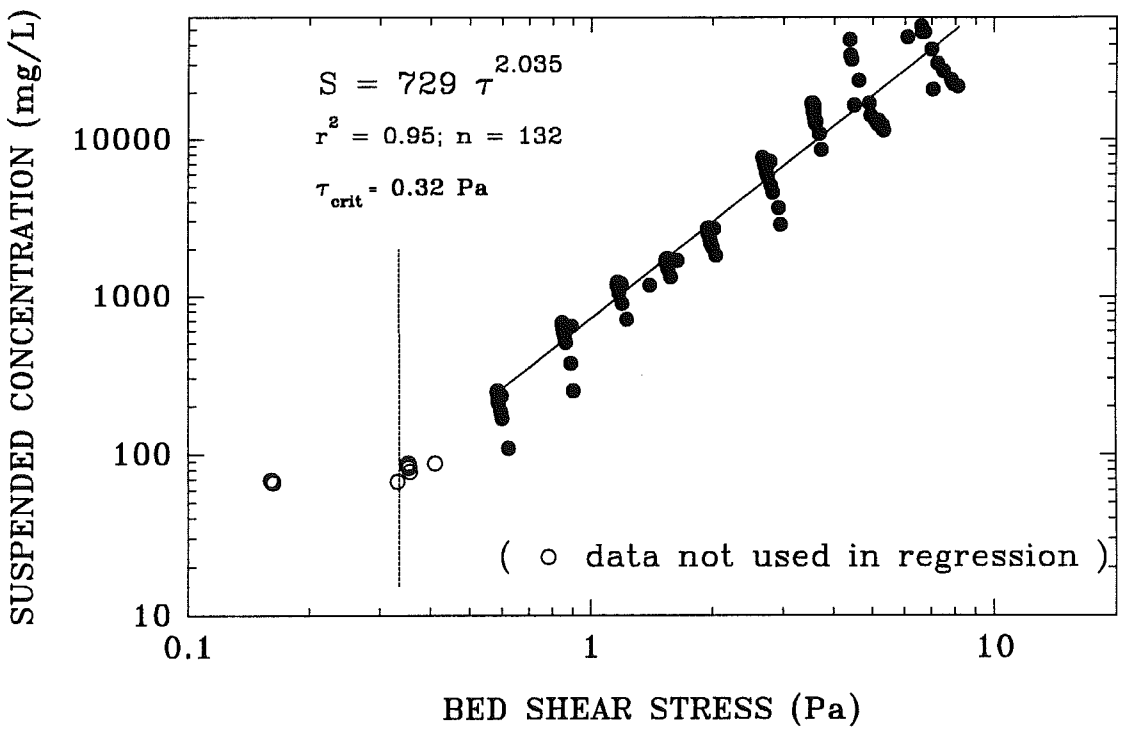

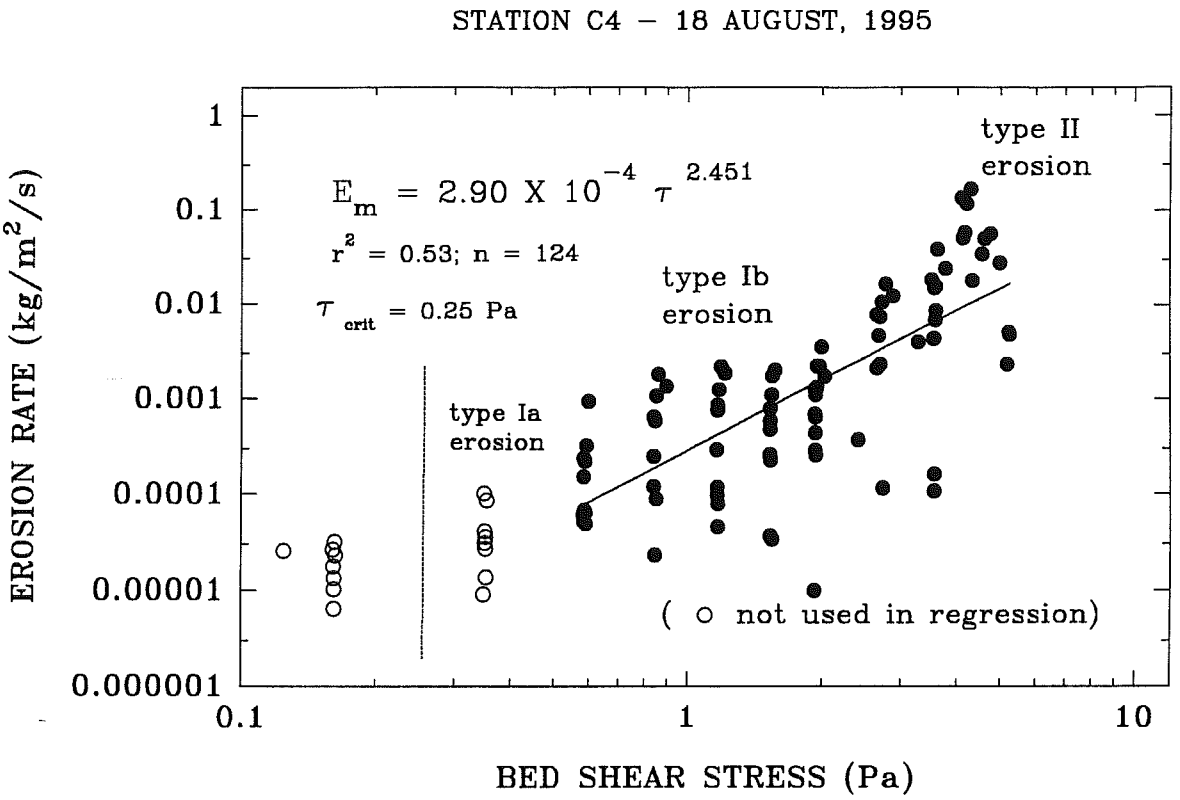

Figure 4.1.1.16 Measured erosion rate (A) and S (B) plotted against applied bed shear stress for control site C4.

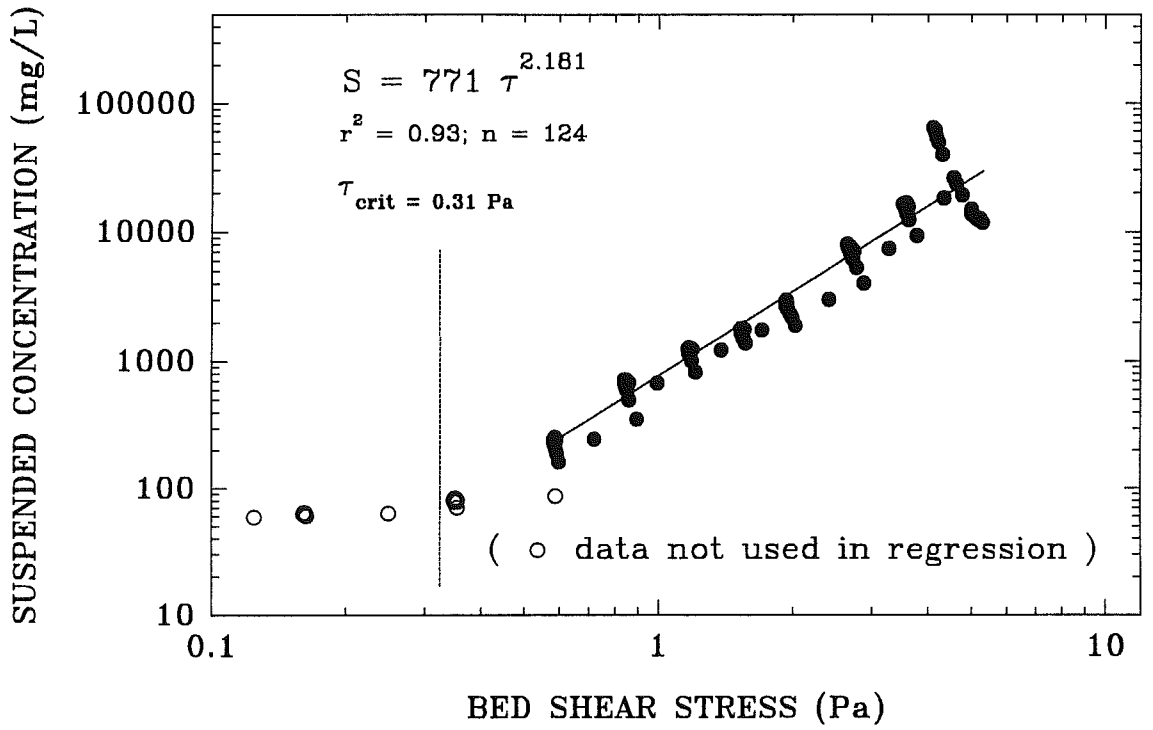

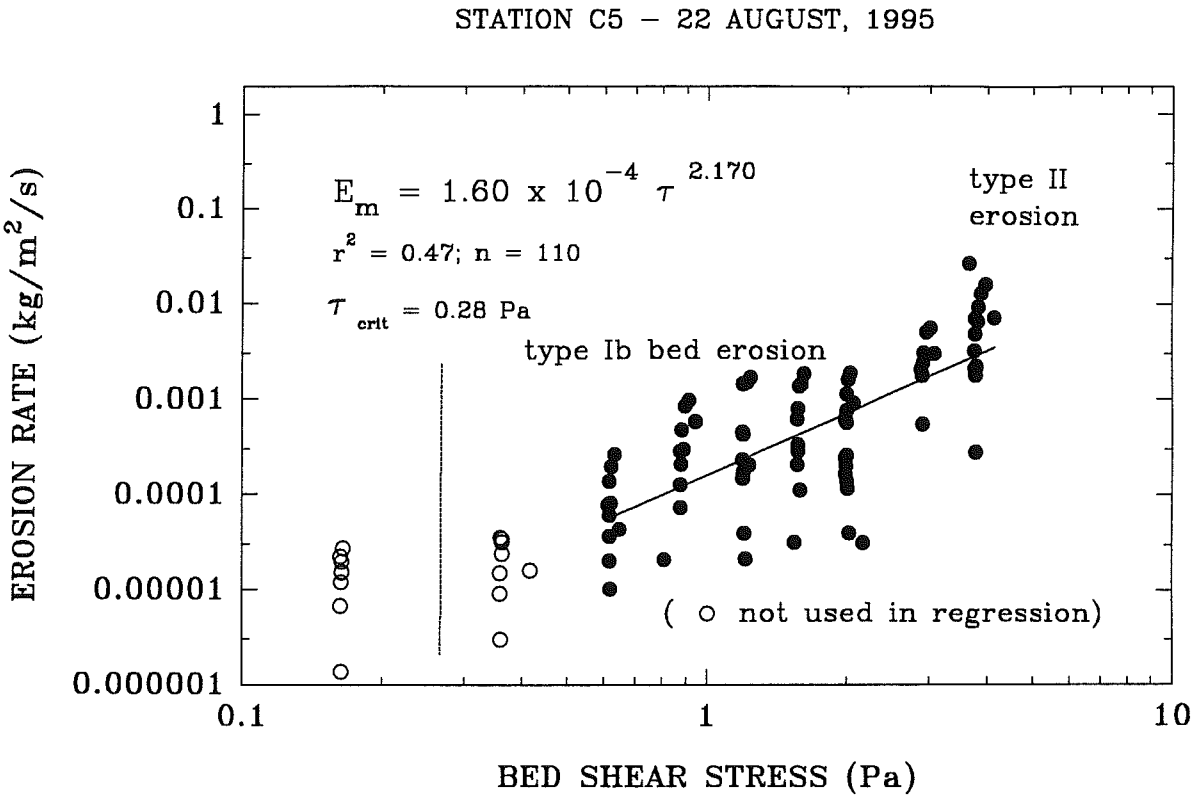

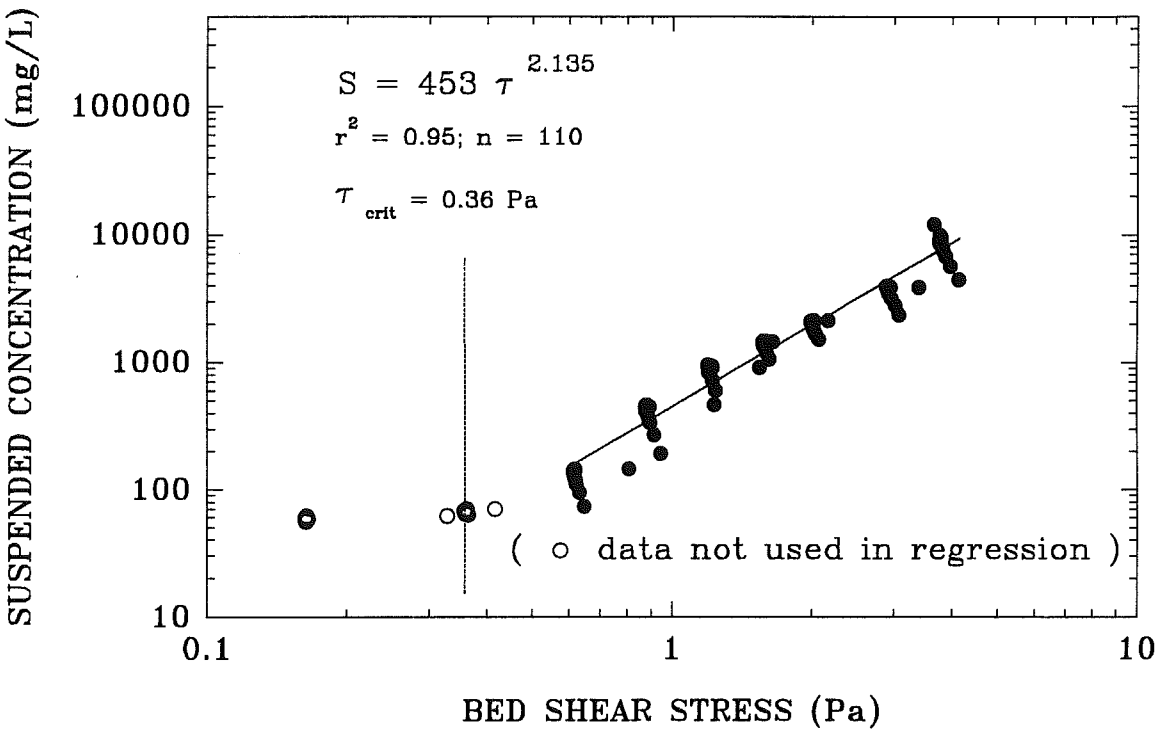

Figure 4.1.1.17 Measured erosion rate (A) and S (B) plotted against applied bed shear stress for

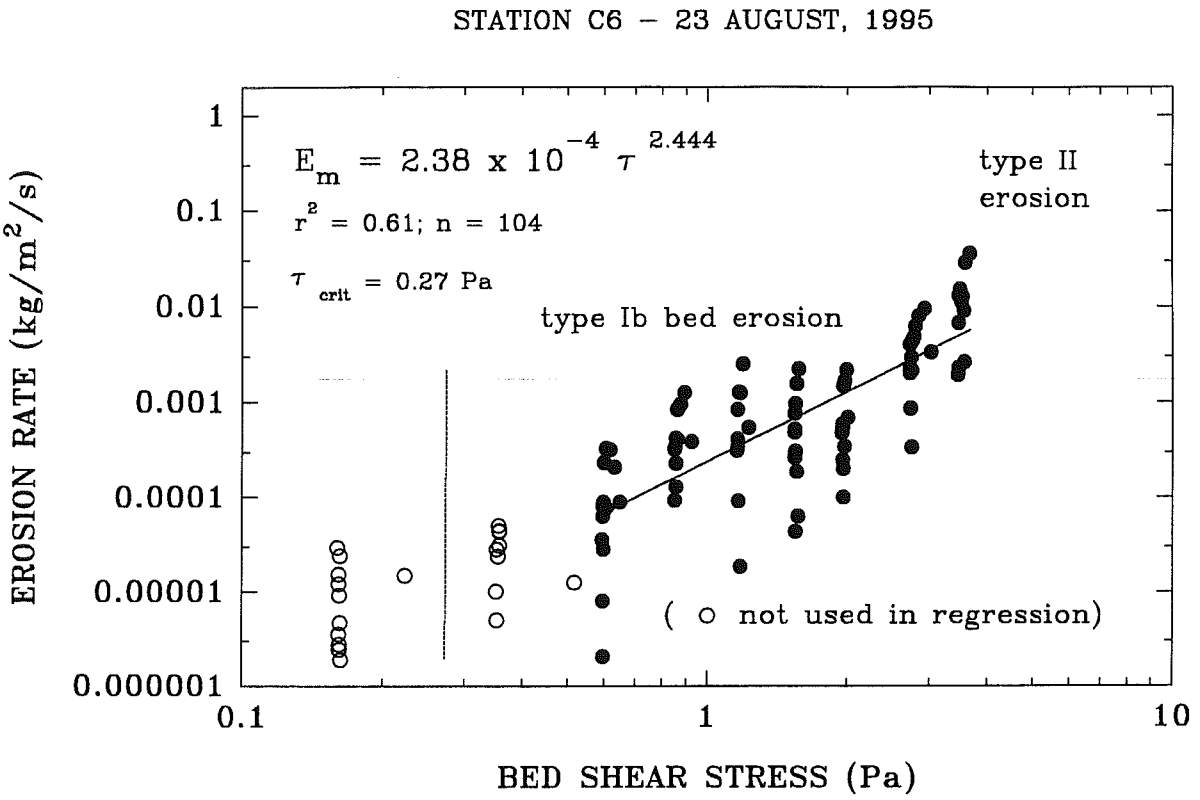

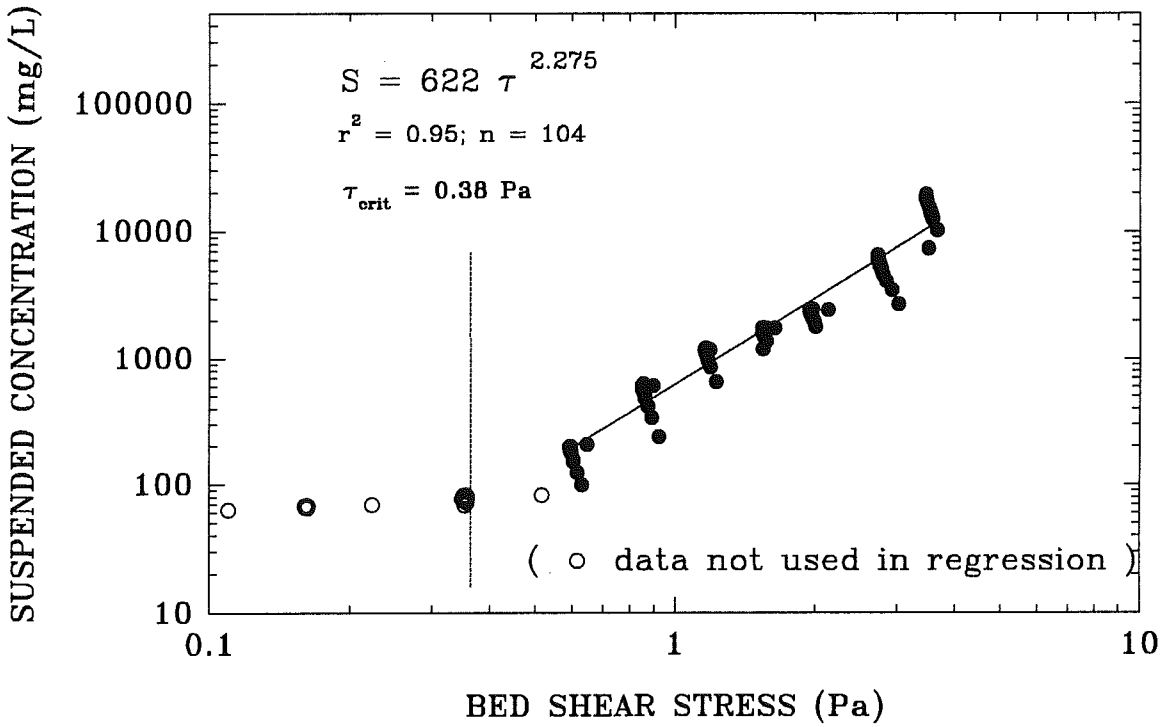

Figure 4.1.1.18 Measured erosion rate (A) and S (B) plotted against applied bed shear stress for control site C6.

Figure 4.1.1.19 Time-series of the still-water S derived in the last stages of each experiment: (A) control sites; (B) water-injection sites; and (C) oxidant-injection sites. The trends are adequately explained as logarithmic decaying concentrations, the decay constants (k) being linear functions of the starting value of S.

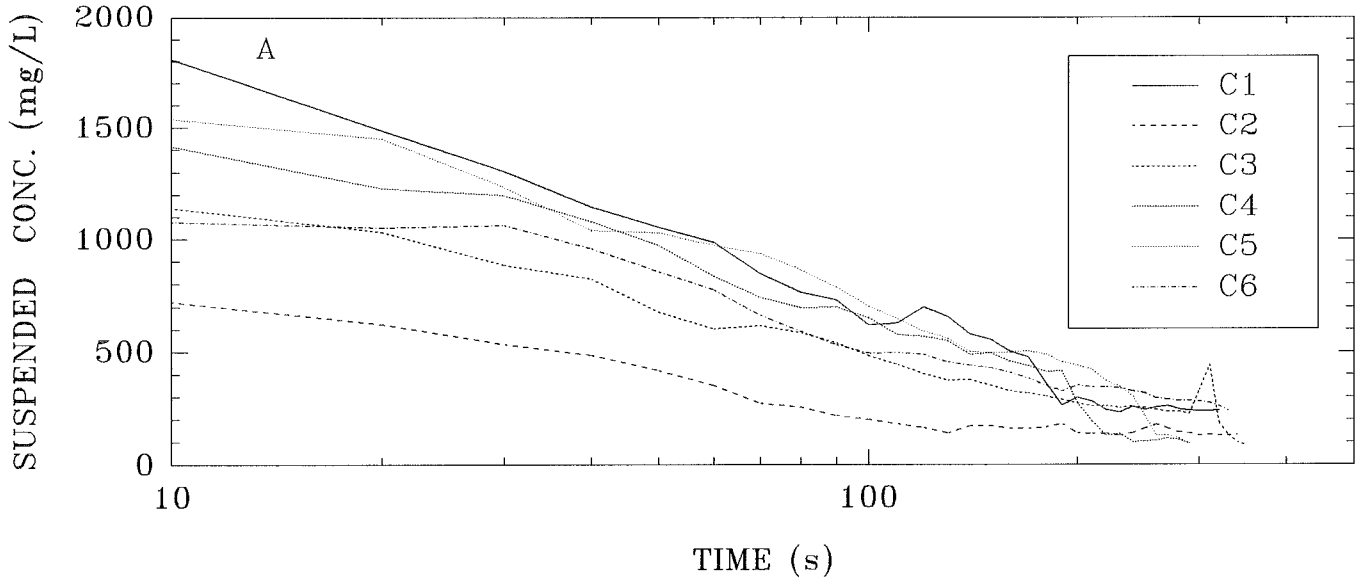
A
SUSPENDED CONC. (mg/L)
2000
1500
1000
500
0
10
100
TIME (s)
C1
C2
C3
C4
C5
C6

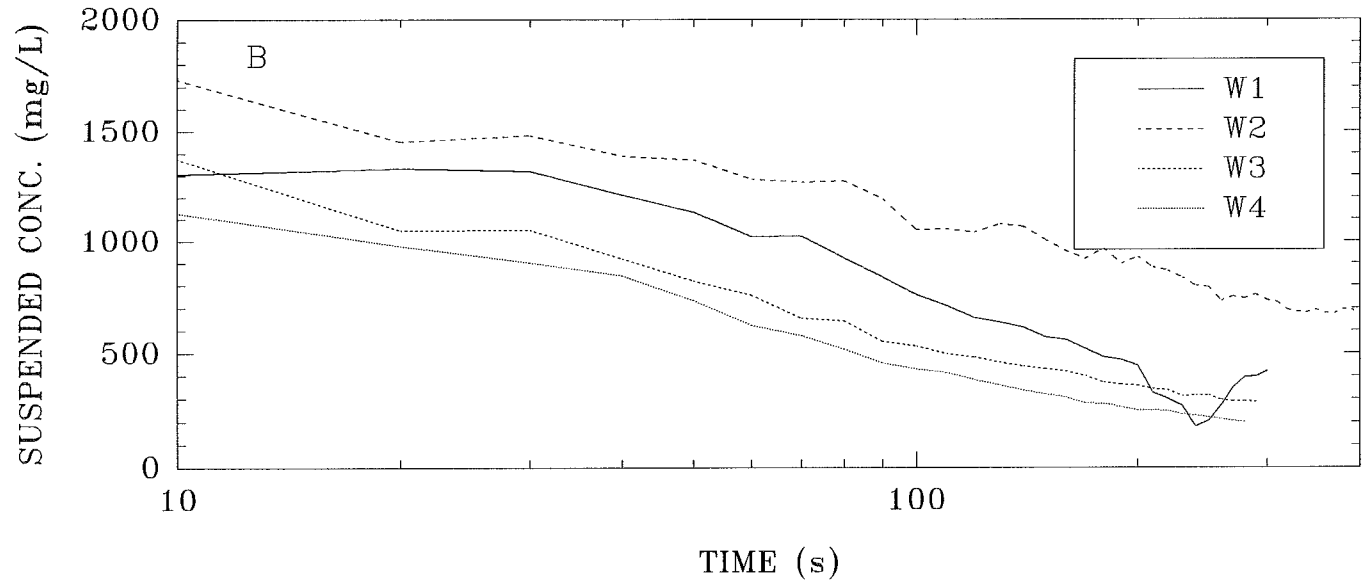
B
SUSPENDED CONC. (mg/L)
2000
1500
1000
500
0
10
100
TIME (s)
W1
W2
W3
W4

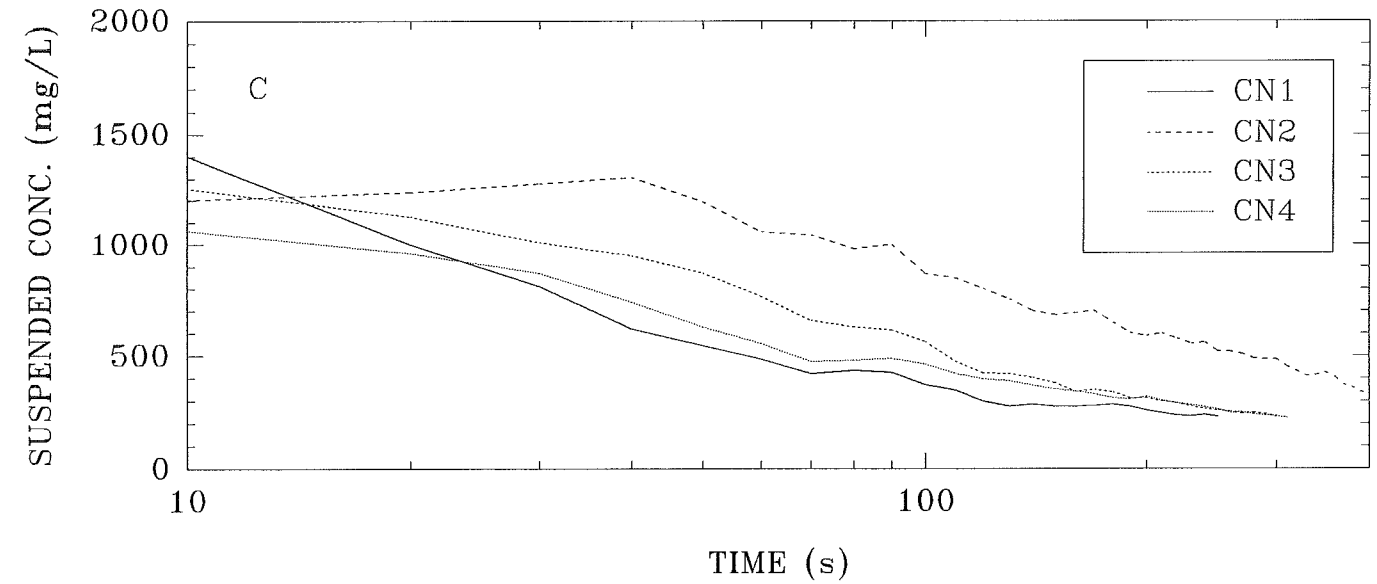
C
SUSPENDED CONC. (mg/L)
2000
1500
1000
500
0
10
100
TIME (s)
CN1
CN2
CN3
CN4

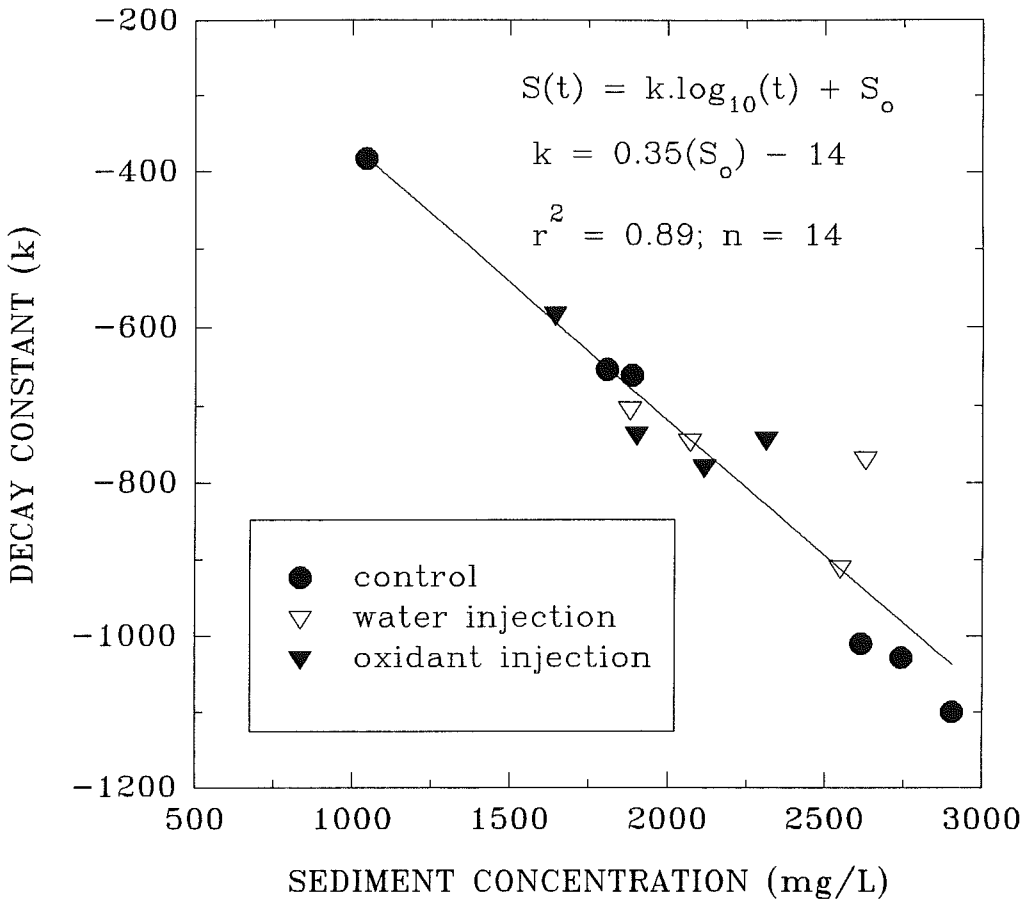

Figure 4.1.1.20 The decay constants derived from the results shown in Figure 4.1.1.19 plotted against starting S. Notice the strongly linear relationship for all plots, which suggests that settling is unaffected by the means of treatment.

Figure 4.1.1.21 Mean S and incremental mass deposition determined for the time-series of Sea Carousel from control site C1. The equivalent mass settling velocity has been determined from these data, as well as the sedimentation diameter (on the assumption that the particle density is that of the bed at the maximum depth of erosion). Notice that the settling rate diminishes with time as does the diameter diagnostic of segregation on settling and a widely distributed size spectrum of suspended aggregates.

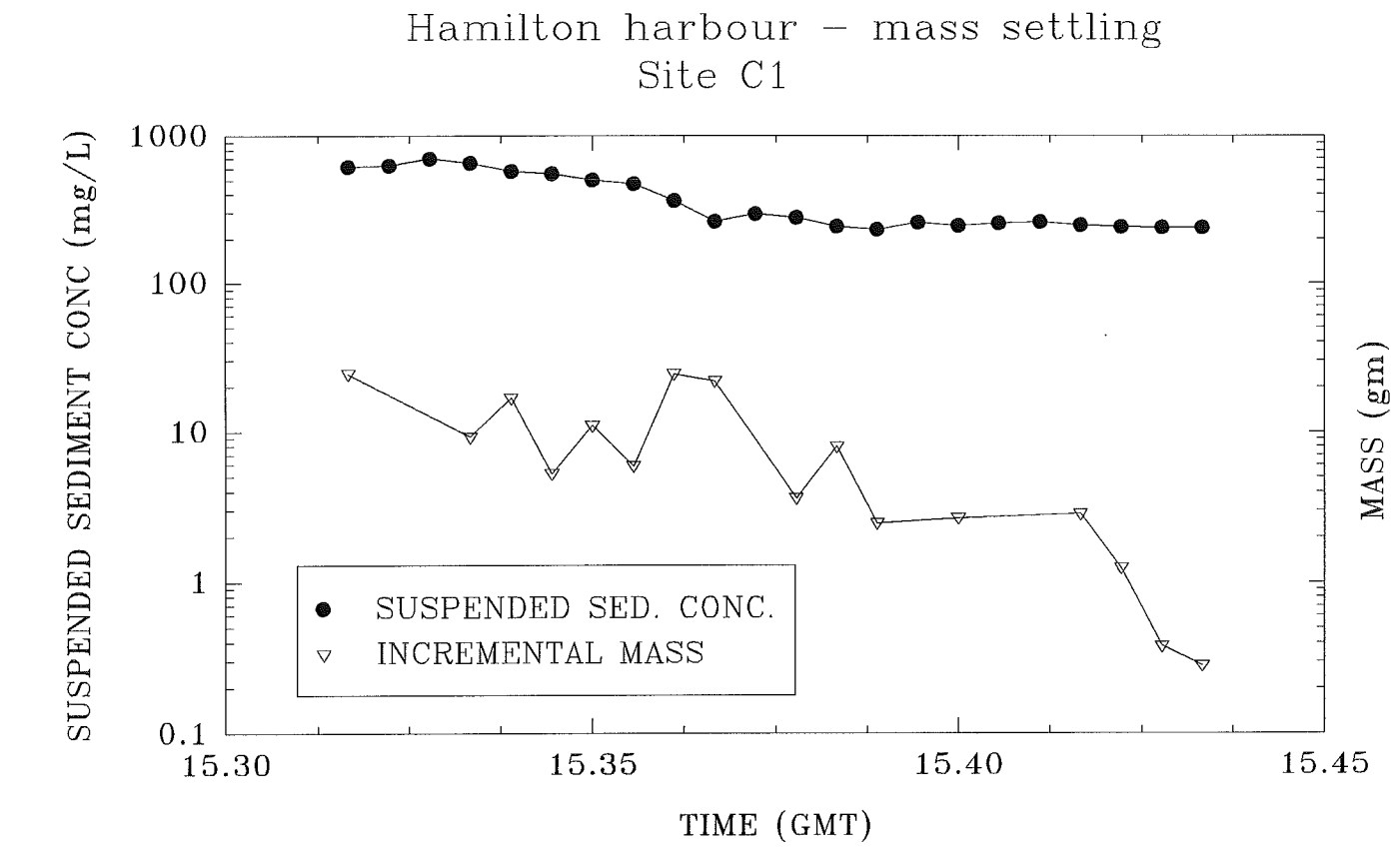
Hamilton harbour – mass settling
Site C1
SUSPENDED SEDIMENT CONC (mg/L)
1000
100
10
1
0.1
MASS (gm)
SUSPENDED SED. CONC.
INCREMENTAL MASS
15.30
15.35
15.40
15.45
TIME (GMT)

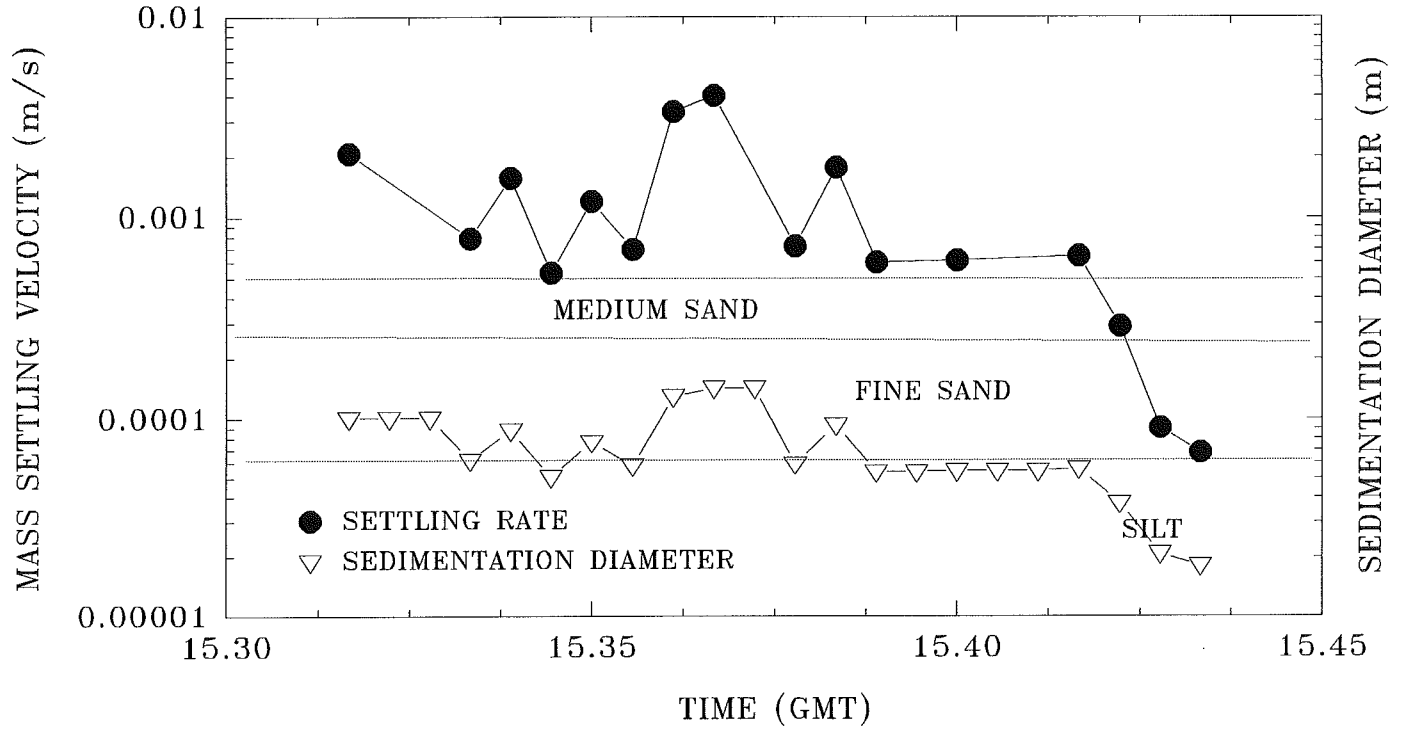
MASS SETTLING VELOCITY (m/s)
0.01
0.001
0.0001
0.00001
SEDIMENTATION DIAMETER (m)
MEDIUM SAND
FINE SAND
SILT
SETTLING RATE
SEDIMENTATION DIAMETER
15.30
15.35
15.40
15.45
TIME (GMT)

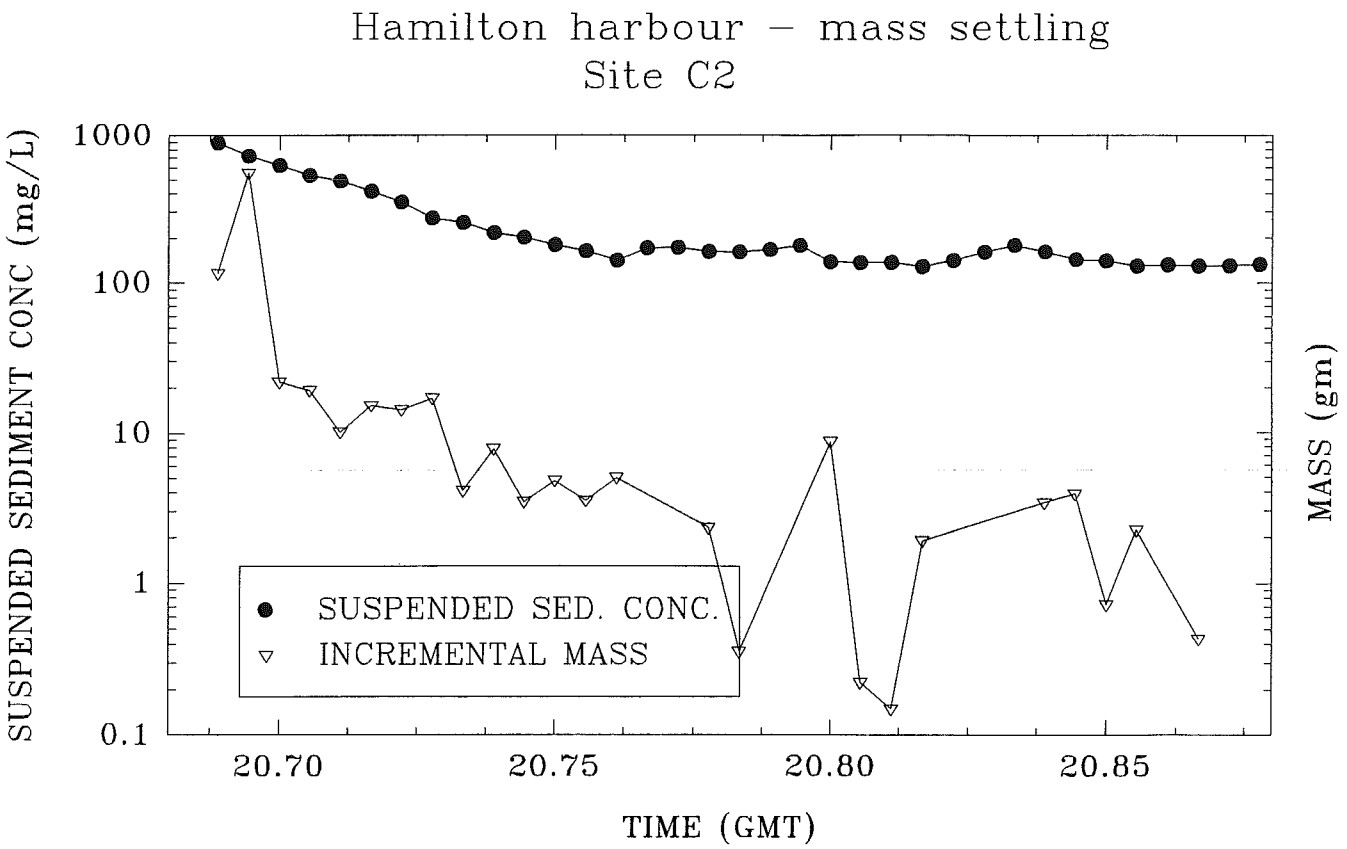

Figure 4.1.1.22 Mean S, incremental mass deposition, mass settling rates, and sedimentation diameter determined for the time-series of Sea Carousel from control site C2. Notice that much of the material in suspension falls into the sand and coarse silt size range.

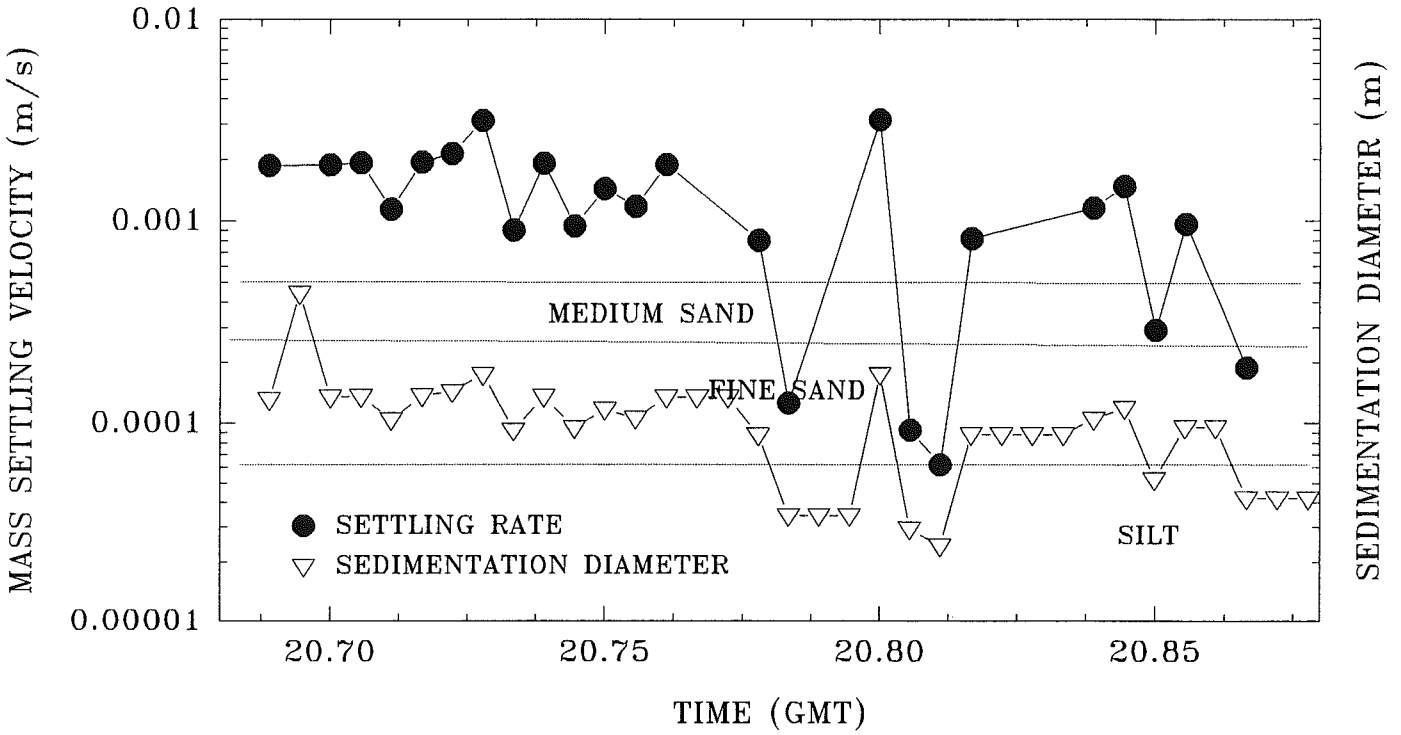

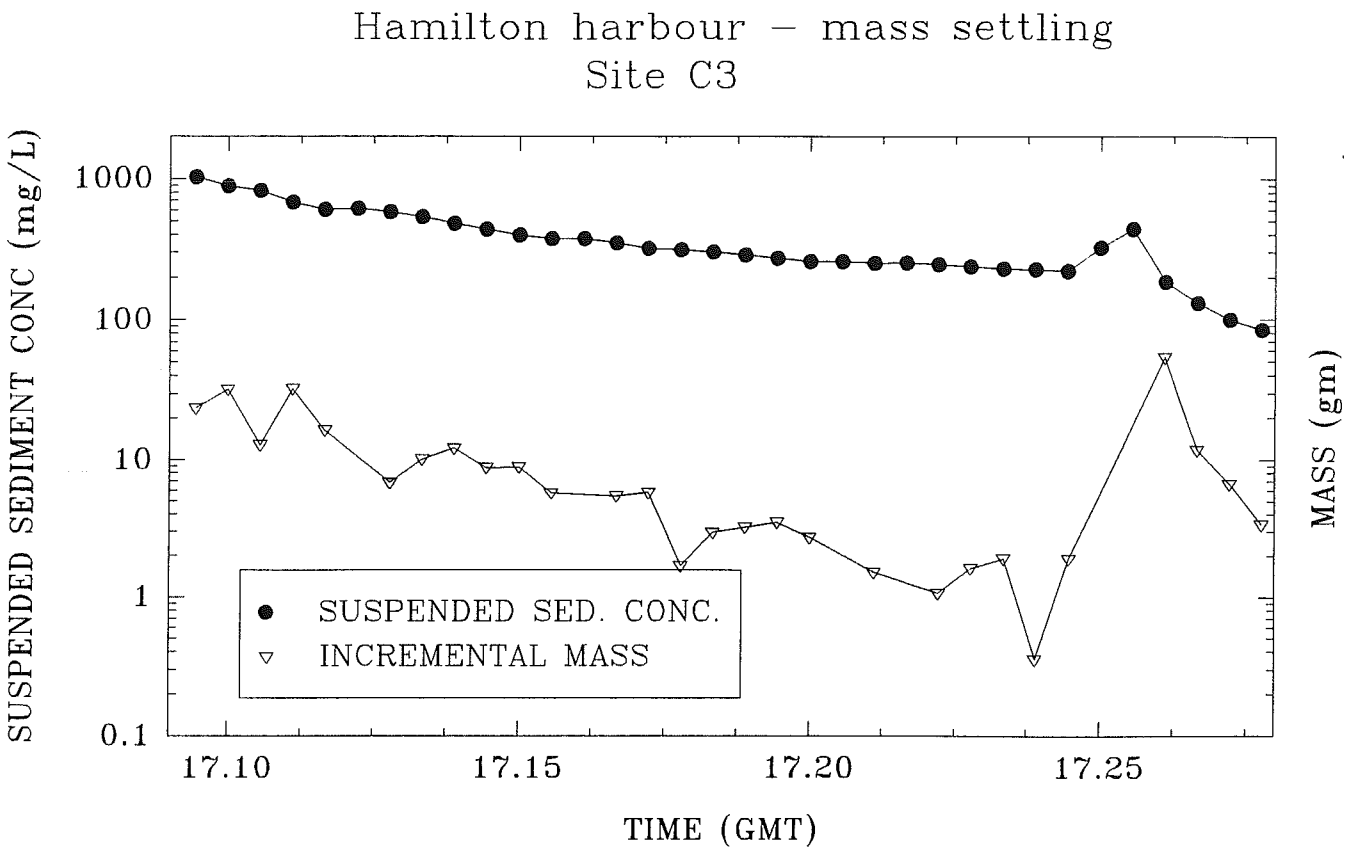

Figure 4.1.1.23 Mean S, incremental mass deposition, mass settling rates, and sedimentation diameter determined for the time-series of Sea Carousel from control site C3. Notice that settling can be quite irregular in time.

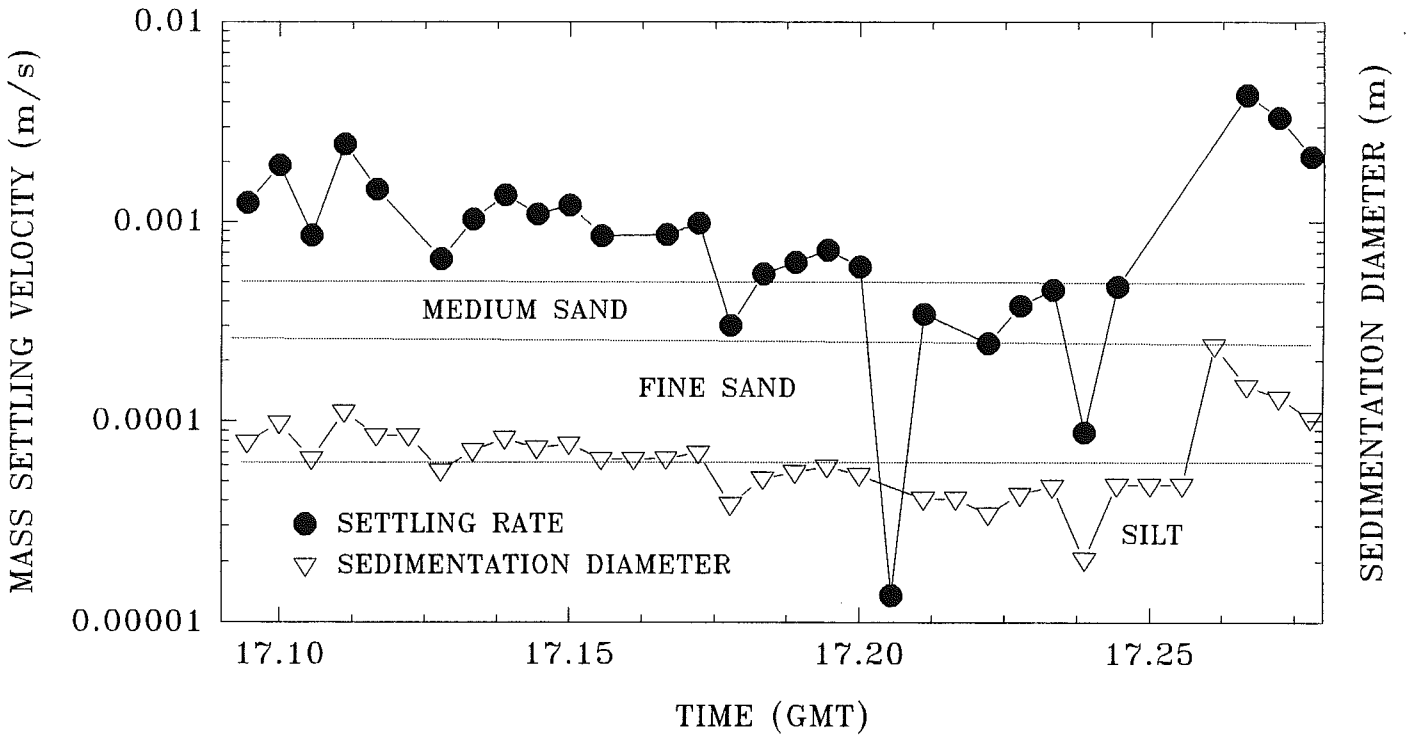

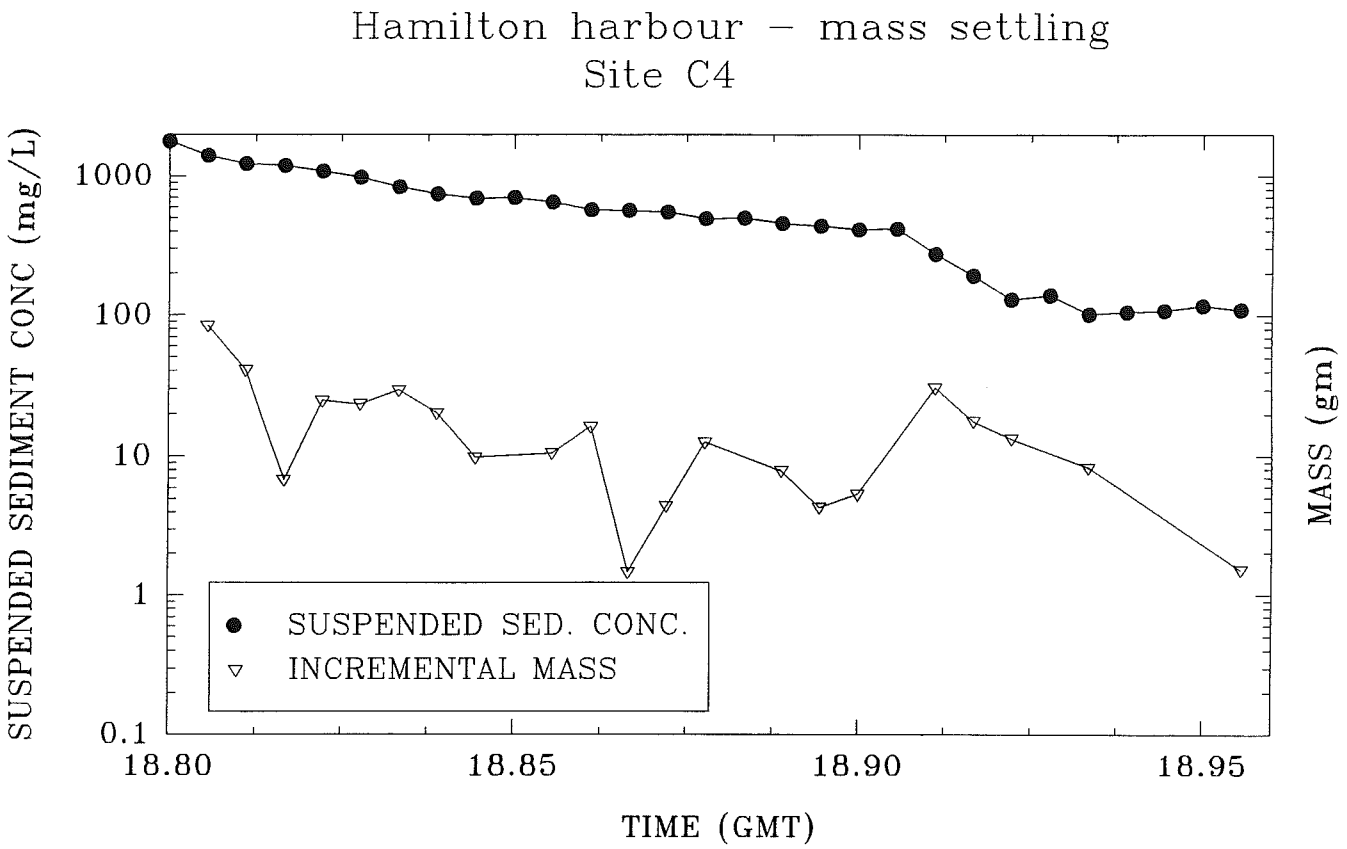

Figure 4.1.1.24 Mean S, incremental mass deposition, mass settling rates, and sedimentation diameter determined for the time-series of Sea Carousel from control site C4.

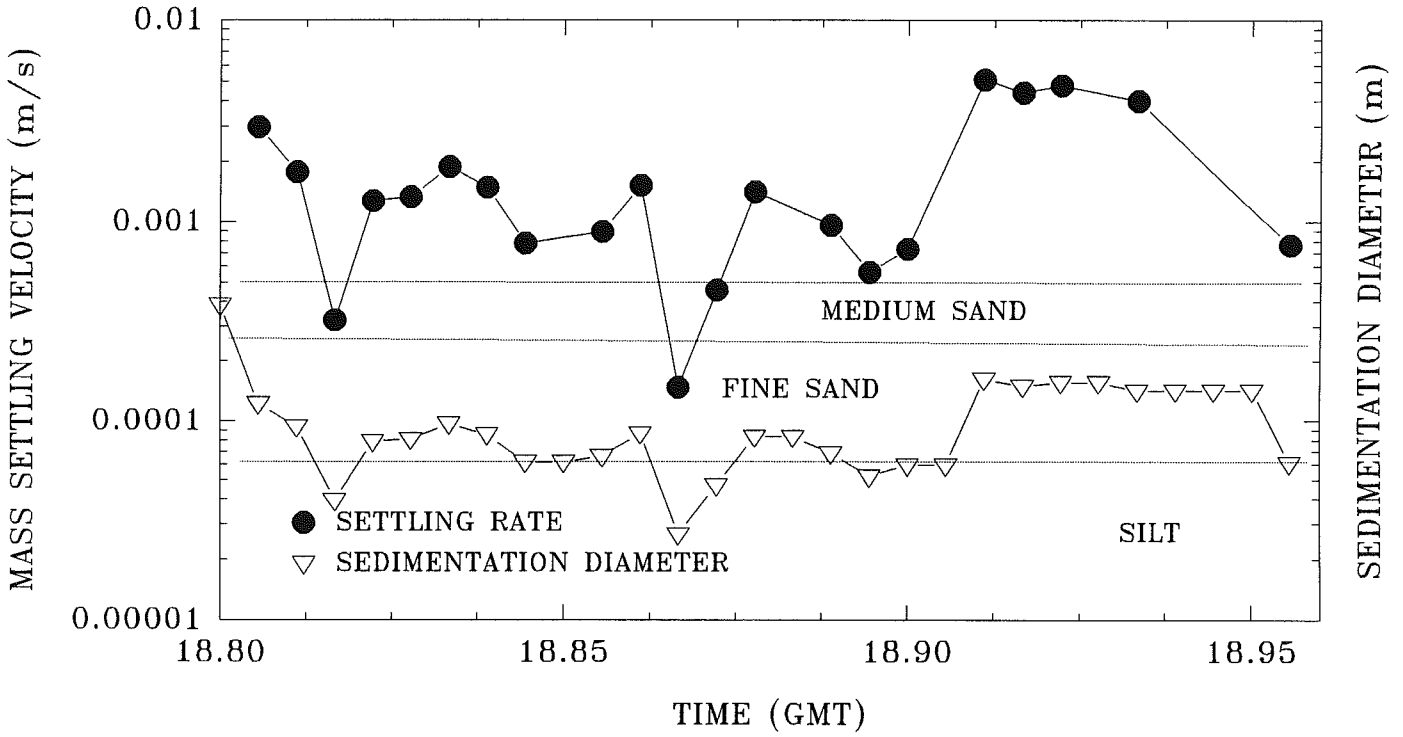

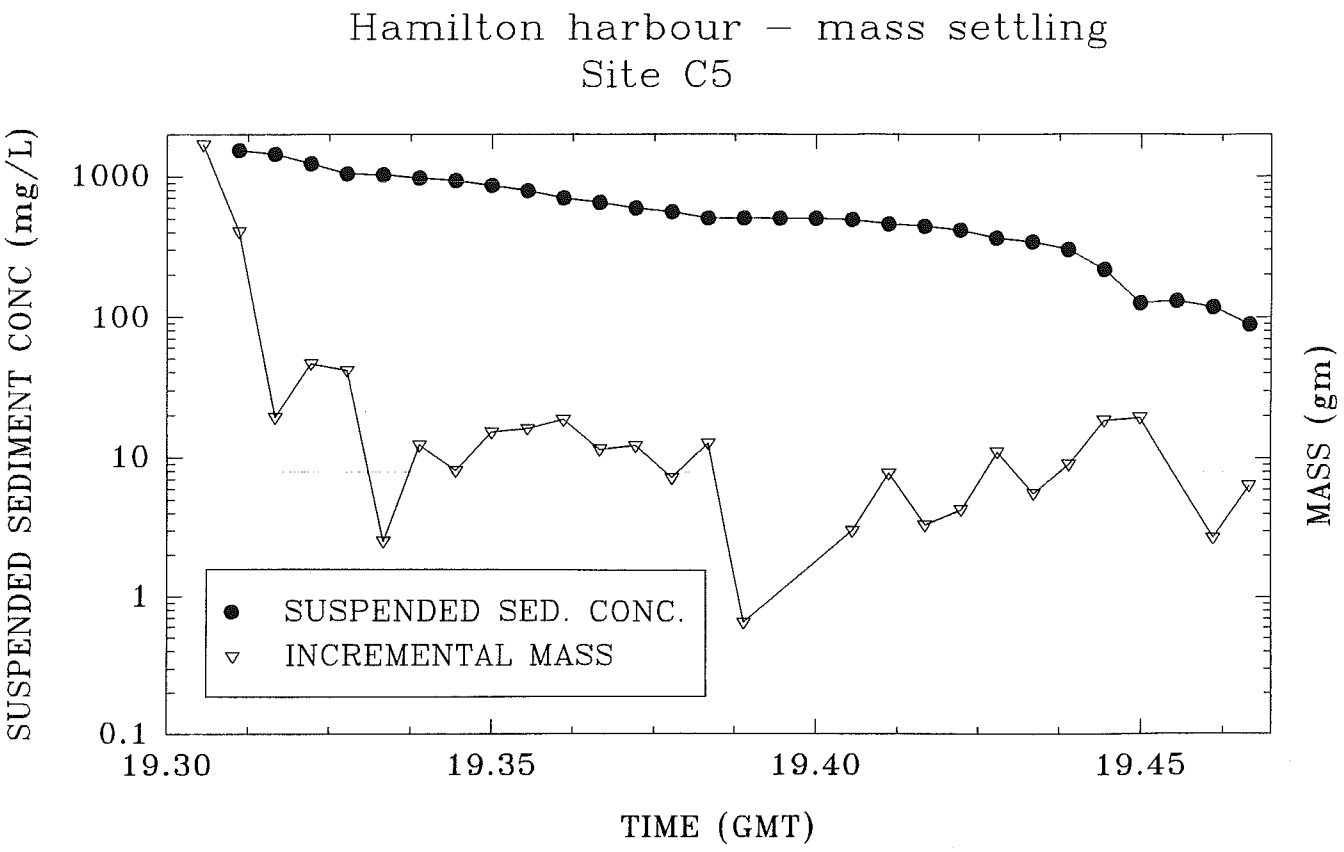

Figure 4.1.1.25 Mean S, incremental mass deposition, mass settling rates, and sedimentation diameter determined for the time-series of Sea Carousel from control site C5.

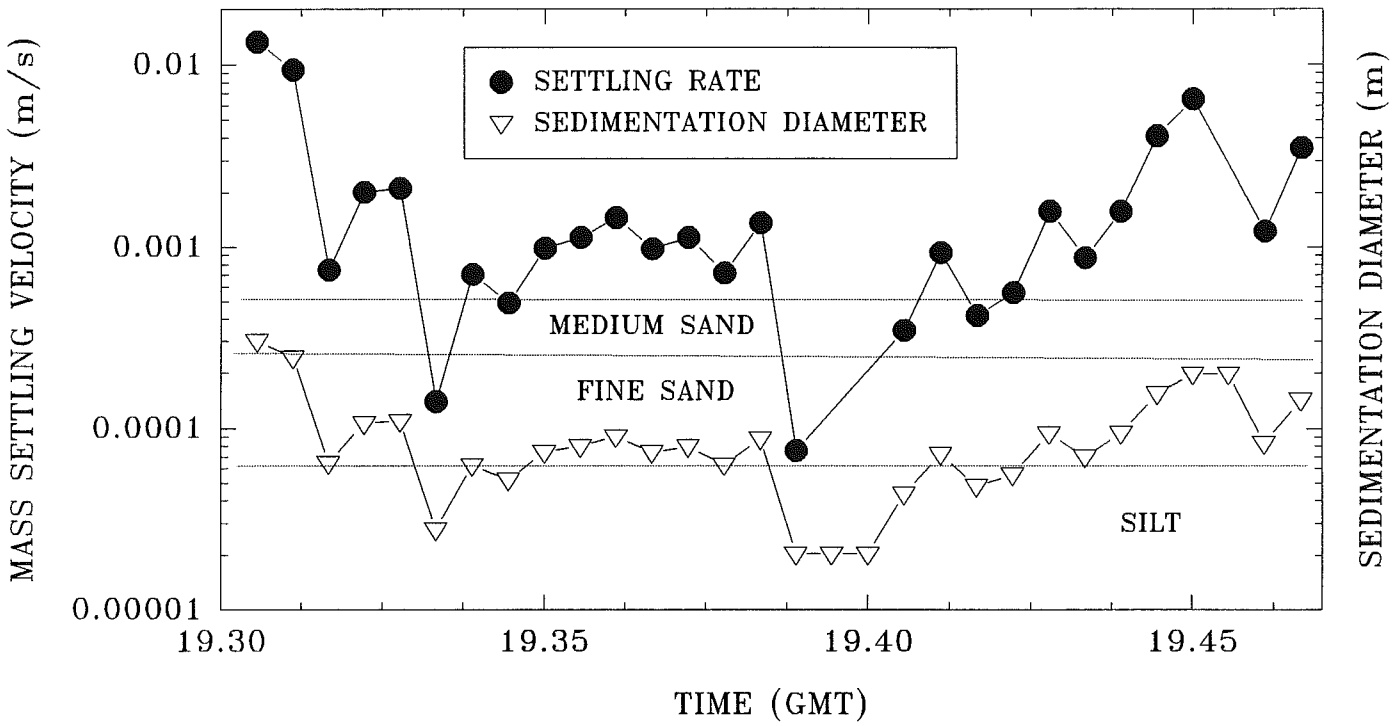

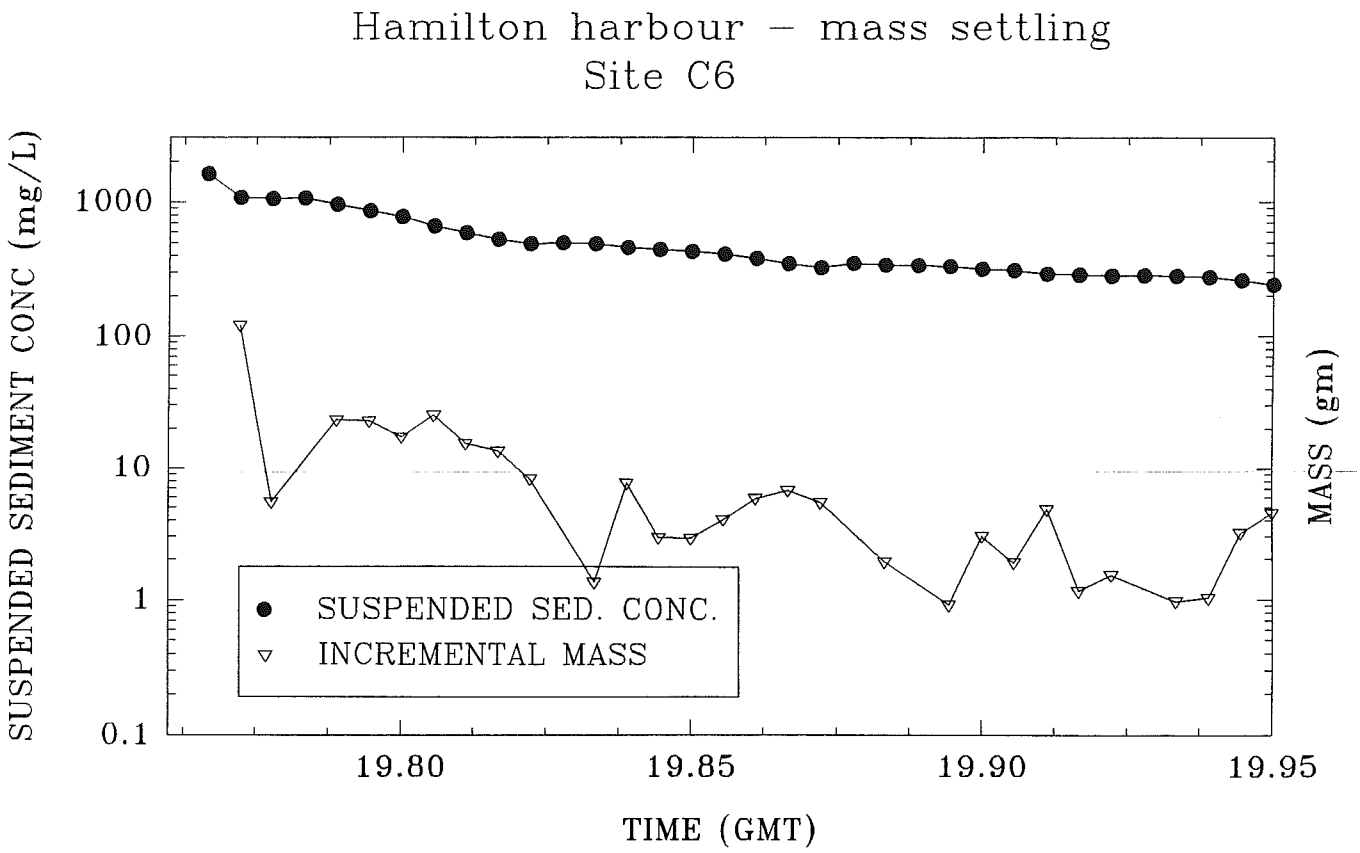

Figure 4.1.1.26 Mean S, incremental mass deposition, mass settling rates, and sedimentation diameter determined for the time-series of Sea Carousel from control site C6.

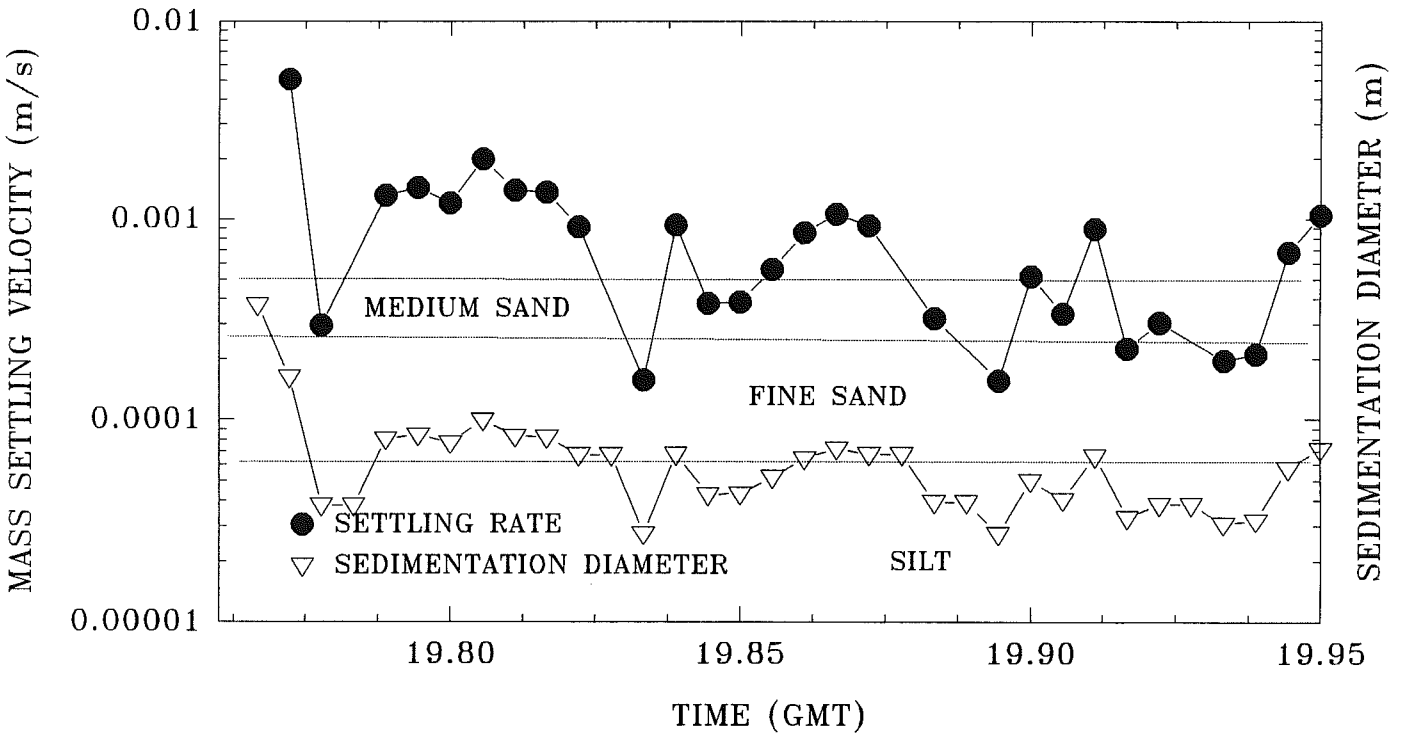

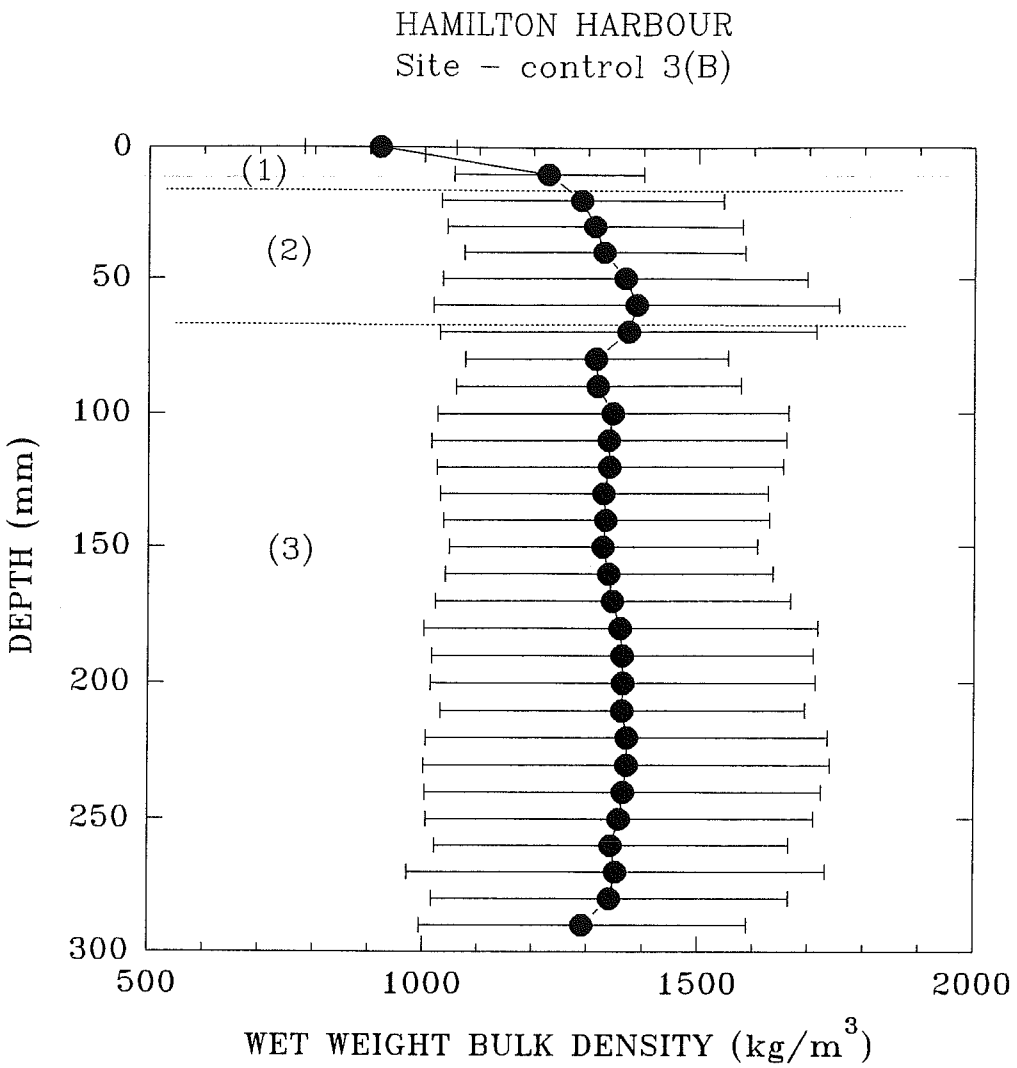

Figure 4.1.2.1 The wet bulk density of a push core taken from an Eckman grab sample from control site C3 determined from Catscan analysis. The core was 10 cm in diameter and 30 cm long. It was frozen slowly upon sampling and has not been corrected for either the effects of freezing or for gas expansion due to removal of hydrostatic pressure. The core depicts three layers: a surface layer of rapidly increasing density; an intermediate layer of transition; and a lower layer of almost constant density (1400 kg/m^3). The horizontal bars denote the scatter in density rather than error in the method.

Figure 4.1.4.1 Conventional optical microscopy micrographs: (A) ambient aggregates/floc remaining in the annulus of the Sea Carousel following the 10 minute initial still-water period; (B) an aggregate eroded from biostabilized surface layer at onset of erosion; and (C) rip-up aggregates eroded from below the biostabilized layer.

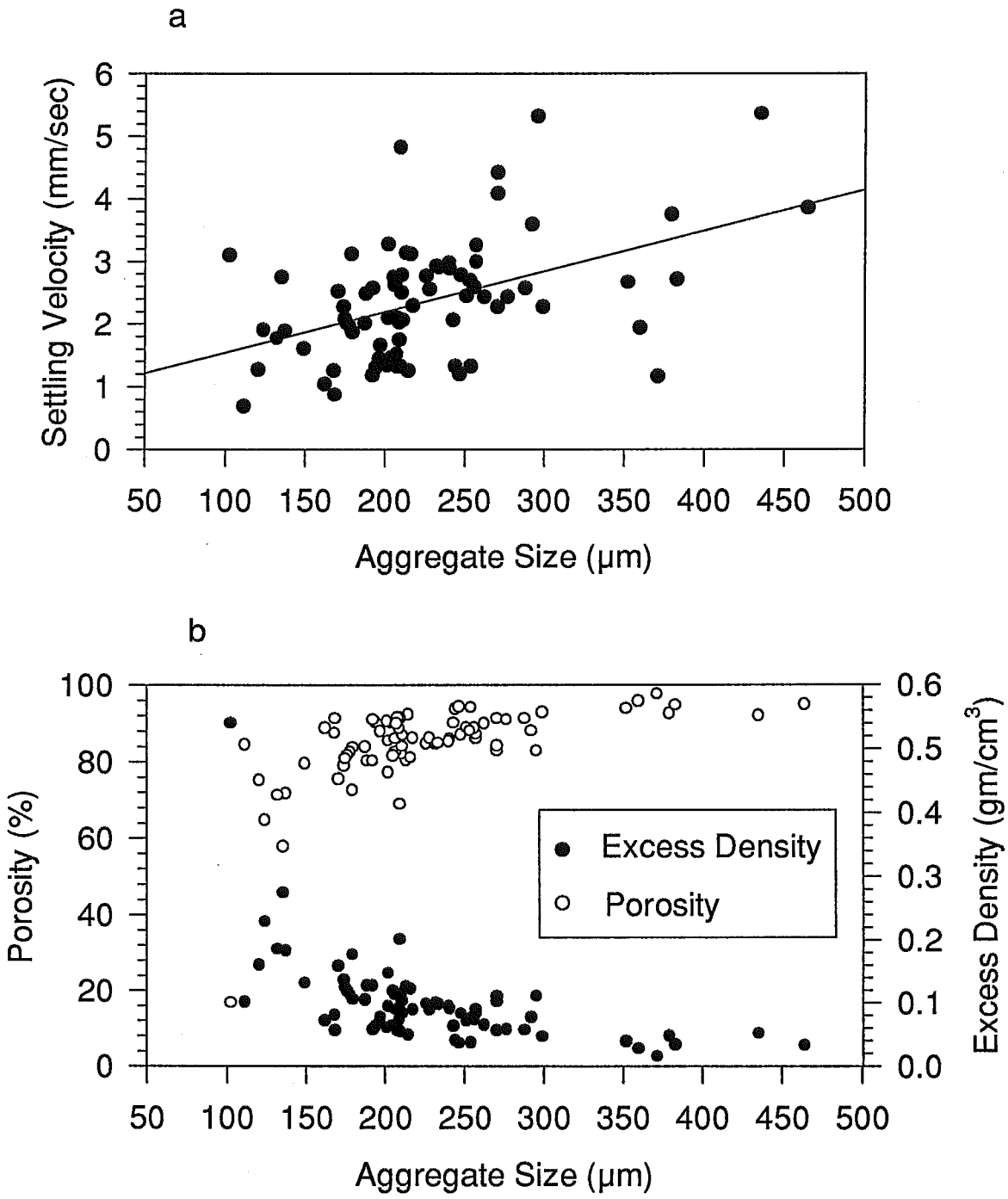

Figure 4.1.6.1. Example of the relationship of eroded aggregate size to (a) settling velocity, and (b) porosity and excess density (CP3: 10th speed increment).

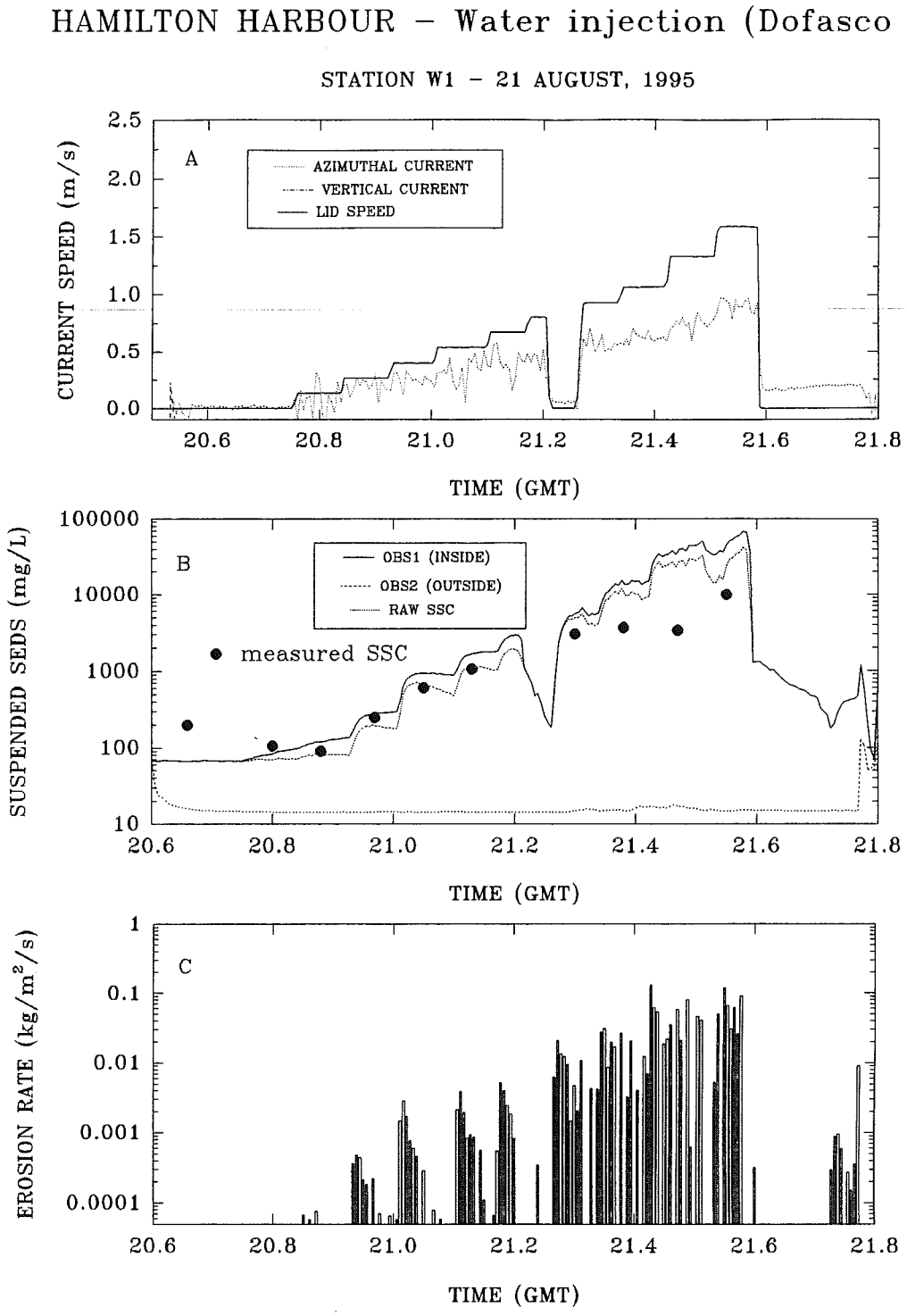

Figure 4.2.1.1 Time-series plots of the Sea Carousel deployment at the water-injection site W1. The brief period of interrupted flow was caused by an overheated power supply. The interruption did not appear to influence the results.

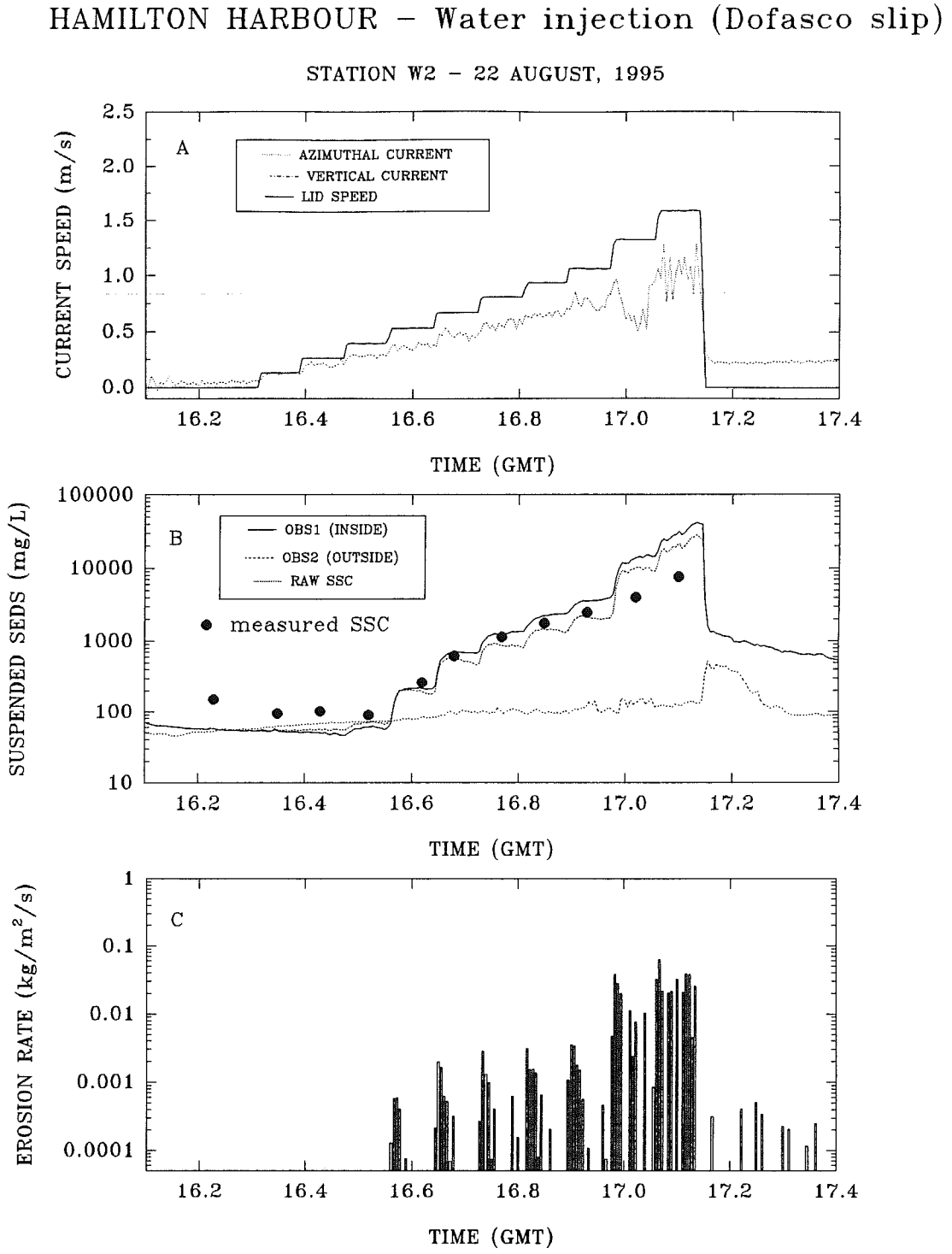

Figure 4.2.1.2 Time-series plots of the Sea Carousel deployment at the water-injection site W2.

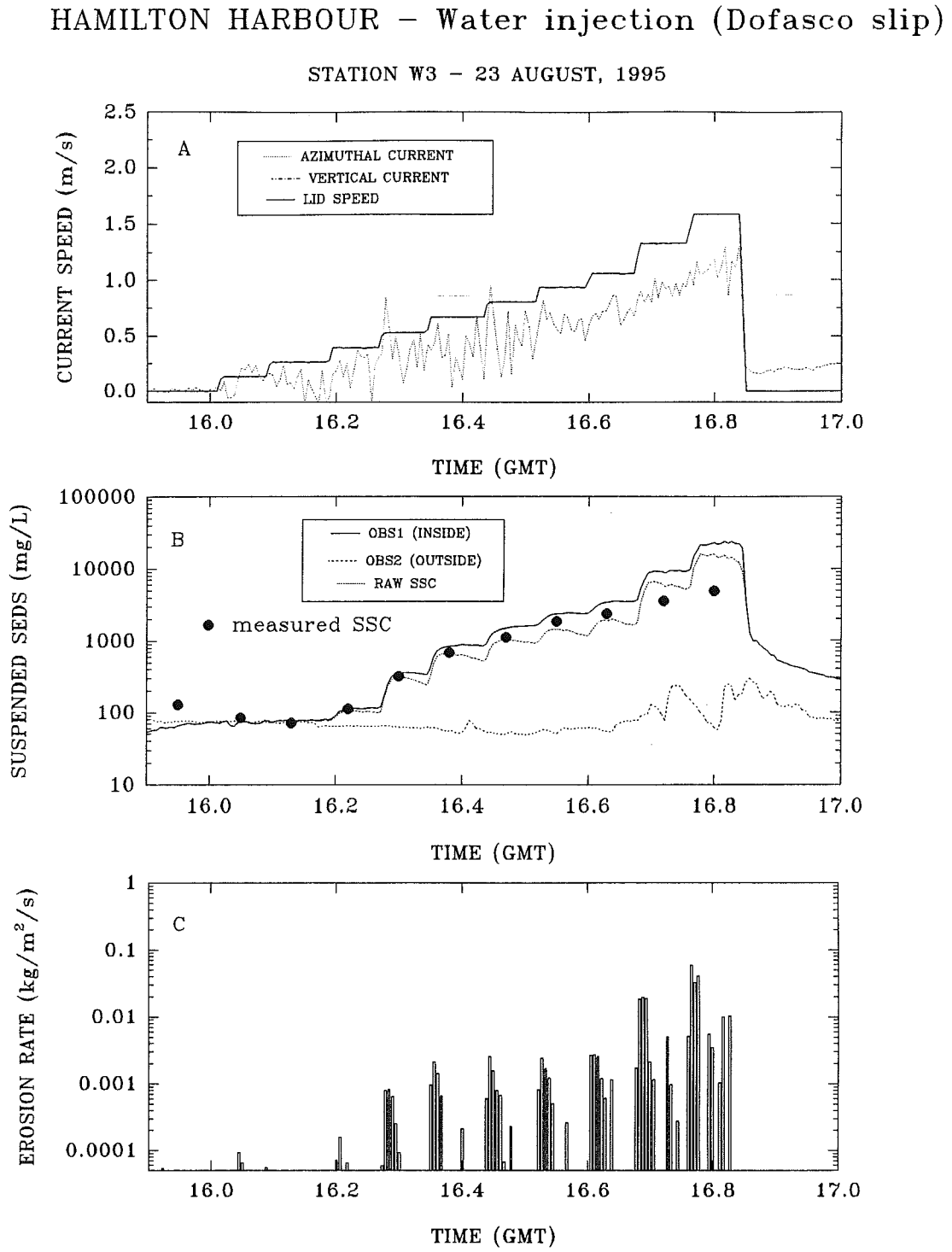

Figure 4.2.1.3 Time-series plots of the Sea Carousel deployment at the water-injection site W3.

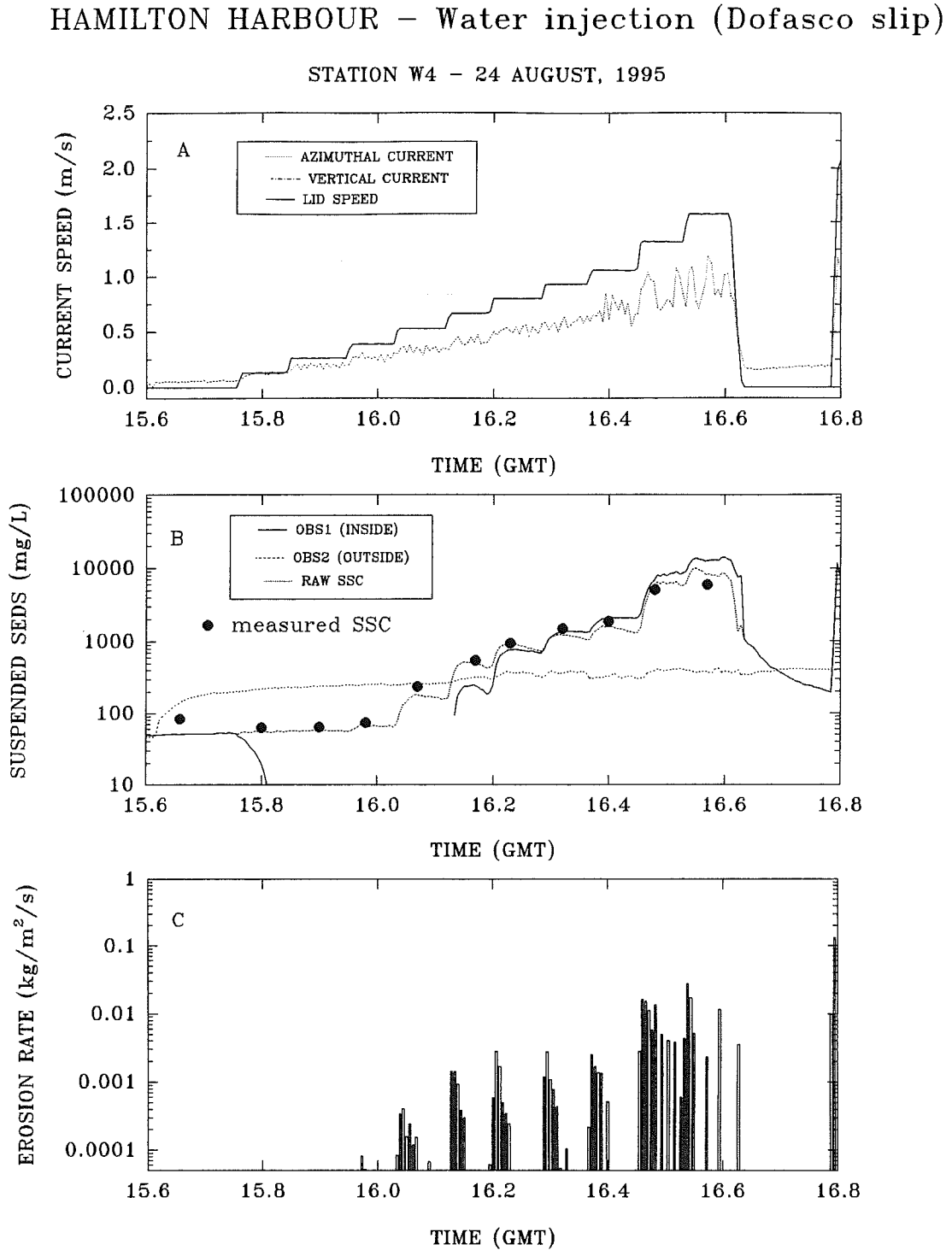

Figure 4.2.1.4 Time-series plots of the Sea Carousel deployment at the water-injection site W4.

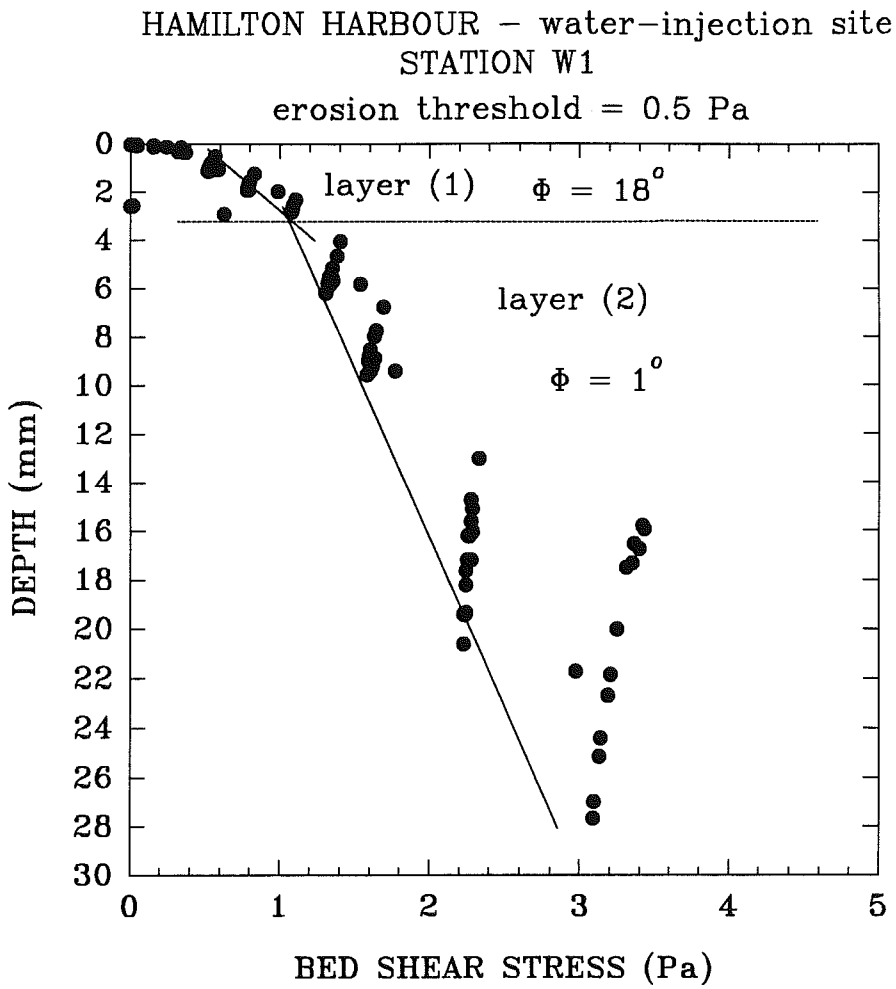

Figure 4.2.1.5 A synthetic core plot of water-injection site W1. The plot shows two layers of increasing strength with depth. The friction coefficients are very low indicating that consolidation is not well advanced. The high surface gradient is suggestive of biostabilization.

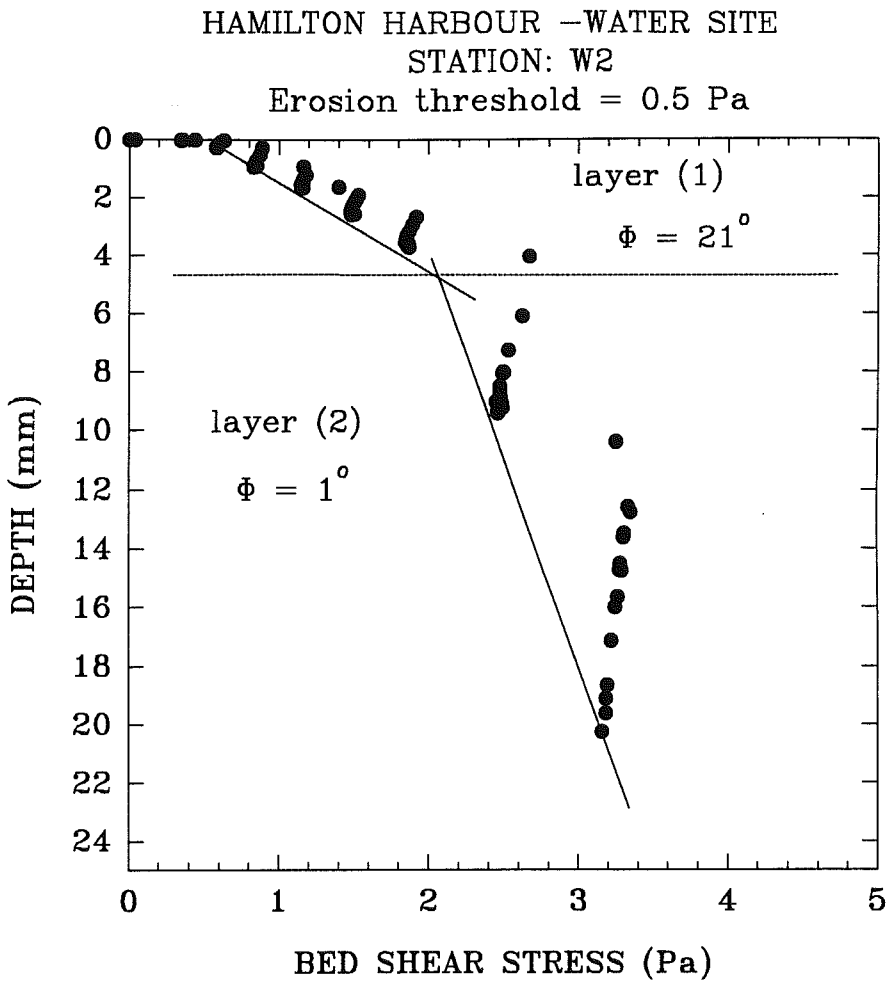

Figure 4.2.1.6 A synthetic core plot of water-injection site W2. The surface 3 mm of this site appears distinct from the underlying material and may be related to biological activity.

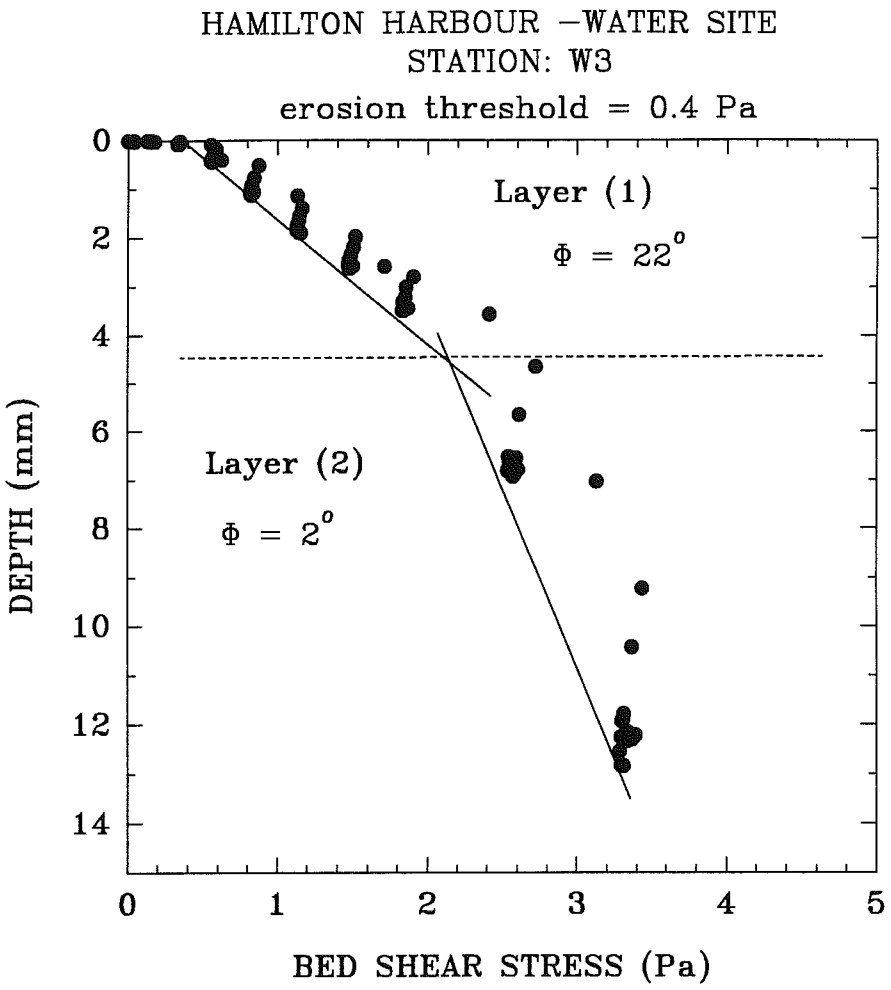

Figure 4.2.1.7 A synthetic core plot of water-injection site W3.

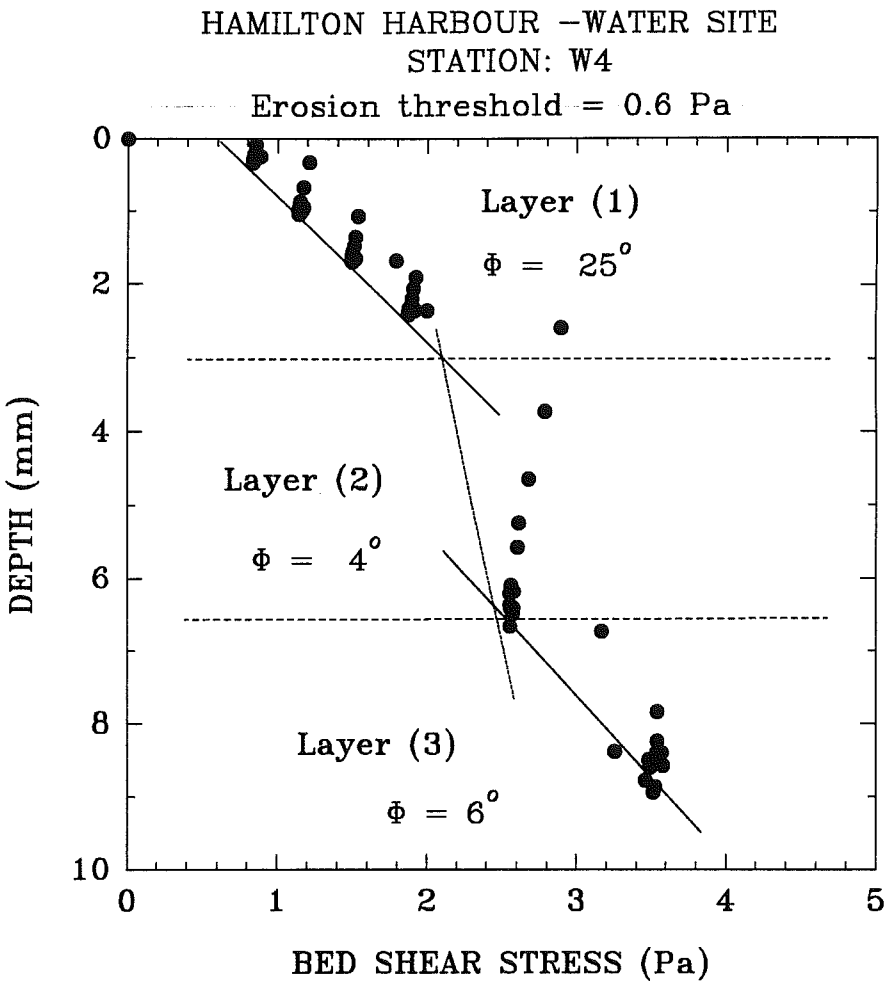

Figure 4.2.1.8 A synthetic core plot of water-injection site W4.

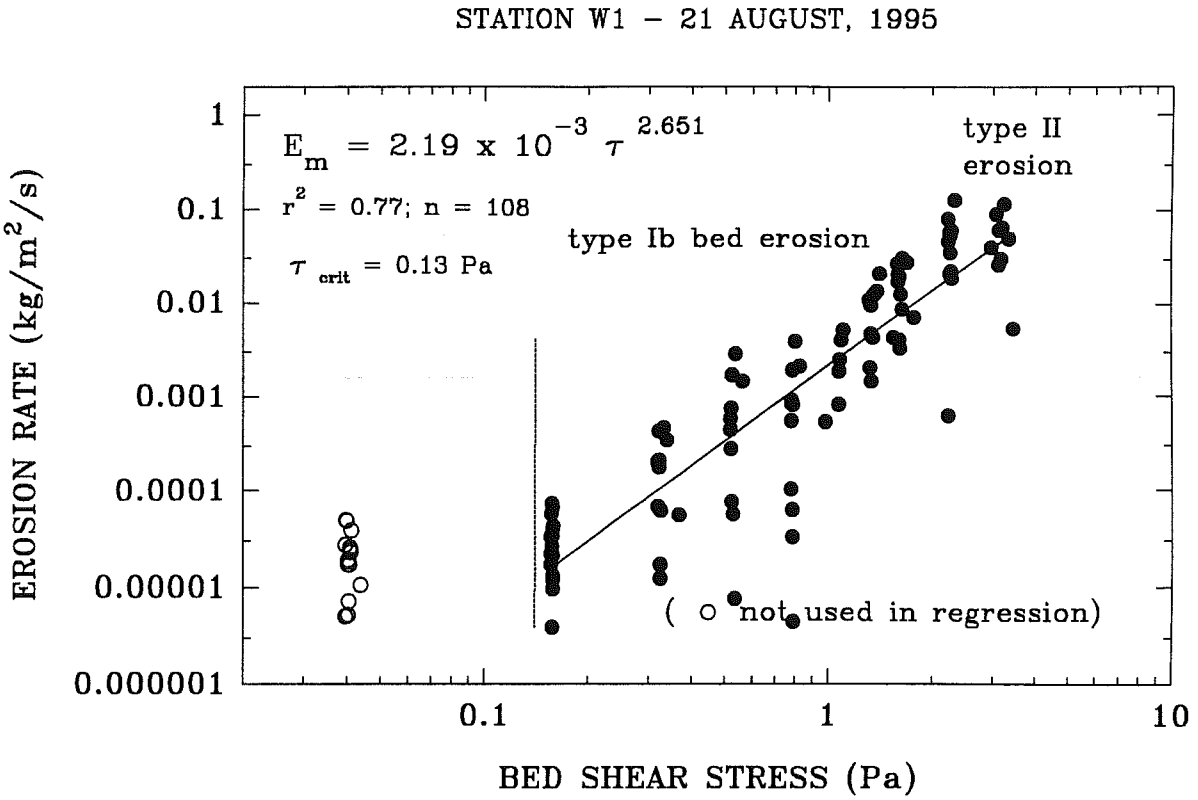

Figure 4.2.1.9 Measured erosion rate (A) and S (B) plotted against applied bed shear stress for water injection site W1.

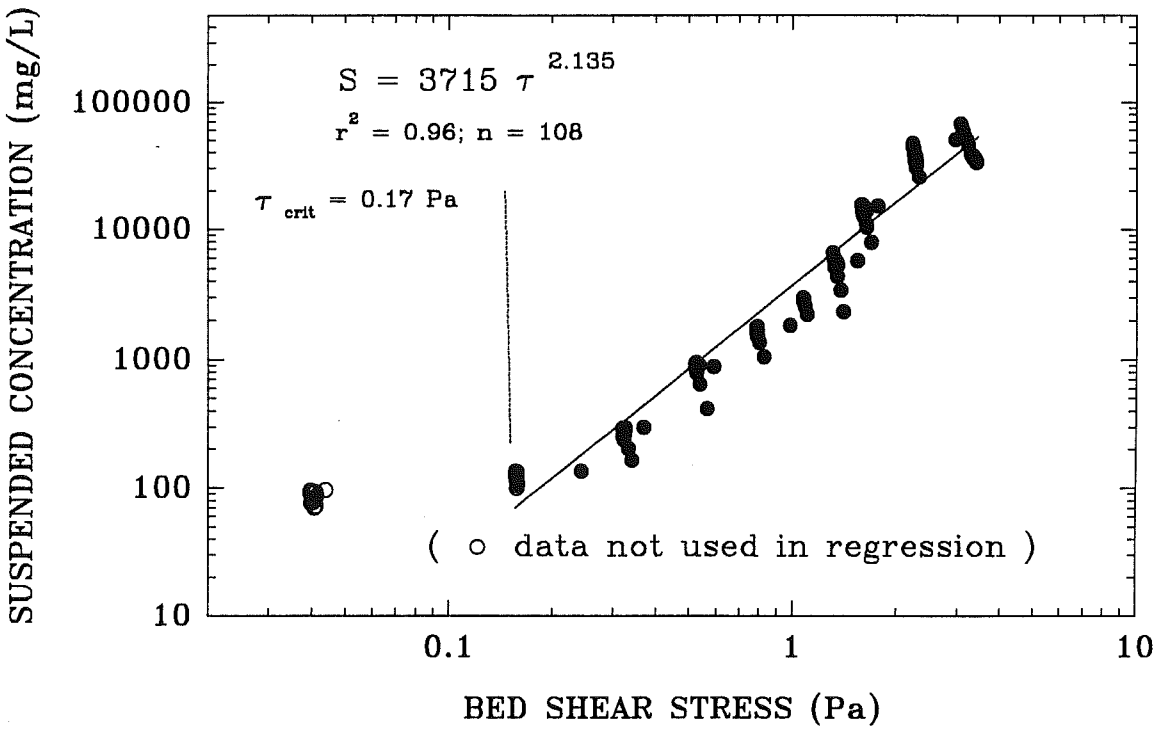

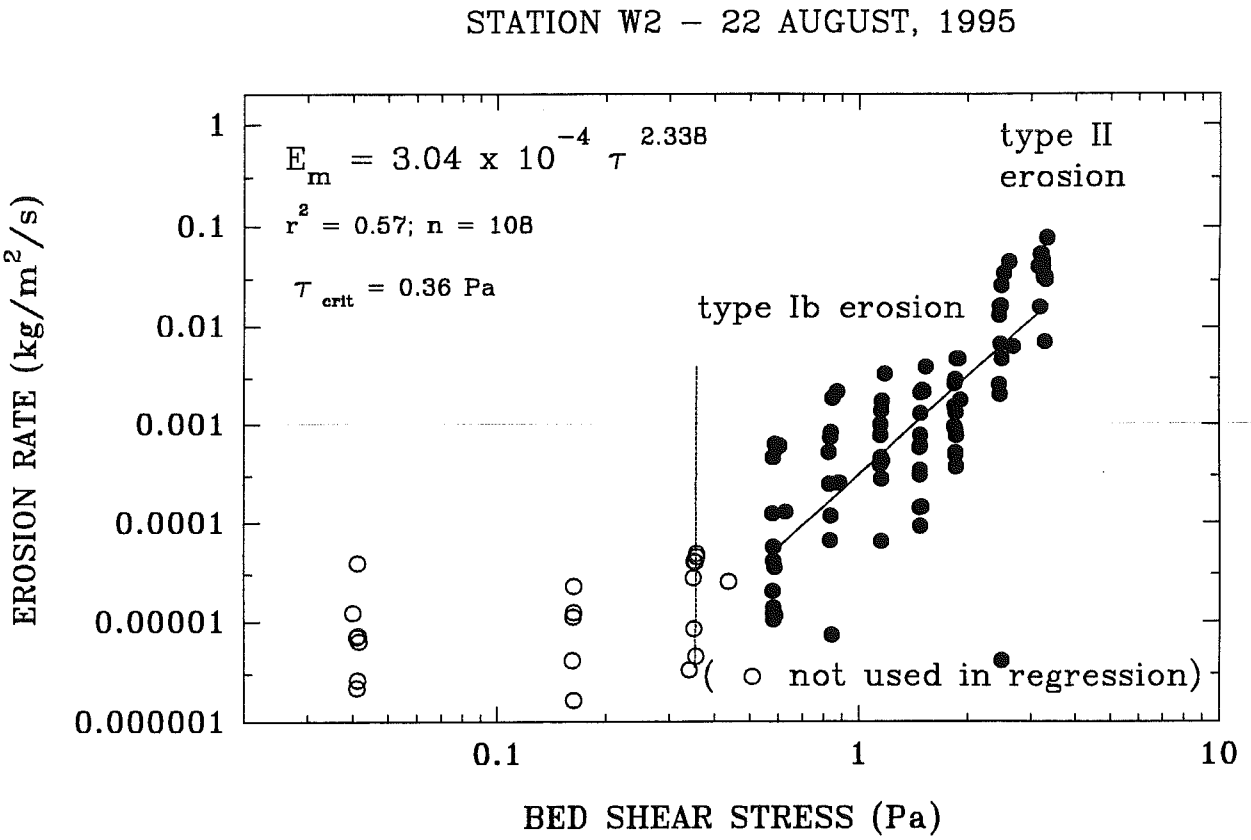

Figure 4.2.1.10 Measured erosion rate (A) and S (B) plotted against applied bed shear stress for water injected site W2.

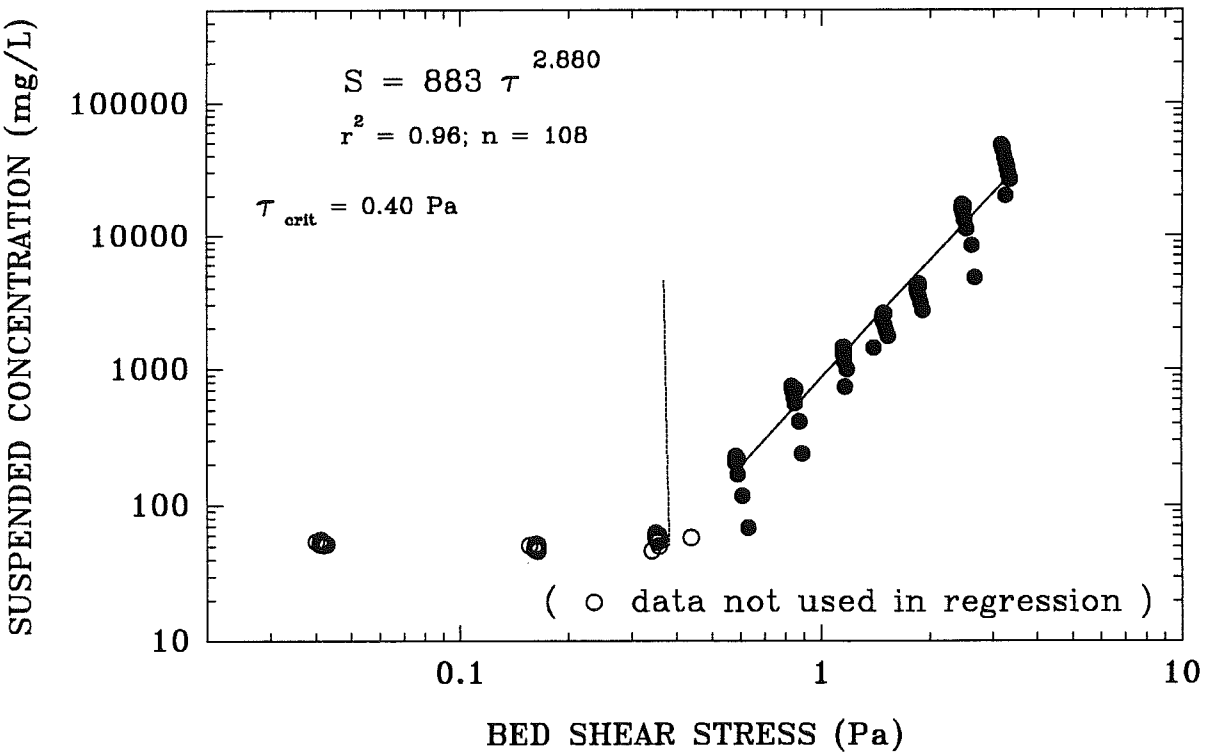

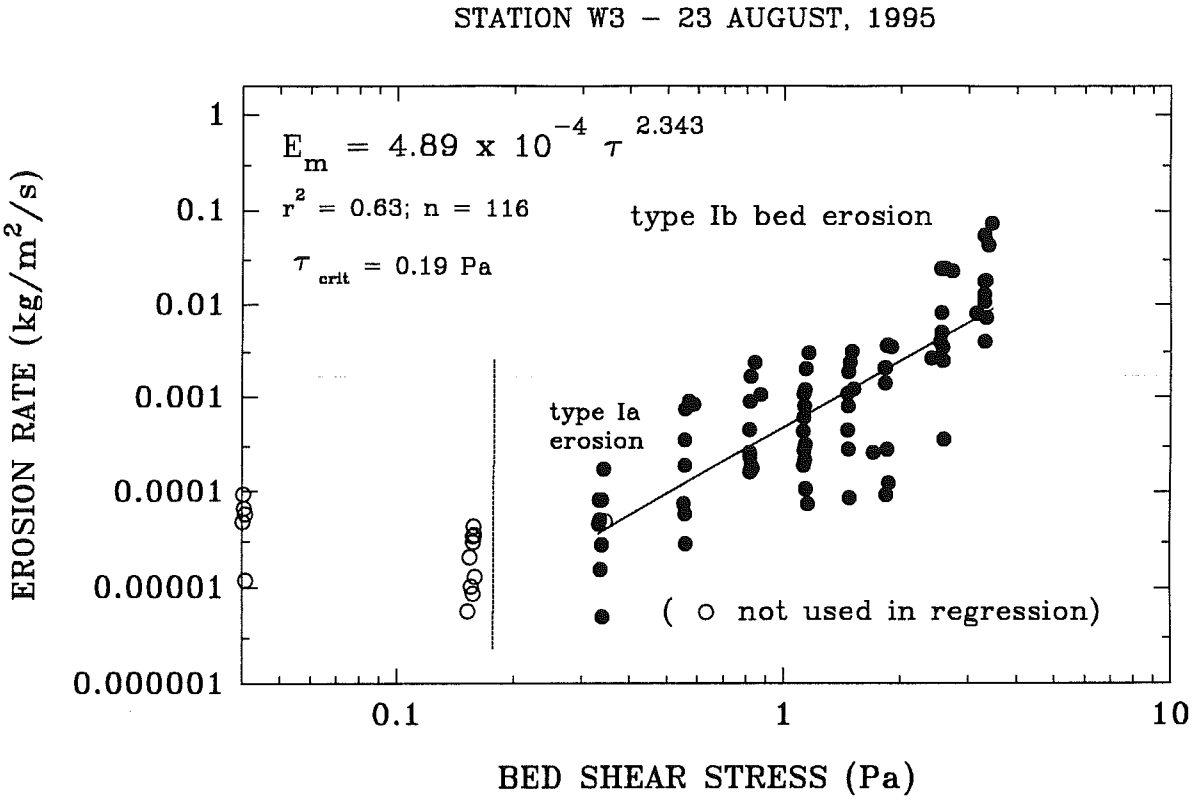

Figure 4.2.1.11 Measured erosion rate (A) and S (B) plotted against applied bed shear stress for water injected site W3.

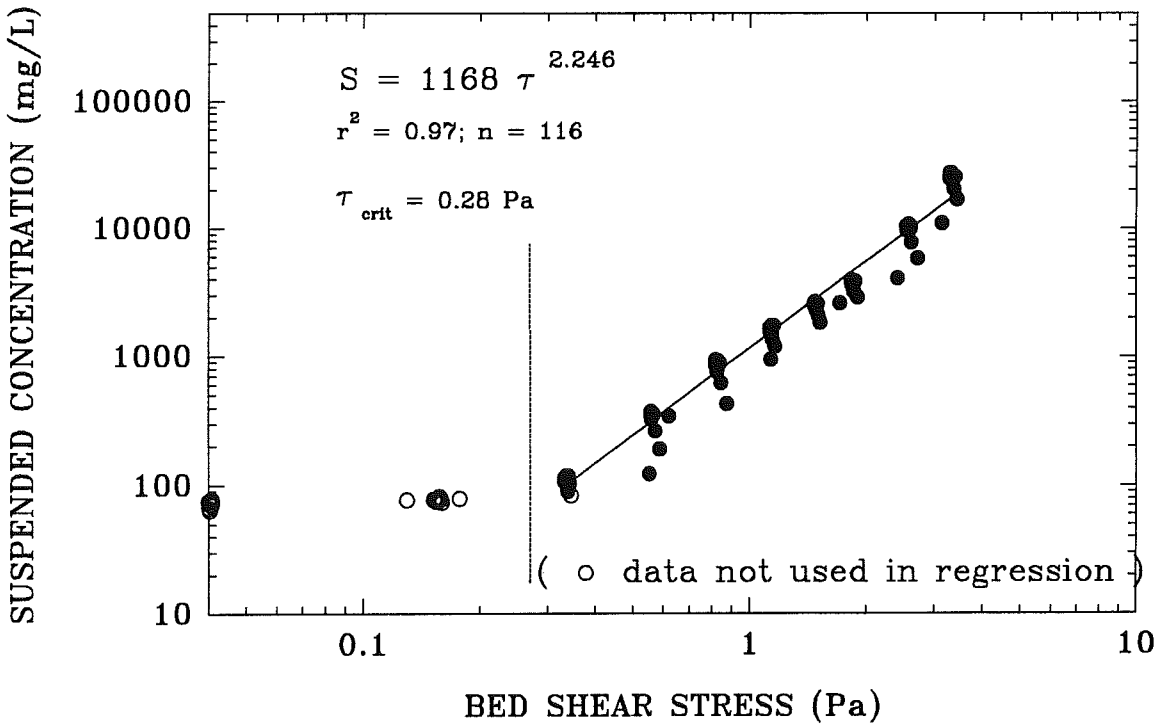

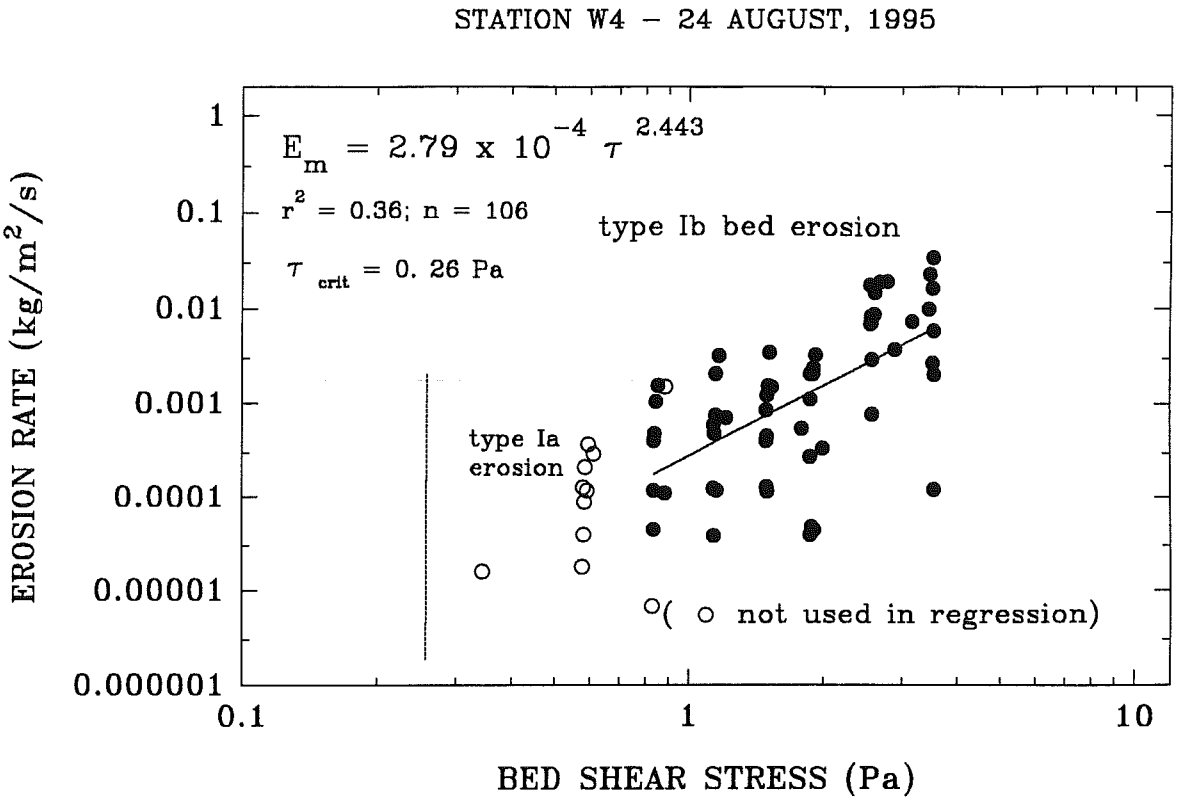

Figure 4.2.1.12 Measured erosion rate (A) and S (B) plotted against applied bed shear stress for water-injected site W4.

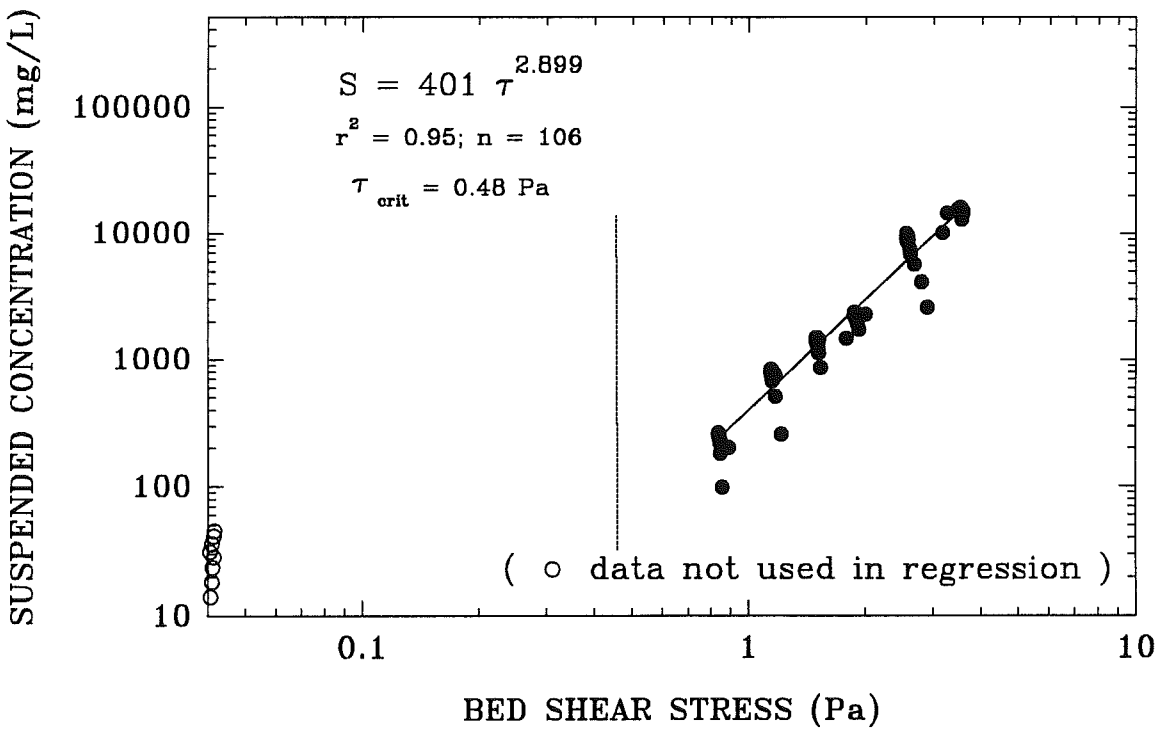

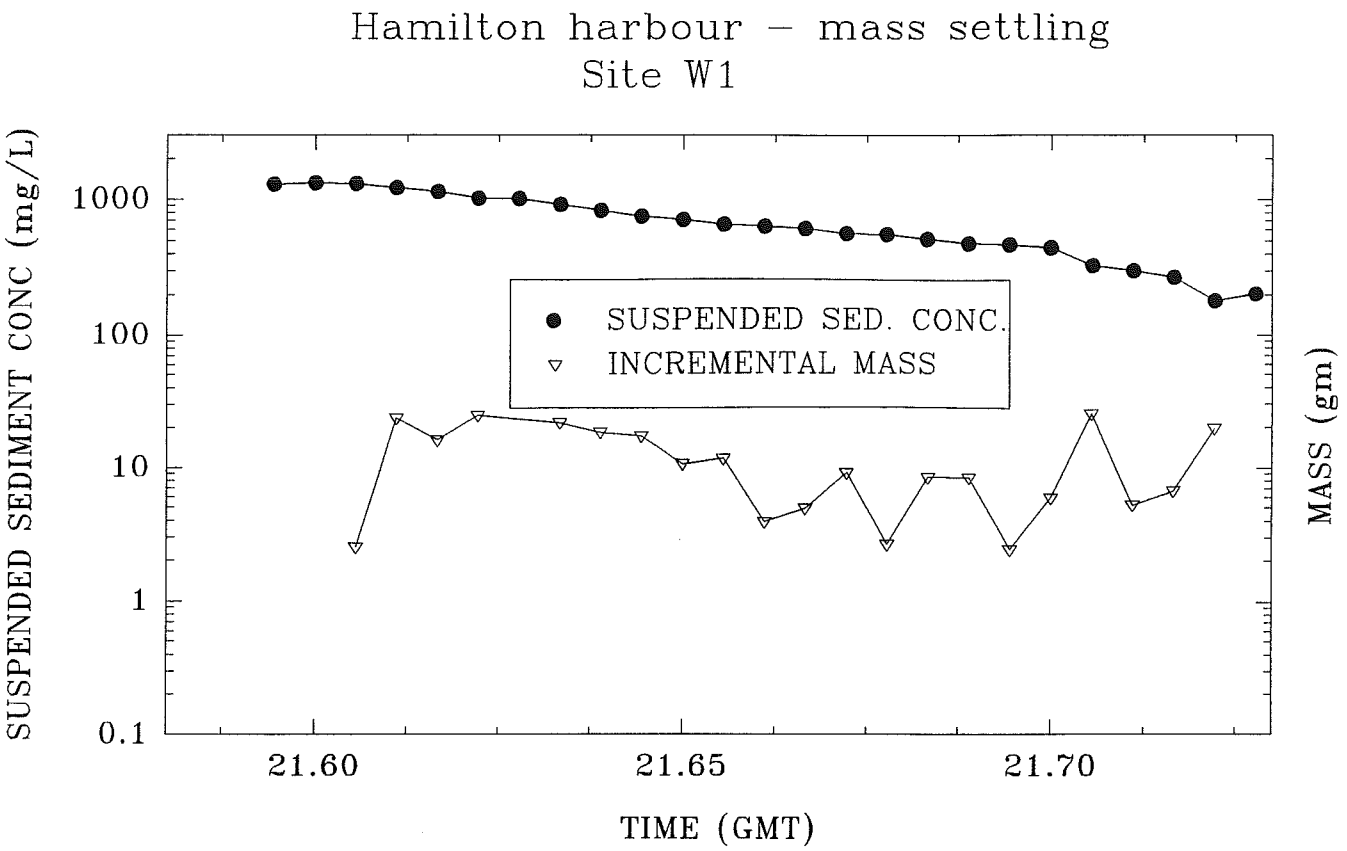

Figure 4.2.1.13 Mean S, incremental mass deposition, mass settling rates, and sedimentation diameter determined for the time-series of Sea Carousel from water-injection site W1. The sedimentation diameter is largely fine sand, though no segregation of size is evident with time.

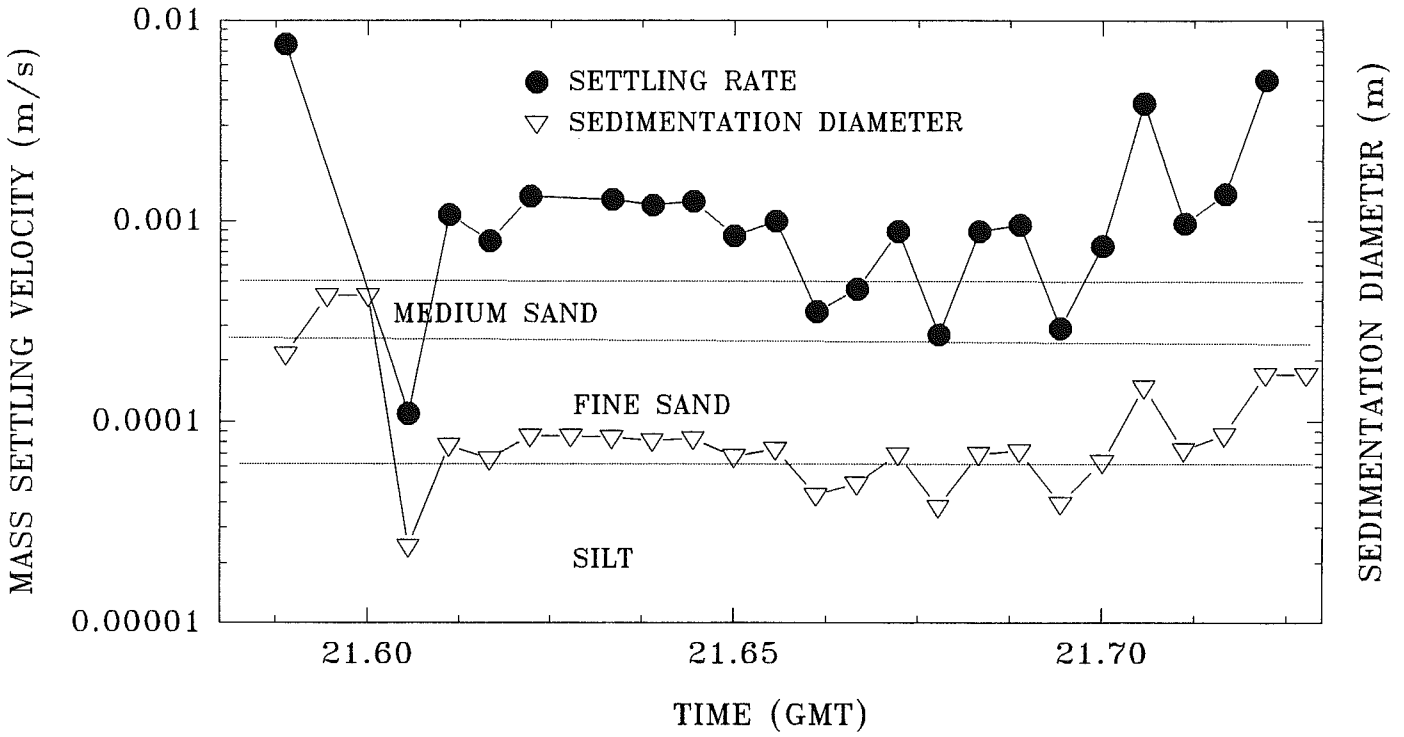

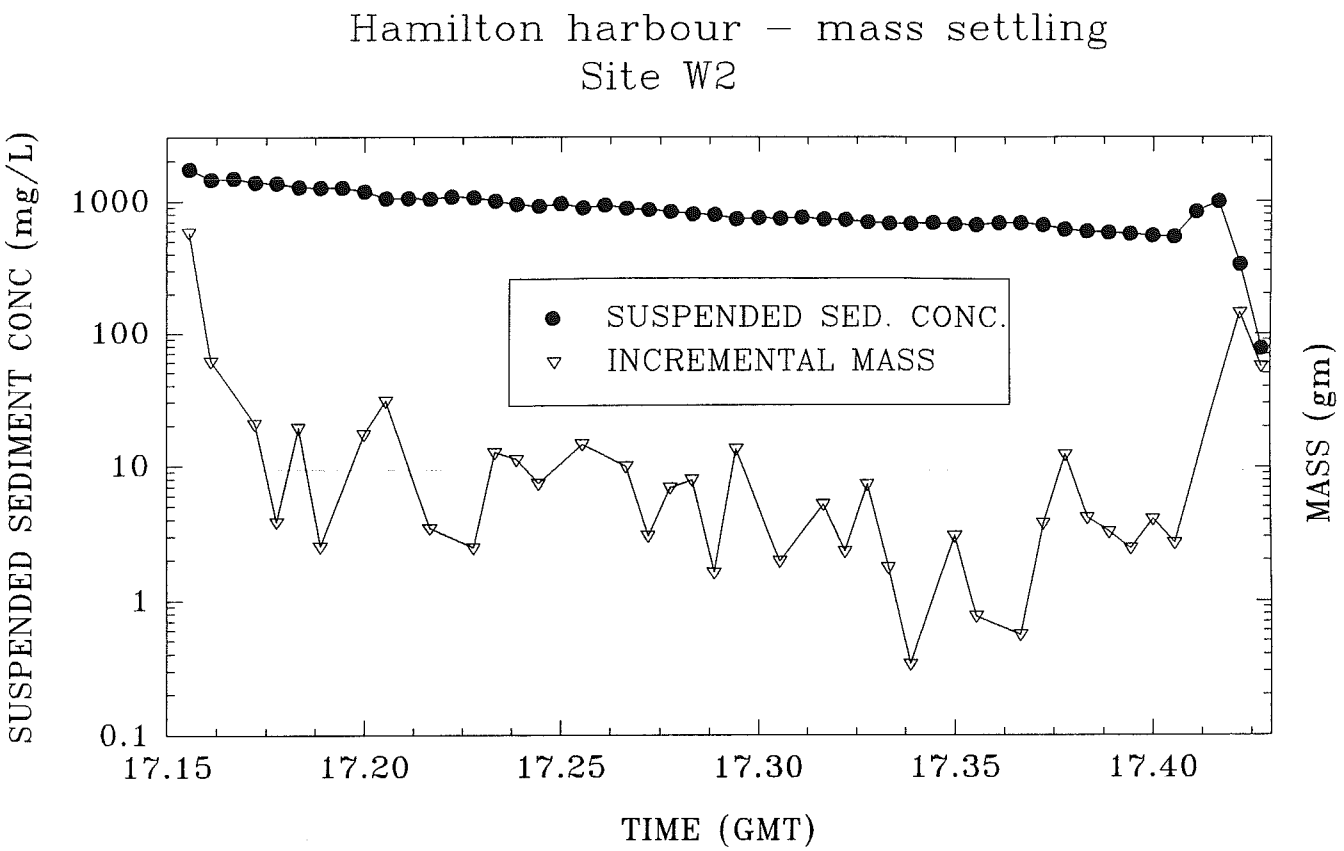

Figure 4.2.1.14 Mean S, incremental mass deposition, mass settling rates, and sedimentation diameter determined for the time-series of Sea Carousel from water-injection site W2. The sedimentation diameter in this case is largely coarse silt.

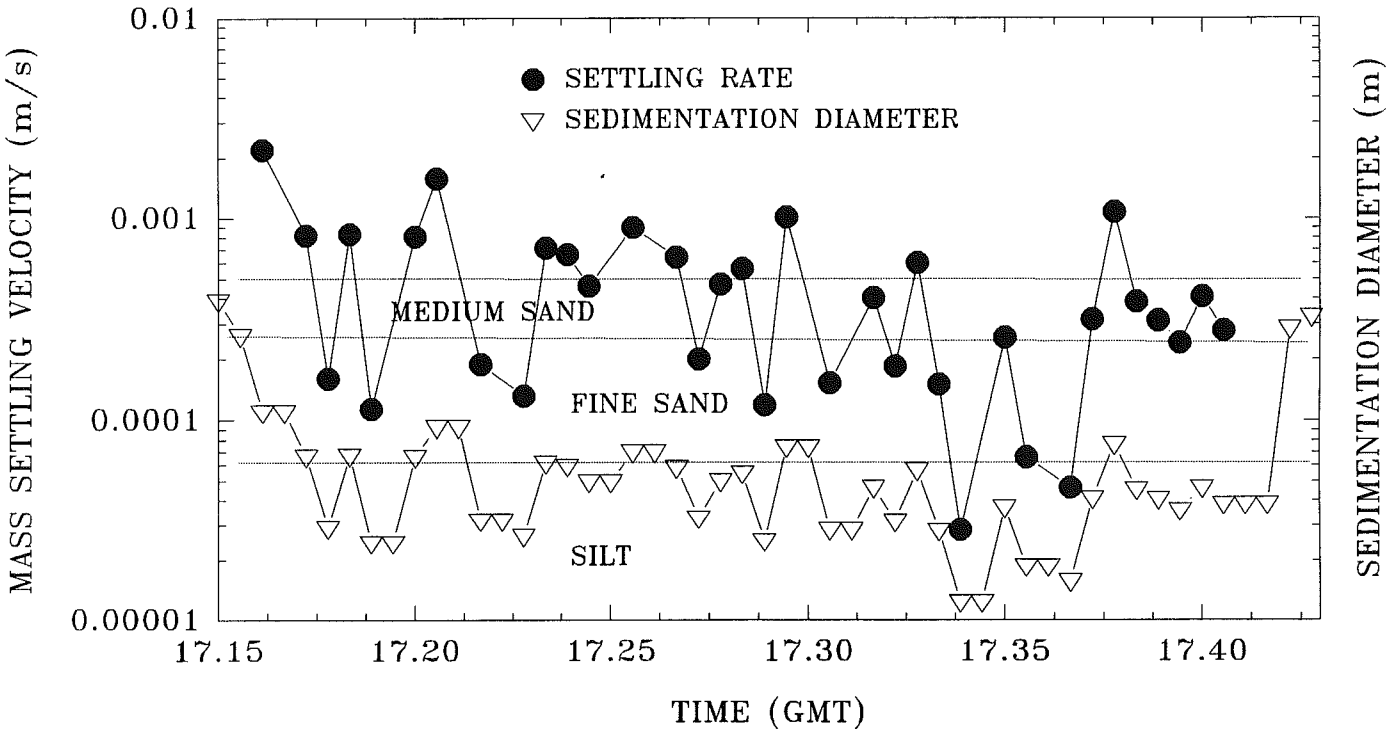

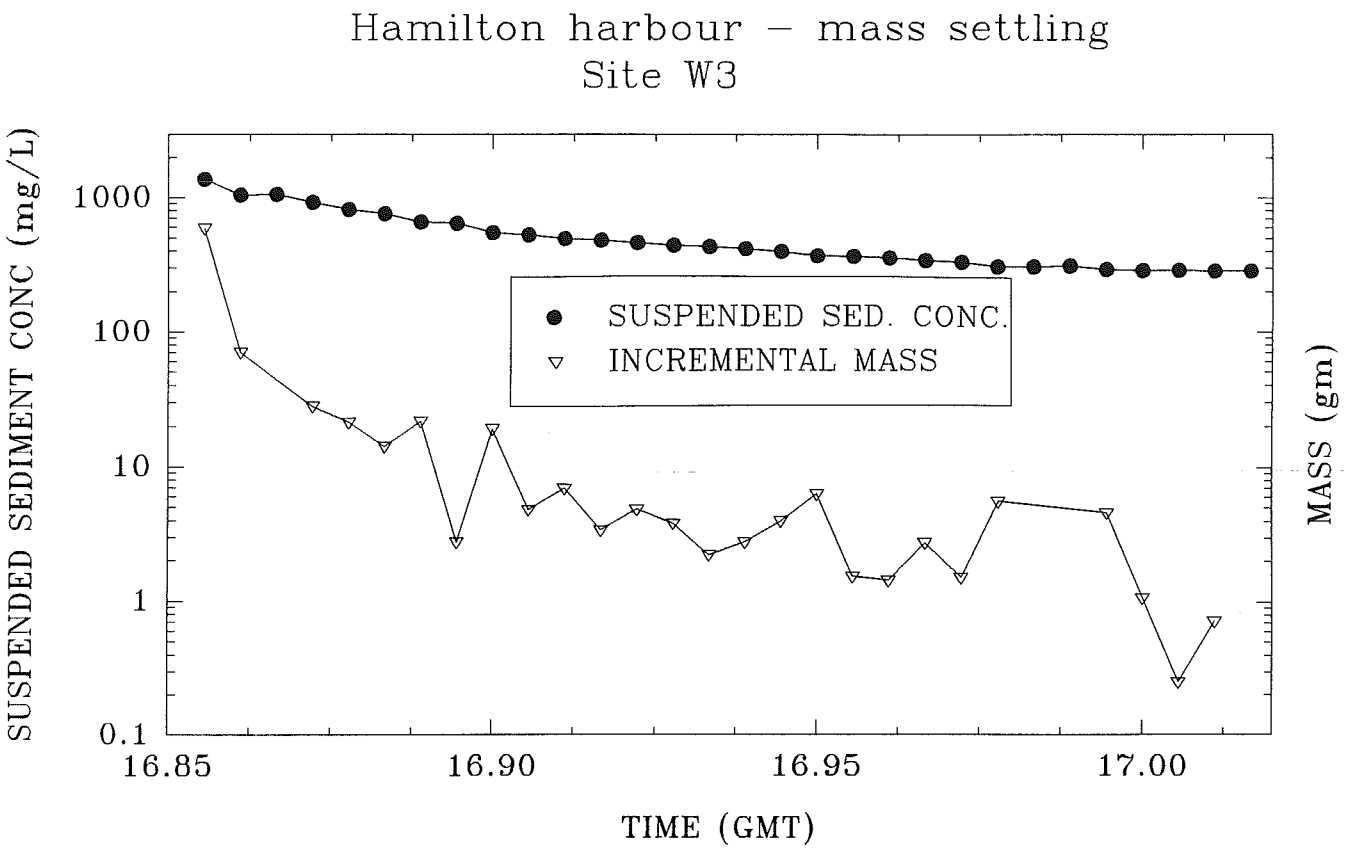

Figure 4.2.1.15 Mean S, incremental mass deposition, mass settling rates, and sedimentation diameter determined for the time-series of Sea Carousel from water-injection site W3. A distinct decrease in settling velocity and sedimentation diameter is evident which is diagnostic of sorting.

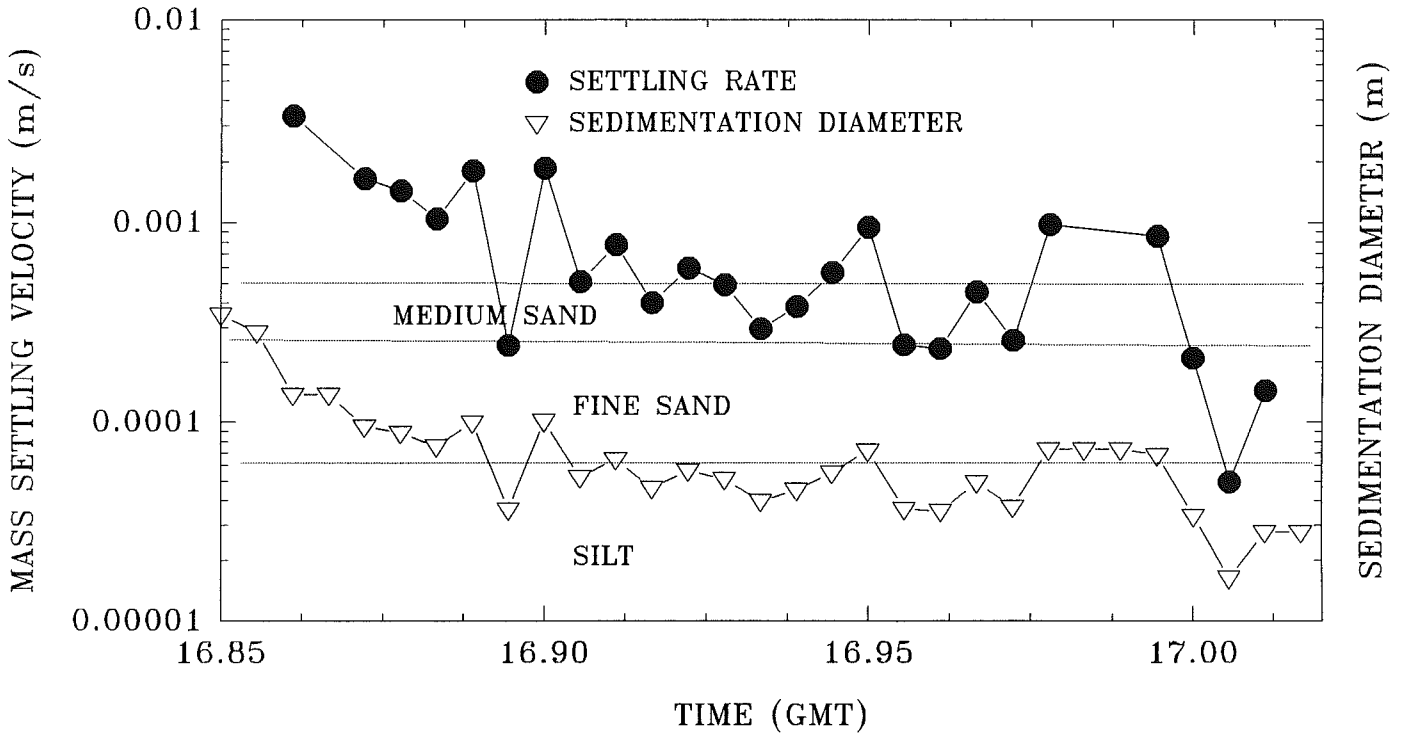

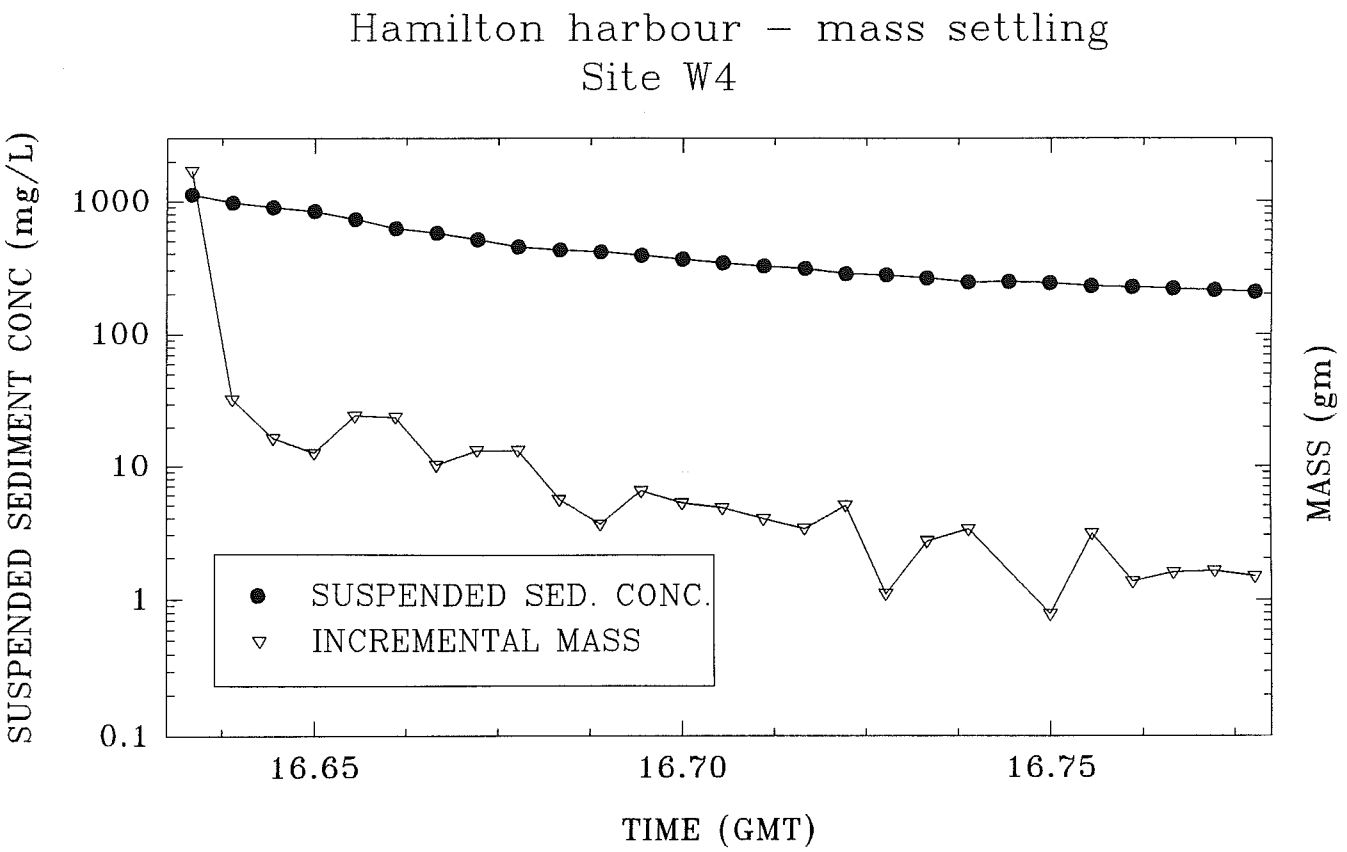

Figure 4.2.1.16 Mean S, incremental mass deposition, mass settling rates, and sedimentation diameter determined for the time-series of Sea Carousel from water-injection site W4.

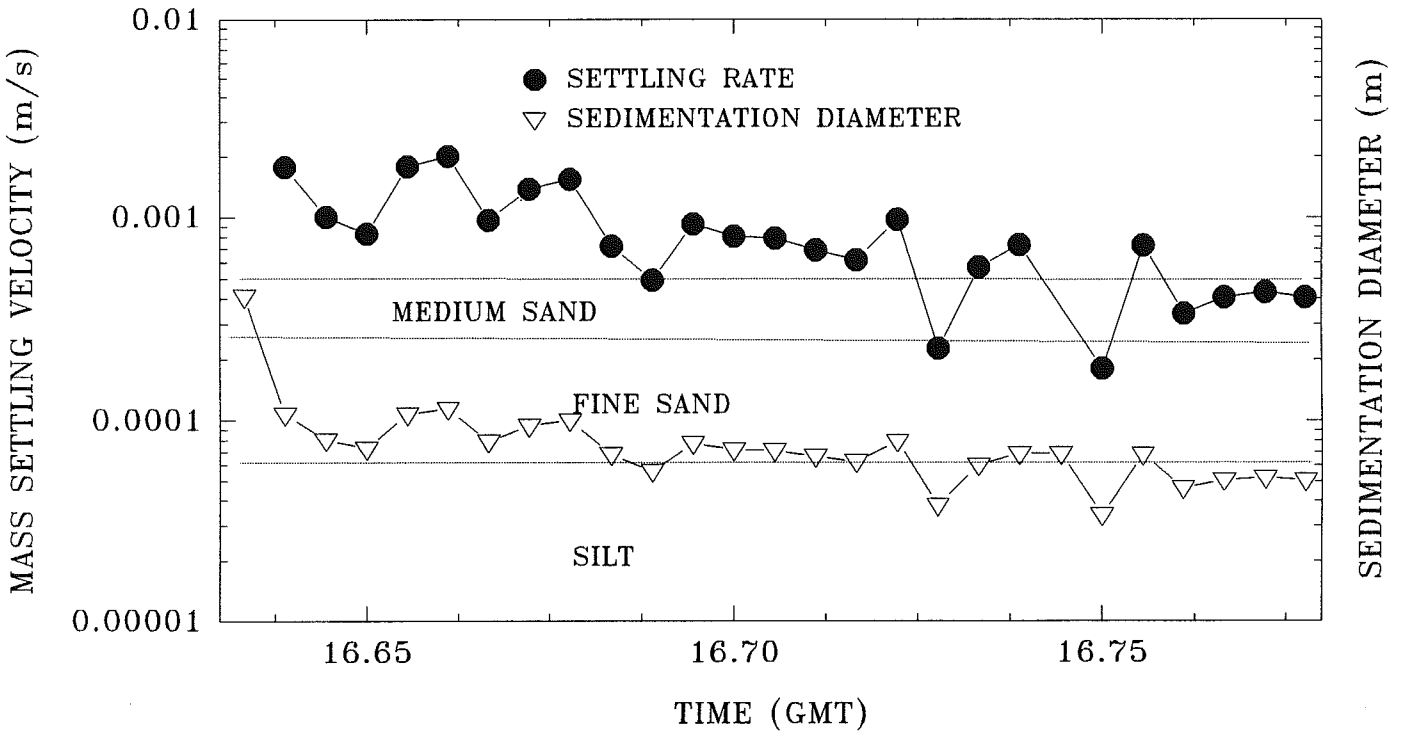

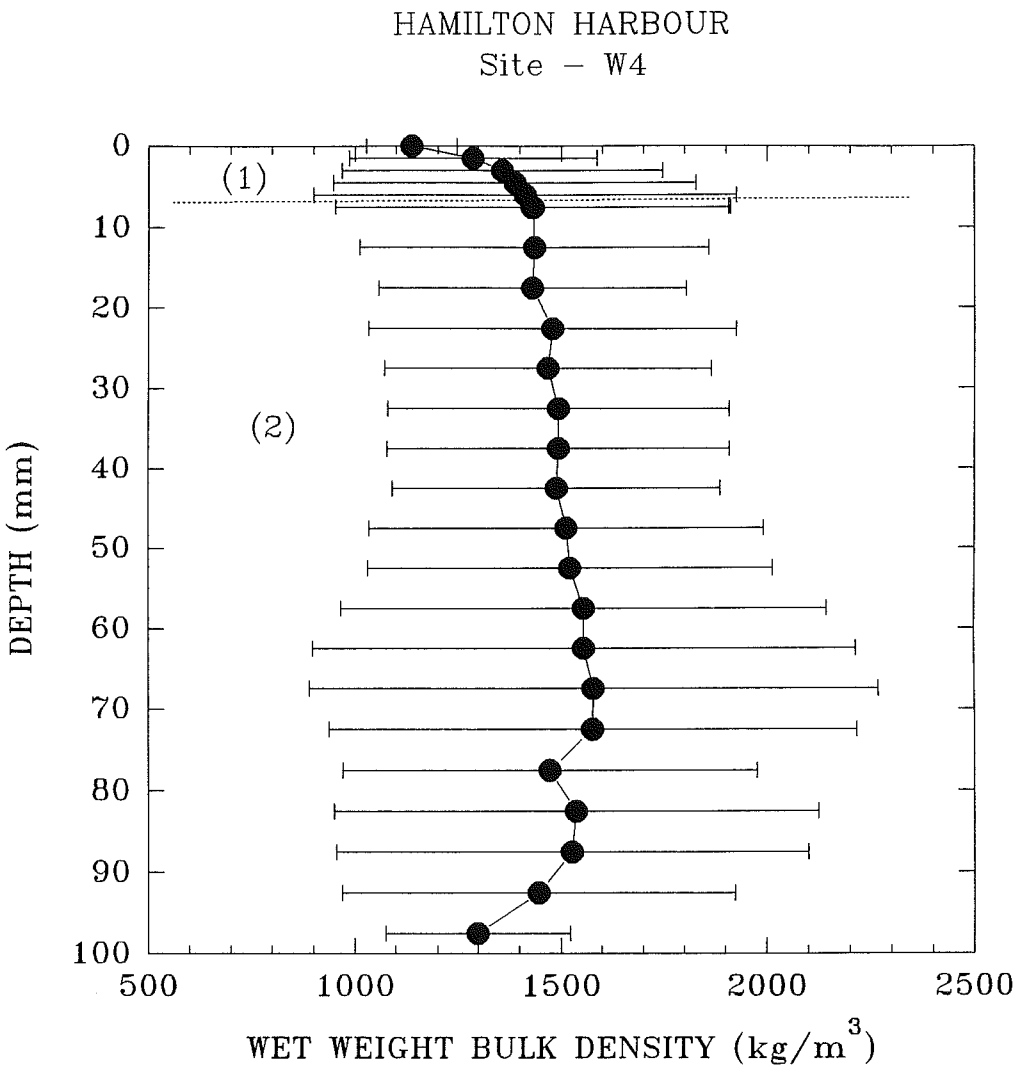

Figure 4.2.2.1 A profile of wet bulk density of a push core (10 cm diameter) taken at water-injection site W4. The core shows a surface layer (5 mm thick) of rapidly increasing density and a substrate of constant density (around 1500 kg/m^3).

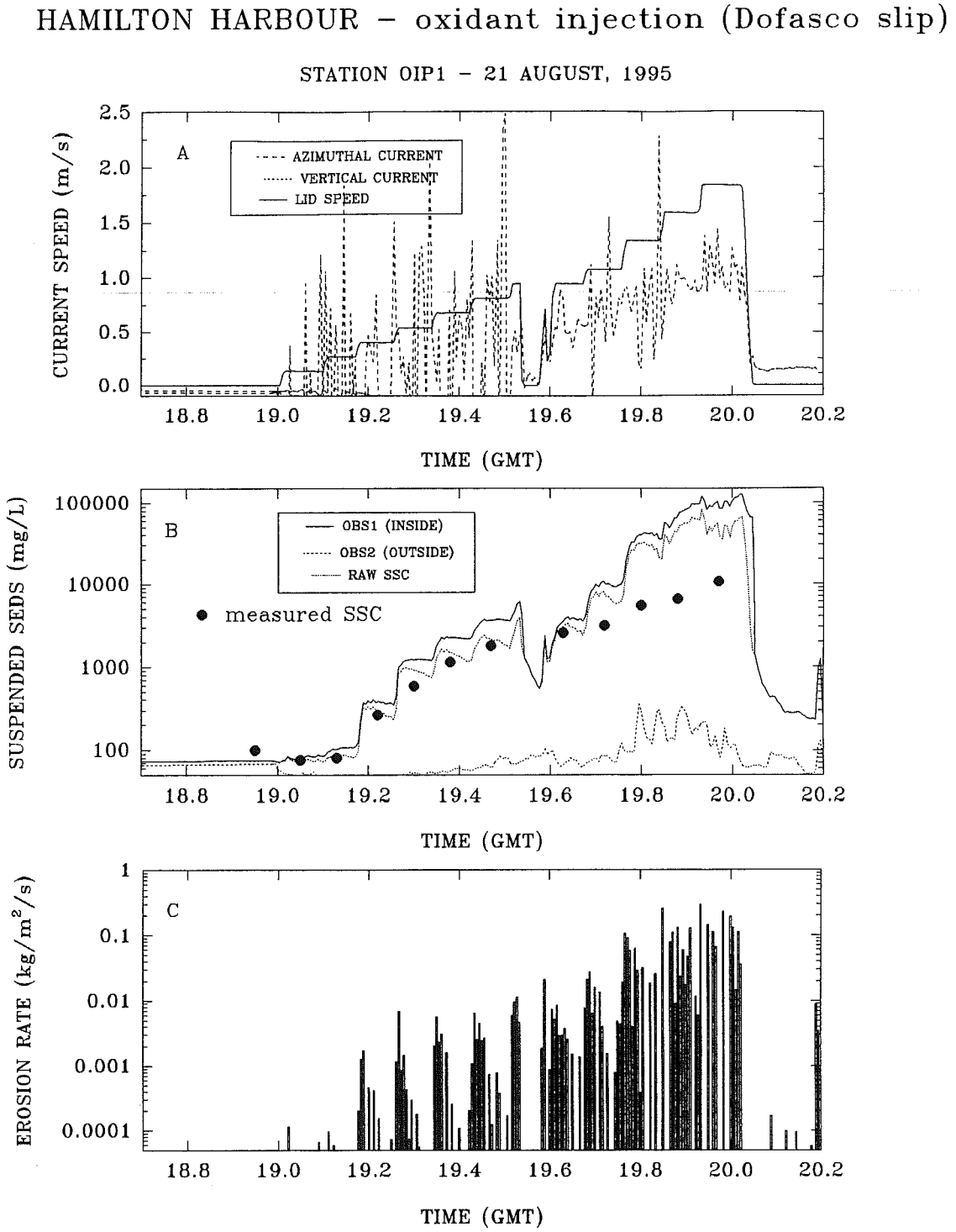

Figure 4.3.1.1 Time-series plots of the Sea Carousel deployment at oxidant-injection site OIP1: (A) lid rotation, azimuthal current speed, and vertical current speed; (B) ambient S, raw S and S corrected for dispersion; and (C) the erosion rate. The dots in panel B denote measured S determined from samples pumped during the experiment. Notice the erratic nature of the current meter which we put down to interference from the injected oxidant.

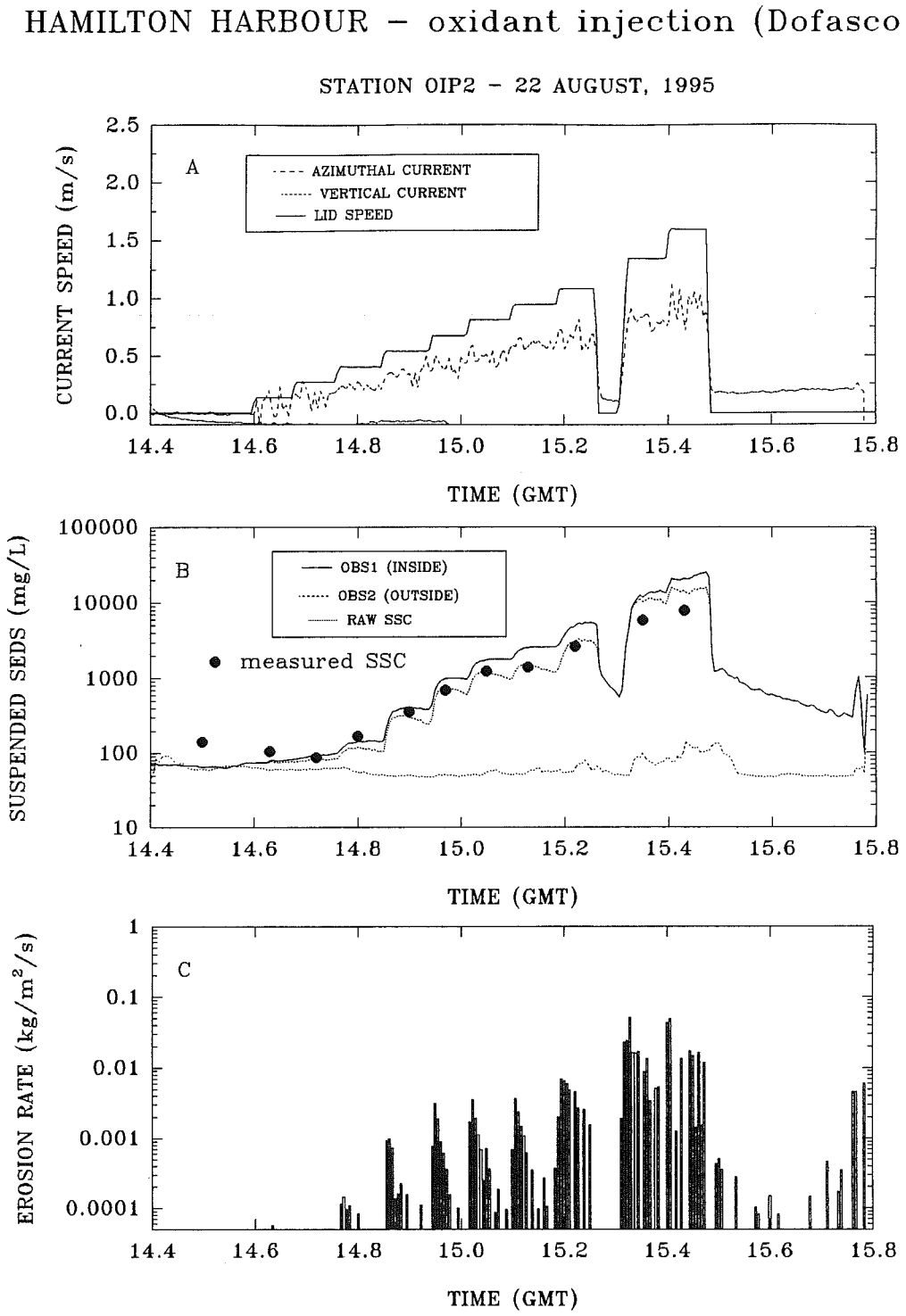

Figure 4.3.1.2 Time-series plots of the Sea Carousel deployment at oxidant-injection site OIP2: (A) lid rotation, azimuthal current speed, and vertical current speed; (B) ambient S, raw S and S corrected for dispersion; and (C) the erosion rate. The dots in panel B denote measured S determined from samples pumped during the experiment. The short break in the lid speed was due to overheating of the power supply.

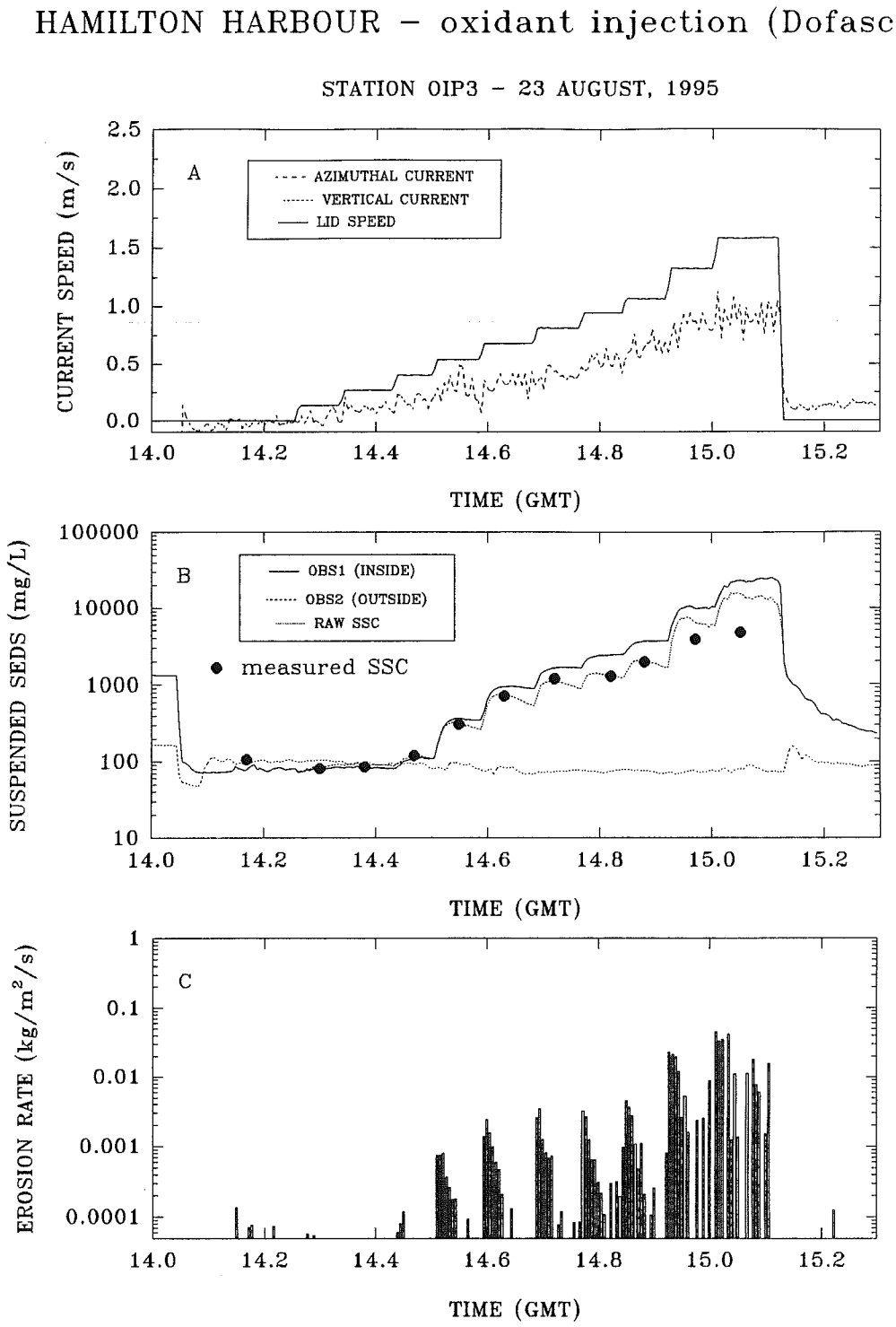

Figure 4.3.1.3 Time-series plots of the Sea Carousel deployment at oxidant-injection site OIP3: (A) lid rotation, azimuthal current speed, and vertical current speed; (B) ambient S, raw S and S corrected for dispersion; and (C) the erosion rate. Notice the change in erosion from type I at early stages of bed erosion to type II during late stages.

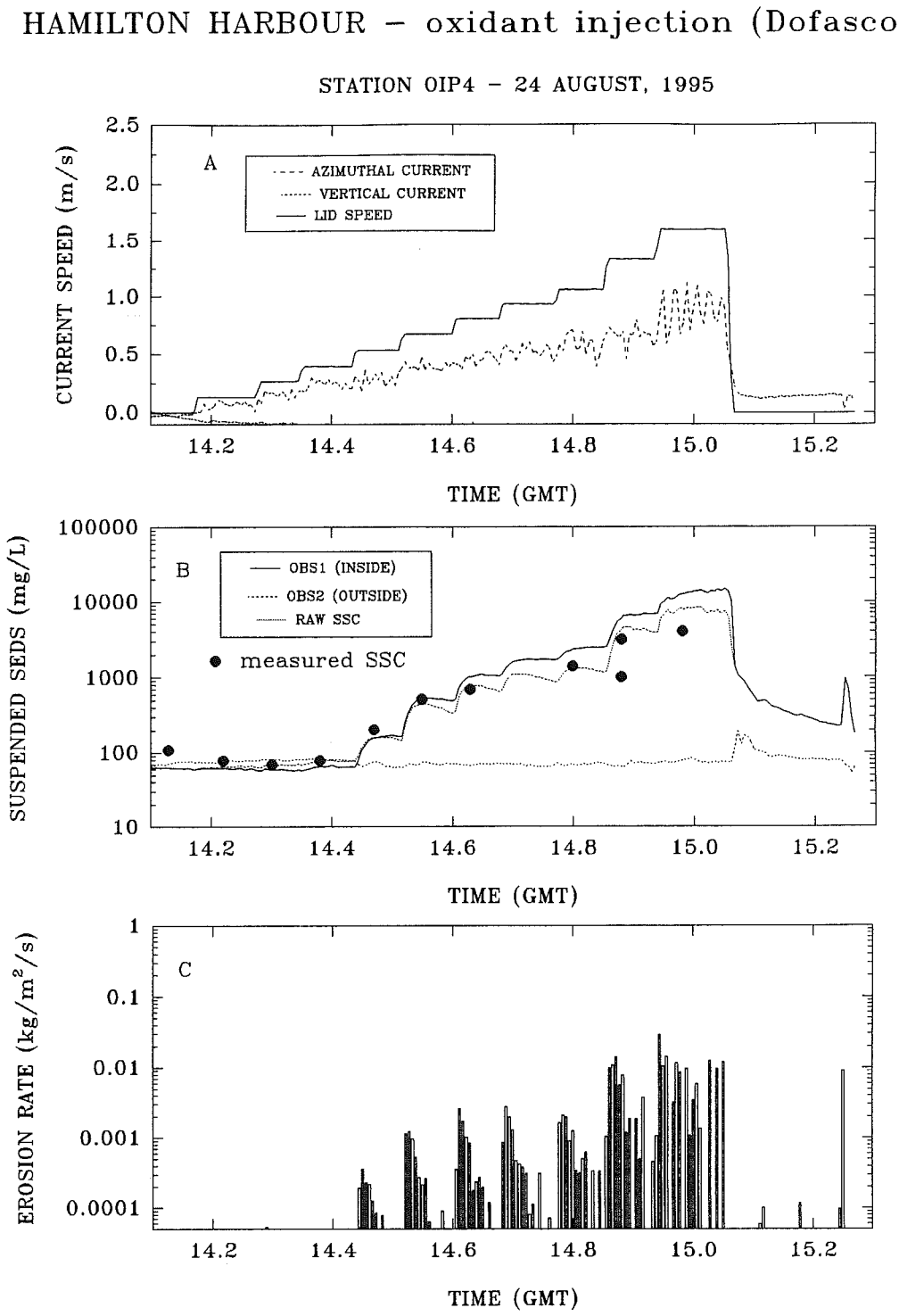

Figure 4.3.1.4 Time-series plots of the Sea Carousel deployment at oxidant-injection site OIP4: (A) lid rotation, azimuthal current speed, and vertical current speed; (B) ambient S, raw S and S corrected for dispersion; and (C) the erosion rate. Notice the erratic behaviour of the flow sensor at high lid speeds.

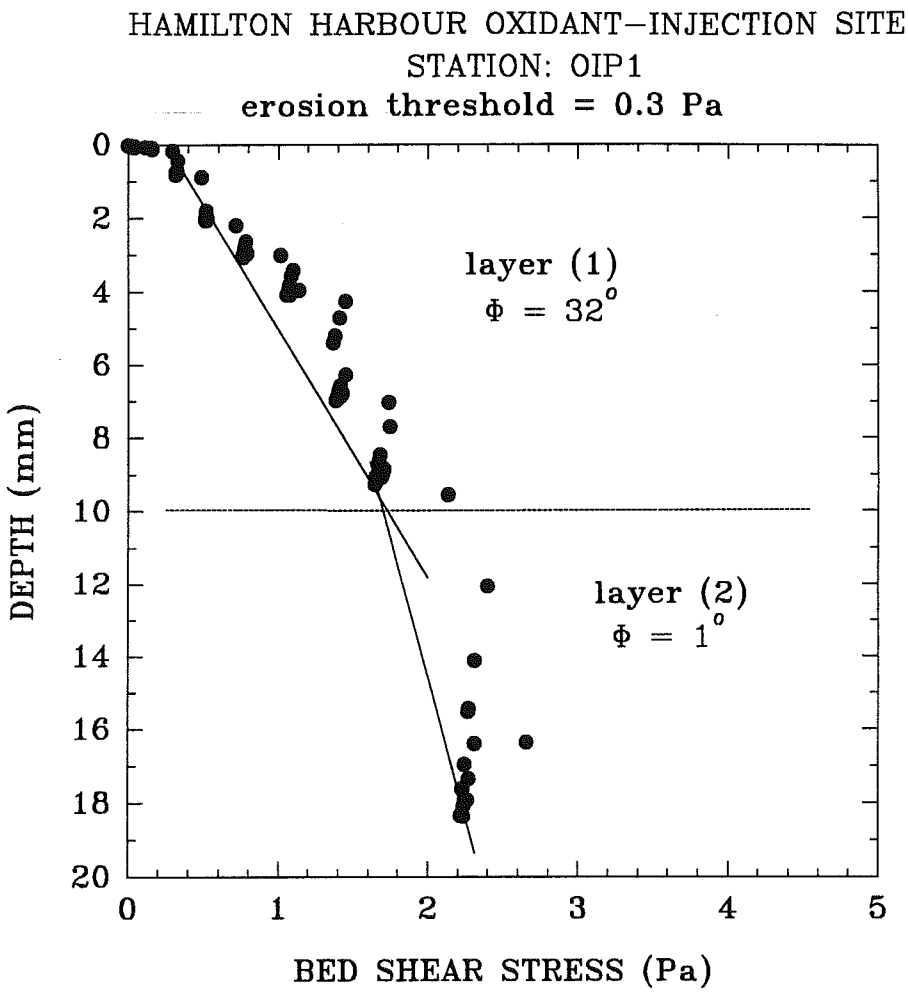

Figure 4.3.1.5 A synthetic core plot of oxidant-injection site OIP1. The high friction angle in the topmost 10 mm may reflect the effects of the treatment, as they exceed values seen at the other plots..

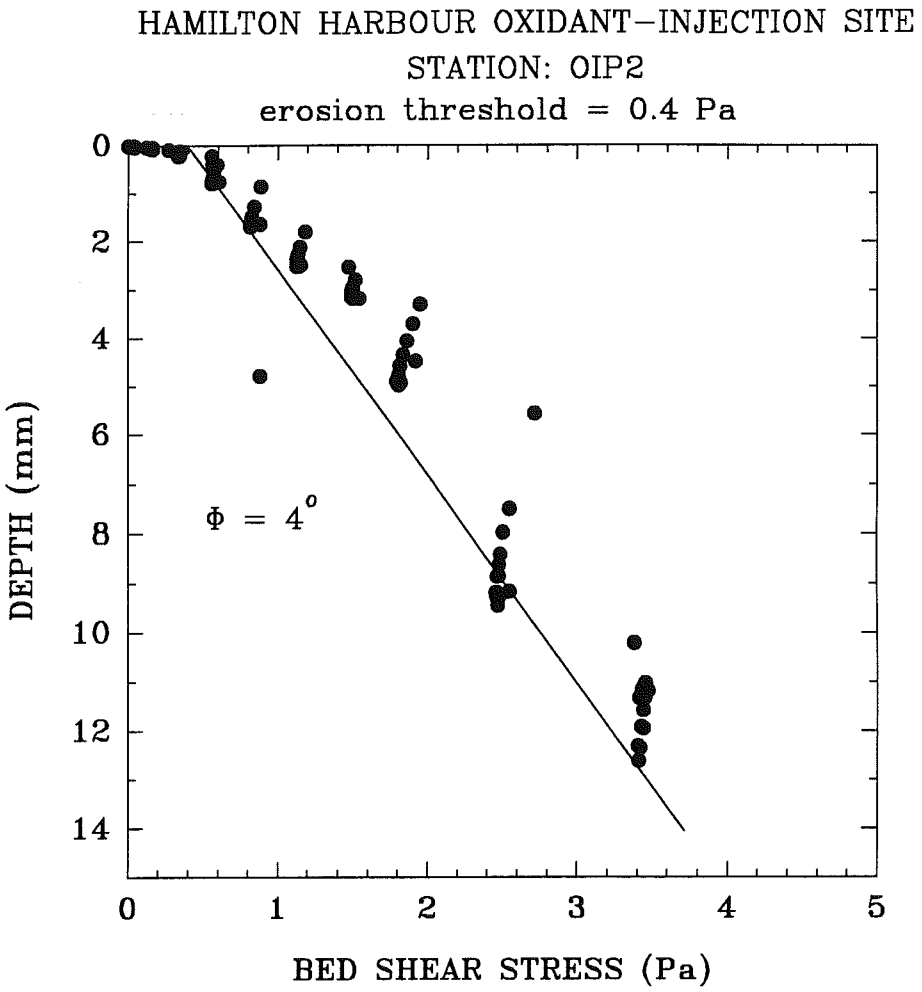

Figure 4.3.1.6 A synthetic core plot of oxidant-injection site OIP2. No bed structure is evident, which may be the result of physical disturbance by the treatment process.

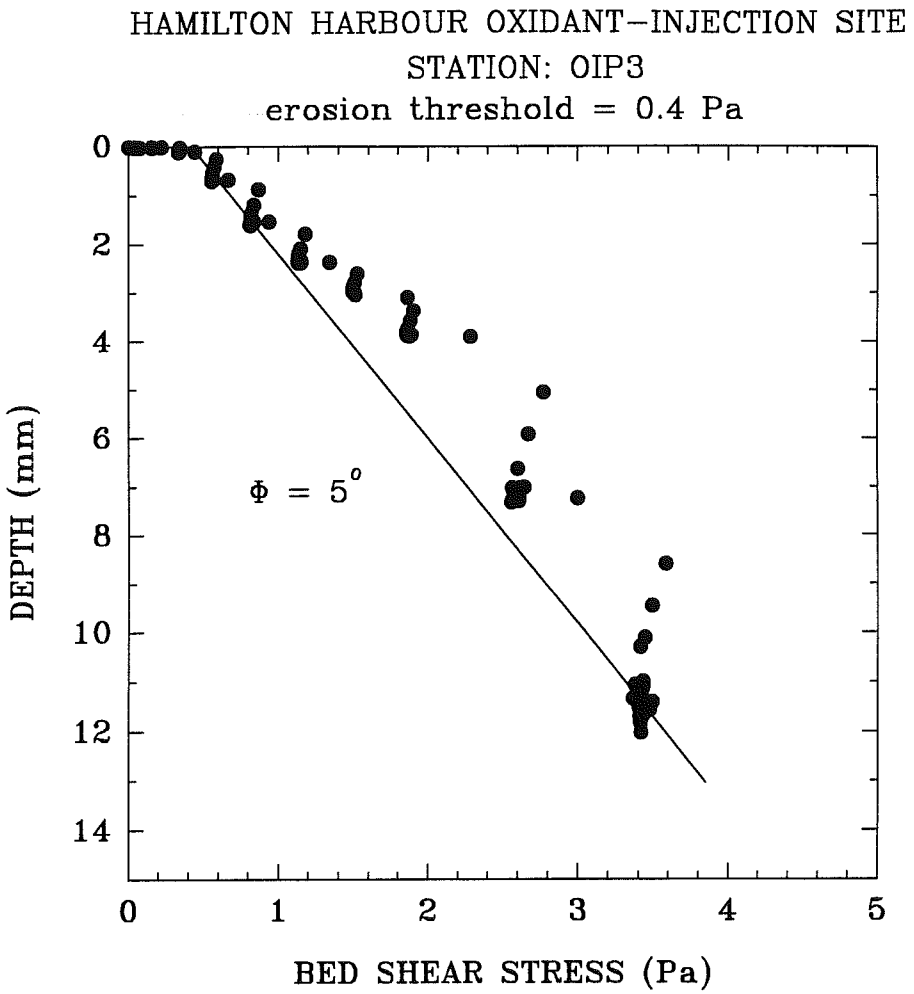

Figure 4.3.1.7 A synthetic core plot of oxidant-injection site OIP3.

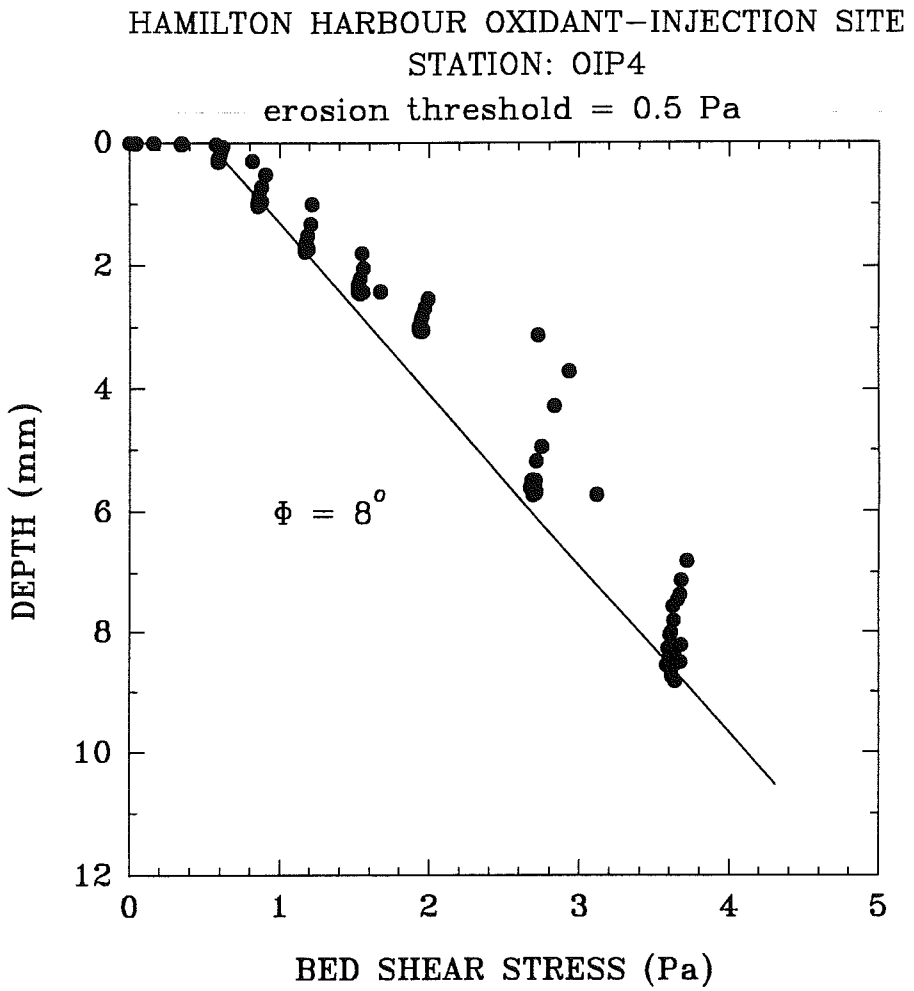

Figure 4.3.1.8 A synthetic core plot of oxidant-injection site OIP4.

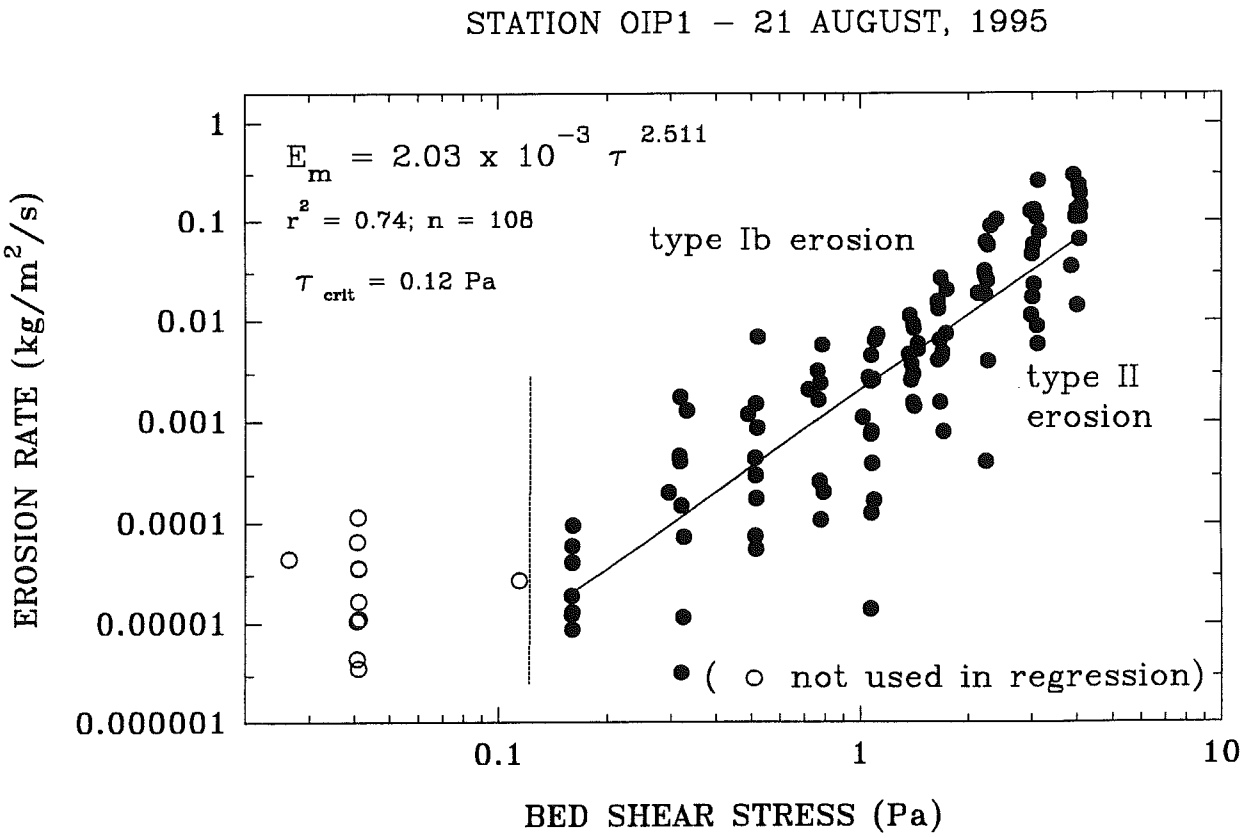

Figure 4.3.1.9 Measured erosion rate (A) and S (B) plotted against applied bed shear stress for oxidant-injection site OIP1.

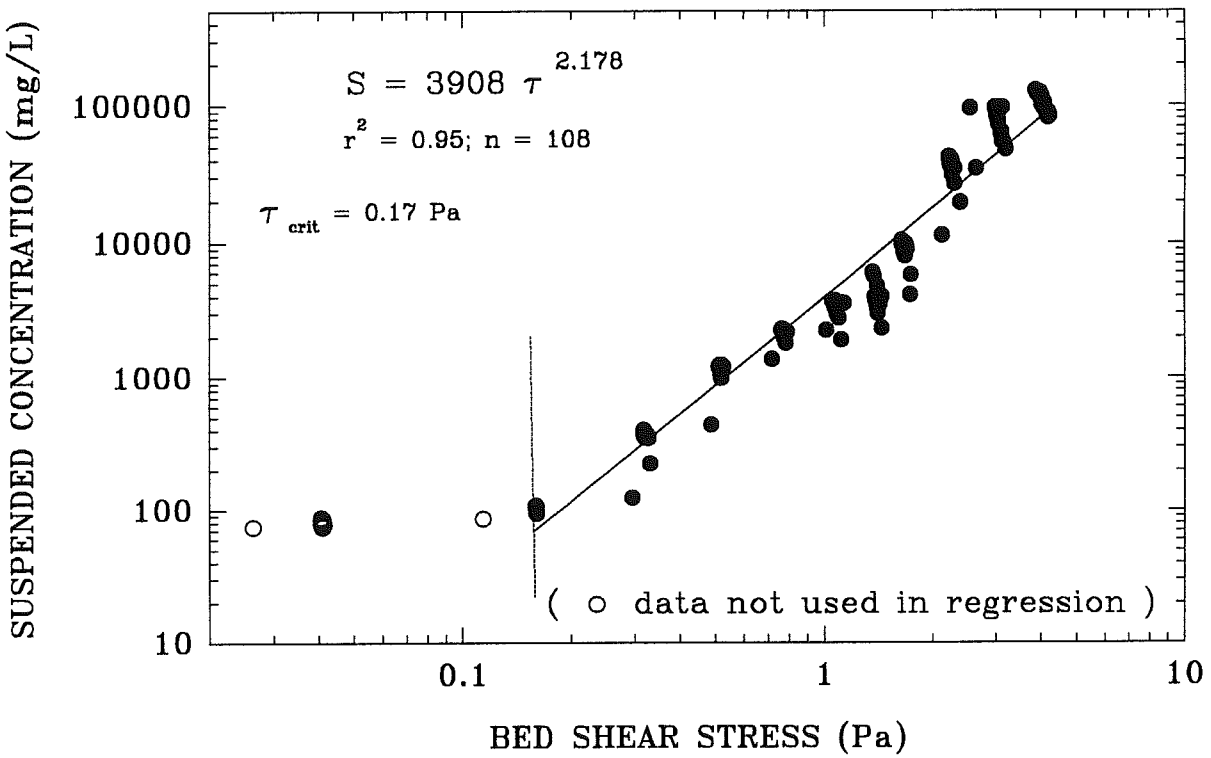

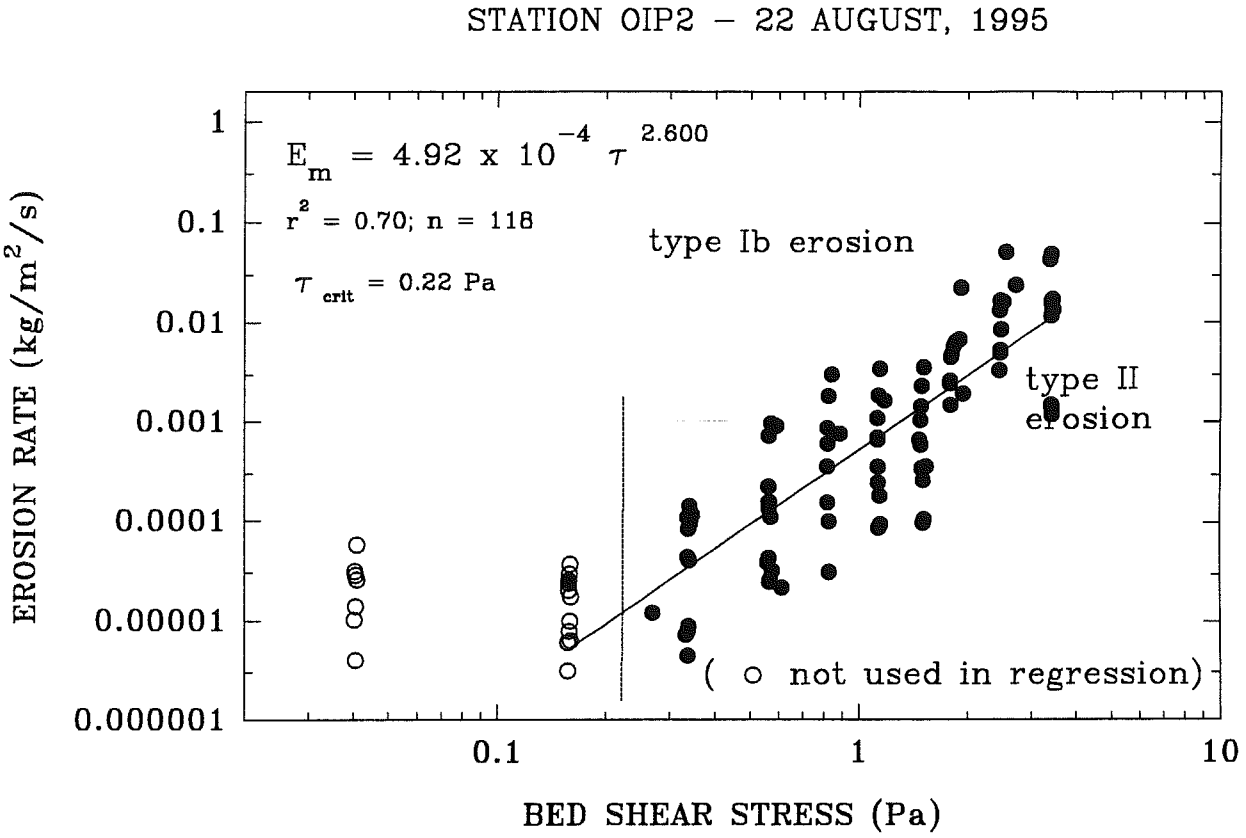

Figure 4.3.1.10 Measured erosion rate (A) and S (B) plotted against applied bed shear stress for oxidant-injection site OIP2.

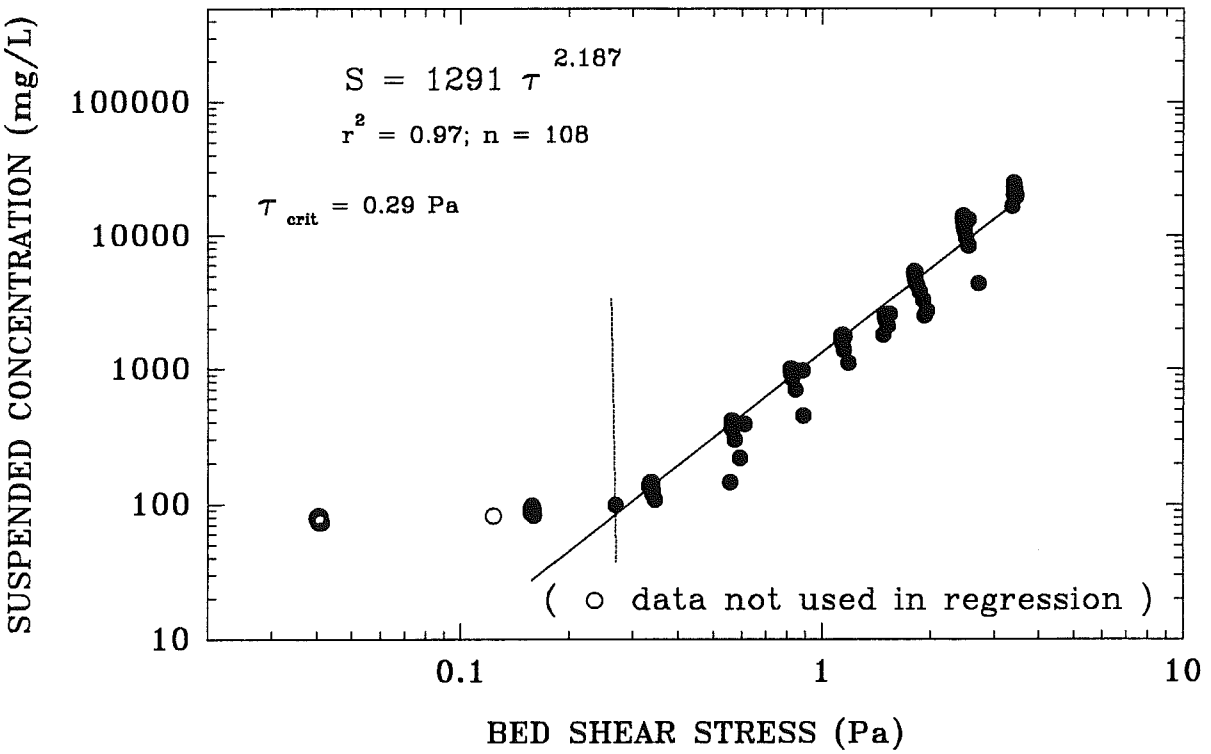

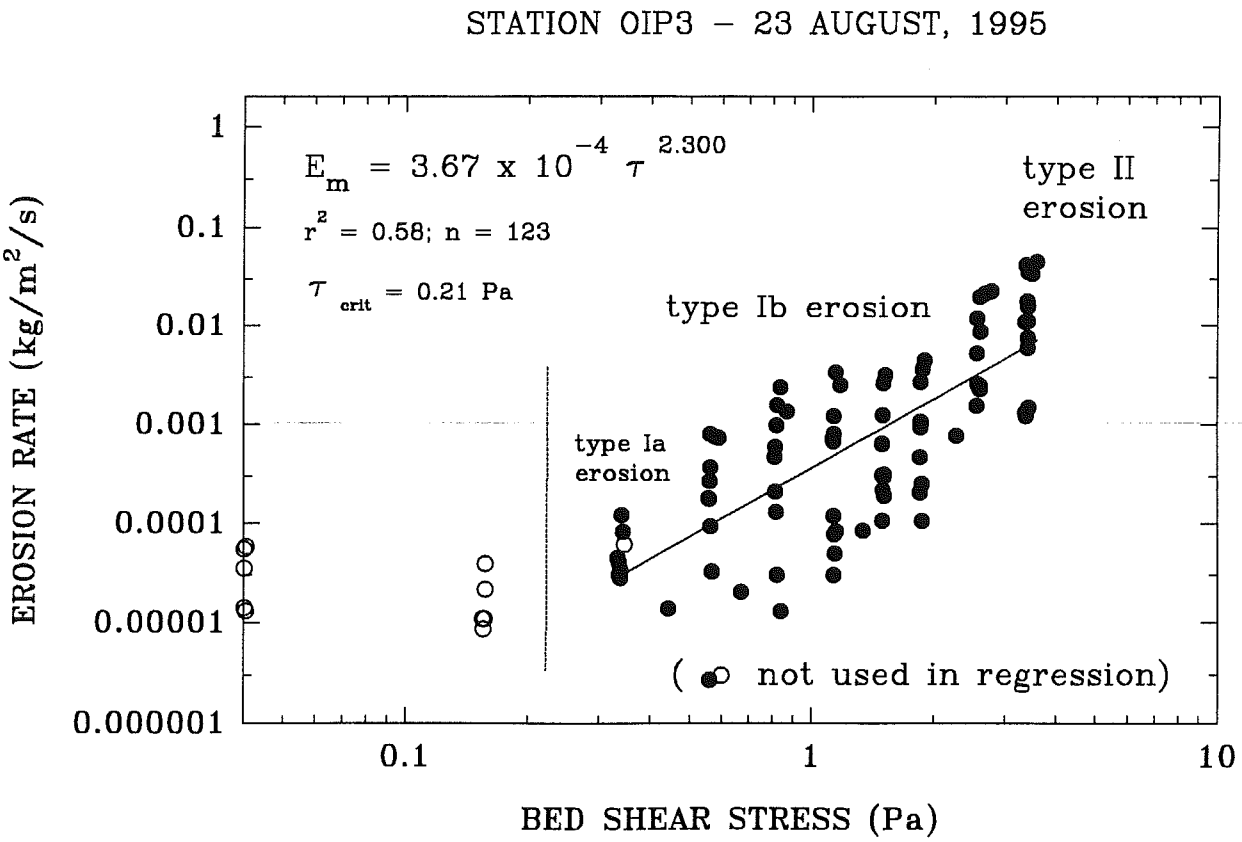

Figure 4.3.1.11 Measured erosion rate (A) and S (B) plotted against applied bed shear stress for oxidant-injection site OIP3.

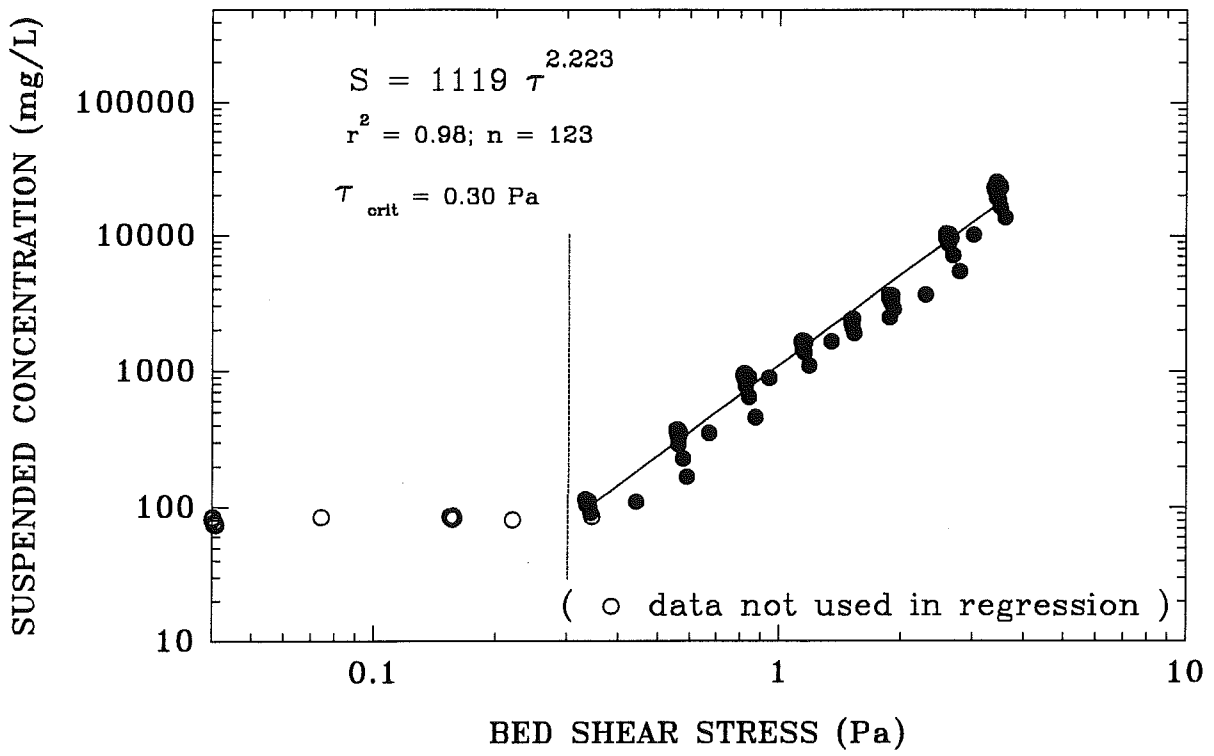

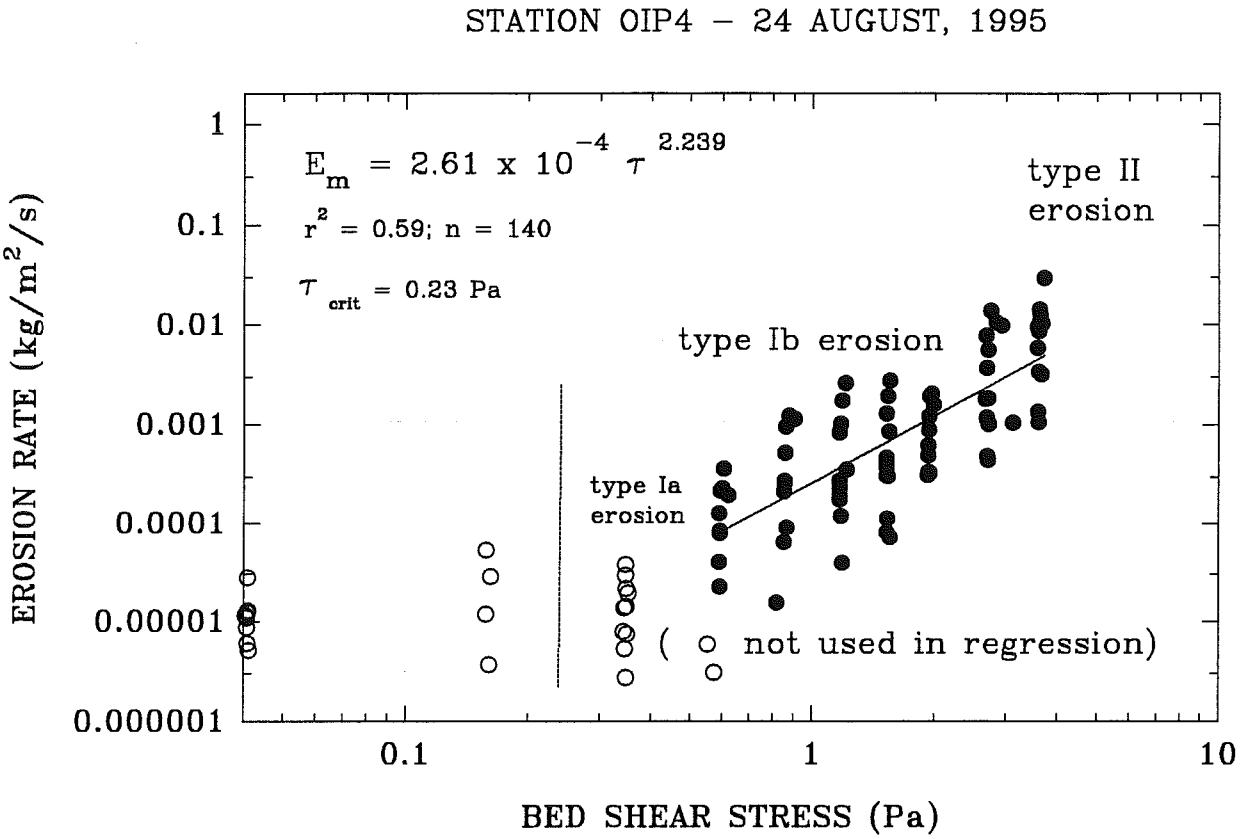

Figure 4.3.1.12 Measured erosion rate (A) and S (B) plotted against applied bed shear stress for oxidant-injection site OIP4.

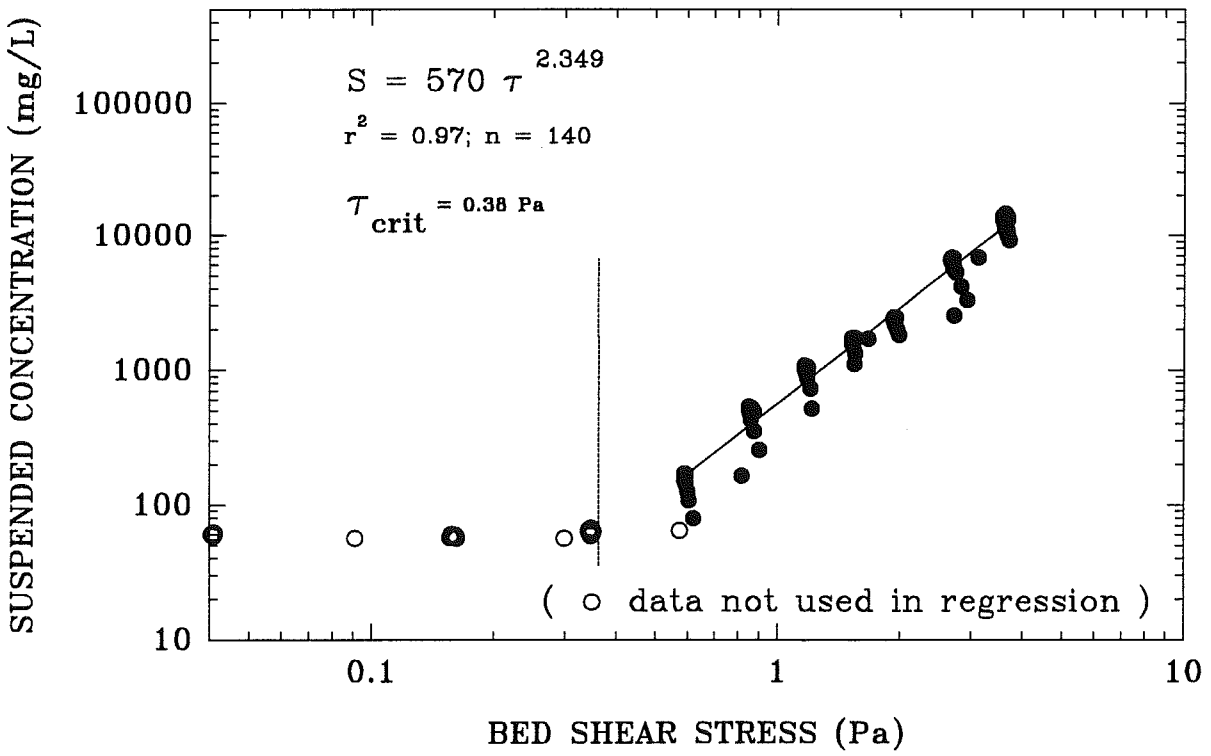

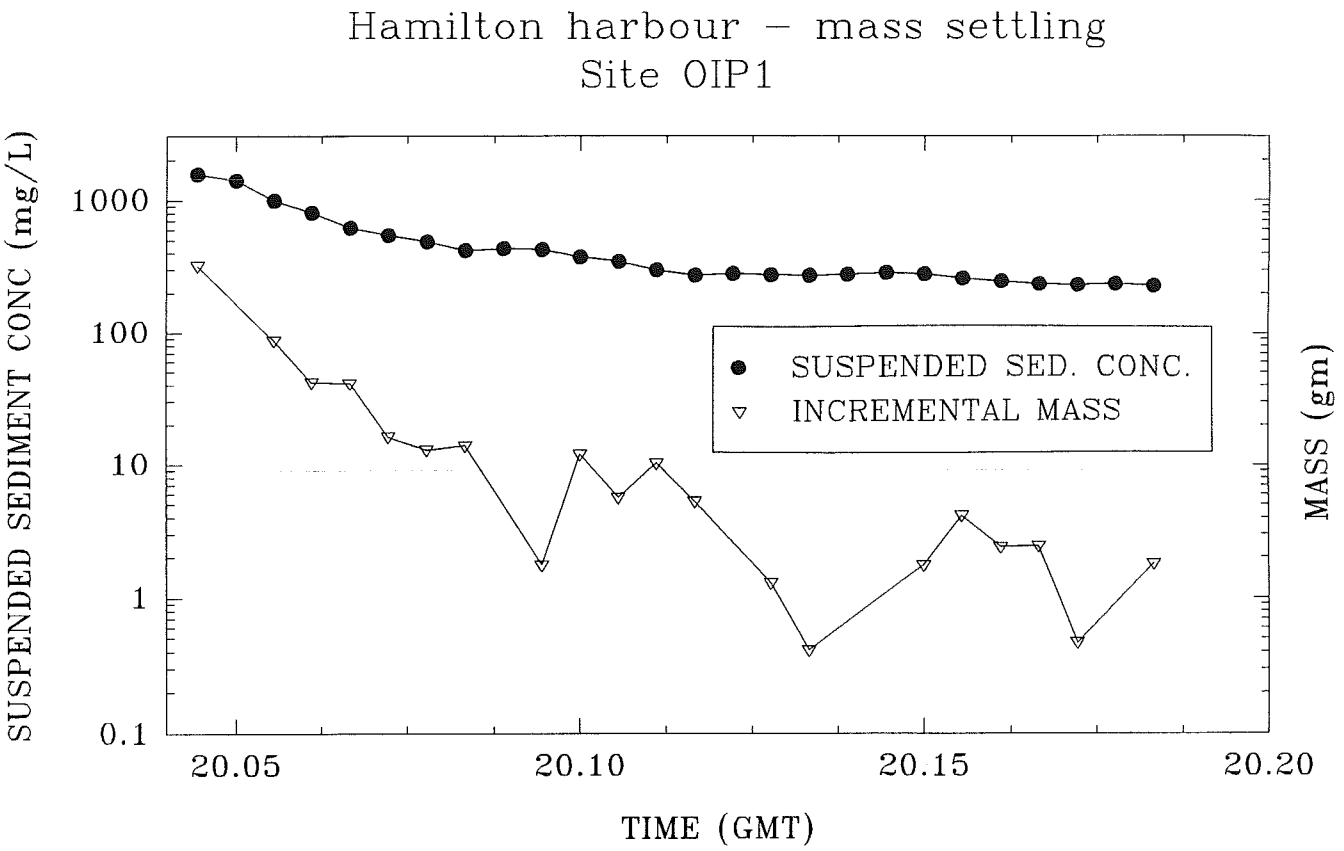

Figure 4.3.1.13 Mean S, incremental mass deposition, mass settling rates, and sedimentation diameter determined for the time-series of Sea Carousel from oxidant-injection site OIP1. Notice the decrease in grain size and settling rate with time through the settling period.

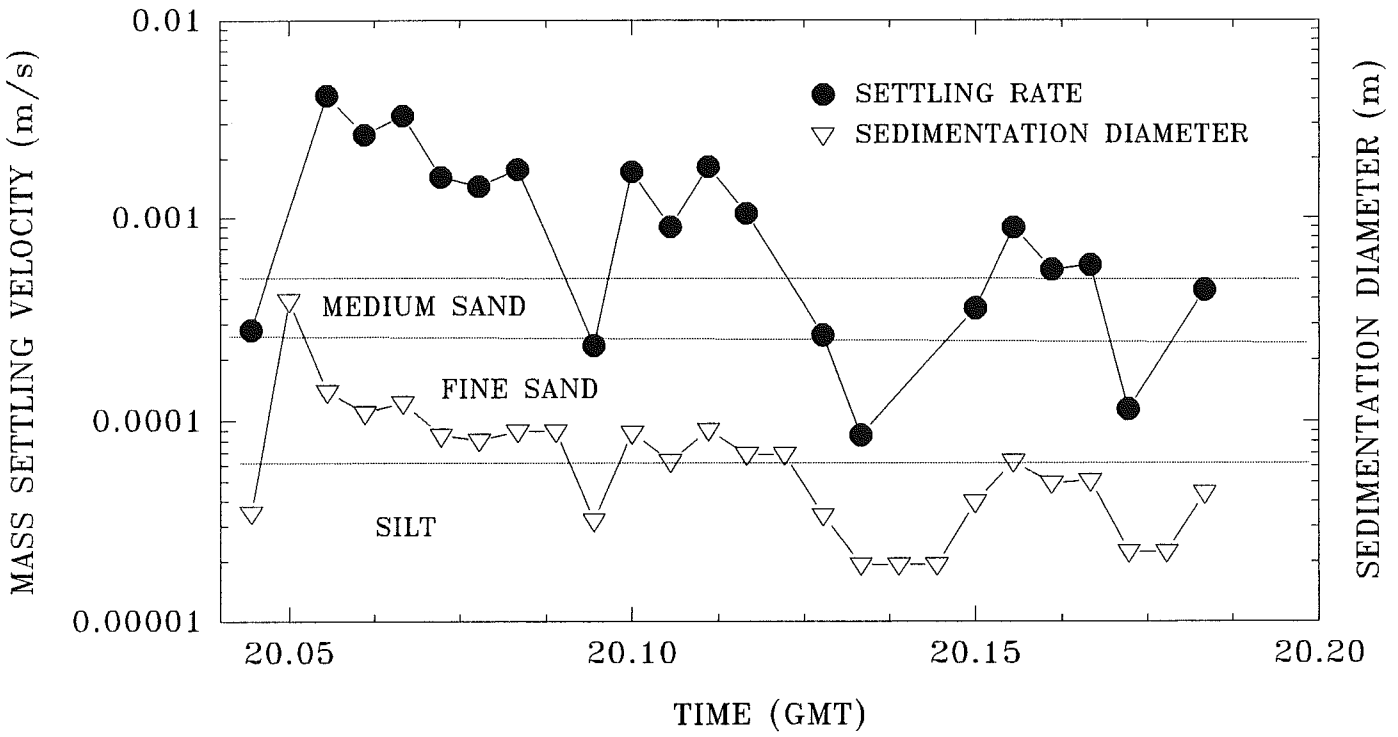

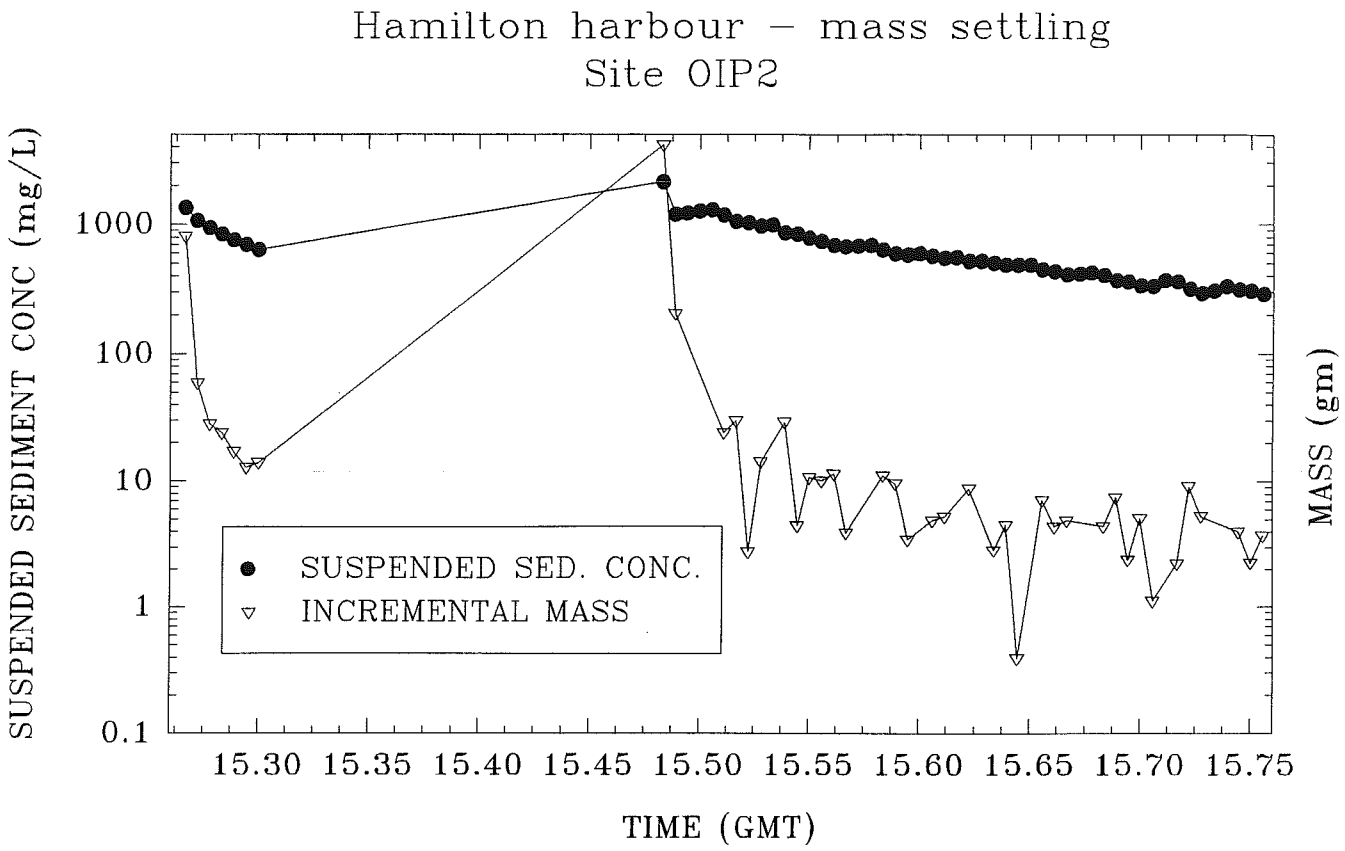

Figure 4.3.1.14 Mean S, incremental mass deposition, mass settling rates, and sedimentation diameter determined for the time-series of Sea Carousel from oxidant-injection site OIP2.

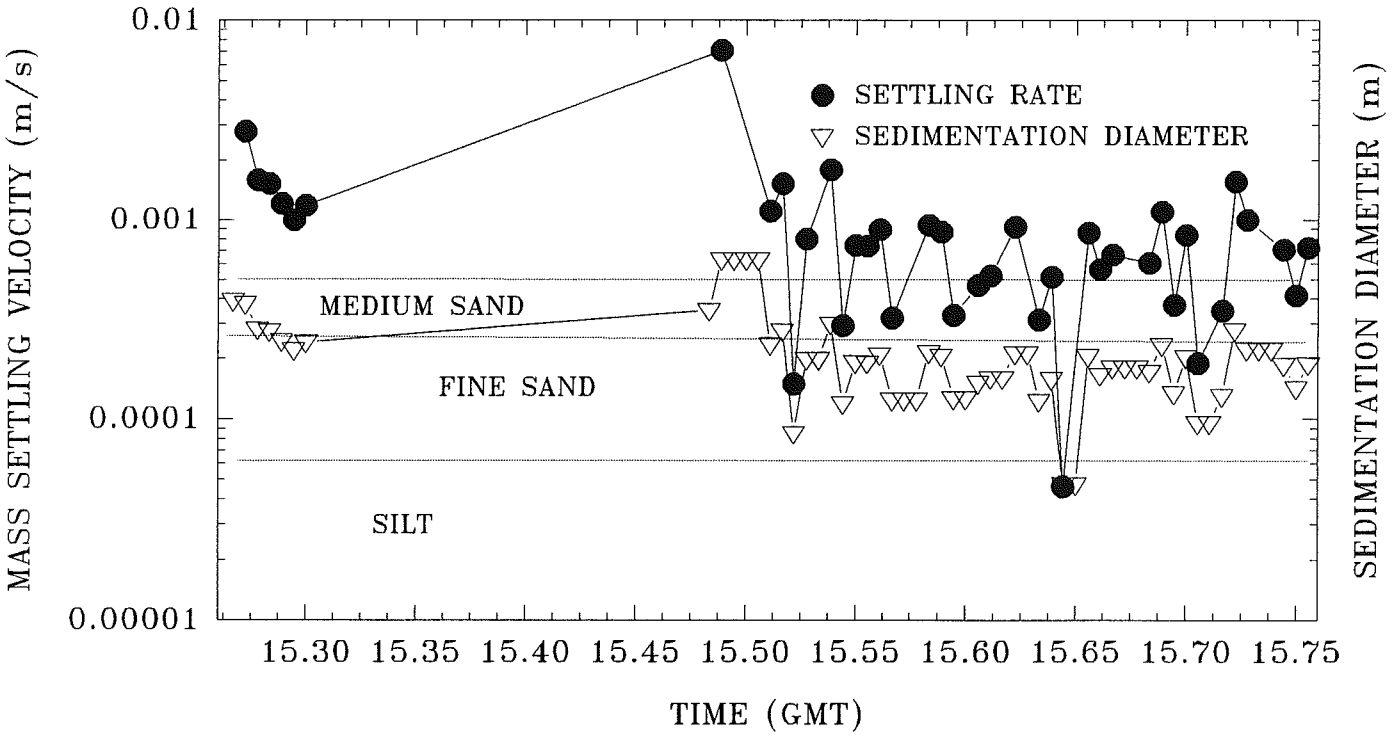

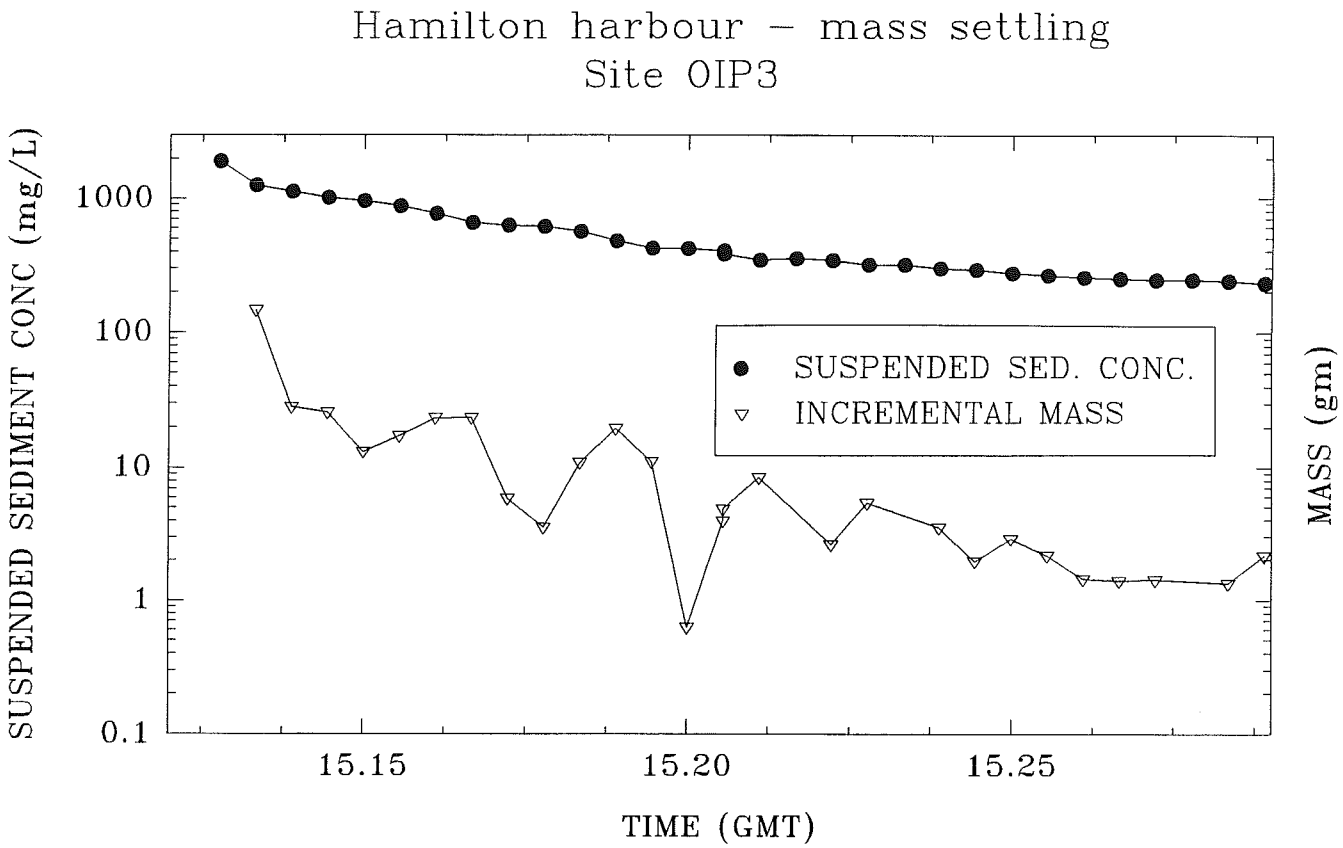

Figure 4.3.1.15 Mean S, incremental mass deposition, mass settling rates, and sedimentation diameter determined for the time-series of Sea Carousel from oxidant-injection site OIP3. The aggregates appear to be up to medium sand in size.

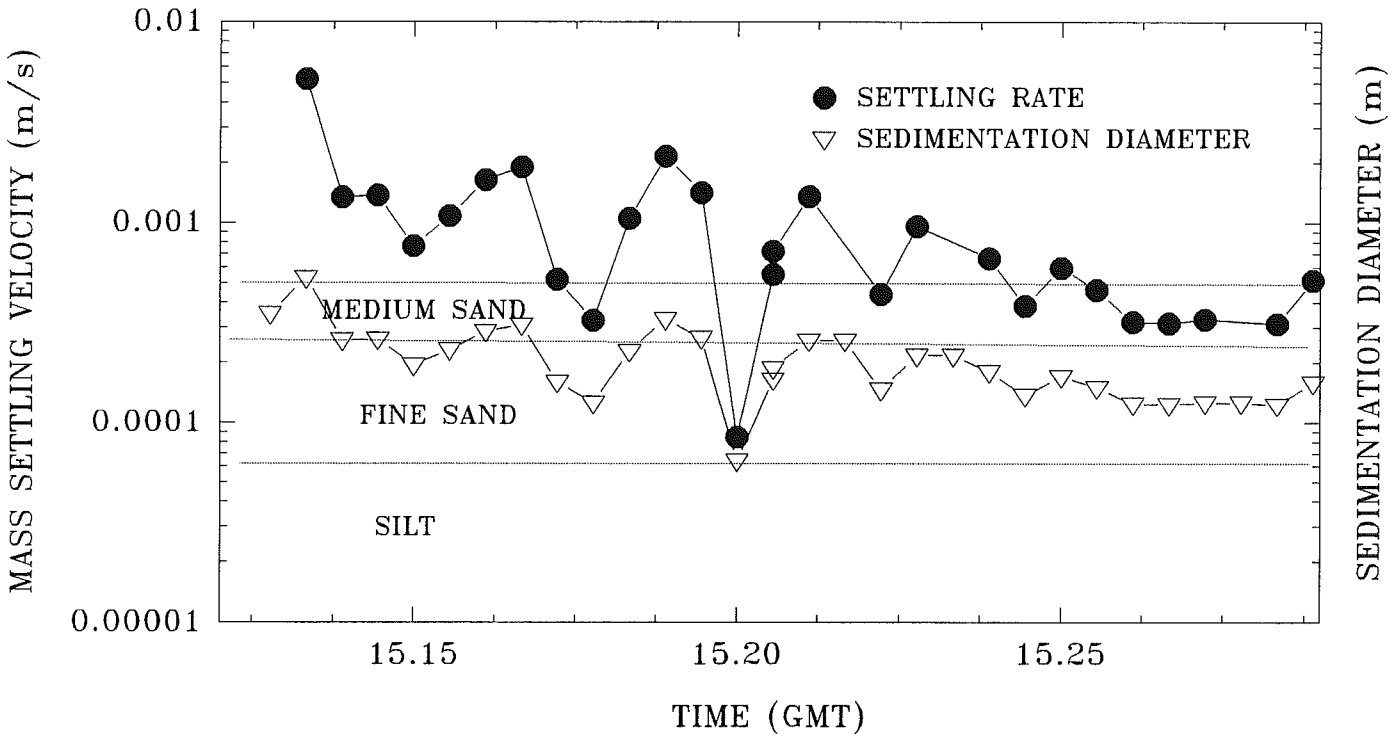

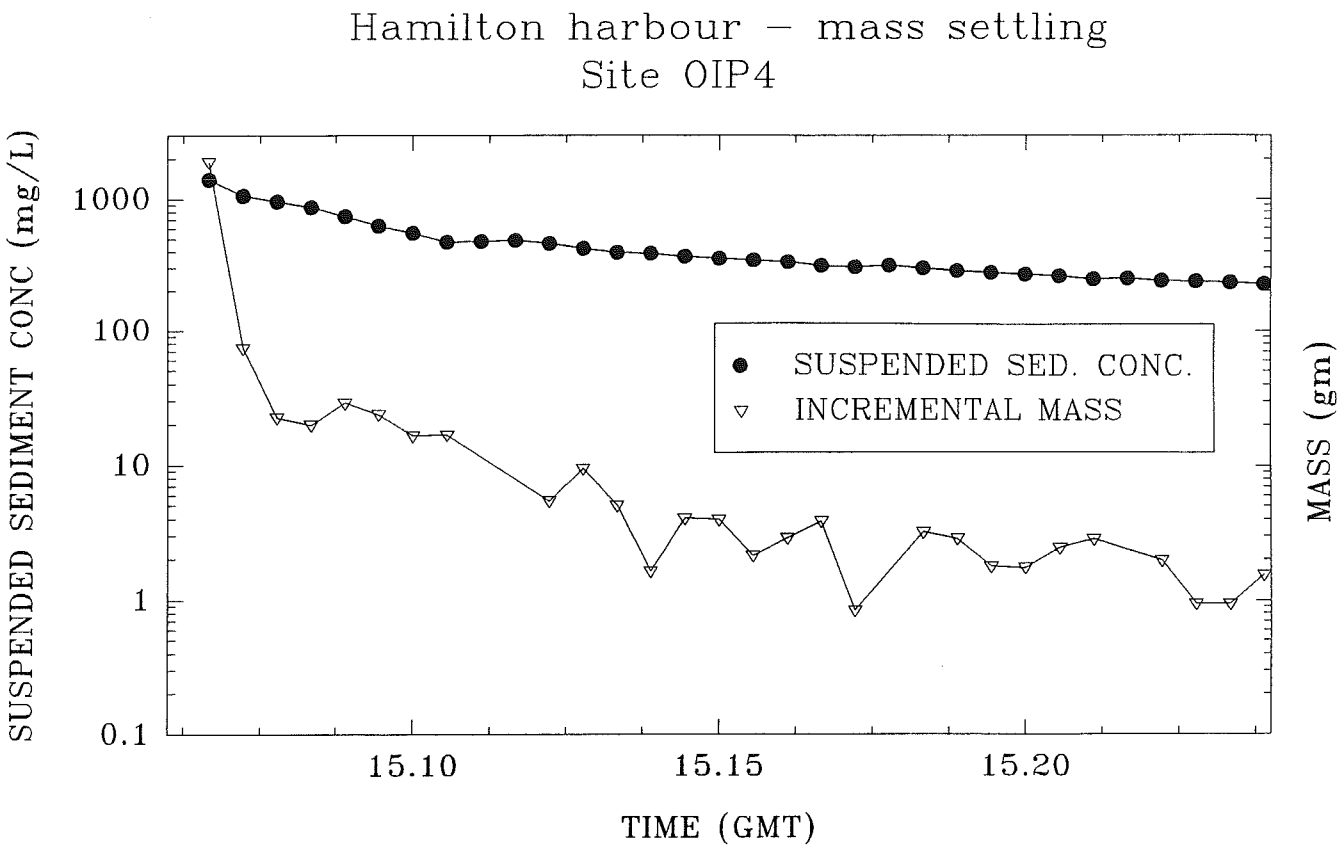

Figure 4.3.1.16 Mean S, incremental mass deposition, mass settling rates, and sedimentation diameter determined for the time-series of Sea Carousel from oxidant-injection site OIP4. Medium/coarse sand was the first to settle out followed by fine sand.

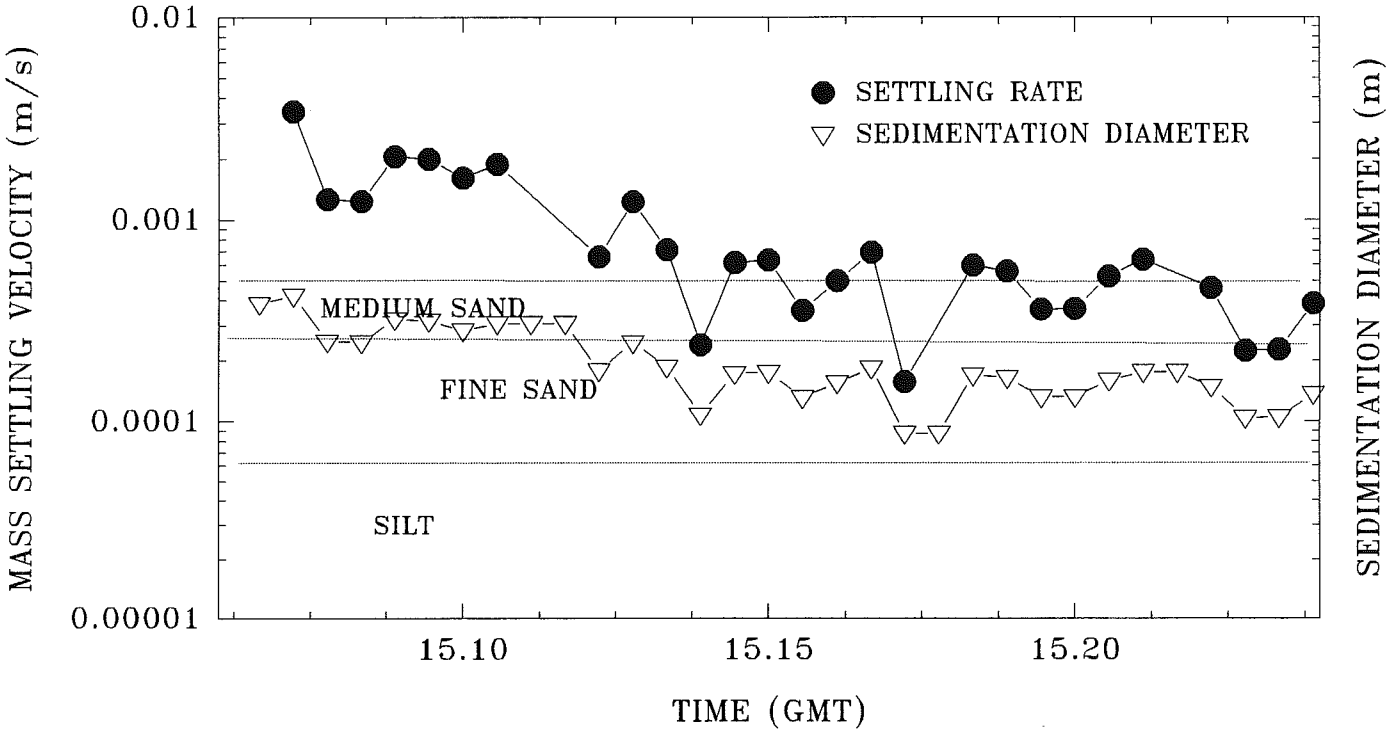

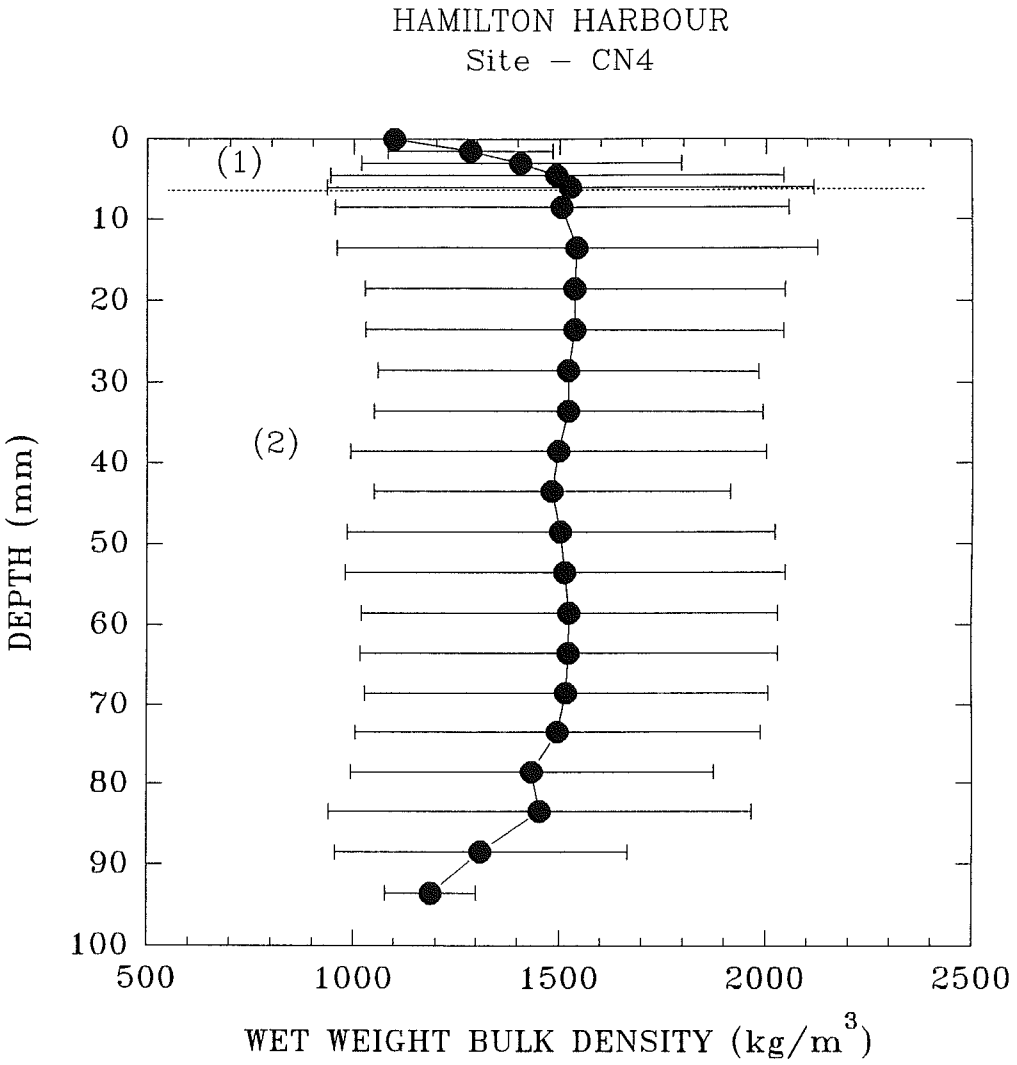

Figure 4.3.2.1 A synthetic core plot of a syringe core (2.5 cm diameter) collected at site OIP4. Notice the presence of a surface layer of rapidly increasing density and the region of constant density beneath.

APPENDIX 1

Video Analysis from Sea Carousel deployments at Hamilton Harbour, Lake Ontario, Canada.

by

Eduardo A. Gómez
Final Report
Acadia Centre for Estuarine Research
Acadia University

March, 1996

Submitted to Dr Carl L. Amos, Geological Survey of Canada - Atlantic

General Considerations

Eleven videos obtained from Sea Carousel deployments at Hamilton Harbour where analyzed for sediment transport magnitude and mode. A SVHF monitor and VCR in slow motion mode were used for this task. All the measurements were taken during a period of two minutes in the middle-end portion of each current speed interval (5 min). The term "aggregate" as used here includes solid particles and flocs because their differentiation is almost impossible in the monitor-screen observations, particularly with the smaller diameters. Due to the low resolution of the monitor and the high speed of the aggregates, only those aggregates with a diameter of 2 mm or larger were discriminated. Also, the error in the counted number of digitised aggregates is larger for smaller diameters than for the biggest.

The transport mode of the aggregates was differentiated into bedload, saltation and suspension. When it was possible (with a good camera angle, focus, illumination and contrast), a surface creep height is given. In those cases, the value was estimated from the general movement of aggregates at actual speed, not from individualizing moving aggregates. So, the heights must be taken as average values. Except for a small and random number of aggregates, it is not possible to measure the saltation length and height from a single aggregate because the saltation length is bigger than the distance recorded on the videos. However, some values of saltation height are given and they were taken from the general pattern of the aggregate trajectories at actual speed, not from individualizing aggregates. So the values for saltation height given in this report must be taken as an average.

As the Sea Carousel current pattern exhibits a small secondary transversal flow, which is upward in the inside wall (where the window is located), the identification and digitalization of aggregates moving in saltation were made according to their trajectory. Those aggregates that showed an appreciable downward component in their trajectories (also reaching the bed) were classified as aggregates transported in saltation. Those aggregates that showed a horizontal trajectory and an upward component of the trajectory at a certain height from the bottom (more than 4 cm) were classified as aggregates in suspension. The speed of aggregates is given as the number of aggregates passing through a point per minute, and the aggregate size distribution is given as a percentage of the total amount of aggregates passing through that point. The aggregates in suspension are given as the number of aggregates per minute across the entire depth of the Sea Carousel (24 cm).

Because the quality of the video records is variable and also because there are some peculiarities occurring at certain water speeds, some notes are added to the specified values.

RESULTS

Symbols

BL: Bed Load
SL: Saltation Load
SpL: Suspended Load
ag: Aggregates
SH: Saltation Height
SLe: Saltation Length
CrH: Creep Height

File: C1.DAT **Sea Carousel Deployment** #174

Water Speed: V0.25 to V1.00 Time: 13:40h-14:25h
No motion

Water Speed: V1.5 Time: 14:25-14:30h
Organic aggregates start to move

Water Speed: V2.0 Time: 14:30-14:35h
Starts BL and SL - Camera out of focus, impossible to measure ag. size.

Water Speed: V2.5 Time: 14:35-14:40h
BL+SL: 35 ag/min.
2mm: 52% 3mm: 35% 4mm: 8.6% 5mm: 4.3%
There are small ripples (length wave=8cm) that moves at 2.25 mm/min. Its presence do not allow to differentiate from BL to SL.

Water Speed: V3.0 Time: 14:40-14:45h
BL+SL: 108 ag/min.
2mm: 73.7% 3mm: 20.8% 4mm: 5.5%
SpL: 306 ag/min.
2mm: 66.6% 3mm: 19.6% 4mm: 13.7%

Water Speed: V3.5 Time:14:45-14:50h
BL: 97 ag/min.
2mm: 46% 3mm: 41.3% 4mm: 9.5% 5mm: 1.6% 6mm: 0% 7mm: 1.6%
CrH: 1-2 mm
SL: 40.5 ag/min.
2mm: 66.6% 3mm: 29.6% 4mm: 3.7%
SH: 1cm
SpL: 298 ag/min.

2mm: 63.4% 3mm: 26.8% 4mm: 7.3% 5mm: 2.4%
The bed roughness (ripple) almost disappear.

Water Speed: V4.0 Time:15:50-15:55h
BL: 74.6 ag/min.
2mm: 67.8% 3mm: 25% 4mm: 7.1%
CrH: 1-2 mm
SL: 44 ag/min.
2mm: 73.3% 3mm: 20% 4mm: 3.3% 5mm: 3.3%
SH: 1 cm SL: ? cm
SpL: 65 ag/min.
2mm: 64.3% 3mm: 21.4% 4mm: 14.3%

Water Speed: V5.0 Time: 14:55-15.00h
The bottom starts to be eroded very fast (2.7 mm/min) passing the materials directly to suspension. From here to the end of the deployment it is not possible to measure anything else.

File: C3.DAT **Sea Carousel Deployment** #175

Water Speed: V0.5-V1.0 Time: 15:53-16:15h
No motion

Water Speed: V1.5 Time: 16:15-16:20h
Organic aggregates start to move as BL.
BL: 42 ag/min. Diameter less than 2 mm.

Water Speed: V2.0 Time: 16:20-16:25h
BL: 46 ag/min. Diameter less than 2 mm.
Sediments start to build up on the window reaching 0.5 cm maximum height.

Water Speed: V2.5 Time: 16:25-16:30h
BL: 70 ag/min.
Diameter < or = to 2mm: 65.7% 3mm: 34.3%

Water Speed: V3.0 Time: 16:30-16:35h
BL: 44 ag/min.
2mm: 33.3% 3mm: 40.0% 4mm: 26.7%

Water Speed: V3.5 Time: 16:35-16:40h
BL: 47 ag/min.
2mm: 30.3% 3mm: 39.4% 4mm: 9.1% 5mm: 15.1% 6mm: 6.1%

Water Speed: V4.0 Time: 16:40-16:45h
BL: 45 ag/min.
2mm: 15.6% 3mm: 19.5% 4mm: 19.5% 5mm: 22.3% 6mm: 9.8% 7mm: 6.7% 10mm: 3.3% 15 mm: 3.3%
CrH: 2 mm
SL: 37 ag/min.
2mm: 51.5% 3mm: 27.1% 4mm: 8.9% 5mm: 12.5%
SH: 0.5-1cm
Erosion starts on the window.

Water Speed: V5.0 Time: 16:45-16:50h
BL: 74 ag/min.
2mm: 13.6% 3mm: 39.0% 4mm: 25.6% 5mm: 17.5% 10mm: 4.3%
SL: 17 ag/min.
2mm: 34.8% 3mm: 38.3% 4mm: 15.2% 5mm: 11.6%
SH: 2 cm SL: ? cm

Water Speed: V6.0 Time: 16:50-16:55h
All the bed is eroded, disappearing from the window. From here to the end of the deployment it is not possible to measure anything else.

File: C4.DAT **Sea Carousel Deployment #176**

Water Speed: V0.5-V1.0 Time: 17:36-18:00h
No motion

Water Speed: V1.5 Time: 18:00-18:05h
Organic flocs moving in suspension. The level of the bed surface inside the window is under the outside bed surface, then it is not possible to observe or measure the BL.

Water Speed: V2.0 Time: 18:05-18:10h
Starts BL, also passing aggregates to suspension. It is not possible to measure the BL. because aggregates size is less than 1 mm and the inside bed surface is observable only through 1.5 cm.

Water Speed: V2.5 Time: 18:10-18:15h
BL: 15 ag/min.
2mm: 66.6% 3mm: 16.6% 4mm: 4.2% 5mm: 4.2% 6mm: 4.2% 9mm: 4.2% CrH: 1-2 mm

Water Speed: V3.0 Time: 18:15-18:20h
BL: 19 ag/min.
2mm: 41.4% 3mm: 41.4% 4mm: 10.3% 5mm: 6.9%
CrH: 1-2 mm
SL: 11.2 ag/min.
2mm: 62.5% 3mm: 37.5%
SH: 0.5 cm SLe: 6 cm (2 ag)
SpL: 134.8 ag/min.
2mm: 69.6% 3mm: 17.4% 4mm: 8.6% 5mm: 4.4%
The bed surface starts to grow up on the window.

Water Speed: V3.5 Time: 18:20-18:25h
BL: 109 ag/min.
2mm: 54.8% 3mm: 30.6% 4mm: 12.9% 5mm: 1.6%
CrH: 1-2 mm
SL: 30 ag/min.
2mm: 50% 3mm: 45% 4mm: 5%
SH: 0.5-1 cm SL: 8 cm (1 ag)
SpL: 168 ag/min.
2mm: 60.7% 3mm: 28.6% 4mm: 3.6% 5mm: 7.1%
Total bed surface grow: 0.5 cm

Water Speed: V4.0 Time: 18:25-18:30h
BL: 50 ag/min.
2mm: 48.5% 3mm: 27.3% 4mm: 9.1% 5mm: 12.0% 10mm: 3%
CrH: 1-2 mm

SL: 28 ag/min.
2mm: 46.6% 3mm: 26.7% 4mm: 20% 5mm: 6.7%
SH: 0.5-1 cm SL: ? cm
SpL: 240 ag/min.
2mm: 54.8% 3mm: 16.1% 4mm: 19.3% 5mm: 9.7%

Water Speed: V5.0 Time: 18:30-18:35h
BL: 12 ag/min.
2mm: 33.3% 3mm: 22.2% 4mm: 11% 5mm: 22.2% 10mm: 11%
The bed starts to be eroded very fast. Sediment is passing directly to suspension disappearing from the window. From here to the end of the deployment it is not possible to measure anything else.

File: CN2.DAT **Sea Carousel Deployment** #179

Water Speed: V0.5-V1.0 Time: 14:12-14:45h
No motion. Problems with camera focus.

Water Speed: V1.5 Time: 14:45-14:50h
Organic flocs in SL and BL starts. Flocs diameter less than 1 mm.

Water Speed: V2.0 Time: 14:50-14:56h
Floc diameter less than 1 mm. There are turbulences because pre-existence of bed roughness. It is not possible to measure anything.

Water Speed: V2.5 Time: 14:56-15:00h
BL: 12 ag/min.
2mm: 15% 3mm: 40% 4mm: 30% 5mm: 10% 6mm: 5%
Poor visibility.

Water Speed: V3.0 Time: 15:00-15:05h
BL: 32 ag/min.
2mm: 42.9% 3mm: 23.8% 4mm: 9.5% 5mm: 19% 6mm: 4.8%
SL: 11 ag/min.
2mm: 60% 3mm: 40%
SH: 0.5 cm
SpL: 93 ag/min.
2mm: 75% 3mm: 8.3% 4mm: 16.7%

Water Speed: V3.0 Time: 15:05-15:10h
BL: 38.6 ag/min.
2mm: 51.8% 3mm: 22.2% 4mm: 18.5% 5mm: 3.7% 10mm: 3.7%
CrH: 1-2 mm
SL: 28.5 ag/min.

2mm: 52.6% 3mm: 26.3% 4mm: 15.8% 5mm: 5.3%
SH: 0.5-1 cm
SpL: 192 ag/min.
2mm: 43.6% 3mm: 28.2% 4mm: 10.3% 5mm: 10.2% 7mm: 2.6% 10mm: 5.1%

Water Speed: V4.0 Time: 15:10-15:18h
BL: Not observable.
SL: 60 ag/min.
2mm: 61% 3mm: 33.6% 4mm: 2.7% 5mm: 2.7%
SH: 1 cm
SpL: 370 ag/min.
2mm: 43% 3mm: 26.4% 4mm: 14% 5mm: 11% 6mm: 2.8% 7mm: 2.8%
The bed becomes to be eroded very fast.

Water Speed: V5.0 Time: 15:18-15:23h
BL: 25 ag/min.
2mm: 58.8% 3mm: 29.4% 5mm: 11.8%
SL: 113 ag/min.
2mm:58.5 % 3mm: 28.3% 4mm: 9.4% 5mm: 3.8%
SH: 1 cm
SpL: 510 ag/min.
2mm: 64.5% 3mm: 16.1% 4mm: 9.7% 5mm: 6.5% 6mm: 1.6% 7mm: 1.6%
Poor quality of BL observations because high speed and low contrast.

Water Speed: V6.0 Time: 15:23-15:28h
Every thing pass to suspension very fast. It is not possible to distinguish anything else.

File: W2.DAT **Sea Carousel Deployment #180**

Water Speed: V0.5-V1.0 Time: 16.02-16.28h
No motion.

Water Speed: V1.5 Time: 16.28-16.33h
Organic flocs in suspension.

Water Speed: V2.0 Time: 16.33-16.38h
Organic flocs moving as BL.
BL: 231 ag/min.
1mm: 37% 2mm: 51.8% 3mm: 11.1%
CrH: 2-3 mm

Water Speed: V2.5 Time: 16:38-16:43h
BL: 61.5 ag/min.
2mm: 66.2% 3mm: 22.2% 4mm: 10% 5mm: 1.25%

SL: Not observable
SpL: 190 ag/min.
2mm: 56% 3mm: 20% 4mm: 20% 5mm: 4%

Water Speed: V3.0 Time: 16:43-16:48h
BL: 70.8 ag/min.
2mm: 50.6% 3mm: 30.6% 4mm: 5.9% 5mm: 10.58% 10mm: 1.17% 13mm: 1.17%
SL: 44 ag/min.
2mm: 63.3% 3mm: 23.4% 4mm: 13.3%
SH: 1 cm
SpL: 374 ag/min.
2mm: 78.4% 3mm: 15.7% 5mm: 3.92% 8mm: 1.96%
Bed surface grows on the window up to 5 mm.

Water Speed: V3.5 Time: 16:48-16:53h
BL: 80.7ag/min.
2mm: 48.7% 3mm: 33.3% 4mm: 7.7% 5mm: 10.2%
SL: 82 ag/min.
2mm: 75% 3mm: 20% 4mm: 4% 5mm: 1%
SH: 1.2 cm
SpL: 281 ag/min.
2mm: 60% 3mm: 26% 4mm: 7.5% 6mm: 1.9% 7mm: % 8mm: 1.9%

Water Speed: V4.0 Time: 16:53-16:58h
BL: 49 ag/min.
2mm: 64% 3mm: 24.4% 4mm: 4.4% 5mm: 6.7%
SL: 91.7 ag/min.
2mm: 71.6% 3mm: 18.5% 4mm: 3.7% 5mm: 4.94% 10mm: 1.23%
SH: 1 cm
SpL: 452 ag/min.
2mm: 60% 3mm: 25.45% 4mm: 5.45% 5mm: 7.27% 6mm: 1.8%

Water Speed: V5.0 Time: 16:58-17:03h
BL: 12 ag/min.
3mm: 37.5% 4mm: 25% 5mm: 37.5%
SL: 76.8 ag/min.
2mm: 81% 3mm: 15.6% 4mm:
SH: 1.3 cm
The bed starts to be eroded fast. It is not possible to observe ag less than 3 mm as BL because inside bed surface is lower that outside. Because the ag speed is to fast, it is not possible to measure those that are dark. The ag that only can be measured are shells because its light colour. From here to the end of the deployment the bed becomes to be eroded very fast, passing all materials directly to suspension. It is not possible to measure anything else.

File: C5.dat **Sea Carousel Deployment #181**

Water Speed: V0.5-V1.0 Time: 18:11-18:35h
No motion

Water Speed: V1.5-V2.0 Time: 18:35-18:45h
Organic flocs as SpL and BL. Because the camera is out of focus it is not possible to make any measurement.

Water Speed: V2.5 Time: 18:45-18:50h
Organic flocs as SpL and BL. Flocs size homogeneous and less than 1 mm.
CrH: 2 mm

Water Speed: V3.0 Time: 18:50-18:56h
BL: 20.5 ag/min.
2mm: 46.7% 3mm: 13.3% 4mm: 20% 5mm: 6.7% 6mm: 13.3%
SL: 27.8 ag/min.
2mm: 57.9% 3mm: 26.3% 4mm: 10.5% 5mm: 5.3%
SH: 1 cm
SpL: 196 ag/min.
2mm: 63.6% 3mm: 18.2% 4mm: 13.6% 6mm: 4.5%

Water Speed: V3.5 Time: 18:56-19:01h
BL: 30.8 ag/min.
2mm: 65% 3mm: 15% 4mm: 15% 5mm: 5%
SL: 44.6 ag/min.
2mm: 37.9% 3mm: 41.38% 4mm: 17.2% 5mm: 3.4%
SH: 1 cm SLe: 4-6 cm (3 ag)
SpL: 368 ag/min.
2mm: 52.7% 3mm: 27.3% 4mm: 9.1% 5mm: 10.9%

Water Speed: V4.0 Time: 19:01-19:11h
BL: 82 ag/min.
2mm: 39.3% 3mm: 28.5% 4mm: 17.8% 5mm: 10.7% 6mm: 3.6%
CrH: 1.5-2 mm
SL: 79 ag/min.
2mm: 33.3% 3mm: 31.7% 4mm: 17.5% 5mm: 12.7% 6mm: 4.8%
SH: 1 cm SL: 6 cm (2 ag)
SpL: 576 ag/min.
2mm: 53.3% 3mm: 26.7% 4mm: 3.3% 5mm: 10% 6mm: 5% 7mm: 1.6%
The camera is too high. Only 2 cm of the bed are visible (left corner)

Water Speed: V5.0 Time: 19:06-19:11h
BL: 43.5 ag/min.
2mm: 34.5% 3mm: 27.6% 4mm: 24.1% 5mm: 6.9% 6mm: 6.9%
SL: 44.6 ag/min.

2mm: 26.9% 3mm: 38.5% 4mm: 15.3% 5mm: 19.2%
SH: 1 cm
SpL: 276 ag/min.
2mm: 57.8% 3mm: 13.2% 4mm: 7.9% 5mm: 18.4% 6mm: 2.6%
The bed starts to be eroded. From here to the end of the deployment the camera is out of focus.

File: CN3.DAT **Sea Carousel Deployment #182**

Water Speed: V0.5-V1.0 Time: 13:54-14:25h
No motion.

Water Speed: V1.5 Time: 14:25-14:30h
Organic flocs in suspension.

Water Speed: V2.0-V2.5-V3.0-V3.5 Time: 14:30-14:50h
A pre-existent bed form strongly modify the flow pattern, generating turbulences that could be confused with SH, SL and CrH. The bed form moves like a sand ripple, and also does the flow pattern over it. Any value measured from the window is only representative of one single point, not representing the average transport conditions inside the Sea Carousel. At speeds V3.0 and V3.5 it is possible to observe some 0.5 cm isolated ag in suspension.

Water Speed: V4.0 Time: 14:50-14:55h
BL: 42 ag/min.
2mm: 60.7% 3mm: 21.4% 4mm: 14.3% 5mm: 3.6% 6
CrH: 2 mm
SL: 34 ag/min.
2mm: 66.7% 3mm: 29% 5mm: 4.2%
SH: 1 cm
SpL: 276.8 ag/min.
2mm: 53.3% 3mm: 26.7% 4mm: 13.3% 5mm: 6.7%

Water Speed: V5.0 Time: 14:55-15:00h
BL: Not distinguishable.
SL: 86.5 ag/min.
2mm: 71.4% 3mm: 20.4% 5mm: 8.2%
SH: 1 cm
SpL: 356 ag/min.
2mm: 58.3% 3mm: 25.6% 4mm: 4.6% 5mm: 4.6% 6mm: 2.3% 7mm: 2.3%
8mm: 2.3%
The bed starts to be eroded fast.

Water Speed: V6.0 Time: 15:00-15:05h
The bed is eroded very fast, passing everything to suspension. Camera out of focus. It is not possible to take any kind of measurement.

File: W3.DAT **Sea Carousel Deployment #183**

Water Speed: V0.5 Time: 16:00-16:05h
No motion

Water Speed: V1.0 Time: 16:05-16:10h
Small amount of organic flocs in suspension.

Water Speed: V1.5 Time: 16:10-16:15h
Not significant BL is observed
SpL: 281 ag/min.
2mm: 85% 3mm: 13% 4mm: 2%

Water Speed: V2.0 Time: 16:15-16:20h
BL: 24.6 ag/min.
2mm: 72% 3mm: 18.7% 4mm: 6.2% 5mm: 3%
CrH: 1-2 mm
SL: 10 ag/min.
2mm: 83% 3mm: 17%
SpL: 142 ag/min.
2mm: 50% 3mm: 39% 4mm: 11%
Bed surface starts to grow up.

Water Speed: V2.5 Time: 16:20-16:25h
BL: 17 ag/min.
2mm: 50% 3mm: 33% 4mm: 7% 5mm: 10%
CrH: 1-2 mm
SL: 19 ag/min.
2mm: 62% 3mm: 27.5% 4mm: 6.9% 5mm: 3.4%
SH: 1-1.5 cm SLe: 5-10 cm (3 ag)
SpL: 116 ag/min.
2mm: 37.8% 3mm: 43.2% 4mm: 13.5% 5mm: 5.4%
Back ground too dark makes difficult to differentiate ag.

Water Speed: V3.0 Time: 16:25-16:30h
BL: 13.9 ag/min.
2mm: 47.4% 3mm: 31.6% 4mm: 21%
CrH: 1-2 mm
SL: 26 ag/min.
2mm: 62% 3mm: 33% 4mm: 4.6%
SH: 1.5 cm
SpL: 166 ag/min.
2mm: 54.5% 3mm: 36.4% 4mm: 9%
Bed surface reach a maximum height of 7 mm.

Water Speed: V3.5 Time: 16:30-16:35h
BL: 15 ag/min.
2mm: 45.5% 3mm: 36.4% 4mm: 18%
CrH: 1-2 mm
SL: 46.6 ag/min.
2mm: 68.9% 3mm: 9.45% 4mm: 10.3%
SH: 1.5 cm
SpL: 190 ag/min.
2mm: 52% 3mm: 36% 4mm: 8% 5mm: 4%

Water Speed: V4.0 Time: 16:40-16:45h
From here to the end of the deployment the camera becomes out of focus. It is not possible to measure anything else.

File: C6.DAT **Sea Carousel Deployment #184**

Water Speed: V0.5 Time: 18:44-19:00h
No motion.

Water Speed: V1.0 Time: 19:00-19:05h
Erosion of organic flocs starts.

Water Speed: V1.5 Time: 19:05-19:10h
Organic flocs moving as BL. Camera out of focus, is not possible to make any measurement.

Water Speed: V2.0 Time: 19:10-19:15h
BL: 3.4 ag/min.
2mm: 33.3% 3mm: 33.3% 4mm: 33.3%
Very poor vision. Only 3 ag could be observed.
SL: 11.7 ag/min.
2mm: 50% 3mm: 25% 4mm: 25%
SH: 2 cm SLe: 10 cm (1 ag)
SpL: 48.3 ag/min.
2mm: 63.6% 3mm: 36.4%

Water Speed: V2.5 Time: 19:15-19:20h
BL: 7.3 ag/min.
2mm: 16.6% 3mm: 33.3% 4mm: 16.6% 5mm: 16.6% 6mm: 16.6%
SL: 6 ag/min.
2mm: 25% 3mm: 50% 4mm: 25%
SpL: 22.5 ag/min.
2mm: 26.6% 3mm: 26.6% 4mm: 20% 5mm: 13.3% 6mm: 6.6% 10mm: 6.6%
Very poor vision.

Water Speed: V3.0 Time: 19:20-19:25h
BL: 16.2 ag/min.
2mm: 40% 3mm: 10% 4mm: 40% 5mm: 0% 6mm: 10%
SL: 30.8 ag/min.
2mm: 40% 3mm: 20% 4mm: 25% 5mm: 15%
SH: 1.5 cm SL: 10 cm (2 ag)
SpL: 106.2 ag/min.
2mm: 52.2% 3mm: 26% 4mm: 17.5% 5mm: 4.3%

Water Speed: V3.5 Time: 19:25-19:30h
BL: 41 ag/min.
2mm: 20.8% 3mm: 33.3% 4mm: 16.7% 5mm: 12.5% 6mm: 12.5% 15mm: 4.2% CrH: 1-2 mm
SL: 16.7 ag/min.
2mm: 40% 3mm: 20% 4mm: 20% 5mm: 20%
SH: 1.5 cm
SpL: 402 ag/min.
2mm: 67.8% 3mm: 23.2% 4mm: 3.6% 5mm: 3.6% 6mm: 1.8%
Bed starts to be eroded.

Water Speed: V4.0 Time: 19:30-19:35h
BL: 20.5 ag/min.
2mm: 26.7% 3mm: 40% 4mm: 13.3% 6mm: 6.6% 8mm: 6.6% 15mm: 6.6% **SL:** 16 ag/min.
2mm: 41.7% 3mm: 8.3% 4mm: 16.7% 5mm: 8.3% 6mm: 8.3% 9 mm: 8.3% 10mm: 8.3%
SpL: 501 ag/min.
2mm: 54.7% 3mm: 20% 4mm: 10.6% 5mm: 8% 6mm: 5.3% 7mm: 1.3%
Very fast bed erosion.

Water Speed: V5.0 Time: 19:35-19:40h
SpL: 396 ag/min.
2mm: 47.7% 3mm: 20.5% 4mm: 9.1% 5mm: 9.1%
The inside bed surface is lower than the external bed surface. Aggregates speed to fast. From here to the end of the deployment it is not possible to make any measure.

File: W4.DAT **Sea Carousel Deployment #186**

Water Speed: V0.5 Time: 15:45-15:50h
No motion

Water Speed: V1.0 Time: 15:50-15:56h
Starts BL of organic flocs.

Water Speed: V1.5 Time: 15:56-16:01h
1-2 mm thick BL layer.

Water Speed: V2.0 Time: 16:01-16:06h
Bed surface starts to grow up. Ag < 1 mm. Small ripples appear (0.5 cm height, 12 cm wavelength)

Water Speed: V2.5 Time: 16:06-16:11h
BL: 57 ag/min.
1mm: 72.4% 2mm: 23% 3mm: 4.6%
CrH: 1-2 mm

Water Speed: V3.0 Time: 16:11-16:16h
BL: 67 ag/min.
1mm: 15% 2mm: 24% 3mm: 12%
CrH: 1-2 mm
SH: 0.9 cm

Water Speed: V3.5 Time: 16:16-16:21h
BL: 54.4 ag/min.
2mm: 37.2% 3mm: 26.9% 4mm: 24.4% 5mm: 7.7% 6mm: 2.5% 7mm: 1.3%
SL: 29 ag/min.
2mm: 40.7% 3mm: 44.4% 4mm: 11.1% 5mm: 3.8%
SH: 0.5-0.7cm
SpL: 216 ag/min.
2mm: 48.3% 3mm: 38% 4mm: 8.6% 5mm: 1.7% 6mm: 1.7% 10mm: 1.7%

Water Speed: V4.0 Time: 16:21-16:26h
BL: 61 ag/min.
2mm: 42.8% 3mm: 27.4% 4mm: 15.5% 5mm: 8.3% 7mm: 1.2% 8mm: 1.2% 10 mm: 1.2% 11mm: 1.2% 13mm: 1.2mm
CrH: 2mm
SL: 39 ag/min.
2mm: 52.8% 3mm: 33.3% 4mm: 11.1% 5mm: 2.8%
SH: 1.0 cm
SpL: 302 ag/min.
2mm: 58% 3mm: 27.2% 4mm: 12.3% 5mm: 1.2% 10mm: 1.2%
Bed surface becomes plane and grows up reaching a maximum height of 1 cm.

Water Speed: V5.0 Time: 16:26-16:31h
BL: 33 ag/min.
2mm: 61.3% 3mm: 24.5% 4mm: 8.2% 5mm: 2% 6mm: 4%
SL: 58 ag/min.
2mm: 57.7% 3mm: 32.7% 4mm: 9.6%
SpL: 480 ag/min.
2mm: 62.7% 3mm: 19.6% 4mm: 10.7% 5mm: 5.3% 6mm: 1.7%
From here to the end of the deployment the turbidity of the outside water makes not possible any further observation.

APPENDIX 2

Major Ions Data

Note: F = filtered sample (dissolved phase)
U = unfiltered (total water sample)
ex. CA-F-VH = Calcium filtered
CA-U-VH = Calcium total

FINAL SAMPLE ANALYSIS REPORT 8-NOV-1995 10:01AM SHEIKH

Project number: 95-563
Project title: FLOCCULATION OF FINE-GRAINED SEDIMENT
Project leader: I. DROPPO

Sample Naqudat proj - Cruise Number Naquadat stn - Mon/Cons. Stn Client sample# - Begin/end depth Sampling date Date last analyzed Date received Date expected Date accepted		9504448 W4-1 23-AUG-1995 23-OCT-1995 28-AUG-1995 23-OCT-1995 08-NOV-1995		9504449 W4-5 23-AUG-1995 23-OCT-1995 28-AUG-1995 23-OCT-1995 08-NOV-1995		9504450 W4-11 23-AUG-1995 23-OCT-1995 28-AUG-1995 23-OCT-1995 08-NOV-1995	
S2 CA-F-VH							
CA (MG/L)	A0018	42.8		42.0		44.3	
S1 CA-U-VH							
CA (MG/L)	A0019	44.9		45.6		56.8	
S8 COBAS-F-VH							
CL (MG/L)	A1974	68.1		66.8		69.3	
SO4 (MG/L)	A1976	54.2		52.1		52.5	
SIO2 (MG/L)	A1978	1.00		1.06		3.74	
S7 COBAS-U-VH							
CL (MG/L)	A1975	67.0		66.7		69.1	
SO4 (MG/L)	A1977	49.4		48.4		83.7	
SIO2 (MG/L)	A1979	1.01		1.42		13.9	
S4 MG-F-VH							
MG (MG/L)	A0022	10.8		10.5		10.8	
S3 MG-U-VH							
MG (MG/L)	A0023	11.3		11.4		12.3	
S6 NA-K-F-VH							
K (MG/L)	A0026	4.04		4.04		4.11	
NA (MG/L)	A0029	41.2		40.5		41.9	
S5 NA-K-U-VH							
K (MG/L)	A0027	4.27		4.21		4.13	
NA (MG/L)	A0030	43.7	R	42.4	R	42.9	R

FİNAL SAMPLE ANALYSIS REPORT 8-NOV-1995 10:01AM SHEIKH

Project number: 95-563
Project title: FLOCCULATION OF FINE-GRAINED SEDIMENT
Project leader: I. DROPPO

Sample Naqudat proj - Cruise Number Naquadat stn - Mon/Cons. Stn Client sample# - Begin/end depth Sampling date Date last analyzed Date received Date expected Date accepted		9504445 CN4-1 23-AUG-1995 23-OCT-1995 28-AUG-1995 23-OCT-1995 08-NOV-1995		9504446 CN4-5 23-AUG-1995 23-OCT-1995 28-AUG-1995 23-OCT-1995 08-NOV-1995		9504447 CN4-11 23-AUG-1995 23-OCT-1995 28-AUG-1995 23-OCT-1995 08-NOV-1995	
S2 CA-F-VH							
CA (MG/L)	A0018	41.8		42.5		43.9	
S1 CA-U-VH							
CA (MG/L)	A0019	44.6		45.0		55.5	
S8 COBAS-F-VH							
CL (MG/L)	A1974	66.3		66.5		66.8	
SO4 (MG/L)	A1976	50.7		53.3		51.2	
SIO2 (MG/L)	A1978	0.99		1.04		3.28	
S7 COBAS-U-VH							
CL (MG/L)	A1975	67.1	R	65.8		67.2	
SO4 (MG/L)	A1977	50.2	R	49.4		83.8	
SIO2 (MG/L)	A1979	1.16	R	1.39		12.1	
S4 MG-F-VH							
MG (MG/L)	A0022	10.7		10.6		10.6	
S3 MG-U-VH							
MG (MG/L)	A0023	11.3		11.3		12.0	
S6 NA-K-F-VH							
K (MG/L)	A0026	4.04		4.04		3.97	
NA (MG/L)	A0029	39.9		40.6		40.6	
S5 NA-K-U-VH							
K (MG/L)	A0027	4.20		4.17		4.08	
NA (MG/L)	A0030	42.4	R	42.4	R	42.0	R

FINAL SAMPLE ANALYSIS REPORT 8-NOV-1995 10:01AM SHEIKH

Project number: 95-563
Project title: FLOCCULATION OF FINE-GRAINED SEDIMENT
Project leader: I. DROPPO

Sample Naqudat proj - Cruise Number Naquadat stn - Mon/Cons. Stn Client sample# - Begin/end depth Sampling date Date last analyzed Date received Date expected Date accepted		9504442 CN3-1 23-AUG-1995 23-OCT-1995 28-AUG-1995 23-OCT-1995 08-NOV-1995		9504443 CN3-4 23-AUG-1995 23-OCT-1995 28-AUG-1995 23-OCT-1995 08-NOV-1995		9504444 CN3-11 23-AUG-1995 23-OCT-1995 28-AUG-1995 23-OCT-1995 08-NOV-1995	
S2 CA-F-VH							
CA (MG/L)	A0018	43.6		43.9		52.5	
S1 CA-U-VH							
CA (MG/L)	A0019	46.1		46.7		66.3	
S8 COBAS-F-VH							
CL (MG/L)	A1974	66.2		64.6		66.0	
SO4 (MG/L)	A1976	51.2		52.9		49.8	
SIO2 (MG/L)	A1978	1.16		1.21		3.70	
S7 COBAS-U-VH							
CL (MG/L)	A1975	66.0		64.7		64.5	
SO4 (MG/L)	A1977	48.3		46.2		67.2	
SIO2 (MG/L)	A1979	1.24		1.32		10.5	
S4 MG-F-VH							
MG (MG/L)	A0022	10.5		10.6		10.8	
S3 MG-U-VH							
MG (MG/L)	A0023	11.2		11.2		12.0	
S6 NA-K-F-VH							
K (MG/L)	A0026	4.04		4.04		3.97	
NA (MG/L)	A0029	40.4		39.4		39.5	
S5 NA-K-U-VH							
K (MG/L)	A0027	4.20		4.18		4.02	
NA (MG/L)	A0030	42.0	R	41.6	R	42.0	R

FINAL SAMPLE ANALYSIS REPORT 8-NOV-1995 10:01AM SHEIKH

Project number: 95-563
Project title: FLOCCULATION OF FINE-GRAINED SEDIMENT
Project leader: I. DROPPO

Sample Naqudat proj - Cruise Number Naquadat stn - Mon/Cons. Stn Client sample# - Begin/end depth Sampling date Date last analyzed Date received Date expected Date accepted		9504439 W2-1 22-AUG-1995 23-OCT-1995 28-AUG-1995 23-OCT-1995 08-NOV-1995		9504440 W2-5 22-AUG-1995 23-OCT-1995 28-AUG-1995 23-OCT-1995 08-NOV-1995		9504441 W2-11 22-AUG-1995 23-OCT-1995 28-AUG-1995 23-OCT-1995 08-NOV-1995	
S2 CA-F-VH							
CA (MG/L)	A0018	46.1		47.4		48.1	
S1 CA-U-VH							
CA (MG/L)	A0019	48.9		50.4		62.3	
S8 COBAS-F-VH							
CL (MG/L)	A1974	63.5		63.1		62.7	
SO4 (MG/L)	A1976	51.6		52.3		50.3	
SIO2 (MG/L)	A1978	1.12		1.20		3.72	
S7 COBAS-U-VH							
CL (MG/L)	A1975	63.4		62.4		63.2	
SO4 (MG/L)	A1977	46.9		45.2		73.8	
SIO2 (MG/L)	A1979	1.22		1.71		13.7	
S4 MG-F-VH							
MG (MG/L)	A0022	10.3		10.5		10.8	
S3 MG-U-VH							
MG (MG/L)	A0023	11.1		11.0		12.2	
S6 NA-K-F-VH							
K (MG/L)	A0026	3.90		3.83		3.76	
NA (MG/L)	A0029	38.6		38.3		37.6	
S5 NA-K-U-VH							
K (MG/L)	A0027	4.06		4.07		3.86	
NA (MG/L)	A0030	40.4	R	39.5	R	40.4	R

FINAL SAMPLE ANALYSIS REPORT 8-NOV-1995 10:01AM SHEIKH

Project number: 95-563
Project title: FLOCCULATION OF FINE-GRAINED SEDIMENT
Project leader: I. DROPPO

Sample		9504436		9504437		9504438	
Naqudat proj - Cruise Number							
Naquadat stn - Mon/Cons. Stn							
Client sample# - Begin/end depth		CN2-1		CN2-4		CN2-11	
Sampling date		22-AUG-1995		22-AUG-1995		22-AUG-1995	
Date last analyzed		23-OCT-1995		23-OCT-1995		23-OCT-1995	
Date received		28-AUG-1995		28-AUG-1995		28-AUG-1995	
Date expected		23-OCT-1995		23-OCT-1995		23-OCT-1995	
Date accepted		08-NOV-1995		08-NOV-1995		08-NOV-1995	
S2 CA-F-VH							
CA (MG/L)	A0018	44.0		45.0		52.3	
S1 CA-U-VH							
CA (MG/L)	A0019	47.3		48.7		79.7	
S8 COBAS-F-VH							
CL (MG/L)	A1974	76.2		70.8	R	64.4	
SO4 (MG/L)	A1976	55.2		56.3	R	52.8	
SIO2 (MG/L)	A1978	1.36		1.49	R	3.90	
S7 COBAS-U-VH							
CL (MG/L)	A1975	71.5		69.1		64.5	
SO4 (MG/L)	A1977	51.4		50.2		75.6	
SIO2 (MG/L)	A1979	1.57		1.60		12.3	
S4 MG-F-VH							
MG (MG/L)	A0022	11.0		10.8		11.0	
S3 MG-U-VH							
MG (MG/L)	A0023	11.5		11.4		13.1	
S6 NA-K-F-VH							
K (MG/L)	A0026	4.40		4.33		4.04	
NA (MG/L)	A0029	44.9		43.2		39.2	
S5 NA-K-U-VH							
K (MG/L)	A0027	4.56		4.52		4.00	
NA (MG/L)	A0030	45.8	R	43.7	R	40.4	R

FINAL SAMPLE ANALYSIS REPORT 8-NOV-1995 09:48AM SHEIKH

Project number: 95-563
Project title: FLOCCULATION OF FINE-GRAINED SEDIMENT
Project leader: I. DROPPO

Sample		9504434		9504435	
Naqudat proj - Cruise Number					
Naquadat stn - Mon/Cons. Stn					
Client sample# - Begin/end depth		W1-4		W1-10	
Sampling date		21-AUG-1995		21-AUG-1995	
Date last analyzed		23-OCT-1995		23-OCT-1995	
Date received		29-AUG-1995		29-AUG-1995	
Date expected		24-OCT-1995		24-OCT-1995	
Date accepted		08-NOV-1995		08-NOV-1995	
S2 CA-F-VH					
CA (MG/L)	A0018	44.7		46.8	
S1 CA-U-VH					
CA (MG/L)	A0019	48.9		62.4	
S8 COBAS-F-VH					
CL (MG/L)	A1974	70.1		70.7	
SO4 (MG/L)	A1976	59.4		59.1	
SIO2 (MG/L)	A1978	1.40		4.31	
S7 COBAS-U-VH					
CL (MG/L)	A1975	69.6		70.0	
SO4 (MG/L)	A1977	49.8		91.1	
SIO2 (MG/L)	A1979	1.83		14.2	
S4 MG-F-VH					
MG (MG/L)	A0022	10.7		11.1	
S3 MG-U-VH					
MG (MG/L)	A0023	11.4		12.5	
S6 NA-K-F-VH					
K (MG/L)	A0026	4.33		4.25	
NA (MG/L)	A0029	43.6		42.9	
S5 NA-K-U-VH					
K (MG/L)	A0027	4.52		4.26	
NA (MG/L)	A0030	44.9	R	44.5	R

FINAL SAMPLE ANALYSIS REPORT 8-NOV-1995 09:48AM SHEIKH

Project number: 95-563
Project title: FLOCCULATION OF FINE-GRAINED SEDIMENT
Project leader: I. DROPPO

Sample Naqudat proj - Cruise Number Naquadat stn - Mon/Cons. Stn Client sample# - Begin/end depth Sampling date Date last analyzed Date received Date expected Date accepted		9504431 CN1-4 21-AUG-1995 23-OCT-1995 29-AUG-1995 24-OCT-1995 08-NOV-1995		9504432 CN1-12 21-AUG-1995 23-OCT-1995 29-AUG-1995 24-OCT-1995 08-NOV-1995		9504433 W1-1 21-AUG-1995 23-OCT-1995 29-AUG-1995 24-OCT-1995 08-NOV-1995	
S2 CA-F-VH							
CA (MG/L)	A0018	46.0		90.3		45.5	
S1 CA-U-VH							
CA (MG/L)	A0019	50.9		100.0		48.4	
S8 COBAS-F-VH							
CL (MG/L)	A1974	72.6		73.5		71.8	
SO4 (MG/L)	A1976	59.7		58.1		57.5	
SIO2 (MG/L)	A1978	1.53		5.24		1.40	
S7 COBAS-U-VH							
CL (MG/L)	A1975	72.3		73.2		71.9	
SO4 (MG/L)	A1977	49.6		98.9		52.1	
SIO2 (MG/L)	A1979	1.90		13.9		1.48	
S4 MG-F-VH							
MG (MG/L)	A0022	10.8		12.2		10.9	
S3 MG-U-VH							
MG (MG/L)	A0023	11.6		13.4		11.3	
S6 NA-K-F-VH							
K (MG/L)	A0026	4.47		4.54		4.47	
NA (MG/L)	A0029	44.7		44.6		43.5	
S5 NA-K-U-VH							
K (MG/L)	A0027	4.67		4.29		4.63	
NA (MG/L)	A0030	46.6	R	46.6	R	45.4	R

FINAL SAMPLE ANALYSIS REPORT 8-NOV-1995 09:48AM SHEIKH

Project number: 95-563
Project title: FLOCCULATION OF FINE-GRAINED SEDIMENT
Project leader: I. DROPPO

Sample		9504428	9504429	9504430
Naqudat proj - Cruise Number				
Naquadat stn - Mon/Cons. Stn				
Client sample# - Begin/end depth		C4-5	C4-12	CN1-1
Sampling date		18-AUG-1995	18-AUG-1995	21-AUG-1995
Date last analyzed		23-OCT-1995	23-OCT-1995	23-OCT-1995
Date received		29-AUG-1995	29-AUG-1995	29-AUG-1995
Date expected		24-OCT-1995	24-OCT-1995	24-OCT-1995
Date accepted		08-NOV-1995	08-NOV-1995	08-NOV-1995
S2 CA-F-VH				
CA (MG/L)	A0018	46.7	47.1	45.9
S1 CA-U-VH				
CA (MG/L)	A0019	49.9	61.6	48.2
S8 COBAS-F-VH				
CL (MG/L)	A1974	66.1	65.8	72.7
SO4 (MG/L)	A1976	56.1	52.7	58.2
SIO2 (MG/L)	A1978	1.35	5.00	1.37
S7 COBAS-U-VH				
CL (MG/L)	A1975	65.5	65.6	72.6
SO4 (MG/L)	A1977	50.3	81.0	48.3
SIO2 (MG/L)	A1979	1.88	14.4	1.50
S4 MG-F-VH				
MG (MG/L)	A0022	10.7	11.0	11.0
S3 MG-U-VH				
MG (MG/L)	A0023	11.3	12.3	11.5
S6 NA-K-F-VH				
K (MG/L)	A0026	4.04	3.97	4.40
NA (MG/L)	A0029	41.2	40.5	44.2
S5 NA-K-U-VH				
K (MG/L)	A0027	4.32	4.01	4.59
NA (MG/L)	A0030	42.4 R	42.0 R	47.4 R

FINAL SAMPLE ANALYSIS REPORT 8-NOV-1995 09:48AM SHEIKH

Project number: 95-563
Project title: FLOCCULATION OF FINE-GRAINED SEDIMENT
Project leader: I. DROPPO

Sample Naqudat proj - Cruise Number Naquadat stn - Mon/Cons. Stn Client sample# - Begin/end depth Sampling date Date last analyzed Date received Date expected Date accepted		9504425 C3-4 18-AUG-1995 23-OCT-1995 29-AUG-1995 24-OCT-1995 08-NOV-1995		9504426 C3-11 18-AUG-1995 23-OCT-1995 29-AUG-1995 24-OCT-1995 08-NOV-1995		9504427 C4-1 18-AUG-1995 23-OCT-1995 29-AUG-1995 24-OCT-1995 08-NOV-1995	
S2 CA-F-VH							
CA (MG/L)	A0018	46.4		47.7		46.2	
S1 CA-U-VH							
CA (MG/L)	A0019	50.2		60.2		48.6	
S8 COBAS-F-VH							
CL (MG/L)	A1974	65.5		66.4		66.8	
SO4 (MG/L)	A1976	56.6		54.6		52.3	
SIO2 (MG/L)	A1978	1.45		5.25		1.22	
S7 COBAS-U-VH							
CL (MG/L)	A1975	65.9	R	66.1		66.4	
SO4 (MG/L)	A1977	49.4	R	85.1		48.7	
SIO2 (MG/L)	A1979	1.92	R	15.8		1.53	
S4 MG-F-VH							
MG (MG/L)	A0022	10.9		11.2		10.7	
S3 MG-U-VH							
MG (MG/L)	A0023	11.1		12.6		11.3	
S6 NA-K-F-VH							
K (MG/L)	A0026	4.04		4.04		4.11	
NA (MG/L)	A0029	40.3		40.7		41.0	
S5 NA-K-U-VH							
K (MG/L)	A0027	4.25		4.01		4.35	
NA (MG/L)	A0030	42.0	R	42.4	R	42.4	R

FINAL SAMPLE ANALYSIS REPORT 8-NOV-1995 09:48AM SHEIKH

Project number: 95-563
Project title: FLOCCULATION OF FINE-GRAINED SEDIMENT
Project leader: I. DROPPO

Sample		9504422		9504423		9504424	
Naqudat proj - Cruise Number							
Naquadat stn - Mon/Cons. Stn							
Client sample# - Begin/end depth		C1-13		C1-14		C3-1	
Sampling date		18-AUG-1995		18-AUG-1995		18-AUG-1995	
Date last analyzed		23-OCT-1995		23-OCT-1995		23-OCT-1995	
Date received		29-AUG-1995		29-AUG-1995		29-AUG-1995	
Date expected		24-OCT-1995		24-OCT-1995		24-OCT-1995	
Date accepted		08-NOV-1995		08-NOV-1995		08-NOV-1995	
S2 CA-F-VH							
CA (MG/L)	A0018	48.7		48.9		45.9	
S1 CA-U-VH							
CA (MG/L)	A0019	66.2		62.4		49.3	
S8 COBAS-F-VH							
CL (MG/L)	A1974	66.6		66.3		66.0	R
SO4 (MG/L)	A1976	52.7		53.2		53.3	R
SIO2 (MG/L)	A1978	5.16		6.01		1.33	R
S7 COBAS-U-VH							
CL (MG/L)	A1975	65.6		66.3		65.9	
SO4 (MG/L)	A1977	84.2		85.9		46.7	
SIO2 (MG/L)	A1979	13.0		16.6		1.79	
S4 MG-F-VH							
MG (MG/L)	A0022	11.0		11.3		10.7	
S3 MG-U-VH							
MG (MG/L)	A0023	12.3		12.6		11.4	
S6 NA-K-F-VH							
K (MG/L)	A0026	3.90		3.97		4.04	
NA (MG/L)	A0029	40.5		40.7		39.9	
S5 NA-K-U-VH							
K (MG/L)	A0027	4.15		3.97		4.25	
NA (MG/L)	A0030	42.4	R	42.4	R	42.9	R

FINAL SAMPLE ANALYSIS REPORT 8-NOV-1995 09:48AM SHEIKH

Project number: 95-563
Project title: FLOCCULATION OF FINE-GRAINED SEDIMENT
Project leader: I. DROPPO

Sample		9504419	9504420	9504421
Naqudat proj - Cruise Number				
Naquadat stn - Mon/Cons. Stn				
Client sample# - Begin/end depth		C1-10	C1-11	C1-12
Sampling date		18-AUG-1995	18-AUG-1995	18-AUG-1995
Date last analyzed		23-OCT-1995	23-OCT-1995	23-OCT-1995
Date received		29-AUG-1995	29-AUG-1995	29-AUG-1995
Date expected		24-OCT-1995	24-OCT-1995	24-OCT-1995
Date accepted		08-NOV-1995	08-NOV-1995	08-NOV-1995
S2 CA-F-VH				
CA (MG/L)	A0018	47.8	48.0	47.7
S1 CA-U-VH				
CA (MG/L)	A0019	55.5	56.6	62.8
S8 COBAS-F-VH				
CL (MG/L)	A1974	66.0	67.1	65.7
SO4 (MG/L)	A1976	50.5	56.4	49.5
SIO2 (MG/L)	A1978	1.88	2.25	3.56
S7 COBAS-U-VH				
CL (MG/L)	A1975	65.6	66.9	66.1
SO4 (MG/L)	A1977	52.1	55.0	68.6
SIO2 (MG/L)	A1979	3.53	4.59	7.95
S4 MG-F-VH				
MG (MG/L)	A0022	10.7	10.9	10.7
S3 MG-U-VH				
MG (MG/L)	A0023	11.4	11.5	11.7
S6 NA-K-F-VH				
K (MG/L)	A0026	3.97	4.04	4.04
NA (MG/L)	A0029	40.0	40.6	40.7
S5 NA-K-U-VH				
K (MG/L)	A0027	4.26	4.28	4.22
NA (MG/L)	A0030	42.4 R	42.0 R	42.4 R

FINAL SAMPLE ANALYSIS REPORT 8-NOV-1995 09:48AM SHEIKH

Project number: 95-563
Project title: FLOCCULATION OF FINE-GRAINED SEDIMENT
Project leader: I. DROPPO

Sample Naqudat proj - Cruise Number Naquadat stn - Mon/Cons. Stn Client sample# - Begin/end depth Sampling date Date last analyzed Date received Date expected Date accepted		9504416 C1-7 18-AUG-1995 23-OCT-1995 29-AUG-1995 24-OCT-1995 08-NOV-1995		9504417 C1-8 18-AUG-1995 23-OCT-1995 29-AUG-1995 24-OCT-1995 08-NOV-1995		9504418 C1-9 18-AUG-1995 23-OCT-1995 29-AUG-1995 24-OCT-1995 08-NOV-1995	
S2 CA-F-VH							
CA (MG/L)	A0018	46.7		46.9		47.8	
S1 CA-U-VH							
CA (MG/L)	A0019	51.4		53.9		54.2	
S8 COBAS-F-VH							
CL (MG/L)	A1974	65.6		65.9		65.7	
SO4 (MG/L)	A1976	51.4		50.5		53.2	
SIO2 (MG/L)	A1978	1.49		1.57		1.81	
S7 COBAS-U-VH							
CL (MG/L)	A1975	65.8		66.0		67.1	
SO4 (MG/L)	A1977	48.0		54.7		52.6	
SIO2 (MG/L)	A1979	2.07		2.72		3.18	
S4 MG-F-VH							
MG (MG/L)	A0022	10.8		10.8		10.8	
S3 MG-U-VH							
MG (MG/L)	A0023	11.5		11.5		11.4	
S6 NA-K-F-VH							
K (MG/L)	A0026	4.04		3.97		4.04	
NA (MG/L)	A0029	40.6		41.1		40.9	
S5 NA-K-U-VH							
K (MG/L)	A0027	4.30		4.30		4.26	
NA (MG/L)	A0030	42.4	R	43.3	R	42.9	R

FINAL SAMPLE ANALYSIS REPORT 8-NOV-1995 09:48AM SHEIKH

Project number: 95-563
Project title: FLOCCULATION OF FINE-GRAINED SEDIMENT
Project leader: I. DROPPO

Sample Naqudat proj - Cruise Number Naquadat stn - Mon/Cons. Stn Client sample# - Begin/end depth Sampling date Date last analyzed Date received Date expected Date accepted		9504413 C1-4 18-AUG-1995 23-OCT-1995 29-AUG-1995 24-OCT-1995 08-NOV-1995		9504414 C1-5 18-AUG-1995 23-OCT-1995 29-AUG-1995 24-OCT-1995 08-NOV-1995		9504415 C1-6 18-AUG-1995 23-OCT-1995 29-AUG-1995 24-OCT-1995 08-NOV-1995	
S2 CA-F-VH							
CA (MG/L)	A0018	45.2		46.4		46.7	
S1 CA-U-VH							
CA (MG/L)	A0019	48.7		49.0		49.3	
S8 COBAS-F-VH							
CL (MG/L)	A1974	64.6		66.4		65.3	
SO4 (MG/L)	A1976	49.2		50.4		51.8	
SIO2 (MG/L)	A1978	1.57		1.48		1.54	
S7 COBAS-U-VH							
CL (MG/L)	A1975	65.5		65.2		65.7	
SO4 (MG/L)	A1977	45.5		46.7		46.6	
SIO2 (MG/L)	A1979	1.51		1.43		1.57	
S4 MG-F-VH							
MG (MG/L)	A0022	10.8		10.9		10.9	
S3 MG-U-VH							
MG (MG/L)	A0023	11.3		11.5		11.3	
S6 NA-K-F-VH							
K (MG/L)	A0026	3.97		4.11		4.04	
NA (MG/L)	A0029	40.1		41.2		40.4	
S5 NA-K-U-VH							
K (MG/L)	A0027	4.30		4.29		4.33	
NA (MG/L)	A0030	42.4	R	42.9	R	42.4	R

Project number: 95-563
Project title: FLOCCULATION OF FINE-GRAINED SEDIMENT
Project leader: I. DROPPO

Sample Naqudat proj - Cruise Number Naquadat stn - Mon/Cons. Stn Client sample# - Begin/end depth Sampling date Date last analyzed Date received Date expected Date accepted		9504410 C1-1 18-AUG-1995 23-OCT-1995 29-AUG-1995 24-OCT-1995 08-NOV-1995		9504411 C1-2 18-AUG-1995 23-OCT-1995 29-AUG-1995 24-OCT-1995 08-NOV-1995		9504412 C1-3 18-AUG-1995 23-OCT-1995 29-AUG-1995 24-OCT-1995 08-NOV-1995	
S2 CA-F-VH							
CA (MG/L)	A0018	46.0	R	47.6	R	48.4	
S1 CA-U-VH							
CA (MG/L)	A0019	48.4		48.2		49.1	
S8 COBAS-F-VH							
CL (MG/L)	A1974	65.7		68.3		69.1	
SO4 (MG/L)	A1976	49.1		49.4		110.	
SIO2 (MG/L)	A1978	1.27		1.40		1.68	
S7 COBAS-U-VH							
CL (MG/L)	A1975	66.5		66.3		66.6	
SO4 (MG/L)	A1977	50.4		49.7		48.0	
SIO2 (MG/L)	A1979	1.32		1.35		1.47	
S4 MG-F-VH							
MG (MG/L)	A0022	10.6	R	11.1	R	11.3	
S3 MG-U-VH							
MG (MG/L)	A0023	11.3		11.3		11.4	
S6 NA-K-F-VH							
K (MG/L)	A0026	4.04		4.18		4.25	
NA (MG/L)	A0029	40.4		42.2		42.4	
S5 NA-K-U-VH							
K (MG/L)	A0027	4.22		4.22		4.28	
NA (MG/L)	A0030	42.4	R	42.4	R	42.4	R

APPENDIX 3

Eroded Suspended Sediment Grain Size Distributions

OPTOMAX V™ - direct microscopic observation
MALVERN™ - laser particle sizing

OPTOMAX V PSA 7.07

Particle distribution by Spherical Diameter

Time : 16:30
Date : 27th July 1995
Title : Hamilton Harbour
Sample name : C1-10
Comment : 500uL in 50mL column

Number of fields : 101
Accumlated Field area : 409195049

Class file selected : OBJ_2-5.SIZ
Volume coefficient : 1.0000
Calibration factor : 3.226 MICRONS /pixel

Size classes			Count	Count %	Volume	Volume %
6.2000	-	7.2000	115	4.0	28817.73	0.0
7.2000	-	8.3000	231	8.1	102004.89	0.0
8.3000	-	9.6000	106	3.7	75129.91	0.0
9.6000	-	11.100	214	7.5	233204.57	0.0
11.100	-	12.900	139	4.8	243387.67	0.0
12.900	-	15.000	158	5.5	418055.76	0.0
15.000	-	17.400	195	6.8	810566.31	0.0
17.400	-	20.100	218	7.6	1417262.3	0.0
20.100	-	23.300	168	5.9	1690499.2	0.0
23.300	-	27.000	168	5.9	2714920.8	0.0
27.000	-	31.300	133	4.6	3313061.2	0.0
31.300	-	36.300	147	5.1	5532181.5	0.1
36.300	-	42.100	116	4.0	6887043.0	0.1
42.100	-	48.800	105	3.7	9786979.8	0.1
48.800	-	56.600	104	3.6	14636516	0.2
56.600	-	65.600	86	3.0	19338495	0.2
65.600	-	76.000	90	3.1	31577926	0.4
76.000	-	88.100	60	2.1	33551855	0.4
88.100	-	102.100	44	1.5	39289403	0.4
102.100	-	118.400	58	2.0	79322149	0.9
118.400	-	137.500	31	1.1	65924091	0.7
137.500	-	158.800	31	1.1	100915203	1.1
158.800	-	184.500	27	0.9	140069037	1.6
184.500	-	214.500	28	1.0	225839122	2.5
214.500	-	249.200	22	0.8	289391505	3.3
249.200	-	289.500	10	0.3	183281496	2.1
289.500	-	336.500	15	0.5	424643626	4.8
336.500	-	391.000	19	0.7	914521373	10.3
391.000	-	454.400	6	0.2	412973909	4.6
454.400	-	528.000	11	0.4	1.32E+009	14.8
528.000	-	614.000	4	0.1	764496208	8.6
614.000	-	713.800	2	0.1	536089225	6.0
713.800	-	829.500	3	0.1	1.40E+009	15.7
829.500	-	964.000	3	0.1	1.88E+009	21.1
964.000	-	1121.00	0	0.0	0	0.0
Total Count within range			2867		8.90E+009	
Undersize			440		39031.24	
Oversize			0			

otal particles examined	3307
otal particles included	3307
otal particles in range	2867

inimum Spherical Diameter of examined particles	3.6399
aximum Spherical Diameter of examined particles	872.613
rea fraction % of examined particles	6.7938

otal Spherical Diameter within range	130224.55
ean Spherical Diameter within range	45.422
tandard Deviation Spherical Diameter within range	76.661
edian Spherical Diameter within range	21.195

inimum Volume	48.226
aximum Volume	664453484
olume Surface mean	397.092

olume Spherical Diameter at 10%	227.289
olume Median Spherical Diameter	542.427
olume Spherical Diameter at 90%	900.217
elative span	1.2406

OPTOMAX V PSA 7.07

Particle distribution by Spherical Diameter

27th July 1995
16:31

:tle : Hamilton Harbour
ample name : C1-10

omment : 500uL in 50mL column
ccumlated Field area : 409195049 over 101 fields
olume coefficient : 1.0000
alibration factor : 3.226 MICRONS/pixel

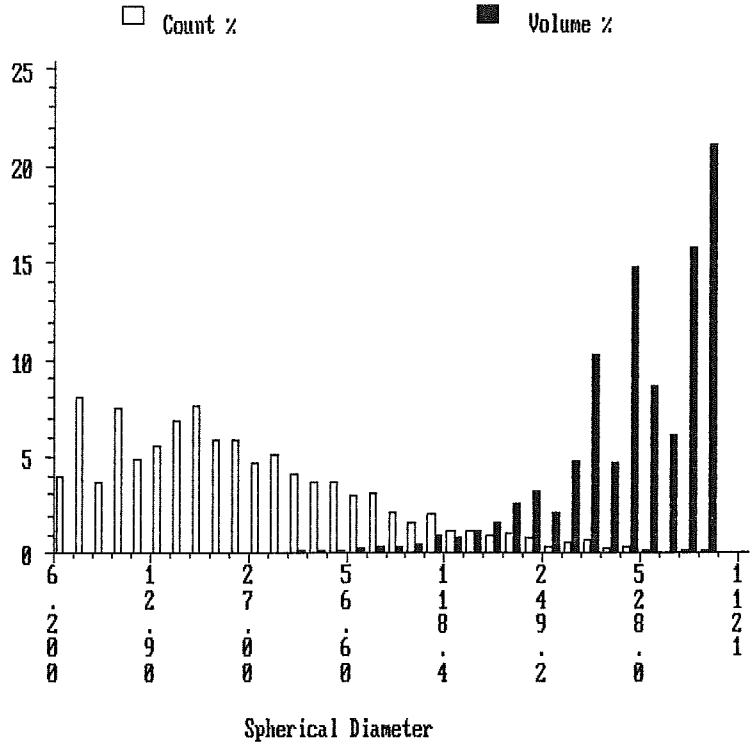

OPTOMAX V PSA 7.07

Particle distribution by Spherical Diameter

ime : 15:56
ate : 27th July 1995
itle : Hamilton Harbour
ample name : C1-11 August 1995
omment : 500uL in 50mL column

umber of fields : 110
ccumlated Field area : 445657974

lass file selected : OBJ_2-5.SIZ
olume coefficient : 1.0000
alibration factor : 3.226 MICRONS /pixel

Size classes			Count	Count %	Volume	Volume %
6.2000	-	7.2000	167	4.0	41848.36	0.0
7.2000	-	8.3000	332	8.0	148946.88	0.0
8.3000	-	9.6000	130	3.1	92140.45	0.0
9.6000	-	11.100	303	7.3	330535.31	0.0
11.100	-	12.900	228	5.5	399109.51	0.0
12.900	-	15.000	231	5.6	619090.05	0.0
15.000	-	17.400	305	7.4	1250601.1	0.0
17.400	-	20.100	274	6.6	1778890.6	0.0
20.100	-	23.300	246	5.9	2489794.1	0.0
23.300	-	27.000	258	6.2	4052412.8	0.0
27.000	-	31.300	201	4.8	4961117.7	0.1
31.300	-	36.300	226	5.5	8715163.6	0.1
36.300	-	42.100	201	4.8	11882506	0.1
42.100	-	48.800	167	4.0	15582827	0.2
48.800	-	56.600	154	3.7	22148253	0.2
56.600	-	65.600	126	3.0	28776941	0.3
65.600	-	76.000	107	2.6	37371919	0.4
76.000	-	88.100	91	2.2	49447578	0.6
88.100	-	102.100	68	1.6	58939458	0.7
102.100	-	118.400	54	1.3	71126313	0.8
118.400	-	137.500	56	1.4	114436596	1.3
137.500	-	158.800	38	0.9	117753038	1.3
158.800	-	184.500	31	0.7	161310166	1.8
184.500	-	214.500	39	0.9	315941034	3.5
214.500	-	249.200	29	0.7	350795555	3.9
249.200	-	289.500	19	0.5	372395109	4.2
289.500	-	336.500	15	0.4	454960158	5.1
336.500	-	391.000	14	0.3	633153799	7.1
391.000	-	454.400	18	0.4	1.36E+009	15.2
454.400	-	528.000	6	0.1	769584941	8.6
528.000	-	614.000	5	0.1	962714190	10.7
614.000	-	713.800	3	0.1	816473230	9.1
713.800	-	829.500	2	0.0	944341129	10.5
829.500	-	964.000	2	0.0	1.26E+009	14.1
964.000	-	1121.00	0	0.0	0	0.0
otal Count within range			4146		8.96E+009	
ndersize			634		54735.84	
versize			0			

otal particles examined	4780
otal particles included	4780
otal particles in range	4146

nimum Spherical Diameter of examined particles	3.6399
aximum Spherical Diameter of examined particles	868.725
ea fraction % of examined particles	8.1466
otal Spherical Diameter within range	174364.10
an Spherical Diameter within range	42.056
andard Deviation Spherical Diameter within range	66.921
edian Spherical Diameter within range	21.440

nimum Volume	48.226
aximum Volume	655611442
olume Surface mean	349.309
olume Spherical Diameter at 10%	201.799
olume Median Spherical Diameter	480.650
olume Spherical Diameter at 90%	868.414
elative span	1.3869

OPTOMAX V PSA 7.07

Particle distribution by Spherical Diameter

27th July 1995
15:56

Title : Hamilton Harbour
Sample name : C1-11 August 1995

Comment : 500uL in 50mL column
Accumlated Field area : 445657974 over 110 fields
Volume coefficient : 1.0000
Calibration factor : 3.226 MICRONS/pixel

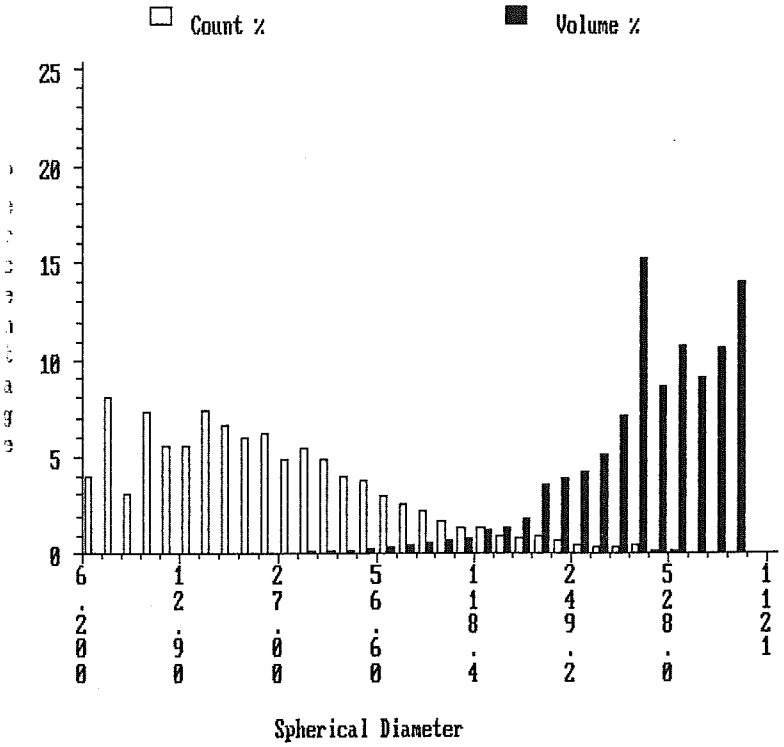

OPTOMAX V PSA 7.07

Particle distribution by Spherical Diameter

ime : 18:06
ate : 26th July 1995
itle : Hamilton Harbour
ample name : C1-12 August 1995
omment : 5 drops 50mL column

umber of fields : 110
ccumlated Field area : 445657974

lass file selected : OBJ_2-5.SIZ
olume coefficient : 1.0000
alibration factor : 3.226 MICRONS /pixel

Size classes			Count	Count %	Volume	Volume %
6.2000	-	7.2000	266	6.2	66656.67	0.0
7.2000	-	8.3000	418	9.7	189795.02	0.0
8.3000	-	9.6000	177	4.1	125452.77	0.0
9.6000	-	11.100	417	9.7	461741.02	0.1
11.100	-	12.900	312	7.3	542676.53	0.1
12.900	-	15.000	307	7.2	813671.59	0.1
15.000	-	17.400	313	7.3	1279755.1	0.1
17.400	-	20.100	363	8.5	2372926.7	0.3
20.100	-	23.300	261	6.1	2647073.9	0.3
23.300	-	27.000	259	6.0	4090303.0	0.4
27.000	-	31.300	207	4.8	5164332.5	0.6
31.300	-	36.300	188	4.4	7274366.4	0.8
36.300	-	42.100	155	3.6	9572483.9	1.0
42.100	-	48.800	124	2.9	11759793	1.3
48.800	-	56.600	125	2.9	17739002	1.9
56.600	-	65.600	103	2.4	23372555	2.6
65.600	-	76.000	90	2.1	31690709	3.5
76.000	-	88.100	44	1.0	23798404	2.6
88.100	-	102.100	44	1.0	38316729	4.2
102.100	-	118.400	35	0.8	46754732	5.1
118.400	-	137.500	30	0.7	61708510	6.7
137.500	-	158.800	11	0.3	37230331	4.1
158.800	-	184.500	15	0.3	80110295	8.7
184.500	-	214.500	13	0.3	107054288	11.7
214.500	-	249.200	7	0.2	77168945	8.4
249.200	-	289.500	4	0.1	80162274	8.7
289.500	-	336.500	2	0.0	59452728	6.5
336.500	-	391.000	2	0.0	97651412	10.7
391.000	-	454.400	1	0.0	87950622	9.6
454.400	-	528.000	0	0.0	0	0.0
528.000	-	614.000	0	0.0	0	0.0
614.000	-	713.800	0	0.0	0	0.0
713.800	-	829.500	0	0.0	0	0.0
829.500	-	964.000	0	0.0	0	0.0
964.000	-	1121.00	0	0.0	0	0.0
otal Count within range			4293		916522565	
ndersize			725		65825.88	
versize			0			

otal particles examined	5018
otal particles included	5018
otal particles in range	4293

inimum Spherical Diameter of examined particles	3.6399
aximum Spherical Diameter of examined particles	444.713
rea fraction % of examined particles	6.5932

otal Spherical Diameter within range	113122.20
ean Spherical Diameter within range	26.350
tandard Deviation Spherical Diameter within range	30.149
edian Spherical Diameter within range	16.913

inimum Volume	48.226
aximum Volume	87950622
olume Surface mean	133.213

olume Spherical Diameter at 10%	66.972
olume Median Spherical Diameter	198.842
olume Spherical Diameter at 90%	388.934
elative span	1.6192

OPTOMAX V PSA 7.07

Particle distribution by Spherical Diameter

26th July 1995
18:06

:tle : Hamilton Harbour
ample name : C1-12 August 1995

omment : 5 drops 50mL column
:cumlated Field area : 445657974 over 110 fields
olume coefficient : 1.0000
alibration factor : 3.226 MICRONS/pixel

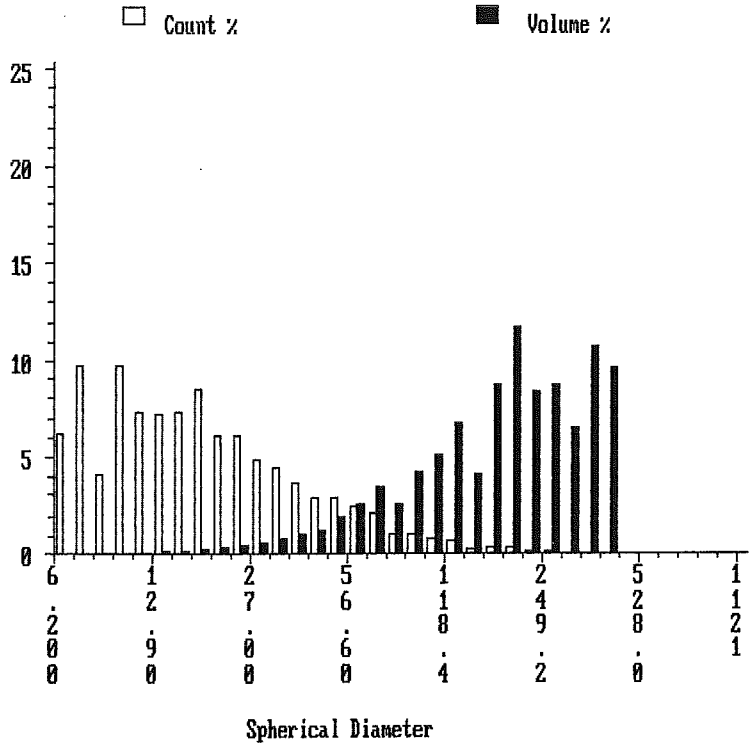

OPTOMAX V PSA 7.07

Particle distribution by Spherical Diameter

Time : 14:11
Date : 28th July 1995
Title : Hamilton Harbour
Sample name : C3-1 August 1995
Comment : 25mL column

Number of fields : 54
Accumlated Field area : 218777551

Class file selected : OBJ_2-5.SIZ
Volume coefficient : 1.0000
Calibration factor : 3.226 MICRONS /pixel

Size classes			Count	Count %	Volume	Volume %
6.2000	-	7.2000	555	5.4	139076.89	0.0
7.2000	-	8.3000	1077	10.6	487753.61	0.0
8.3000	-	9.6000	462	4.5	327453.00	0.0
9.6000	-	11.100	1009	9.9	1082441.4	0.0
11.100	-	12.900	775	7.6	1352508.3	0.1
12.900	-	15.000	742	7.3	1962763.4	0.1
15.000	-	17.400	841	8.2	3426480.0	0.1
17.400	-	20.100	737	7.2	4767651.3	0.2
20.100	-	23.300	636	6.2	6420773.8	0.2
23.300	-	27.000	629	6.2	9951065.9	0.4
27.000	-	31.300	466	4.6	11392149	0.4
31.300	-	36.300	439	4.3	16705578	0.6
36.300	-	42.100	341	3.3	20456711	0.8
42.100	-	48.800	276	2.7	25873737	1.0
48.800	-	56.600	228	2.2	33000430	1.3
56.600	-	65.600	207	2.0	47241267	1.8
65.600	-	76.000	181	1.8	64301740	2.4
76.000	-	88.100	157	1.5	84682525	3.2
88.100	-	102.100	119	1.2	99738073	3.8
102.100	-	118.400	91	0.9	118767456	4.5
118.400	-	137.500	72	0.7	153212379	5.8
137.500	-	158.800	60	0.6	193141461	7.3
158.800	-	184.500	27	0.3	135558302	5.2
184.500	-	214.500	26	0.3	201318288	7.7
214.500	-	249.200	16	0.2	204086900	7.8
249.200	-	289.500	14	0.1	271232098	10.3
289.500	-	336.500	7	0.1	214060011	8.1
336.500	-	391.000	3	0.0	139600004	5.3
391.000	-	454.400	1	0.0	79834925	3.0
454.400	-	528.000	2	0.0	198637252	7.6
528.000	-	614.000	0	0.0	0	0.0
614.000	-	713.800	1	0.0	285220954	10.9
713.800	-	829.500	0	0.0	0	0.0
829.500	-	964.000	0	0.0	0	0.0
964.000	-	1121.00	0	0.0	0	0.0
Total Count within range			10197		2.63E+009	
Undersize			1809		160604.29	
Oversize			0			

Total particles examined	12006
Total particles included	12006
Total particles in range	10197

Minimum Spherical Diameter of examined particles	3.6399
Maximum Spherical Diameter of examined particles	658.254
Area fraction % of examined particles	9.4650

Total Spherical Diameter within range	270155.50
Mean Spherical Diameter within range	26.494
Standard Deviation Spherical Diameter within range	32.001
Median Spherical Diameter within range	16.366

Minimum Volume	48.226
Maximum Volume	285220954
Volume Surface mean	150.983

Volume Spherical Diameter at 10%	77.987
Volume Median Spherical Diameter	227.878
Volume Spherical Diameter at 90%	621.846
Relative span	2.3866

OPTOMAX V PSA 7.07

Particle distribution by Spherical Diameter

itle : Hamilton Harbour 28th July 1995

ample name : C3-1 August 1995 14:13

omment : 25mL column

ccumlated Field area : 218777551 over 54 fields

olume coefficient : 1.0000

alibration factor : 3.226 MICRONS/pixel

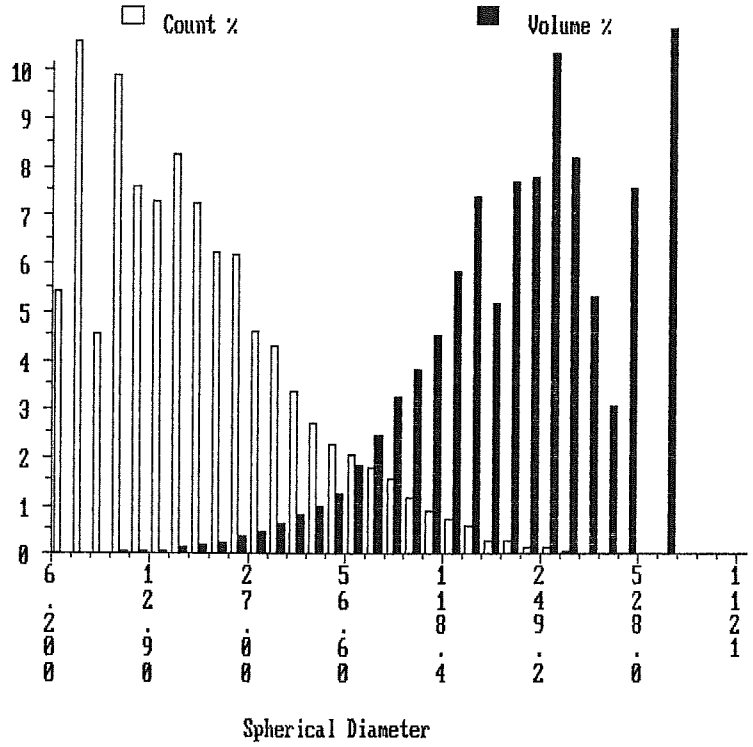

OPTOMAX V PSA 7.07

Particle distribution by Spherical Diameter

Time : 14:54
Date : 28th July 1995
Title : Hamilton Harbour
Sample name : C3-2 August 1995
Comment : 25mL column

Number of fields : 28
Accumlated Field area : 113440212

Class file selected : OBJ_2-5.SIZ
Volume coefficient : 1.0000
Calibration factor : 3.226 MICRONS /pixel

Size classes			Count	Count %	Volume	Volume %
6.2000	-	7.2000	564	5.5	141332.19	0.0
7.2000	-	8.3000	1146	11.2	516521.54	0.0
8.3000	-	9.6000	510	5.0	361474.09	0.0
9.6000	-	11.100	1118	10.9	1212562.0	0.1
11.100	-	12.900	821	8.0	1438156.7	0.1
12.900	-	15.000	845	8.3	2244274.7	0.2
15.000	-	17.400	901	8.8	3689691.9	0.3
17.400	-	20.100	775	7.6	5040109.9	0.4
20.100	-	23.300	686	6.7	6946393.1	0.6
23.300	-	27.000	649	6.4	10250783	0.9
27.000	-	31.300	485	4.7	11937911	1.0
31.300	-	36.300	405	4.0	15448877	1.3
36.300	-	42.100	287	2.8	16963474	1.4
42.100	-	48.800	193	1.9	17799312	1.5
48.800	-	56.600	196	1.9	28575938	2.4
56.600	-	65.600	130	1.3	29235897	2.5
65.600	-	76.000	122	1.2	43317801	3.6
76.000	-	88.100	107	1.0	59154051	5.0
88.100	-	102.100	84	0.8	73572683	6.2
102.100	-	118.400	54	0.5	70762848	5.9
118.400	-	137.500	51	0.5	107413399	9.0
137.500	-	158.800	35	0.3	109174953	9.2
158.800	-	184.500	19	0.2	97960827	8.2
184.500	-	214.500	14	0.1	104376647	8.8
214.500	-	249.200	10	0.1	122346699	10.3
249.200	-	289.500	9	0.1	174907989	14.7
289.500	-	336.500	1	0.0	27436949	2.3
336.500	-	391.000	1	0.0	47806919	4.0
391.000	-	454.400	0	0.0	0	0.0
454.400	-	528.000	0	0.0	0	0.0
528.000	-	614.000	0	0.0	0	0.0
614.000	-	713.800	0	0.0	0	0.0
713.800	-	829.500	0	0.0	0	0.0
829.500	-	964.000	0	0.0	0	0.0
964.000	-	1121.00	0	0.0	0	0.0
Total Count within range			10218		1.19E+009	
Undersize			1927		174495.45	
Oversize			0			

otal particles examined	12145
otal particles included	12145
otal particles in range	10218

inimum Spherical Diameter of examined particles	3.6399
aximum Spherical Diameter of examined particles	362.936
rea fraction % of examined particles	9.1312

otal Spherical Diameter within range	231436.35
ean Spherical Diameter within range	22.650
tandard Deviation Spherical Diameter within range	24.576
edian Spherical Diameter within range	15.280

inimum Volume	48.226
aximum Volume	47806919
olume Surface mean	105.297

olume Spherical Diameter at 10%	55.627
olume Median Spherical Diameter	154.863
olume Spherical Diameter at 90%	279.417
elative span	1.4451

OPTOMAX V PSA 7.07

Particle distribution by Spherical Diameter

28th July 1995
14:55

itle : Hamilton Harbour
ample name : C3-2 August 1995

omment : 25mL column
ccumlated Field area : 113440212 over 28 fields
olume coefficient : 1.0000
alibration factor : 3.226 MICRONS/pixel

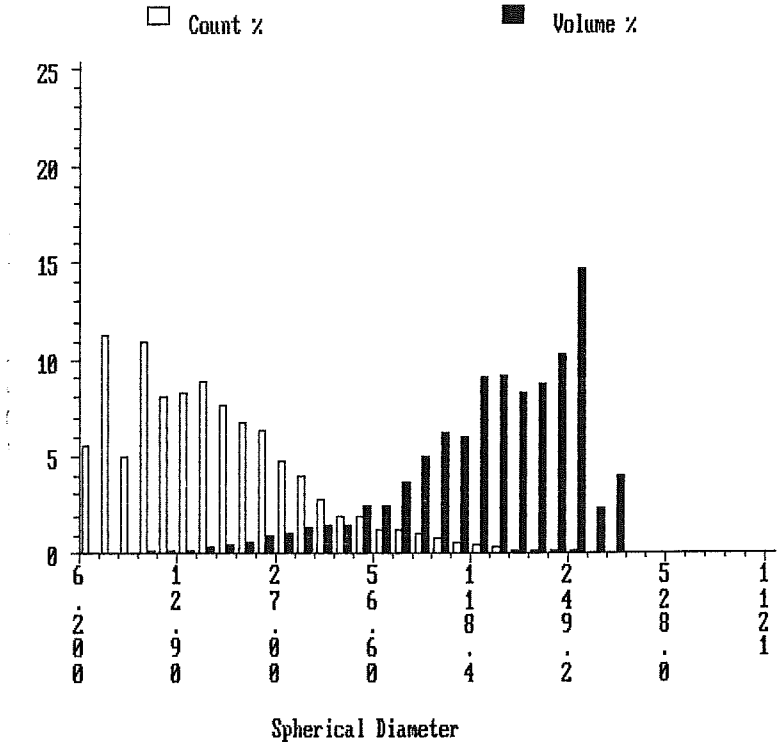

OPTOMAX V PSA 7.07

Particle distribution by Spherical Diameter

me : 15:31
te : 28th July 1995
tle : Hamilton Harbour
mple name : C3-3 August 1995
mment : 25mL column

mber of fields : 62
cumlated Field area : 251189040

ass file selected : OBJ_2-5.SIZ
olume coefficient : 1.0000
alibration factor : 3.226 MICRONS /pixel

Size classes			Count	Count %	Volume	Volume %
6.2000	-	7.2000	556	5.5	139327.48	0.0
7.2000	-	8.3000	1051	10.4	476035.51	0.0
8.3000	-	9.6000	405	4.0	287052.95	0.0
9.6000	-	11.100	930	9.2	998285.26	0.0
11.100	-	12.900	670	6.7	1172707.6	0.0
12.900	-	15.000	679	6.7	1795649.9	0.0
15.000	-	17.400	790	7.8	3231078.7	0.1
17.400	-	20.100	711	7.1	4669586.4	0.1
20.100	-	23.300	616	6.1	6194883.5	0.1
23.300	-	27.000	627	6.2	9905228.3	0.2
27.000	-	31.300	487	4.8	11963478	0.3
31.300	-	36.300	465	4.6	17679030	0.4
36.300	-	42.100	368	3.7	22249947	0.5
42.100	-	48.800	324	3.2	30378480	0.7
48.800	-	56.600	276	2.7	40004879	0.9
56.600	-	65.600	231	2.3	52056405	1.2
65.600	-	76.000	172	1.7	60571938	1.4
76.000	-	88.100	154	1.5	84635463	2.0
88.100	-	102.100	139	1.4	119216049	2.8
102.100	-	118.400	101	1.0	134803465	3.1
118.400	-	137.500	78	0.8	162080989	3.8
137.500	-	158.800	54	0.5	177285748	4.1
158.800	-	184.500	56	0.6	275362805	6.4
184.500	-	214.500	42	0.4	326256134	7.6
214.500	-	249.200	32	0.3	390279995	9.0
249.200	-	289.500	22	0.2	410261107	9.5
289.500	-	336.500	19	0.2	593278939	13.7
336.500	-	391.000	4	0.0	161681046	3.7
391.000	-	454.400	3	0.0	191962263	4.4
454.400	-	528.000	1	0.0	100074034	2.3
528.000	-	614.000	1	0.0	192933116	4.5
614.000	-	713.800	1	0.0	299864421	6.9
713.800	-	829.500	1	0.0	435440731	10.1
829.500	-	964.000	0	0.0	0	0.0
964.000	-	1121.00	0	0.0	0	0.0
otal Count within range			10066		4.32E+009	
idersize			1753		152436.63	
versize			0			

otal particles examined	11819
otal particles included	11819
otal particles in range	10066

inimum Spherical Diameter of examined particles	3.6399
aximum Spherical Diameter of examined particles	757.954
rea fraction % of examined particles	12.593

otal Spherical Diameter within range	295273.80
ean Spherical Diameter within range	29.334
tandard Deviation Spherical Diameter within range	38.287
edian Spherical Diameter within range	17.254

inimum Volume	48.226
aximum Volume	435440731
olume Surface mean	187.178

olume Spherical Diameter at 10%	97.907
olume Median Spherical Diameter	271.390
olume Spherical Diameter at 90%	714.736
elative span	2.2728

OPTOMAX V PSA 7.07

Particle distribution by Spherical Diameter

28th July 1995
15:32

itle : Hamilton Harbour
ample name : C3-3 August 1995

omment : 25mL column
cumlated Field area : 251189040 over 62 fields
olume coefficient : 1.0000
alibration factor : 3.226 MICRONS/pixel

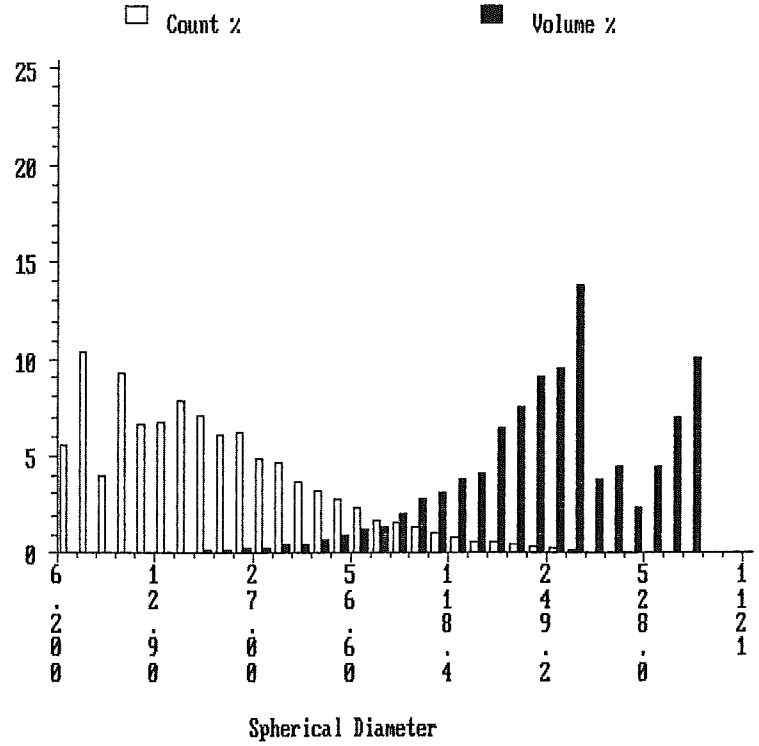

OPTOMAX V PSA 7.07

Particle distribution by Spherical Diameter

ime : 14:47
ate : 29th July 1995
itle : Hamilton Harbour
ample name : C3-4 August 1995

umber of fields : 90
ccumlated Field area : 364629251

lass file selected : OBJ_2-5.SIZ
olume coefficient : 1.0000
alibration factor : 3.226 MICRONS /pixel

Size classes			Count	Count %	Volume	Volume %
6.2000	-	7.2000	397	5.1	99483.83	0.0
7.2000	-	8.3000	739	9.4	333117.65	0.0
8.3000	-	9.6000	300	3.8	212631.82	0.0
9.6000	-	11.100	645	8.2	698478.63	0.0
11.100	-	12.900	491	6.3	851486.17	0.0
12.900	-	15.000	527	6.7	1391328.0	0.0
15.000	-	17.400	546	7.0	2242881.3	0.0
17.400	-	20.100	504	6.4	3279573.0	0.1
20.100	-	23.300	414	5.3	4168590.8	0.1
23.300	-	27.000	440	5.6	6987633.0	0.1
27.000	-	31.300	358	4.6	8777947.6	0.2
31.300	-	36.300	352	4.5	13583047	0.3
36.300	-	42.100	298	3.8	17708757	0.3
42.100	-	48.800	302	3.9	28339009	0.5
48.800	-	56.600	273	3.5	39855727	0.8
56.600	-	65.600	219	2.8	49124909	0.9
65.600	-	76.000	202	2.6	70864030	1.4
76.000	-	88.100	160	2.0	87630257	1.7
88.100	-	102.100	135	1.7	114608522	2.2
102.100	-	118.400	147	1.9	192610411	3.7
118.400	-	137.500	84	1.1	172493638	3.3
137.500	-	158.800	71	0.9	229546513	4.4
158.800	-	184.500	65	0.8	329776030	6.3
184.500	-	214.500	51	0.7	406017171	7.7
214.500	-	249.200	44	0.6	534127935	10.2
249.200	-	289.500	32	0.4	631693759	12.1
289.500	-	336.500	20	0.3	630332919	12.0
336.500	-	391.000	10	0.1	494125784	9.4
391.000	-	454.400	5	0.1	364787156	7.0
454.400	-	528.000	1	0.0	129586718	2.5
528.000	-	614.000	2	0.0	363536863	6.9
614.000	-	713.800	1	0.0	312738123	6.0
713.800	-	829.500	0	0.0	0	0.0
829.500	-	964.000	0	0.0	0	0.0
964.000	-	1121.00	0	0.0	0	0.0
otal Count within range			7835		5.24E+009	
ndersize			1262		110328.63	
versize			0			

otal particles examined	9097
otal particles included	9097
otal particles in range	7835

inimum Spherical Diameter of examined particles	3.6399
aximum Spherical Diameter of examined particles	678.777
rea fraction % of examined particles	7.9398

otal Spherical Diameter within range	277047.10
ean Spherical Diameter within range	35.360
tandard Deviation Spherical Diameter within range	46.395
edian Spherical Diameter within range	18.860

inimum Volume	48.226
aximum Volume	312738123
olume Surface mean	197.423

olume Spherical Diameter at 10%	108.316
olume Median Spherical Diameter	268.705
olume Spherical Diameter at 90%	563.972
elative span	1.6957

OPTOMAX V PSA 7.07

Particle distribution by Spherical Diameter

29th July 1995
14:48

itle : Hamilton Harbour
ample name : C3-4 August 1995

ccumlated Field area : 364629251 over 90 fields
olume coefficient : 1.0000
alibration factor : 3.226 MICRONS/pixel

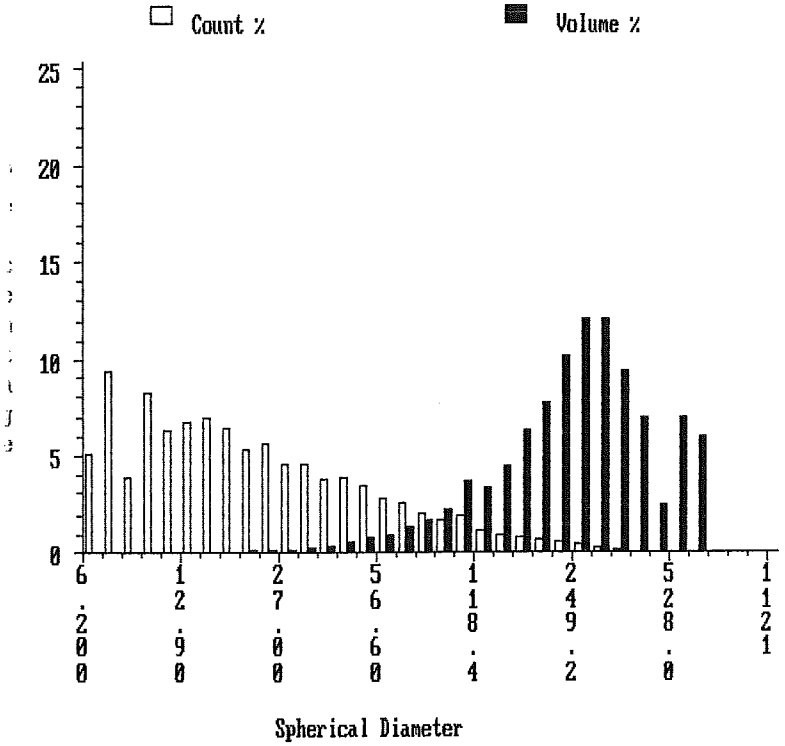

OPTOMAX V PSA 7.07

Particle distribution by Spherical Diameter

ime : 19:40
ate : 30th July 1995
itle : Hamilton Harbour
ample name : C3-5 August 1995

umber of fields : 103
ccumlated Field area : 417297921

lass file selected : OBJ_2-5.SIZ
olume coefficient : 1.0000
alibration factor : 3.226 MICRONS /pixel

Size classes			Count	Count %	Volume	Volume %
6.2000	–	7.2000	333	4.3	83446.14	0.0
7.2000	–	8.3000	539	6.9	243072.77	0.0
8.3000	–	9.6000	213	2.7	150968.59	0.0
9.6000	–	11.100	508	6.5	550493.69	0.0
11.100	–	12.900	384	4.9	670030.74	0.0
12.900	–	15.000	422	5.4	1102531.2	0.0
15.000	–	17.400	437	5.6	1802854.8	0.0
17.400	–	20.100	462	5.9	3008765.7	0.0
20.100	–	23.300	409	5.2	4150236.7	0.0
23.300	–	27.000	417	5.3	6699706.9	0.1
27.000	–	31.300	391	5.0	9582676.7	0.1
31.300	–	36.300	412	5.3	15840866	0.2
36.300	–	42.100	366	4.7	22150683	0.2
42.100	–	48.800	367	4.7	34161353	0.3
48.800	–	56.600	324	4.1	47310891	0.5
56.600	–	65.600	317	4.1	71947036	0.7
65.600	–	76.000	269	3.4	93892958	0.9
76.000	–	88.100	232	3.0	127823847	1.2
88.100	–	102.100	214	2.7	180822890	1.7
102.100	–	118.400	198	2.5	259905565	2.5
118.400	–	137.500	146	1.9	308183138	3.0
137.500	–	158.800	120	1.5	385238756	3.7
158.800	–	184.500	92	1.2	466180602	4.5
184.500	–	214.500	59	0.8	458371528	4.4
214.500	–	249.200	61	0.8	749426159	7.2
249.200	–	289.500	50	0.6	931823447	8.9
289.500	–	336.500	35	0.4	1.06E+009	10.1
336.500	–	391.000	18	0.2	864407429	8.3
391.000	–	454.400	11	0.1	815393001	7.8
454.400	–	528.000	7	0.1	761448445	7.3
528.000	–	614.000	4	0.1	713916720	6.8
614.000	–	713.800	7	0.1	2.05E+009	19.6
713.800	–	829.500	0	0.0	0	0.0
829.500	–	964.000	0	0.0	0	0.0
964.000	–	1121.00	0	0.0	0	0.0
Total Count within range			7824		1.04E+010	
Undersize			972		84262.81	
Oversize			0			

otal particles examined	8796
otal particles included	8796
otal particles in range	7824

inimum Spherical Diameter of examined particles	3.6399
aximum Spherical Diameter of examined particles	696.722
rea fraction % of examined particles	13.371

otal Spherical Diameter within range	356381.20
ean Spherical Diameter within range	45.550
tandard Deviation Spherical Diameter within range	58.813
edian Spherical Diameter within range	25.119

inimum Volume	48.226
laximum Volume	338203233
olume Surface mean	244.333

olume Spherical Diameter at 10%	128.483
olume Median Spherical Diameter	335.749
olume Spherical Diameter at 90%	662.968
elative span	1.5919

OPTOMAX V FSA 7.07

Particle distribution by Spherical Diameter

30th July 1995
19:40

tle : Hamilton Harbour
ample name : C3-5 August 1995

ccumlated Field area : 417297921 over 103 fields
olume coefficient : 1.0000
alibration factor : 3.226 MICRONS/pixel

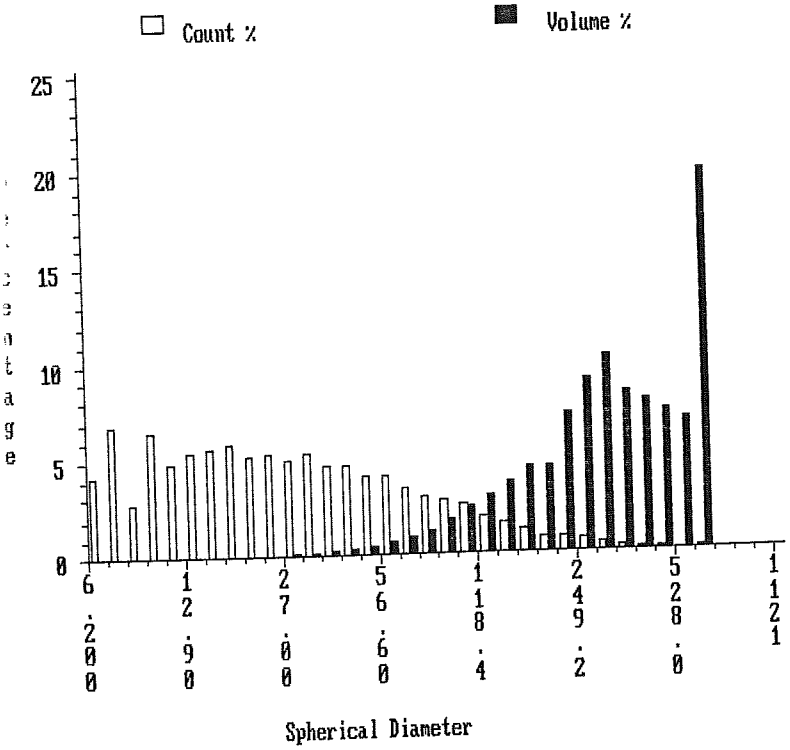

OPTOMAX V PSA 7.07

Particle distribution by Spherical Diameter

ime : 16:18
ate : 29th July 1995
itle : Hamilton Harbour
ample name : C3-6 August 1995

umber of fields : 112
ccumlated Field area : 453760846

lass file selected : OBJ_2-5.SIZ
olume coefficient : 1.0000
alibration factor : 3.226 MICRONS /pixel

Size classes			Count	Count %	Volume	Volume %
6.2000	-	7.2000	408	4.8	102240.31	0.0
7.2000	-	8.3000	786	9.3	352324.20	0.0
8.3000	-	9.6000	318	3.7	225389.72	0.0
9.6000	-	11.100	684	8.1	740269.79	0.0
11.100	-	12.900	528	6.2	928762.04	0.0
12.900	-	15.000	536	6.3	1425447.0	0.0
15.000	-	17.400	575	6.8	2384303.9	0.0
17.400	-	20.100	578	6.8	3758875.1	0.0
20.100	-	23.300	471	5.5	4760876.1	0.0
23.300	-	27.000	486	5.7	7632487.2	0.1
27.000	-	31.300	407	4.8	9981662.6	0.1
31.300	-	36.300	413	4.9	15793617	0.1
36.300	-	42.100	355	4.2	21443709	0.2
42.100	-	48.800	320	3.8	29846103	0.2
48.800	-	56.600	238	2.8	35056064	0.3
56.600	-	65.600	240	2.8	54333976	0.4
65.600	-	76.000	215	2.5	74997554	0.5
76.000	-	88.100	189	2.2	104070272	0.7
88.100	-	102.100	164	1.9	139383868	1.0
102.100	-	118.400	129	1.5	169697014	1.2
118.400	-	137.500	88	1.0	181022695	1.3
137.500	-	158.800	69	0.8	227619269	1.6
158.800	-	184.500	69	0.8	359011383	2.6
184.500	-	214.500	52	0.6	393262211	2.8
214.500	-	249.200	45	0.5	561342613	4.0
249.200	-	289.500	42	0.5	825689154	5.9
289.500	-	336.500	25	0.3	751203426	5.4
336.500	-	391.000	16	0.2	761613071	5.5
391.000	-	454.400	15	0.2	1.14E+009	8.2
454.400	-	528.000	16	0.2	1.83E+009	13.2
528.000	-	614.000	8	0.1	1.42E+009	10.2
614.000	-	713.800	5	0.1	1.45E+009	10.4
713.800	-	829.500	3	0.0	1.56E+009	11.2
829.500	-	964.000	1	0.0	650972713	4.7
964.000	-	1121.00	1	0.0	1.10E+009	7.9
Total Count within range			8495		1.39E+010	
Undersize			1548		132850.80	
Oversize			0			

otal particles examined	10043
otal particles included	10043
otal particles in range	8495

inimum Spherical Diameter of examined particles	3.6399
aximum Spherical Diameter of examined particles	1033.11
rea fraction % of examined particles	11.319

otal Spherical Diameter within range	321587.70
ean Spherical Diameter within range	37.856
tandard Deviation Spherical Diameter within range	58.501
edian Spherical Diameter within range	19.327

inimum Volume	48.226
aximum Volume	1.10E+009
olume Surface mean	330.490

olume Spherical Diameter at 10%	180.538
olume Median Spherical Diameter	497.208
olume Spherical Diameter at 90%	904.792
elative span	1.4566

OPTOMAX V PSA 7.07

Particle distribution by Spherical Diameter

29th July 1995
16:19

itle : Hamilton Harbour
ample name : C3-6 August 1995

ccumlated Field area : 453760846 over 112 fields
olume coefficient : 1.0000
alibration factor : 3.226 MICRONS/pixel

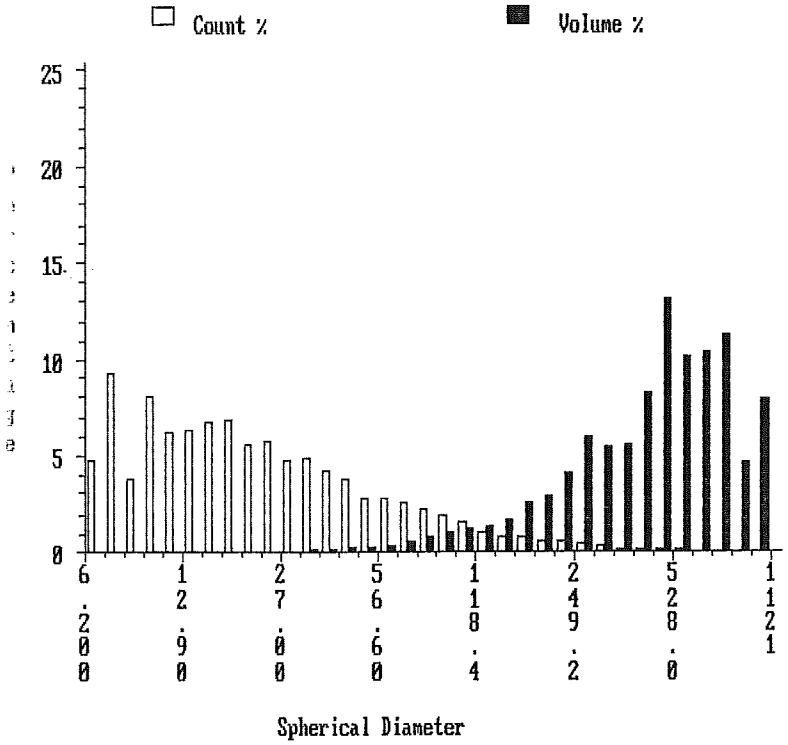

OPTOMAX V PSA 7.07

Particle distribution by Spherical Diameter

Time : 17:48
Date : 30th July 1995
Title : Hamilton Harbour
Sample name : C3-7 August 1995

Number of fields : 99
Accumlated Field area : 401092176

Class file selected : OBJ_2-5.SIZ
Volume coefficient : 1.0000
Calibration factor : 3.226 MICRONS /pixel

Size classes			Count	Count %	Volume	Volume %
6.2000	-	7.2000	283	3.8	70916.69	0.0
7.2000	-	8.3000	469	6.3	212538.67	0.0
8.3000	-	9.6000	208	2.8	147424.73	0.0
9.6000	-	11.100	490	6.5	529982.52	0.0
11.100	-	12.900	342	4.6	598615.17	0.0
12.900	-	15.000	373	5.0	988721.93	0.0
15.000	-	17.400	412	5.5	1691851.2	0.0
17.400	-	20.100	391	5.2	2557910.0	0.0
20.100	-	23.300	388	5.2	3905313.7	0.0
23.300	-	27.000	417	5.6	6594139.4	0.0
27.000	-	31.300	323	4.3	8021615.4	0.1
31.300	-	36.300	405	5.4	15473649	0.1
36.300	-	42.100	377	5.0	22443866	0.2
42.100	-	48.800	354	4.7	33153271	0.2
48.800	-	56.600	335	4.5	49545874	0.3
56.600	-	65.600	306	4.1	69328144	0.5
65.600	-	76.000	270	3.6	95670569	0.7
76.000	-	88.100	245	3.3	133882646	0.9
88.100	-	102.100	212	2.8	182179938	1.3
102.100	-	118.400	198	2.6	261275326	1.8
118.400	-	137.500	138	1.8	290315488	2.0
137.500	-	158.800	128	1.7	415912367	2.9
158.800	-	184.500	134	1.8	665491917	4.6
184.500	-	214.500	85	1.1	659470083	4.6
214.500	-	249.200	56	0.7	690247560	4.8
249.200	-	289.500	46	0.6	860505292	6.0
289.500	-	336.500	45	0.6	1.37E+009	9.5
336.500	-	391.000	31	0.4	1.50E+009	10.4
391.000	-	454.400	14	0.2	1.04E+009	7.2
454.400	-	528.000	10	0.1	1.23E+009	8.5
528.000	-	614.000	9	0.1	1.57E+009	10.9
614.000	-	713.800	3	0.0	777626119	5.4
713.800	-	829.500	1	0.0	380999277	2.6
829.500	-	964.000	1	0.0	838568659	5.8
964.000	-	1121.00	1	0.0	1.25E+009	8.7
Total Count within range			7500		1.44E+010	
Undersize			925		80938.06	
Oversize			0			

otal particles examined	8425
otal particles included	8425
otal particles in range	7500

nimum Spherical Diameter of examined particles	3.6399
ximum Spherical Diameter of examined particles	1077.45
ea fraction % of examined particles	15.474

otal Spherical Diameter within range	373159.05
an Spherical Diameter within range	49.755
andard Deviation Spherical Diameter within range	64.948
dian Spherical Diameter within range	26.796

nimum Volume	48.226
ximum Volume	1.25E+009
olume Surface mean	283.971

olume Spherical Diameter at 10%	151.046
olume Median Spherical Diameter	386.558
olume Spherical Diameter at 90%	933.158
elative span	2.0233

OPTOMAX V FSA 7.07

Particle distribution by Spherical Diameter

itle : Hamilton Harbour 30th July 1995

ample name : C3-7 August 1995 17:49

ccumlated Field area : 401092176 over 99 fields

olume coefficient : 1.0000

alibration factor : 3.226 MICRONS/pixel

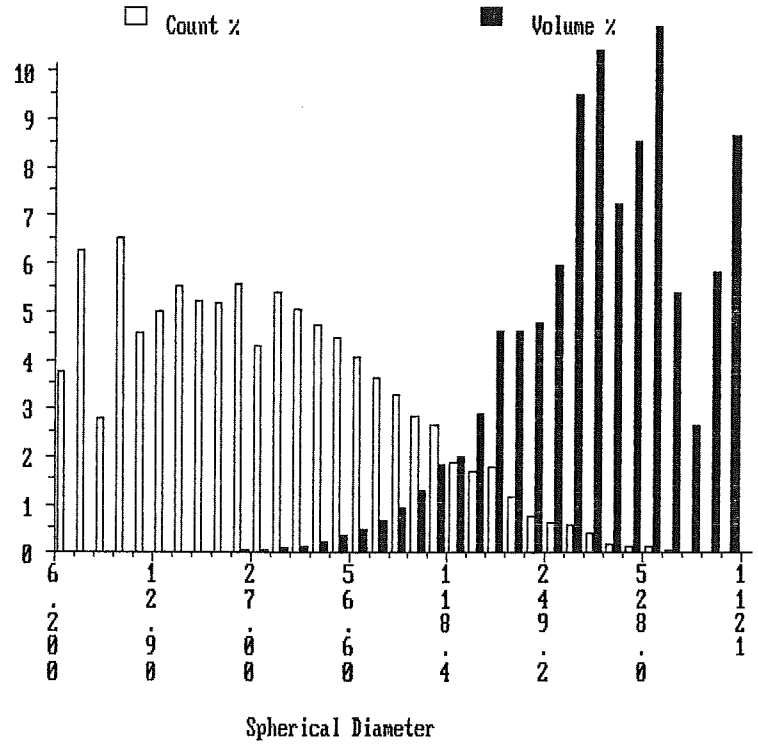

OPTOMAX V PSA 7.07

Particle distribution by Spherical Diameter

me : 17:38
te : 29th July 1995
tle : Hamilton Harbour
mple name : C3-8 August 1995

mber of fields : 66
cumlated Field area : 267394784

ass file selected : OBJ_2-5.SIZ
lume coefficient : 1.0000
libration factor : 3.226 MICRONS /pixel

Size classes			Count	Count %	Volume	Volume %
6.2000	-	7.2000	446	4.5	111762.69	0.0
7.2000	-	8.3000	811	8.1	366263.86	0.0
8.3000	-	9.6000	300	3.0	212631.82	0.0
9.6000	-	11.100	732	7.3	794962.21	0.0
11.100	-	12.900	526	5.3	921787.27	0.0
12.900	-	15.000	551	5.5	1470009.0	0.0
15.000	-	17.400	672	6.7	2755088.9	0.0
17.400	-	20.100	641	6.4	4185082.4	0.0
20.100	-	23.300	572	5.7	5806587.9	0.0
23.300	-	27.000	584	5.8	9189354.6	0.1
27.000	-	31.300	516	5.2	12772944	0.1
31.300	-	36.300	534	5.3	20320556	0.2
36.300	-	42.100	459	4.6	27483318	0.2
42.100	-	48.800	386	3.9	36432084	0.3
48.800	-	56.600	371	3.7	53696954	0.4
56.600	-	65.600	331	3.3	75358127	0.6
65.600	-	76.000	289	2.9	100266697	0.8
76.000	-	88.100	232	2.3	126021275	1.0
88.100	-	102.100	199	2.0	170381148	1.3
102.100	-	118.400	175	1.7	230674128	1.8
118.400	-	137.500	146	1.5	308046718	2.4
137.500	-	158.800	133	1.3	429263157	3.3
158.800	-	184.500	113	1.1	591442857	4.5
184.500	-	214.500	81	0.8	646940377	5.0
214.500	-	249.200	60	0.6	736495438	5.7
249.200	-	289.500	53	0.5	1.04E+009	8.0
289.500	-	336.500	38	0.4	1.18E+009	9.0
336.500	-	391.000	24	0.2	1.08E+009	8.3
391.000	-	454.400	14	0.1	1.07E+009	8.2
454.400	-	528.000	13	0.1	1.55E+009	11.9
528.000	-	614.000	8	0.1	1.49E+009	11.4
614.000	-	713.800	3	0.0	931858573	7.2
713.800	-	829.500	2	0.0	1.10E+009	8.4
829.500	-	964.000	0	0.0	0	0.0
964.000	-	1121.00	0	0.0	0	0.0
tal Count within range			10015		1.30E+010	
dersize			1404		123437.31	
ersize			0			

Total particles examined	11419
Total particles included	11419
Total particles in range	10015

Minimum Spherical Diameter of examined particles	3.6399
Maximum Spherical Diameter of examined particles	826.409
Area fraction % of examined particles	23.688

Total Spherical Diameter within range	412814.15
Mean Spherical Diameter within range	41.220
Standard Deviation Spherical Diameter within range	57.165
Median Spherical Diameter within range	21.938

Minimum Volume	48.226
Maximum Volume	564397666
Volume Surface mean	261.756

Volume Spherical Diameter at 10%	143.171
Volume Median Spherical Diameter	371.943
Volume Spherical Diameter at 90%	691.846
Relative span	1.4752

OPTOMAX V PSA 7.07

Particle distribution by Spherical Diameter

29th July 1995
17:39

itle : Hamilton Harbour
ample name : C3-8 August 1995

ccumlated Field area : 267394784 over 66 fields
olume coefficient : 1.0000
alibration factor : 3.226 MICRONS/pixel

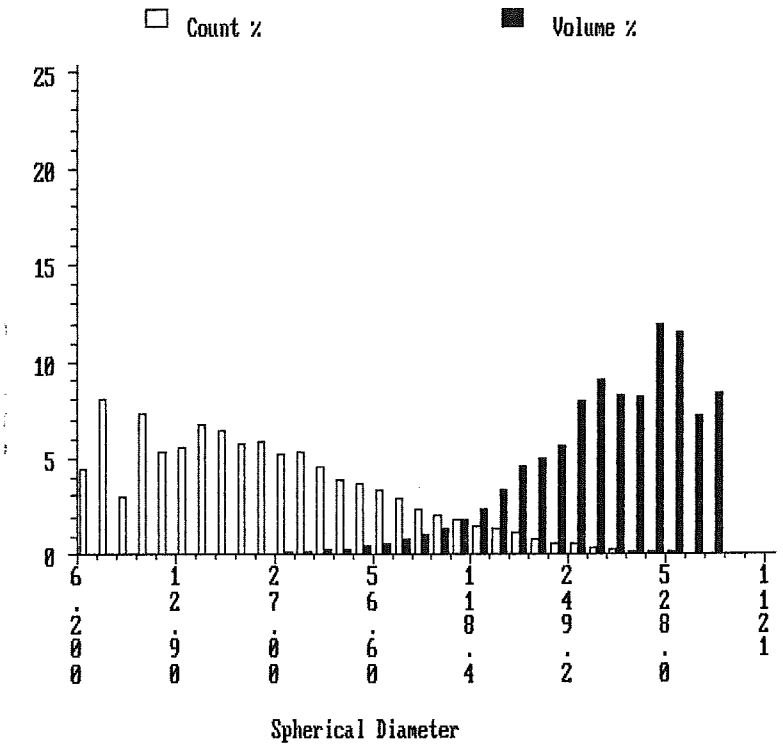

OPTOMAX V PSA 7.07

Particle distribution by Spherical Diameter

ime : 14:25
ate : 27th July 1995
itle : Hamilton Harbour
ample name : C3-9 August 1995
omment : 500 uL 50 mL column

umber of fields : 98
ccumlated Field area : 397040740

lass file selected : OBJ_2-5.SIZ
olume coefficient : 1.0000
alibration factor : 3.226 MICRONS /pixel

Size classes			Count	Count %	Volume	Volume %
6.2000	-	7.2000	493	4.9	123540.38	0.0
7.2000	-	8.3000	939	9.3	422702.40	0.0
8.3000	-	9.6000	376	3.7	266498.54	0.0
9.6000	-	11.100	824	8.1	893668.79	0.0
11.100	-	12.900	670	6.6	1176190.6	0.0
12.900	-	15.000	658	6.5	1744943.8	0.0
15.000	-	17.400	753	7.4	3088246.1	0.0
17.400	-	20.100	683	6.8	4464316.2	0.0
20.100	-	23.300	648	6.4	6571881.0	0.0
23.300	-	27.000	619	6.1	9781994.5	0.1
27.000	-	31.300	495	4.9	12043442	0.1
31.300	-	36.300	497	4.9	19008199	0.1
36.300	-	42.100	402	4.0	24110915	0.1
42.100	-	48.800	331	3.3	30714355	0.2
48.800	-	56.600	299	3.0	43627741	0.2
56.600	-	65.600	242	2.4	54491516	0.3
65.600	-	76.000	223	2.2	77756212	0.4
76.000	-	88.100	181	1.8	99131775	0.5
88.100	-	102.100	146	1.4	125908936	0.7
102.100	-	118.400	117	1.2	160142934	0.8
118.400	-	137.500	95	0.9	195779994	1.0
137.500	-	158.800	89	0.9	293393581	1.5
158.800	-	184.500	70	0.7	336234170	1.8
184.500	-	214.500	52	0.5	411076736	2.2
214.500	-	249.200	51	0.5	640587991	3.4
249.200	-	289.500	37	0.4	707188025	3.7
289.500	-	336.500	43	0.4	1.32E+009	7.0
336.500	-	391.000	19	0.2	908930885	4.8
391.000	-	454.400	22	0.2	1.64E+009	8.7
454.400	-	528.000	12	0.1	1.39E+009	7.3
528.000	-	614.000	12	0.1	2.34E+009	12.3
614.000	-	713.800	10	0.1	2.67E+009	14.1
713.800	-	829.500	6	0.1	2.54E+009	13.4
829.500	-	964.000	3	0.0	1.94E+009	10.2
964.000	-	1121.00	1	0.0	948858825	5.0
otal Count within range			10118		1.90E+010	
ndersize			1522		133360.48	
versize			0			

otal particles examined	11640
otal particles included	11640
otal particles in range	10118

inimum Spherical Diameter of examined particles	3.6399
aximum Spherical Diameter of examined particles	982.654
rea fraction % of examined particles	17.222

otal Spherical Diameter within range	370219.95
ean Spherical Diameter within range	36.590
tandard Deviation Spherical Diameter within range	61.316
edian Spherical Diameter within range	18.768

inimum Volume	48.226
aximum Volume	948858825
olume Surface mean	366.460

olume Spherical Diameter at 10%	213.364
olume Median Spherical Diameter	563.380
olume Spherical Diameter at 90%	898.359
elative span	1.2159

OPTOMAX V PSA 7.07

Particle distribution by Spherical Diameter

27th July 1995
14:25

itle : Hamilton Harbour
ample name : C3-9 August 1995

omment : 500 uL 50 mL column
cumlated Field area : 397040740 over 98 fields
olume coefficient : 1.0000
alibration factor : 3.226 MICRONS/pixel

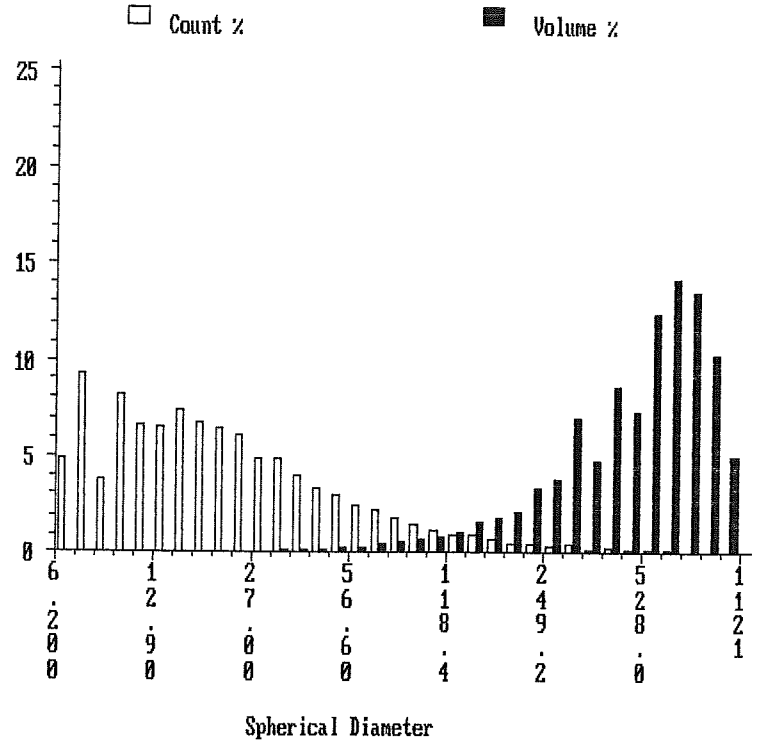

OPTOMAX V PSA 7.07

Particle distribution by Spherical Diameter

ime : 18:08
ate : 21st July 1995
itle : Hamilton Harbour
ample name : C3-10 Aug. 18/95
omment : 1 drop 50mL column

umber of fields : 94
ccumlated Field area : 380834996

lass file selected : OBJ_2-5.SIZ
olume coefficient : 1.0000
alibration factor : 3.226 MICRONS /pixel

Size classes			Count	Count %	Volume	Volume %
6.2000	-	7.2000	405	5.3	101488.54	0.0
7.2000	-	8.3000	799	10.5	355499.19	0.0
8.3000	-	9.6000	344	4.5	243817.81	0.0
9.6000	-	11.100	711	9.3	769253.91	0.1
11.100	-	12.900	550	7.2	961724.05	0.1
12.900	-	15.000	602	7.9	1592553.0	0.1
15.000	-	17.400	613	8.0	2512554.5	0.2
17.400	-	20.100	596	7.8	3893135.9	0.4
20.100	-	23.300	506	6.6	5068604.3	0.5
23.300	-	27.000	470	6.2	7404119.1	0.7
27.000	-	31.300	367	4.8	9040256.5	0.8
31.300	-	36.300	374	4.9	14112764	1.3
36.300	-	42.100	258	3.4	15476372	1.4
42.100	-	48.800	222	2.9	20583575	1.9
48.800	-	56.600	188	2.5	26637733	2.4
56.600	-	65.600	148	1.9	33381458	3.0
65.600	-	76.000	126	1.7	44039845	4.0
76.000	-	88.100	100	1.3	54196173	4.9
88.100	-	102.100	77	1.0	64315235	5.8
102.100	-	118.400	39	0.5	49727885	4.5
118.400	-	137.500	36	0.5	74359350	6.7
137.500	-	158.800	25	0.3	80407919	7.3
158.800	-	184.500	27	0.4	136085138	12.3
184.500	-	214.500	13	0.2	98437999	8.9
214.500	-	249.200	10	0.1	125073557	11.3
249.200	-	289.500	9	0.1	168241731	15.2
289.500	-	336.500	1	0.0	26590204	2.4
336.500	-	391.000	1	0.0	42507543	3.8
391.000	-	454.400	0	0.0	0	0.0
454.400	-	528.000	0	0.0	0	0.0
528.000	-	614.000	0	0.0	0	0.0
614.000	-	713.800	0	0.0	0	0.0
713.800	-	829.500	0	0.0	0	0.0
829.500	-	964.000	0	0.0	0	0.0
964.000	-	1121.00	0	0.0	0	0.0
otal Count within range			7617		1.11E+009	
ndersize			1552		133660.95	
versize			0			

otal particles examined	9169
otal particles included	9169
otal particles in range	7617

inimum Spherical Diameter of examined particles	3.6399
aximum Spherical Diameter of examined particles	348.997
rea fraction % of examined particles	5.8958

otal Spherical Diameter within range	190446.40
ean Spherical Diameter within range	25.003
tandard Deviation Spherical Diameter within range	26.937
edian Spherical Diameter within range	16.556

inimum Volume	48.226
aximum Volume	42507543
olume Surface mean	109.317

olume Spherical Diameter at 10%	57.101
olume Median Spherical Diameter	167.086
olume Spherical Diameter at 90%	279.556
elative span	1.3314

OPTOMAX V PSA 7.07

Particle distribution by Spherical Diameter

itle : Hamilton Harbour 21st July 1995

ample name : C3-10 Aug. 18/95 18:09

omment : 1 drop 50mL column

ccumlated Field area : 380834996 over 94 fields

olume coefficient : 1.0000

alibration factor : 3.226 MICRONS/pixel

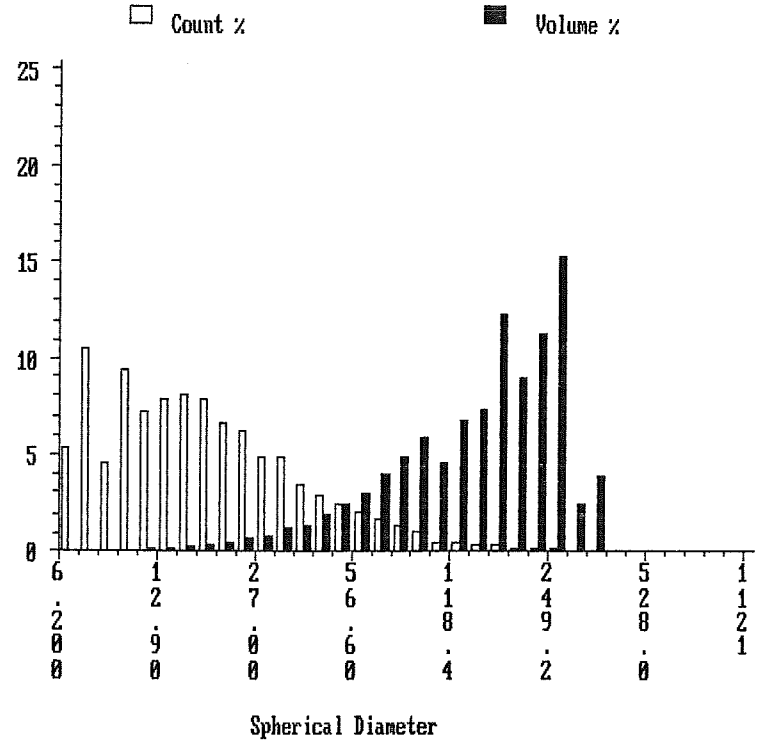

OPTOMAX V PSA 7.07

Particle distribution by Spherical Diameter

ime : 13:59
ate : 29th July 1995
itle : Hamilton Harbour
ample name : C3-11 August 1995

umber of fields : 22
ccumlated Field area : 89131595

lass file selected : OBJ_2-5.SIZ
olume coefficient : 1.0000
alibration factor : 3.226 MICRONS /pixel

Size classes			Count	Count %	Volume	Volume %
6.2000	-	7.2000	514	5.0	128802.74	0.0
7.2000	-	8.3000	1025	9.9	464777.53	0.0
8.3000	-	9.6000	426	4.1	301937.18	0.0
9.6000	-	11.100	974	9.4	1051692.3	0.0
11.100	-	12.900	735	7.1	1280016.5	0.1
12.900	-	15.000	747	7.2	1966307.8	0.1
15.000	-	17.400	819	7.9	3363230.6	0.1
17.400	-	20.100	727	7.0	4706086.9	0.2
20.100	-	23.300	729	7.0	7352591.8	0.3
23.300	-	27.000	643	6.2	10151487	0.4
27.000	-	31.300	558	5.4	13913031	0.6
31.300	-	36.300	512	4.9	19554876	0.8
36.300	-	42.100	410	4.0	24414864	1.1
42.100	-	48.800	362	3.5	33559107	1.5
48.800	-	56.600	277	2.7	40180553	1.7
56.600	-	65.600	240	2.3	54014755	2.3
65.600	-	76.000	158	1.5	56148230	2.4
76.000	-	88.100	138	1.3	75918937	3.3
88.100	-	102.100	112	1.1	95542563	4.1
102.100	-	118.400	78	0.8	102456717	4.4
118.400	-	137.500	60	0.6	122208219	5.3
137.500	-	158.800	33	0.3	104402564	4.5
158.800	-	184.500	28	0.3	137451118	5.9
184.500	-	214.500	23	0.2	179916005	7.8
214.500	-	249.200	9	0.1	108011166	4.7
249.200	-	289.500	11	0.1	217805210	9.4
289.500	-	336.500	5	0.0	144308573	6.2
336.500	-	391.000	2	0.0	90273856	3.9
391.000	-	454.400	2	0.0	142628906	6.2
454.400	-	528.000	2	0.0	232558544	10.1
528.000	-	614.000	0	0.0	0	0.0
614.000	-	713.800	1	0.0	285050906	12.3
713.800	-	829.500	0	0.0	0	0.0
829.500	-	964.000	0	0.0	0	0.0
964.000	-	1121.00	0	0.0	0	0.0
otal Count within range			10360		2.31E+009	
ndersize			1601		140961.96	
versize			0			

otal particles examined	11961
otal particles included	11961
otal particles in range	10360

inimum Spherical Diameter of examined particles	3.6399
aximum Spherical Diameter of examined particles	658.124
rea fraction % of examined particles	17.348

otal Spherical Diameter within range	272324.05
ean Spherical Diameter within range	26.286
tandard Deviation Spherical Diameter within range	29.614
edian Spherical Diameter within range	17.224

inimum Volume	48.226
aximum Volume	285050906
olume Surface mean	144.182

olume Spherical Diameter at 10%	68.324
olume Median Spherical Diameter	235.412
olume Spherical Diameter at 90%	632.886
elative span	2.3982

OPTOMAX V PSA 7.07

Particle distribution by Spherical Diameter

tle : Hamilton Harbour 29th July 1995

mple name : C3-11 August 1995 14:00

cumlated Field area : 89131595 over 22 fields

lume coefficient : 1.0000

libration factor : 3.226 MICRONS/pixel

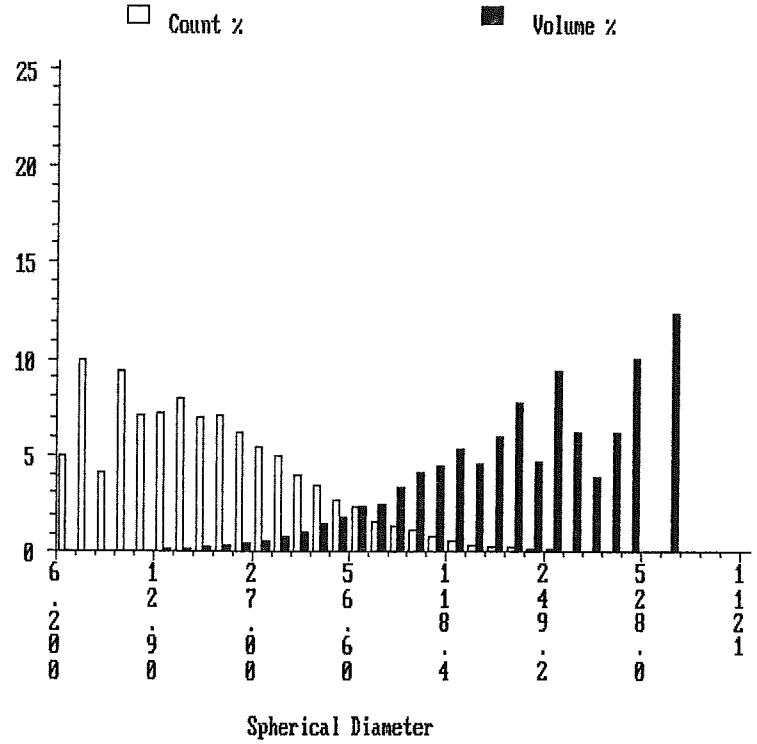

MALVERN Series 2600 SB.09 Master Mode Thu 14 Sep 1995 2:06 pm

High Size	Under %	High Size	Under %	High Size	Under %	High Size	Under %	High Size	Under %	High Size	Under %	Span 1.78
188	100	84.5	77.8	38.0	33.7	17.1	9.3	7.69	2.3	3.46	0.0	D[4,3] 60.32µm
175	99.0	78.6	73.6	35.4	30.4	15.9	8.2	7.15	2.0	3.21	0.0	
163	97.9	73.1	69.1	32.9	27.0	14.8	7.2	6.65	1.7	2.99	0.0	D[3,2] 34.73µm
151	96.7	68.0	64.5	30.6	23.9	13.7	6.3	6.18	1.4	2.78	0.0	
141	95.3	63.2	59.8	28.4	21.0	12.8	5.6	5.75	1.1	2.59	0.0	D[v,0.9] 113.29µm
131	93.8	58.8	55.3	26.4	18.7	11.9	5.0	5.35	0.9	2.40	0.0	
122	92.0	54.7	51.0	24.6	16.7	11.1	4.5	4.97	0.6	2.24	0.0	D[v,0.1] 17.76µm
113	89.9	50.8	47.1	22.9	15.1	10.3	4.0	4.62	0.4	2.08	0.0	
105	87.5	47.3	43.5	21.3	13.5	9.56	3.5	4.30	0.3	1.93	0.0	
97.8	84.7	44.0	40.2	19.8	12.1	8.89	3.1	4.00	0.2			D[v,0.5] 53.71µm
90.9	81.5	40.9	37.0	18.4	10.6	8.27	2.7	3.72	0.1			

Source = :Sample | Beam length = 14.3 mm | Model indp
Log. Diff. = 4.554
Focal length = 100 mm | Obscuration = 0.1237 | Volume Conc. = 0.0107%
Presentation = pil | Volume distribution | Sp.S.A 0.1728 m²/cc.

2560 pil lfu1479
Hamilton Harbour Sampling.....Dofasco
August 18,1995 Sample.....C3 - 1

MALVERN Series 2600 SB.09 Master Mode Thu 14 Sep 1995 2:06 pm

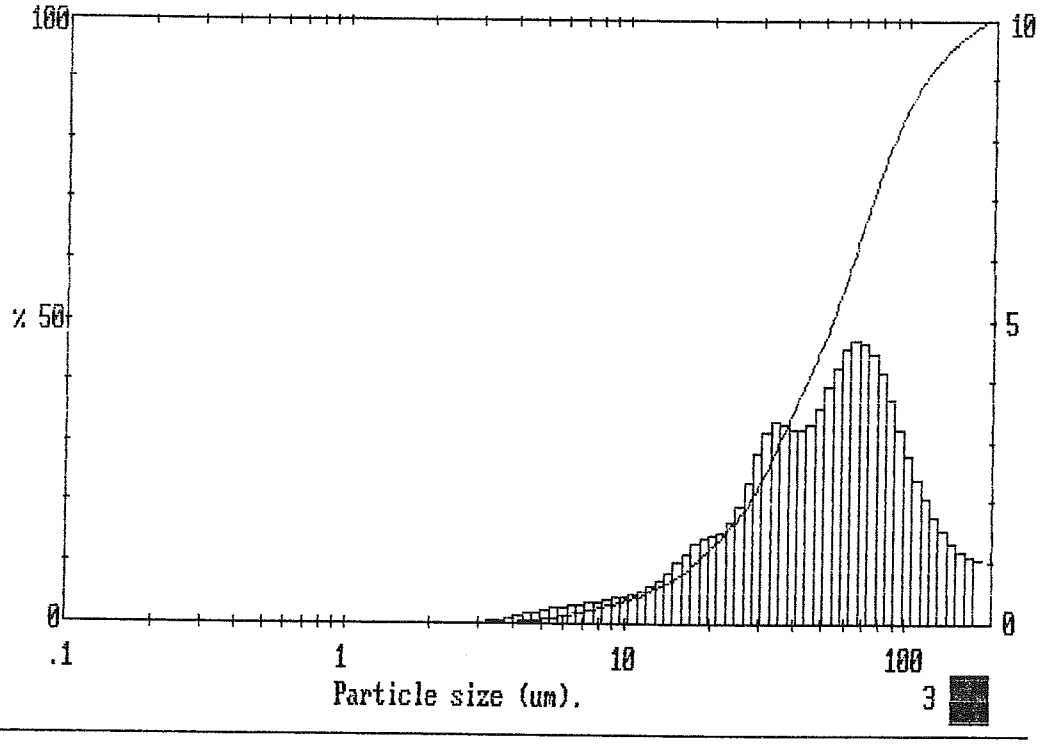

2560 pil lfu1479
Hamilton Harbour Sampling.....Dofasco
August 18,1995 Sample.....C3 - 1

MALVERN Series 2600 SB.09 Master Mode Thu 14 Sep 1995 2:57 pm

High Size	Under %	High Size	Under %	High Size	Under %	High Size	Under %	High Size	Under %	High Size	Under %	Span 2.60
564	100	254	97.3	114	87.2	51.3	57.8	23.1	19.6	10.4	5.0	D[4,3] 64.42µm
524	99.9	236	96.8	106	85.5	47.7	53.9	21.4	17.3	9.64	4.4	
488	99.7	219	96.3	98.6	83.5	44.4	50.0	19.9	15.2	8.97	3.8	D[3,2] 29.52µm
454	99.5	204	95.7	91.7	81.3	41.2	46.1	18.5	13.5	8.34	3.3	
422	99.4	190	95.0	85.3	79.0	38.4	42.3	17.2	11.9	7.76	2.9	D[v,0.9] 130.61µm
392	99.2	176	94.3	79.3	76.6	35.7	38.6	16.0	10.6	7.21	2.4	
365	99.0	164	93.4	73.8	74.1	33.2	35.0	14.9	9.3	6.71	2.0	D[v,0.1] 15.53µm
339	98.7	153	92.4	68.6	71.3	30.8	31.6	13.9	8.3	6.24	1.6	
315	98.4	142	91.4	63.8	68.3	28.7	28.3	12.9	7.3	5.80	1.2	
293	98.1	132	90.2	59.3	65.0	26.7	25.1	12.0	6.4			
273	97.7	123	88.8	55.2	61.5	24.8	22.2	11.2	5.7			

Source = :Sample	Beam length = 14.3 mm	Model indp	D[v,0.5] 44.34µm
	Log. Diff. = 2.630		
Focal length = 300 mm	Obscuration = 0.0892	Volume Conc. = 0.0064%	
Presentation = pil	Volume distribution	Sp.S.A 0.2033 m²/cc.	

2560 pil 1fu1479
Hamilton Harbour Sampling.....Dofasco
August 18,1995 Sample.....C3 -2

MALVERN Series 2600 SB.09 Master Mode Thu 14 Sep 1995 2:57 pm

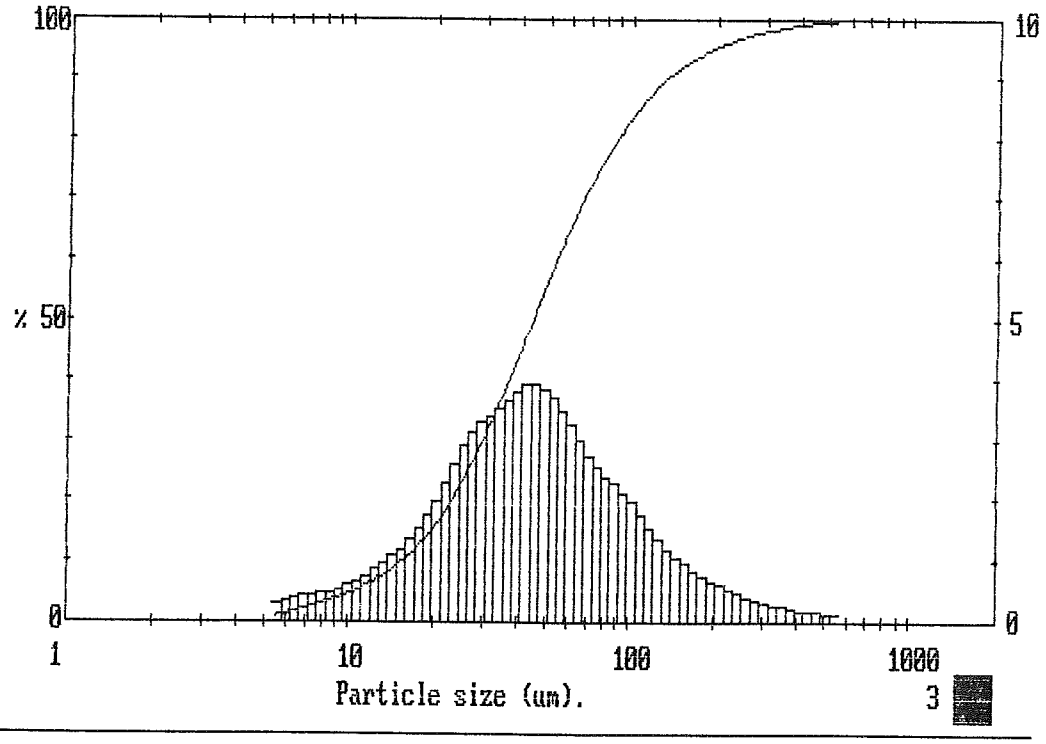

2560 pil 1fu1479
Hamilton Harbour Sampling.....Dofasco
August 18,1995 Sample.....C3 -2

MALVERN Series 2600 SB.09 Master Mode Thu 14 Sep 1995 3:01 pm

High Size	Under %	High Size	Under %	High Size	Under %	High Size	Under %	High Size	Under %	High Size	Under %	Span 2.58
564	100	254	95.4	114	85.9	51.3	53.5	23.1	17.9	10.4	4.7	D[4,3] 72.52µm
524	99.6	236	95.0	106	84.1	47.7	49.5	21.4	16.0	9.64	4.2	
488	99.1	219	94.5	98.6	82.0	44.4	45.5	19.9	14.3	8.97	3.7	D[3,2] 30.97µm
454	98.7	204	94.0	91.7	79.8	41.2	41.6	18.5	12.7	8.34	3.2	
422	98.3	190	93.5	85.3	77.3	38.4	38.0	17.2	11.3	7.76	2.8	D[v,0.9] 140.26µm
392	97.9	176	92.9	79.3	74.7	35.7	34.5	16.0	10.1	7.21	2.4	
365	97.5	164	92.1	73.8	71.8	33.2	31.2	14.9	8.9	6.71	2.0	D[v,0.1] 15.97µm
339	97.0	153	91.2	68.6	68.7	30.8	28.2	13.9	7.9	6.24	1.6	
315	96.6	142	90.2	63.8	65.3	28.7	25.3	12.9	6.9	5.80	1.2	
293	96.2	132	89.0	59.3	61.6	26.7	22.6	12.0	6.1			
273	95.8	123	87.6	55.2	57.6	24.8	20.1	11.2	5.4			

Source = :Sample	Beam length = 14.3 mm	Model indp	D[v,0.5] 48.15µm
Focal length = 300 mm	Log. Diff. = 2.833		
Presentation = pil	Obscuration = 0.1369	Volume Conc. = 0.0106%	
	Volume distribution	Sp.S.A 0.1938 m²/cc.	

2560 pil lfu1479
Hamilton Harbour Sampling.....Dofasco
August 18,1995 Sample.....C3 -3

MALVERN Series 2600 SB.09 Master Mode Thu 14 Sep 1995 3:01 pm

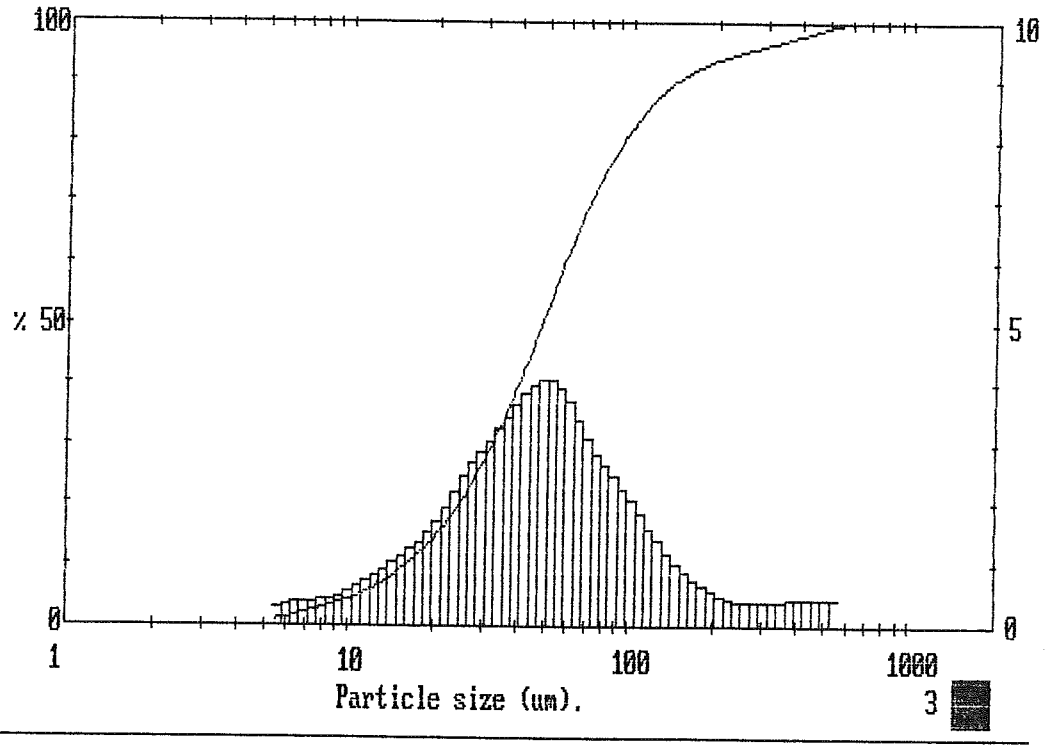

2560 pil lfu1479
Hamilton Harbour Sampling.....Dofasco
August 18,1995 Sample.....C3 -3

MALVERN Series 2600 SB.09 Master Mode Thu 14 Sep 1995 3:05 pm

High Size	Under %	High Size	Under %	High Size	Under %	High Size	Under %	High Size	Under %	High Size	Under %	Span 2.68
564	100	254	97.8	114	87.4	51.3	60.8	23.1	20.7	10.4	4.9	D[4,3] 61.71µm
524	99.9	236	97.3	106	85.7	47.7	56.7	21.4	18.2	9.64	4.3	
488	99.8	219	96.8	98.6	83.9	44.4	52.4	19.9	16.1	8.97	3.8	D[3,2] 28.99µm
454	99.7	204	96.2	91.7	82.0	41.2	48.1	18.5	14.2	8.34	3.3	
422	99.6	190	95.5	85.3	80.1	38.4	44.0	17.2	12.5	7.76	2.8	D[v,0.9] 129.40µm
392	99.4	176	94.7	79.3	78.1	35.7	40.1	16.0	11.0	7.21	2.4	
365	99.3	164	93.8	73.8	76.0	33.2	36.4	14.9	9.6	6.71	1.9	D[v,0.1] 15.26µm
339	99.1	153	92.8	68.6	73.6	30.8	32.9	13.9	8.4	6.24	1.5	
315	98.8	142	91.6	63.8	71.0	28.7	29.5	12.9	7.3	5.80	1.2	
293	98.5	132	90.4	59.3	67.9	26.7	26.3	12.0	6.4			
273	98.2	123	89.0	55.2	64.5	24.8	23.3	11.2	5.6			

Source = :Sample	Beam length = 14.3 mm	Model indp	D[v,0.5] 42.56µm
	Log. Diff. = 2.764		
Focal length = 300 mm	Obscuration = 0.2431	Volume Conc. = 0.0188%	
Presentation = pil	Volume distribution	Sp.S.A 0.2070 m²/cc.	

2560 pil lfu1479
Hamilton Harbour Sampling.....Dofasco
August 18,1995 Sample.....C3 - 4

MALVERN Series 2600 SB.09 Master Mode Thu 14 Sep 1995 3:05 pm

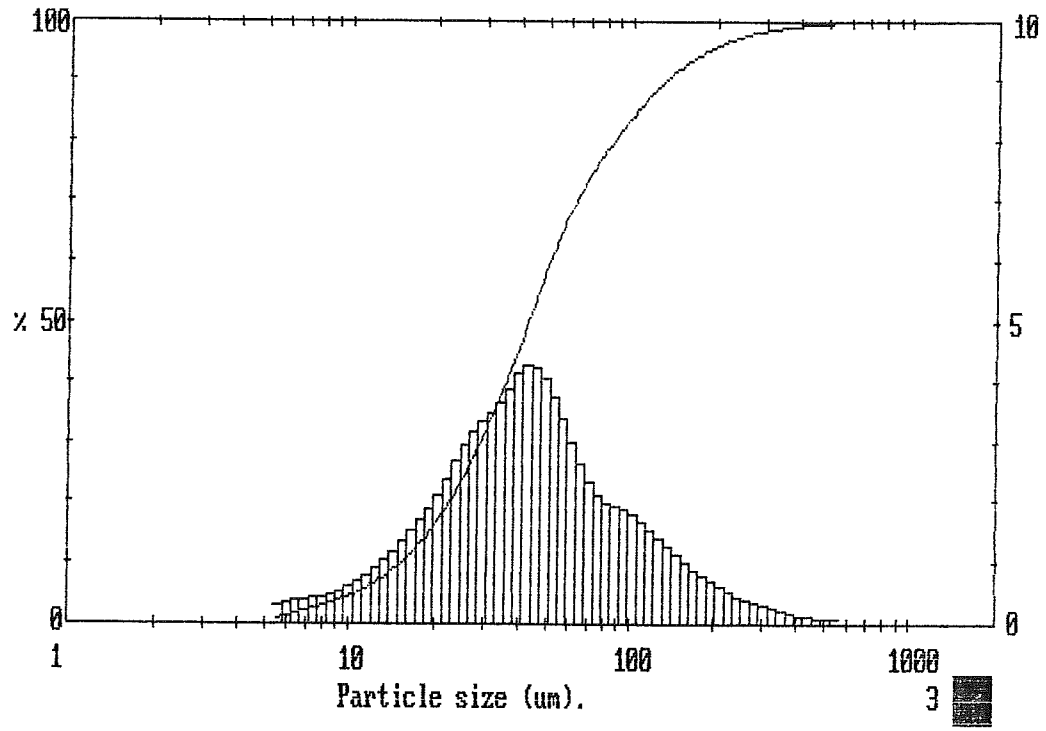

2560 pil lfu1479
Hamilton Harbour Sampling.....Dofasco
August 18,1995 Sample.....C3 - 4

MALVERN Series 2600 SB.09 Master Mode Fri 15 Sep 1995 8:39 am

High Size	Under %	High Size	Under %	High Size	Under %	High Size	Under %	High Size	Under %	High Size	Under %	Span 2.99
564	100	254	95.7	114	87.8	51.3	62.3	23.1	24.5	10.4	6.6	D[4,3] 64.96µm
524	99.7	236	95.2	106	86.6	47.7	58.7	21.4	21.9	9.64	5.8	
488	99.3	219	94.7	98.6	85.2	44.4	55.0	19.9	19.6	8.97	5.1	D[3,2] 25.94µm
454	98.9	204	94.1	91.7	83.7	41.2	51.3	18.5	17.5	8.34	4.5	
422	98.6	190	93.5	85.3	81.9	38.4	47.6	17.2	15.6	7.76	3.9	
392	98.2	176	92.9	79.3	79.9	35.7	44.0	16.0	13.9	7.21	3.3	D[v,0.9] 133.57µm
365	97.8	164	92.2	73.8	77.7	33.2	40.5	14.9	12.3	6.71	2.8	
339	97.4	153	91.5	68.6	75.1	30.8	37.0	13.9	10.9	6.24	2.2	
315	97.0	142	90.7	63.8	72.3	28.7	33.6	12.9	9.6	5.80	1.7	D[v,0.1] 13.20µm
293	96.6	132	89.8	59.3	69.2	26.7	30.4	12.0	8.5			
273	96.2	123	88.9	55.2	65.8	24.8	27.3	11.2	7.5			

Source = :Sample	Beam length = 14.3 mm	Model indp	D[v,0.5] 40.21µm
	Log. Diff. = 2.440		
Focal length = 300 mm	Obscuration = 0.3473	Volume Conc. = 0.0258%	
Presentation = pil	Volume distribution	Sp.S.A 0.2313 m²/cc.	

2560 pil lfu1479
Hamilton Harbour Sampling.....Dofasco
August 18,1995 Sample.....C3 - 5

MALVERN Series 2600 SB.09 Master Mode Fri 15 Sep 1995 8:39 am

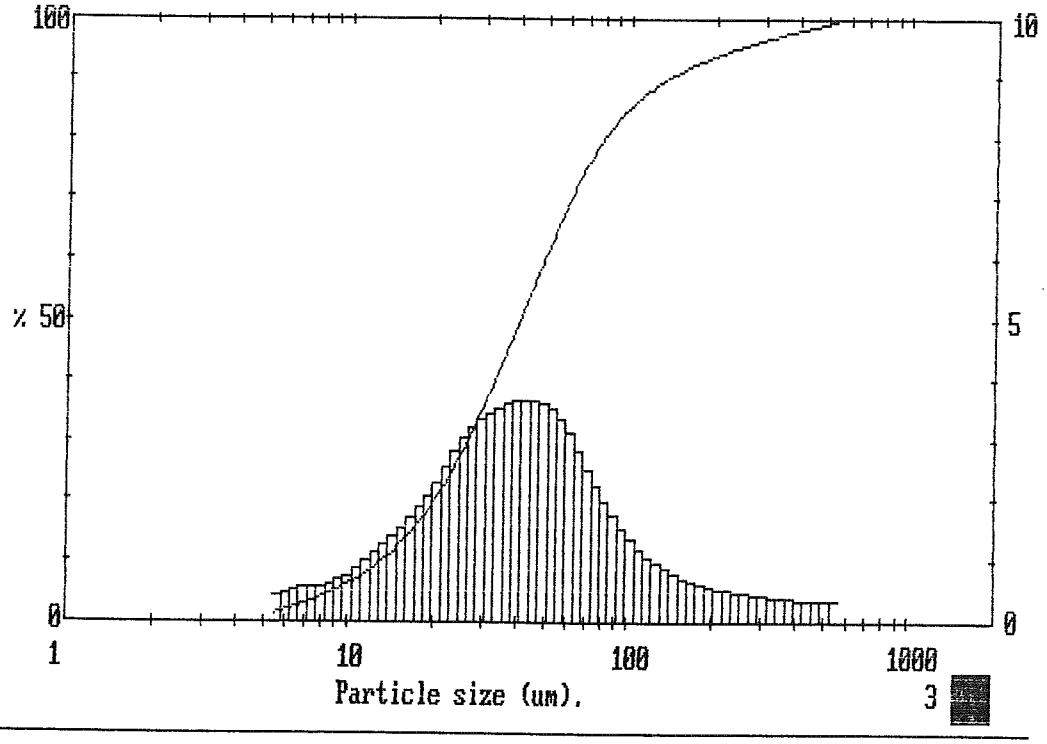

2560 pil lfu1479
Hamilton Harbour Sampling.....Dofasco
August 18,1995 Sample.....C3 - 5

MALVERN Series 2600 SB.09 Master Mode Fri 15 Sep 1995 8:42 am

High Size	Under %	High Size	Under %	High Size	Under %	High Size	Under %	High Size	Under %	High Size	Under %	Span 2.22
564	100	254	97.9	114	88.5	51.3	54.4	23.1	17.1	10.4	4.3	D[4,3] 63.55µm
524	99.9	236	97.5	106	86.9	47.7	50.0	21.4	15.1	9.64	3.8	
488	99.8	219	97.0	98.6	85.0	44.4	45.8	19.9	13.3	8.97	3.4	D[3,2] 31.31µm
454	99.7	204	96.5	91.7	82.9	41.2	41.8	18.5	11.8	8.34	3.0	
422	99.6	190	95.9	85.3	80.4	38.4	38.0	17.2	10.4	7.76	2.6	D[v,0.9] 122.57µm
392	99.4	176	95.2	79.3	77.7	35.7	34.3	16.0	9.2	7.21	2.2	
365	99.2	164	94.4	73.8	74.6	33.2	30.9	14.9	8.1	6.71	1.8	D[v,0.1] 16.84µm
339	99.0	153	93.5	68.6	71.1	30.8	27.7	13.9	7.2	6.24	1.5	
315	98.8	142	92.5	63.8	67.3	28.7	24.7	12.9	6.3	5.80	1.1	D[v,0.5] 47.68µm
293	98.6	132	91.3	59.3	63.1	26.7	21.9	12.0	5.5			
273	98.2	123	90.0	55.2	58.8	24.8	19.3	11.2	4.9			

Source = :Sample
Focal length = 300 mm
Presentation = pil

Beam length = 14.3 mm
Log. Diff. = 2.831
Obscuration = 0.3274
Volume distribution

Model indp
Volume Conc. = 0.0289%
Sp.S.A 0.1916 m²/cc.

2560 pil lfu1479
Hamilton Harbour Sampling.....Dofasco
August 18,1995 Sample.....C3 - 6

MALVERN Series 2600 SB.09 Master Mode Fri 15 Sep 1995 8:42 am

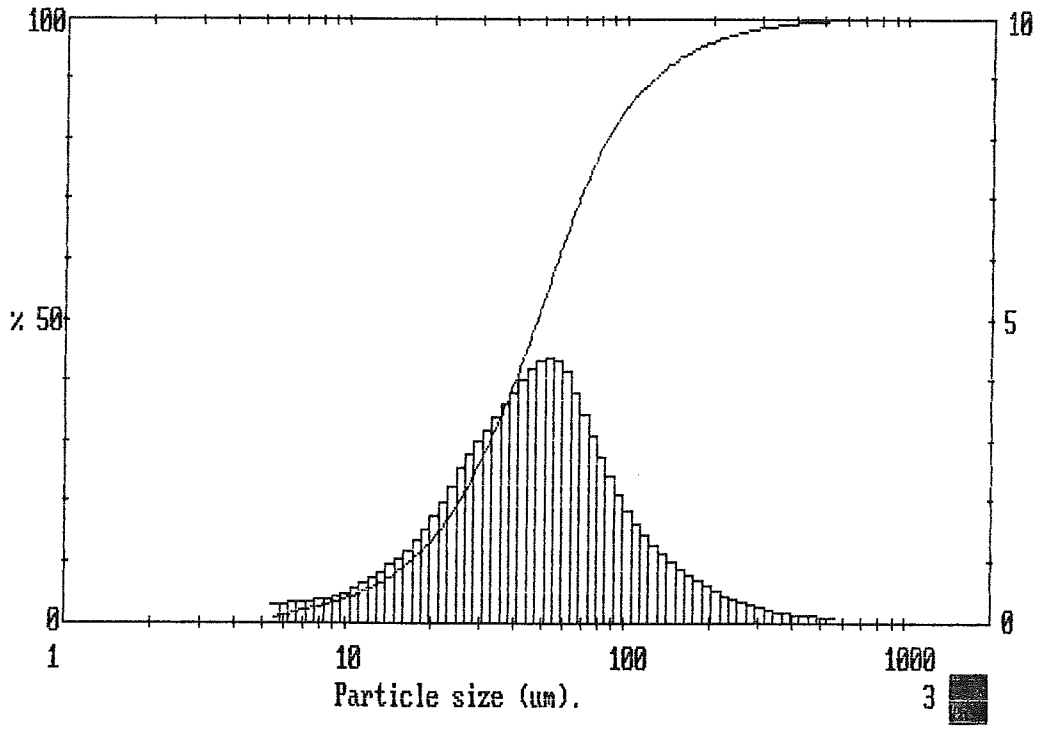

2560 pil lfu1479
Hamilton Harbour Sampling.....Dofasco
August 18,1995 Sample.....C3 - 6

MALVERN Series 2600 SB.09 Master Mode Fri 15 Sep 1995 8:47 am

High Size	Under %	High Size	Under %	High Size	Under %	High Size	Under %	High Size	Under %	High Size	Under %	Span 2.49
564	100	254	96.1	114	83.9	51.3	47.3	23.1	14.9	10.4	3.9	D[4,3] 75.48µm
524	99.7	236	95.5	106	81.9	47.7	43.4	21.4	13.2	9.64	3.4	
488	99.5	219	94.8	98.6	79.6	44.4	39.7	19.9	11.7	8.97	3.0	D[3,2] 34.33µm
454	99.2	204	94.0	91.7	77.1	41.2	36.2	18.5	10.4	8.34	2.7	
422	98.9	190	93.2	85.3	74.2	38.4	32.9	17.2	9.2	7.76	2.3	D[v,0.9] 151.96µm
392	98.6	176	92.3	79.3	71.1	35.7	29.7	16.0	8.2	7.21	2.0	
365	98.3	164	91.2	73.8	67.6	33.2	26.7	14.9	7.2	6.71	1.6	D[v,0.1] 18.13µm
339	97.9	153	90.1	68.6	63.8	30.8	24.0	13.9	6.4	6.24	1.3	
315	97.5	142	88.8	63.8	59.8	28.7	21.4	12.9	5.6	5.80	1.0	
293	97.1	132	87.3	59.3	55.6	26.7	19.0	12.0	5.0			
273	96.6	123	85.7	55.2	51.4	24.8	16.8	11.2	4.4			D[v,0.5] 53.79µm

Source = :Sample
Focal length = 300 mm
Presentation = pil

Beam length = 14.3 mm
Log. Diff. = 2.711
Obscuration = 0.2977
Volume distribution

Model indp
Volume Conc. = 0.0283%
Sp.S.A 0.1748 m²/cc.

2560 pil lfu1479
Hamilton Harbour Sampling.....Dofasco
August 18,1995 Sample.....C3 - 7

MALVERN Series 2600 SB.09 Master Mode Fri 15 Sep 1995 8:47 am

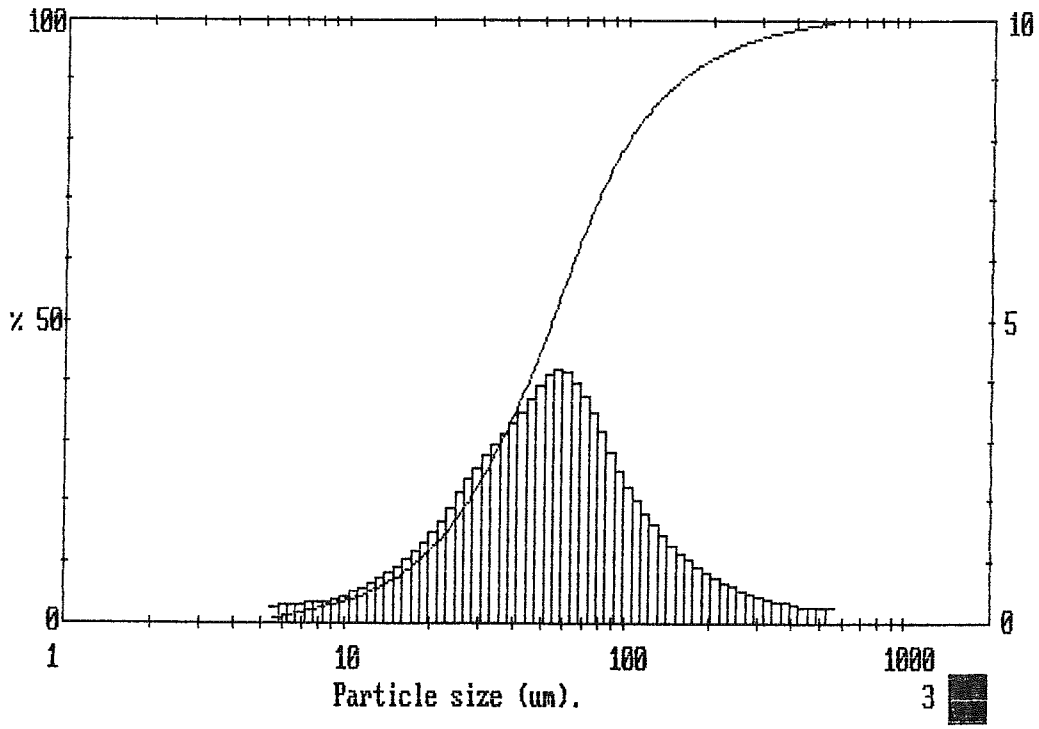

2560 pil lfu1479
Hamilton Harbour Sampling.....Dofasco
August 18,1995 Sample.....C3 - 7

MALVERN Series 2600 SB.09 Master Mode Fri 15 Sep 1995 8:50 am

High Size	Under %	High Size	Under %	High Size	Under %	High Size	Under %	High Size	Under %	High Size	Under %	Span 2.22
564	100	254	98.1	114	87.1	51.3	51.5	23.1	15.7	10.4	3.9	D[4,3] 65.96µm
524	99.9	236	97.6	106	85.1	47.7	47.2	21.4	13.8	9.64	3.4	
488	99.9	219	97.1	98.6	82.8	44.4	43.0	19.9	12.2	8.97	3.0	D[3,2] 33.06µm
454	99.8	204	96.6	91.7	80.3	41.2	39.0	18.5	10.8	8.34	2.6	
422	99.7	190	95.9	85.3	77.6	38.4	35.3	17.2	9.6	7.76	2.3	D[v,0.9] 128.95µm
392	99.5	176	95.1	79.3	74.7	35.7	31.8	16.0	8.5	7.21	1.9	
365	99.4	164	94.2	73.8	71.5	33.2	28.6	14.9	7.5	6.71	1.6	D[v,0.1] 17.70µm
339	99.2	153	93.1	68.6	68.0	30.8	25.7	13.9	6.6	6.24	1.3	
315	99.0	142	91.9	63.8	64.2	28.7	22.8	12.9	5.8	5.80	1.0	D[v,0.5] 50.03µm
293	98.7	132	90.5	59.3	60.2	26.7	20.2	12.0	5.1			
273	98.4	123	88.9	55.2	55.9	24.8	17.8	11.2	4.4			

Source = :Sample	Beam length = 14.3 mm Log. Diff. = 2.740	Model indp
Focal length = 300 mm	Obscuration = 0.3109	Volume Conc. = 0.0287%
Presentation = pil	Volume distribution	Sp.S.A 0.1815 m²/cc.

2560 pil lfu1479
Hamilton Harbour Sampling.....Dofasco
August 18,1995 Sample.....C3 - 8

MALVERN Series 2600 SB.09 Master Mode Fri 15 Sep 1995 8:50 am

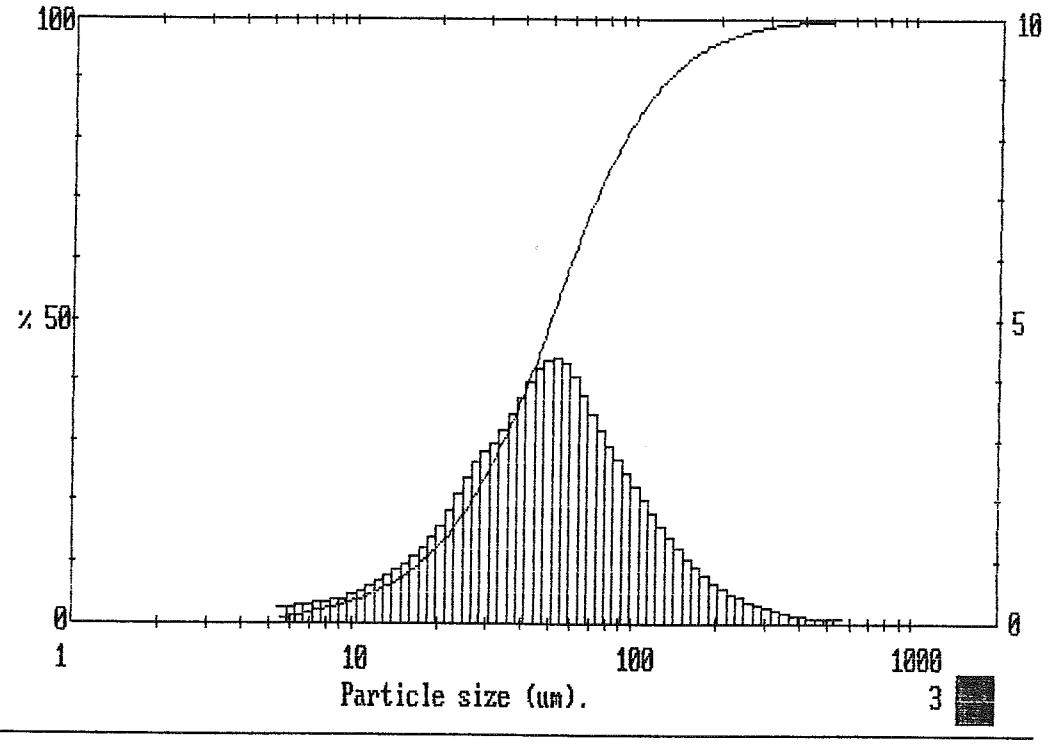

2560 pil lfu1479
Hamilton Harbour Sampling.....Dofasco
August 18,1995 Sample.....C3 - 8

MALVERN Series 2600 SB.09 Master Mode Fri 15 Sep 1995 8:57 am

High Size	Under %	High Size	Under %	High Size	Under %	High Size	Under %	High Size	Under %	High Size	Under %	Span 2.39
564	100	254	97.8	114	86.3	51.3	52.6	23.1	17.9	10.4	4.7	D[4,3] 66.41µm
524	99.9	236	97.3	106	84.3	47.7	48.6	21.4	15.9	9.64	4.2	
488	99.8	219	96.8	98.6	81.9	44.4	44.7	19.9	14.2	8.97	3.7	D[3,2] 30.97µm
454	99.7	204	96.2	91.7	79.4	41.2	41.0	18.5	12.6	8.34	3.2	
422	99.6	190	95.5	85.3	76.8	38.4	37.4	17.2	11.2	7.76	2.8	D[v,0.9] 132.86µm
392	99.4	176	94.6	79.3	73.9	35.7	34.1	16.0	10.0	7.21	2.4	
365	99.3	164	93.7	73.8	70.9	33.2	31.0	14.9	8.8	6.71	2.0	D[v,0.1] 16.06µm
339	99.1	153	92.6	68.6	67.7	30.8	28.1	13.9	7.8	6.24	1.6	
315	98.8	142	91.3	63.8	64.2	28.7	25.3	12.9	6.9	5.80	1.3	D[v,0.5] 48.95µm
293	98.5	132	89.8	59.3	60.5	26.7	22.6	12.0	6.1			
273	98.2	123	88.2	55.2	56.5	24.8	20.2	11.2	5.4			

Source = :Sample	Beam length = 14.3 mm Log. Diff. = 2.843	Model indp
Focal length = 300 mm	Obscuration = 0.4408	Volume Conc. = 0.0420%
Presentation = pil	Volume distribution	Sp.S.A 0.1938 m²/cc.

2560 pil 1fu1479
Hamilton Harbour Sampling.....Dofasco
August 18,1995 Sample.....C3 - 9

MALVERN Series 2600 SB.09 Master Mode Fri 15 Sep 1995 8:57 am

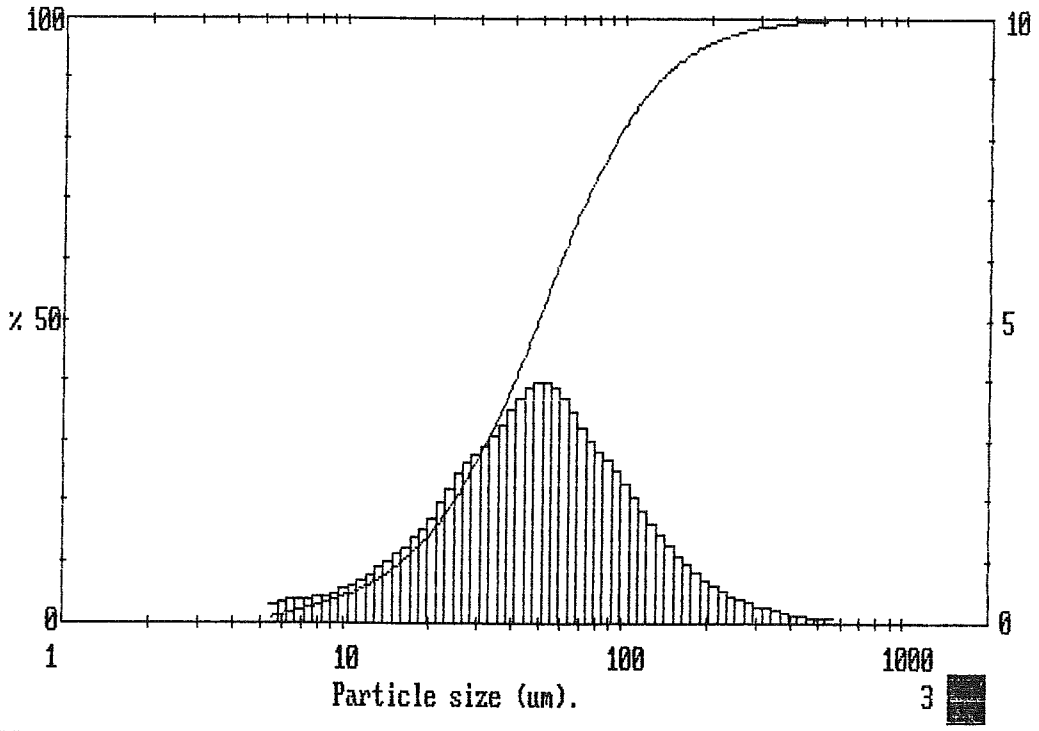

2560 pil 1fu1479
Hamilton Harbour Sampling.....Dofasco
August 18,1995 Sample.....C3 - 9

MALVERN Series 2600 SB.09 Master Mode Fri 15 Sep 1995 9:00 am

High Size	Under %	High Size	Under %	High Size	Under %	High Size	Under %	High Size	Under %	High Size	Under %	Span 2.79
564	100	254	96.9	114	84.2	51.3	53.7	23.1	19.7	10.4	5.3	D[4,3] 69.60µm
524	99.9	236	96.3	106	82.2	47.7	50.0	21.4	17.6	9.64	4.7	
488	99.7	219	95.6	98.6	80.0	44.4	46.4	19.9	15.7	8.97	4.1	D[3,2] 29.77µm
454	99.5	204	94.8	91.7	77.8	41.2	42.9	18.5	14.0	8.34	3.6	
422	99.4	190	93.9	85.3	75.4	38.4	39.5	17.2	12.5	7.76	3.1	
392	99.1	176	92.9	79.3	72.8	35.7	36.3	16.0	11.1	7.21	2.7	D[v,0.9] 148.09µm
365	98.9	164	91.8	73.8	70.2	33.2	33.2	14.9	9.8	6.71	2.2	
339	98.6	153	90.5	68.6	67.3	30.8	30.2	13.9	8.7	6.24	1.8	
315	98.3	142	89.2	63.8	64.2	28.7	27.4	12.9	7.7	5.80	1.4	
293	97.9	132	87.6	59.3	60.9	26.7	24.6	12.0	6.8			D[v,0.1] 15.05µm
273	97.4	123	86.0	55.2	57.3	24.8	22.0	11.2	6.0			

Source = :Sample	Beam length = 14.3 mm	Model indp	D[v,0.5] 47.69µm
	Log. Diff. = 2.812		
Focal length = 300 mm	Obscuration = 0.5441	Volume Conc. = 0.0545%	
Presentation = pil	Volume distribution	Sp.S.A 0.2015 m²/cc.	

2560 pil lfu1479
Hamilton Harbour Sampling.....Dofasco
August 18,1995 Sample.....C3 - 10

MALVERN Series 2600 SB.09 Master Mode Fri 15 Sep 1995 9:00 am

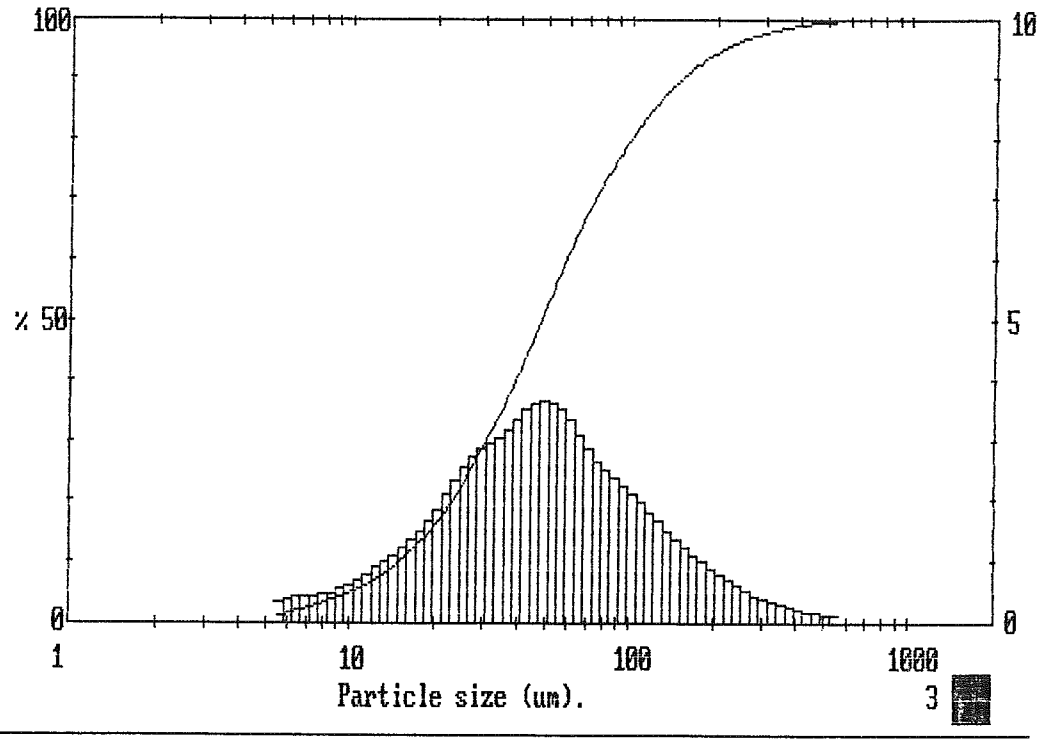

2560 pil lfu1479
Hamilton Harbour Sampling.....Dofasco
August 18,1995 Sample.....C3 - 10

MALVERN Series 2600 SB.09 Master Mode Fri 15 Sep 1995 12:47 pm

High Size	Under %	High Size	Under %	High Size	Under %	High Size	Under %	High Size	Under %	High Size	Under %	Span 3.95
188	100	84.5	98.8	38.0	88.5	17.1	69.5	7.69	39.9	3.46	17.2	D[4,3] 16.37µm
175	100	78.6	98.4	35.4	87.3	15.9	67.2	7.15	37.4	3.21	16.3	
163	100	73.1	97.9	32.9	86.2	14.8	64.9	6.65	35.1	2.99	15.5	D[3,2] 4.86µm
151	100	68.0	97.3	30.6	85.1	13.7	62.5	6.18	32.8	2.78	14.8	
141	100	63.2	96.6	28.4	83.7	12.8	59.9	5.75	30.4	2.59	13.9	D[v,0.9] 41.41µm
131	100	58.8	95.8	26.4	82.2	11.9	57.2	5.35	28.1	2.40	12.9	
122	99.9	54.7	94.8	24.6	80.4	11.1	54.3	4.97	25.7	2.24	11.7	D[v,0.1] 2.03µm
113	99.9	50.8	93.6	22.9	78.4	10.3	51.3	4.62	23.5	2.08	10.4	
105	99.7	47.3	92.4	21.3	76.3	9.56	48.3	4.30	21.5	1.93	9.1	
97.8	99.5	44.0	91.1	19.8	74.1	8.89	45.4	4.00	19.8			D[v,0.5] 9.96µm
90.9	99.2	40.9	89.8	18.4	71.8	8.27	42.5	3.72	18.3			

Source = :Sample
Focal length = 100 mm
Presentation = pil

Beam length = 14.3 mm
Log. Diff. = 2.424
Obscuration = 0.4850
Volume distribution

Model indp
Volume Conc. = 0.0075%
Sp.S.A 1.2345 m²/cc.

2560 pil lfu1479
mamilton Harbour Sampling .....Dofasco
August 18th, 1995..... C3 - 10 2 min. sonitated

MALVERN Series 2600 SB.09 Master Mode Fri 15 Sep 1995 12:47 pm

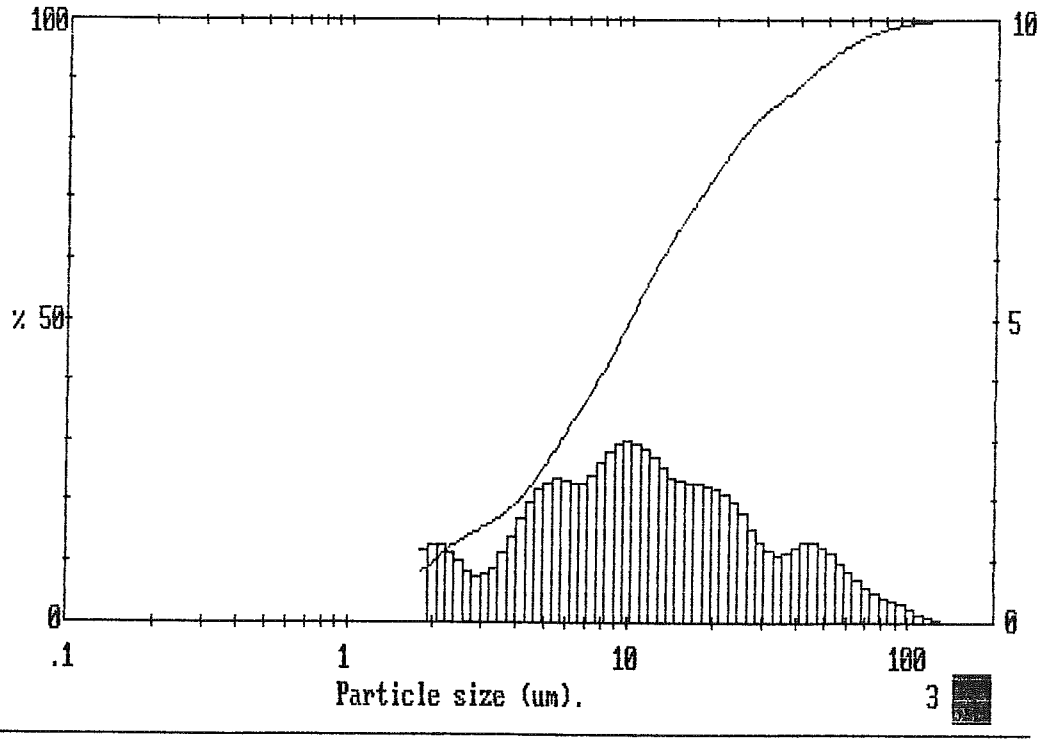

2560 pil lfu1479
mamilton Harbour Sampling .....Dofasco
August 18th, 1995..... C3 - 10 2 min. sonitated

MALVERN Series 2600 SB.09 Master Mode Thu 14 Sep 1995 2:51 pm

High Size	Under %	High Size	Under %	High Size	Under %	High Size	Under %	High Size	Under %	High Size	Under %	Span 3.94
564	100	254	86.1	114	64.9	51.3	38.1	23.1	14.7	10.4	4.0	D[4,3] 120.33µm
524	98.9	236	84.5	106	62.6	47.7	35.7	21.4	13.2	9.64	3.6	
488	97.8	219	82.8	98.6	60.2	44.4	33.3	19.9	11.8	8.97	3.2	D[3,2] 38.31µm
454	96.7	204	81.0	91.7	57.7	41.2	30.8	18.5	10.6	8.34	2.8	
422	95.5	190	79.2	85.3	55.2	38.4	28.5	17.2	9.5	7.76	2.4	D[v,0.9] 306.44µm
392	94.4	176	77.3	79.3	52.7	35.7	26.2	16.0	8.4	7.21	2.1	
365	93.1	164	75.4	73.8	50.2	33.2	23.9	14.9	7.5	6.71	1.7	
339	91.9	153	73.4	68.6	47.7	30.8	21.8	13.9	6.6	6.24	1.4	
315	90.5	142	71.4	63.8	45.3	28.7	19.8	12.9	5.8	5.80	1.1	D[v,0.1] 17.87µm
293	89.2	132	69.3	59.3	42.9	26.7	18.0	12.0	5.2			
273	87.7	123	67.2	55.2	40.5	24.8	16.3	11.2	4.6			

Source = :Sample	Beam length = 14.3 mm		Model indp	D[v,0.5] 73.31µm
	Log. Diff. = 2.471			
Focal length = 300 mm	Obscuration = 0.3659		Volume Conc. = 0.0407%	
Presentation = pil	Volume distribution		Sp.S.A 0.1566 m²/cc.	

2560 pil 1fu1479
Hamilton Harbour Sampling.....Dofasco
August 18,1995 Sample.....C3 -11

MALVERN Series 2600 SB.09 Master Mode Thu 14 Sep 1995 2:51 pm

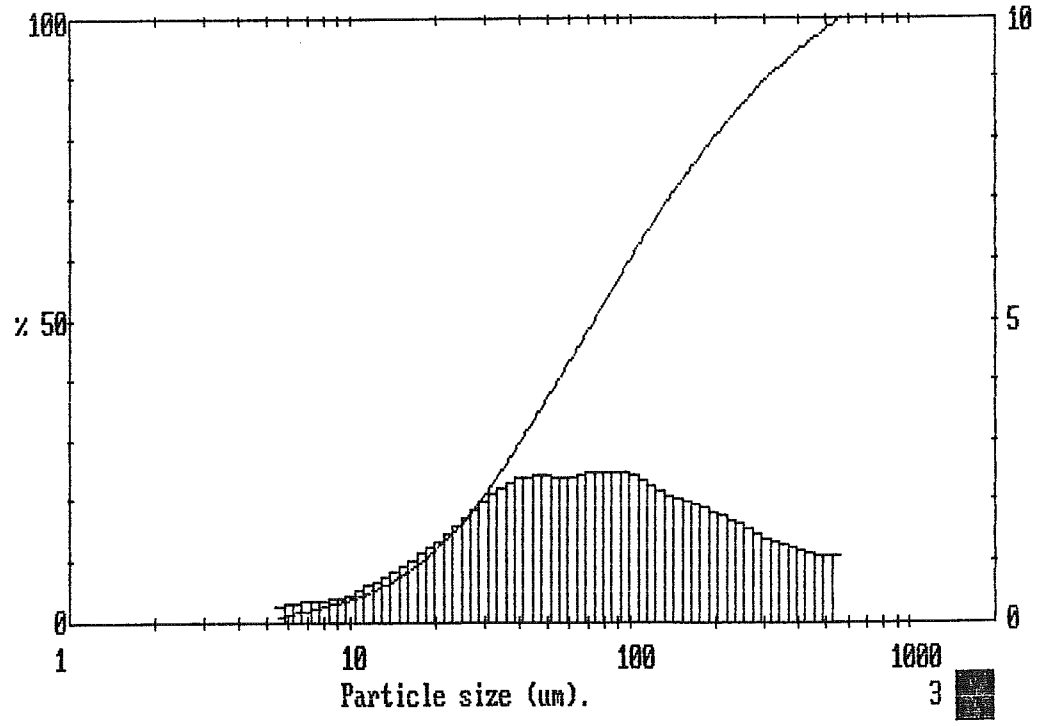

2560 pil 1fu1479
Hamilton Harbour Sampling.....Dofasco
August 18,1995 Sample.....C3 -11

MALVERN Series 2600 SB.09 Master Mode Fri 15 Sep 1995 9:06 am

High Size	Under %	High Size	Under %	High Size	Under %	High Size	Under %	High Size	Under %	High Size	Under %
564	100	254	95.0	114	82.2	51.3	47.2	23.1	13.9	10.4	3.5
524	99.7	236	94.3	106	80.2	47.7	43.2	21.4	12.2	9.64	3.1
488	99.3	219	93.6	98.6	78.0	44.4	39.5	19.9	10.8	8.97	2.7
454	99.0	204	92.7	91.7	75.6	41.2	35.9	18.5	9.5	8.34	2.4
422	98.6	190	91.8	85.3	72.9	38.4	32.4	17.2	8.4	7.76	2.1
392	98.2	176	90.8	79.3	69.9	35.7	29.1	16.0	7.4	7.21	1.8
365	97.8	164	89.7	73.8	66.7	33.2	26.0	14.9	6.5	6.71	1.5
339	97.3	153	88.4	68.6	63.2	30.8	23.1	13.9	5.8	6.24	1.2
315	96.8	142	87.1	63.8	59.4	28.7	20.4	12.9	5.1	5.80	0.9
293	96.3	132	85.6	59.3	55.4	26.7	18.0	12.0	4.5		
273	95.7	123	84.0	55.2	51.3	24.8	15.8	11.2	4.0		

Span 2.75

D[4,3] 79.71µm

D[3,2] 35.59µm

D[v,0.9] 167.52µm

D[v,0.1] 19.07µm

D[v,0.5] 53.95µm

Source = :Sample
Focal length = 300 mm
Presentation = pil

Beam length = 14.3 mm
Log. Diff. = 2.721
Obscuration = 0.0539
Volume distribution

Model indp
Volume Conc. = 0.0046%
Sp.S.A 0.1686 m²/cc.

2560 pil lfu1479
Hamilton Harbour Sampling.....Dofasco
August 22,1995 Sample.....C5 - 1

MALVERN Series 2600 SB.09 Master Mode Fri 15 Sep 1995 9:06 am

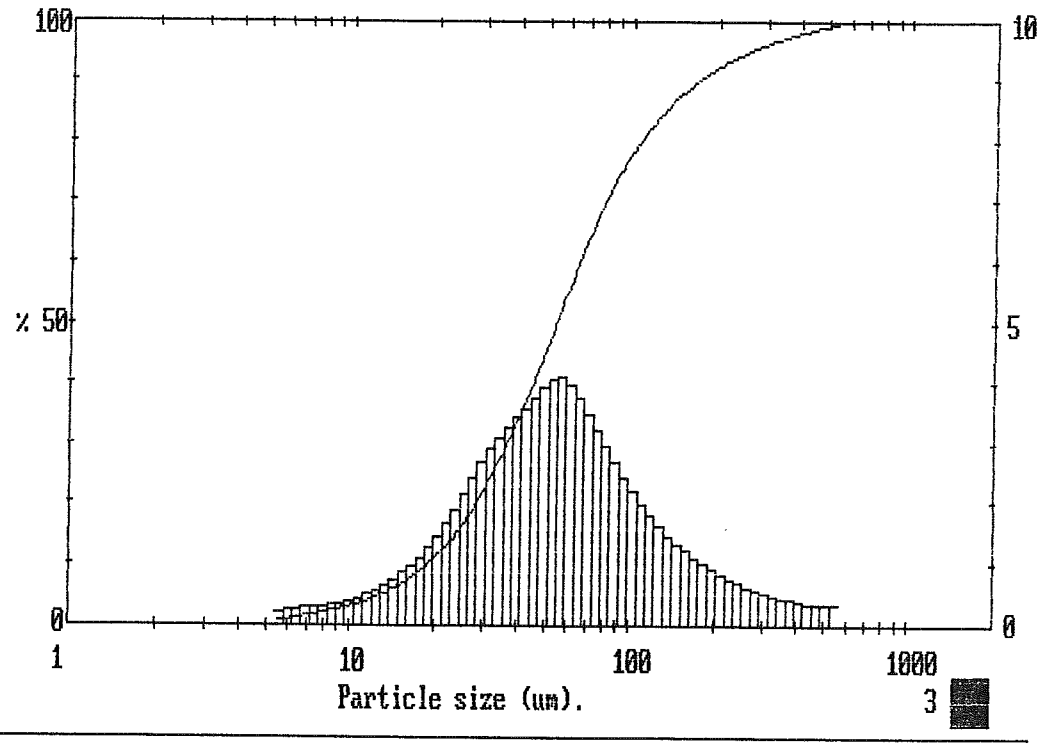

2560 pil lfu1479
Hamilton Harbour Sampling.....Dofasco
August 22,1995 Sample.....C5 - 1

MALVERN Series 2600 SB.09 Master Mode Fri 15 Sep 1995 9:37 am

High Size	Under %	High Size	Under %	High Size	Under %	High Size	Under %	High Size	Under %	High Size	Under %	Span 3.24
564	100	254	93.4	114	78.9	51.3	45.7	23.1	13.6	10.4	3.7	D[4,3] 87.00µm
524	99.6	236	92.5	106	77.0	47.7	41.8	21.4	12.0	9.64	3.2	
488	99.1	219	91.5	98.6	75.0	44.4	38.1	19.9	10.7	8.97	2.9	D[3,2] 36.02µm
454	98.6	204	90.4	91.7	72.8	41.2	34.6	18.5	9.5	8.34	2.5	
422	98.1	190	89.2	85.3	70.4	38.4	31.2	17.2	8.4	7.76	2.2	D[v,0.9] 198.98µm
392	97.6	176	88.0	79.3	67.6	35.7	28.1	16.0	7.5	7.21	1.9	
365	97.1	164	86.7	73.8	64.6	33.2	25.1	14.9	6.7	6.71	1.6	D[v,0.1] 19.15µm
339	96.5	153	85.3	68.6	61.2	30.8	22.3	13.9	5.9	6.24	1.3	
315	95.8	142	83.8	63.8	57.6	28.7	19.8	12.9	5.3	5.80	1.0	D[v,0.5] 55.49µm
293	95.1	132	82.2	59.3	53.7	26.7	17.5	12.0	4.6			
273	94.3	123	80.6	55.2	49.7	24.8	15.4	11.2	4.1			

Source = :Sample	Beam length = 14.3 mm	Model indp
	Log. Diff. = 2.687	
Focal length = 300 mm	Obscuration = 0.0530	Volume Conc. = 0.0046%
Presentation = pil	Volume distribution	Sp.S.A 0.1666 m²/cc.

2560 pil lfu1479
Hamilton Harbour Sampling.....Dofasco
August 22,1995 Sample.....C5 - 2

MALVERN Series 2600 SB.09 Master Mode Fri 15 Sep 1995 9:37 am

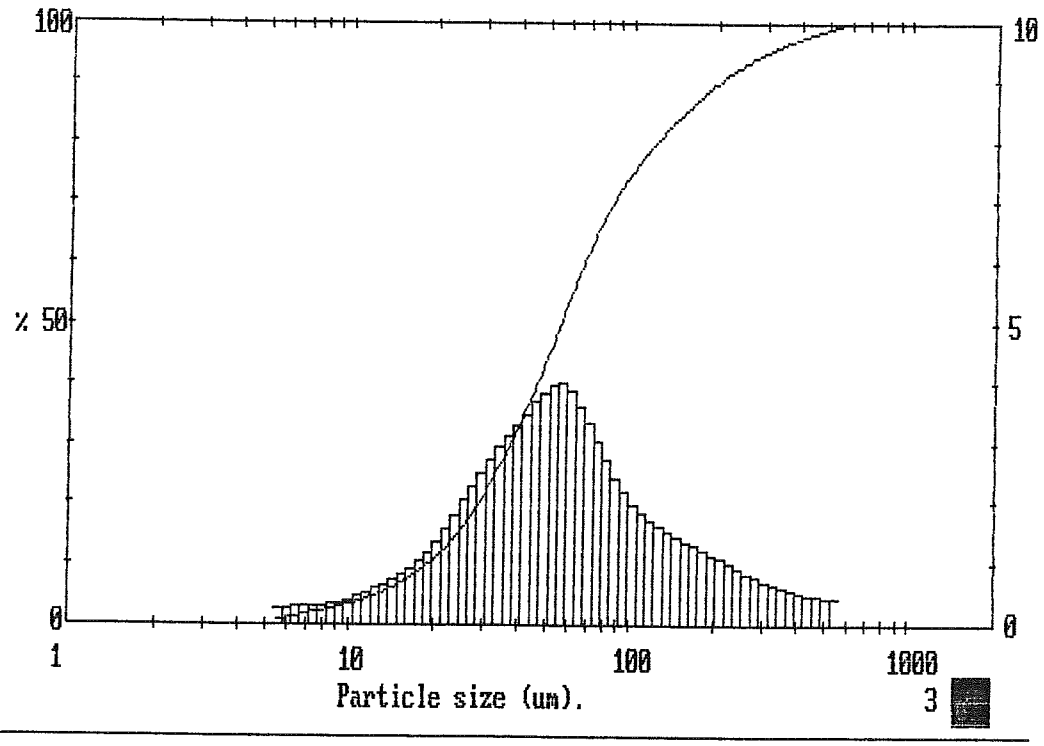

2560 pil lfu1479
Hamilton Harbour Sampling.....Dofasco
August 22,1995 Sample.....C5 - 2

MALVERN Series 2600 SB.09 Master Mode Fri 15 Sep 1995 9:41 am

High Size	Under %	High Size	Under %	High Size	Under %	High Size	Under %	High Size	Under %	High Size	Under %
564	100	254	94.1	114	79.2	51.3	45.0	23.1	16.1	10.4	4.6
524	99.6	236	93.2	106	77.0	47.7	41.7	21.4	14.4	9.64	4.1
488	99.2	219	92.3	98.6	74.7	44.4	38.6	19.9	12.9	8.97	3.6
454	98.8	204	91.3	91.7	72.1	41.2	35.7	18.5	11.6	8.34	3.2
422	98.4	190	90.1	85.3	69.3	38.4	32.9	17.2	10.4	7.76	2.8
392	97.9	176	88.9	79.3	66.2	35.7	30.1	16.0	9.3	7.21	2.4
365	97.4	164	87.6	73.8	62.9	33.2	27.4	14.9	8.4	6.71	2.0
339	96.8	153	86.2	68.6	59.4	30.8	24.9	13.9	7.5	6.24	1.6
315	96.3	142	84.6	63.8	55.8	28.7	22.4	12.9	6.7	5.80	1.2
293	95.6	132	83.0	59.3	52.1	26.7	20.1	12.0	5.9		
273	94.9	123	81.1	55.2	48.5	24.8	18.0	11.2	5.2		

Span 3.01

D[4,3] 84.96µm

D[3,2] 33.53µm

D[v,0.9] 188.09µm

D[v,0.1] 16.79µm

D[v,0.5] 56.84µm

Source = :Sample
Focal length = 300 mm
Presentation = pil

Beam length = 14.3 mm
Log. Diff. = 2.490
Obscuration = 0.0399
Volume distribution

Model indp
Volume Conc. = 0.0032%
Sp.S.A 0.1789 m²/cc.

2560 pil lfu1479
Hamilton Harbour Sampling.....Dofasco
August 22,1995 Sample.....C5 - 3

MALVERN Series 2600 SB.09 Master Mode Fri 15 Sep 1995 9:42 am

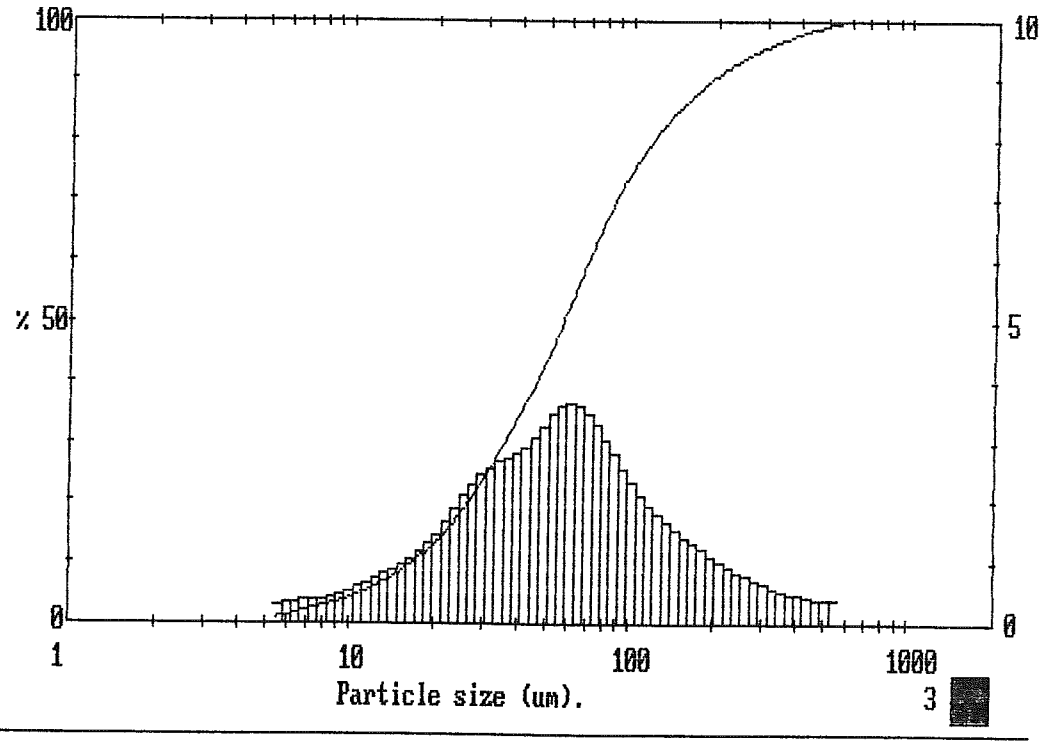

2560 pil lfu1479
Hamilton Harbour Sampling.....Dofasco
August 22,1995 Sample.....C5 - 3

MALVERN Series 2600 SB.09 Master Mode Fri 15 Sep 1995 9:46 am

High Size	Under %	High Size	Under %	High Size	Under %	High Size	Under %	High Size	Under %	High Size	Under %	Span 2.82
564	100	254	94.8	114	82.9	51.3	47.5	23.1	13.6	10.4	3.6	D[4,3] 79.67µm
524	99.6	236	94.0	106	81.1	47.7	43.2	21.4	11.9	9.64	3.1	
488	99.3	219	93.2	98.6	79.1	44.4	39.1	19.9	10.5	8.97	2.8	D[3,2] 35.57µm
454	98.9	204	92.4	91.7	76.8	41.2	35.3	18.5	9.3	8.34	2.4	
422	98.5	190	91.5	85.3	74.3	38.4	31.8	17.2	8.2	7.76	2.1	D[v,0.9] 170.06µm
392	98.1	176	90.5	79.3	71.3	35.7	28.5	16.0	7.3	7.21	1.8	
365	97.6	164	89.5	73.8	68.1	33.2	25.5	14.9	6.5	6.71	1.5	D[v,0.1] 19.39µm
339	97.1	153	88.4	68.6	64.5	30.8	22.7	13.9	5.8	6.24	1.2	
315	96.6	142	87.2	63.8	60.5	28.7	20.1	12.9	5.1	5.80	0.9	
293	96.0	132	85.9	59.3	56.3	26.7	17.7	12.0	4.5			D[v,0.5] 53.49µm
273	95.4	123	84.5	55.2	51.9	24.8	15.5	11.2	4.0			

Source = :Sample	Beam length = 14.3 mm	Model indp
	Log. Diff. = 2.816	
Focal length = 300 mm	Obscuration = 0.0718	Volume Conc. = 0.0062%
Presentation = pil	Volume distribution	Sp.S.A 0.1687 m²/cc.

2560 pil lfu1479
Hamilton Harbour Sampling.....Dofasco
August 22,1995 Sample.....C5 - 4

MALVERN Series 2600 SB.09 Master Mode Fri 15 Sep 1995 9:46 am

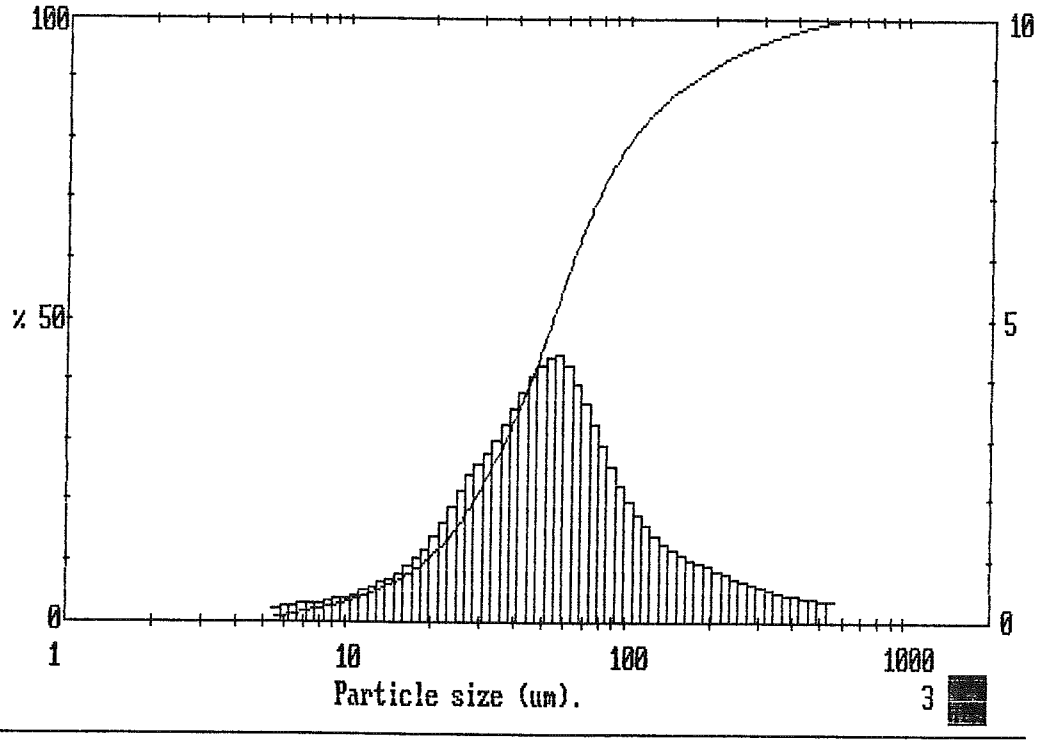

2560 pil lfu1479
Hamilton Harbour Sampling.....Dofasco
August 22,1995 Sample.....C5 - 4

MALVERN Series 2600 SB.09 Master Mode Fri 15 Sep 1995 9:49 am

High Size	Under %	High Size	Under %	High Size	Under %	High Size	Under %	High Size	Under %	High Size	Under %	Span 2.35
564	100	254	95.3	114	82.4	51.3	41.7	23.1	11.2	10.4	2.8	D[4,3] 81.89µm
524	99.7	236	94.7	106	80.1	47.7	37.7	21.4	9.8	9.64	2.5	
488	99.3	219	94.0	98.6	77.5	44.4	34.0	19.9	8.6	8.97	2.2	D[3,2] 39.24µm
454	98.9	204	93.3	91.7	74.5	41.2	30.5	18.5	7.6	8.34	1.9	
422	98.6	190	92.4	85.3	71.2	38.4	27.2	17.2	6.7	7.76	1.7	D[v,0.9] 160.08µm
392	98.2	176	91.5	79.3	67.5	35.7	24.2	16.0	5.9	7.21	1.5	
365	97.8	164	90.4	73.8	63.4	33.2	21.4	14.9	5.2	6.71	1.2	D[v,0.1] 21.65µm
339	97.3	153	89.2	68.6	59.1	30.8	18.9	13.9	4.6	6.24	1.0	
315	96.9	142	87.8	63.8	54.7	28.7	16.6	12.9	4.0	5.80	0.8	D[v,0.5] 59.01µm
293	96.4	132	86.2	59.3	50.3	26.7	14.6	12.0	3.6			
273	95.9	123	84.5	55.2	45.9	24.8	12.8	11.2	3.1			

Source = :Sample	Beam length = 14.3 mm	Model indp
	Log. Diff. = 2.609	
Focal length = 300 mm	Obscuration = 0.2354	Volume Conc. = 0.0246%
Presentation = pil	Volume distribution	Sp.S.A 0.1529 m²/cc.

2560 pil lfu1479
Hamilton Harbour Sampling.....Dofasco
August 22,1995 Sample.....C5 - 5

MALVERN Series 2600 SB.09 Master Mode Fri 15 Sep 1995 9:49 am

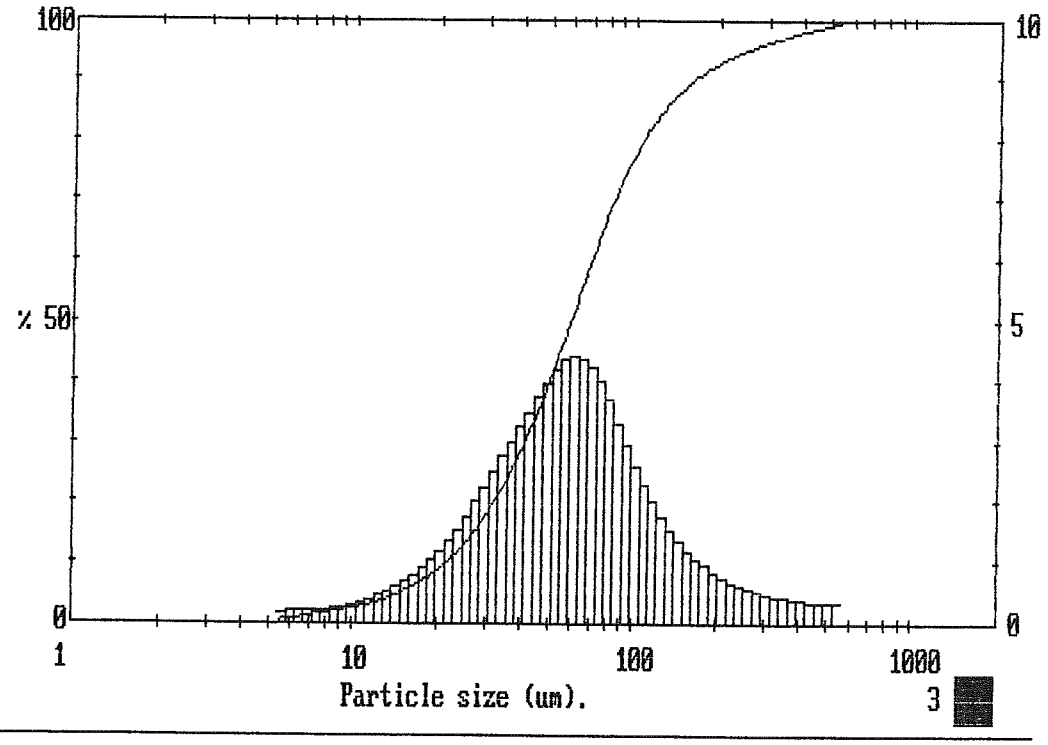

2560 pil lfu1479
Hamilton Harbour Sampling.....Dofasco
August 22,1995 Sample.....C5 - 5

MALVERN Series 2600 SB.09 Master Mode Fri 15 Sep 1995 9:53 am

High Size	Under %	High Size	Under %	High Size	Under %	High Size	Under %	High Size	Under %	High Size	Under %
564	100	254	97.7	114	85.4	51.3	45.1	23.1	12.6	10.4	3.2
524	99.9	236	97.2	106	83.0	47.7	40.7	21.4	11.1	9.64	2.8
488	99.8	219	96.7	98.6	80.4	44.4	36.7	19.9	9.8	8.97	2.5
454	99.6	204	96.1	91.7	77.4	41.2	32.9	18.5	8.7	8.34	2.2
422	99.5	190	95.3	85.3	74.2	38.4	29.4	17.2	7.7	7.76	1.9
392	99.3	176	94.5	79.3	70.8	35.7	26.3	16.0	6.8	7.21	1.6
365	99.2	164	93.5	73.8	67.1	33.2	23.5	14.9	6.0	6.71	1.4
339	98.9	153	92.3	68.6	63.1	30.8	20.9	13.9	5.3	6.24	1.1
315	98.7	142	90.9	63.8	58.8	28.7	18.6	12.9	4.7	5.80	0.9
293	98.4	132	89.3	59.3	54.3	26.7	16.3	12.0	4.1		
273	98.1	123	87.5	55.2	49.7	24.8	14.3	11.2	3.6		

Source = :Sample	Beam length = 14.3 mm	Model indp	Span 2.09
	Log. Diff. = 2.799		D[4,3] 71.67µm
Focal length = 300 mm	Obscuration = 0.3232	Volume Conc. = 0.0334%	D[3,2] 36.66µm
Presentation = pil	Volume distribution	Sp.S.A 0.1637 m²/cc.	D[v,0.9] 135.94µm
			D[v,0.1] 20.21µm
			D[v,0.5] 55.43µm

2560 pil lfu1479
Hamilton Harbour Sampling.....Dofasco
August 22,1995 Sample.....C5 - 6

MALVERN Series 2600 SB.09 Master Mode Fri 15 Sep 1995 9:53 am

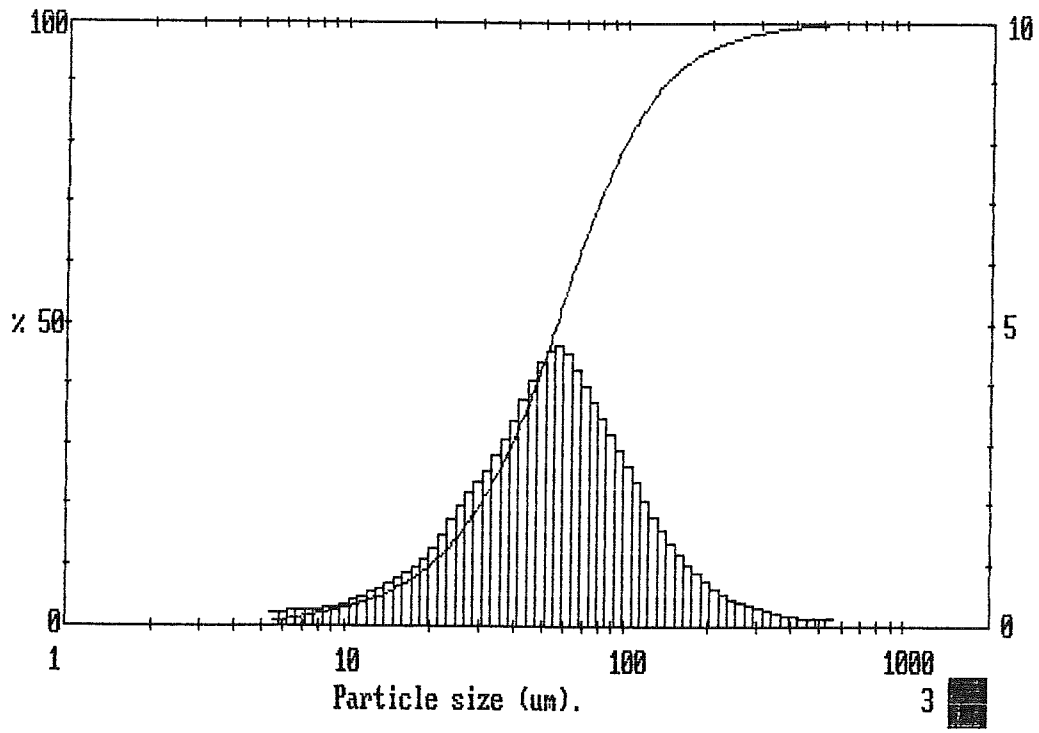

2560 pil lfu1479
Hamilton Harbour Sampling.....Dofasco
August 22,1995 Sample.....C5 - 6

MALVERN Series 2600 SB.09 Master Mode Fri 15 Sep 1995 9:57 am

High Size	Under %	High Size	Under %	High Size	Under %	High Size	Under %	High Size	Under %	High Size	Under %
564	100	254	97.5	114	86.6	51.3	53.0	23.1	17.4	10.4	4.5
524	99.9	236	97.0	106	84.6	47.7	49.0	21.4	15.4	9.64	4.0
488	99.7	219	96.5	98.6	82.4	44.4	45.0	19.9	13.7	8.97	3.5
454	99.6	204	95.9	91.7	79.9	41.2	41.1	18.5	12.2	8.34	3.0
422	99.4	190	95.2	85.3	77.3	38.4	37.5	17.2	10.8	7.76	2.6
392	99.2	176	94.4	79.3	74.5	35.7	34.0	16.0	9.6	7.21	2.2
365	99.0	164	93.5	73.8	71.5	33.2	30.8	14.9	8.5	6.71	1.9
339	98.8	153	92.5	68.6	68.2	30.8	27.7	13.9	7.5	6.24	1.5
315	98.5	142	91.3	63.8	64.7	28.7	24.8	12.9	6.6	5.80	1.2
293	98.2	132	89.9	59.3	61.0	26.7	22.1	12.0	5.8		
273	97.9	123	88.4	55.2	57.1	24.8	19.6	11.2	5.1		

Span 2.39

D[4,3] 67.00µm

D[3,2] 31.42µm

D[v,0.9] 132.35µm

D[v,0.1] 16.44µm

D[v,0.5] 48.59µm

Source = :Sample
Focal length = 300 mm
Presentation = pil

Beam length = 14.3 mm
Log. Diff. = 2.751
Obscuration = 0.3690
Volume distribution

Model indp
Volume Conc. = 0.0337%
Sp.S.A 0.1909 m²/cc.

2560 pil lfu1479
Hamilton Harbour Sampling.....Dofasco
August 22,1995 Sample.....C5 - 7

MALVERN Series 2600 SB.09 Master Mode Fri 15 Sep 1995 9:57 am

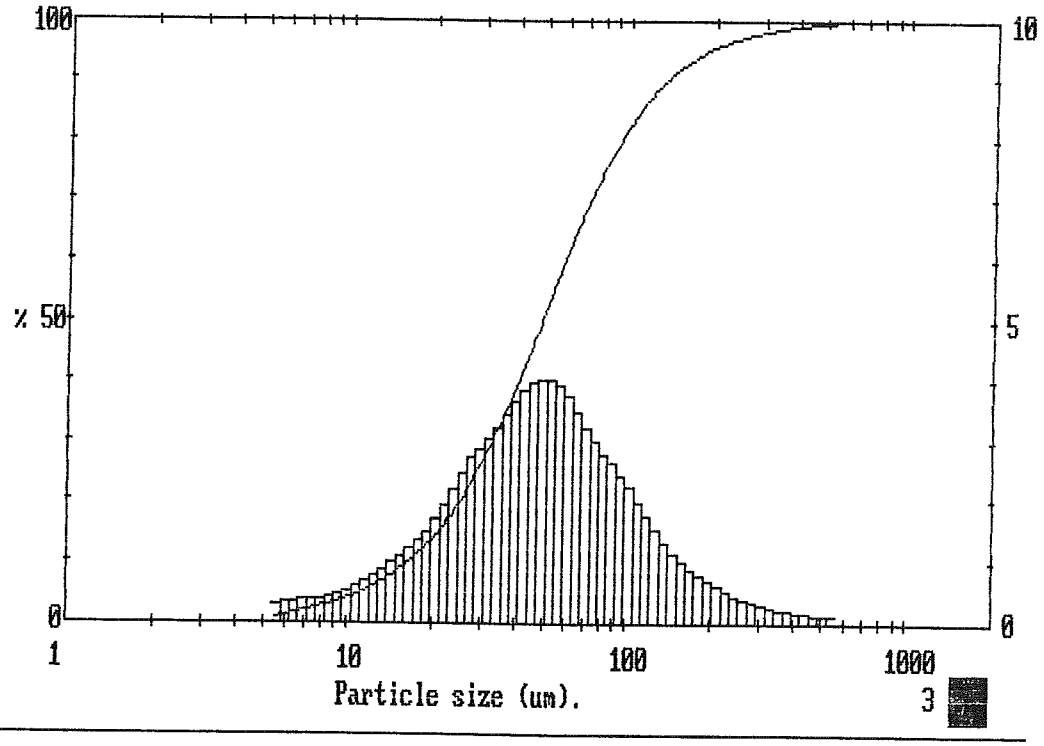

2560 pil lfu1479
Hamilton Harbour Sampling.....Dofasco
August 22,1995 Sample.....C5 - 7

MALVERN Series 2600 SB.09 Master Mode Fri 15 Sep 1995 10:01 am

High Size	Under %	High Size	Under %	High Size	Under %	High Size	Under %	High Size	Under %	High Size	Under %	Span 2.57
564	100	254	97.3	114	87.2	51.3	57.2	23.1	20.5	10.4	5.4	D[4,3] 64.56µm
524	99.8	236	96.9	106	85.4	47.7	53.4	21.4	18.3	9.64	4.7	
488	99.7	219	96.4	98.6	83.3	44.4	49.6	19.9	16.3	8.97	4.2	D[3,2] 28.77µm
454	99.5	204	95.8	91.7	81.0	41.2	45.7	18.5	14.6	8.34	3.7	
422	99.3	190	95.2	85.3	78.6	38.4	42.0	17.2	13.0	7.76	3.2	D[v,0.9] 129.67µm
392	99.1	176	94.5	79.3	76.1	35.7	38.4	16.0	11.5	7.21	2.7	
365	98.9	164	93.6	73.8	73.5	33.2	35.0	14.9	10.2	6.71	2.3	D[v,0.1] 14.76µm
339	98.6	153	92.7	68.6	70.7	30.8	31.7	13.9	9.0	6.24	1.8	
315	98.4	142	91.6	63.8	67.7	28.7	28.6	12.9	7.9	5.80	1.4	
293	98.0	132	90.3	59.3	64.4	26.7	25.7	12.0	6.9			
273	97.7	123	88.9	55.2	60.9	24.8	23.0	11.2	6.1			

Source = :Sample	Beam length = 14.3 mm	Model indp	D[v,0.5] 44.70µm
	Log. Diff. = 2.564		
Focal length = 300 mm	Obscuration = 0.3198	Volume Conc. = 0.0258%	
Presentation = pil	Volume distribution	Sp.S.A 0.2086 m²/cc.	

2560 pil lfu1479
Hamilton Harbour Sampling.....Dofasco
August 22,1995 Sample.....C5 - 8

MALVERN Series 2600 SB.09 Master Mode Fri 15 Sep 1995 10:02 am

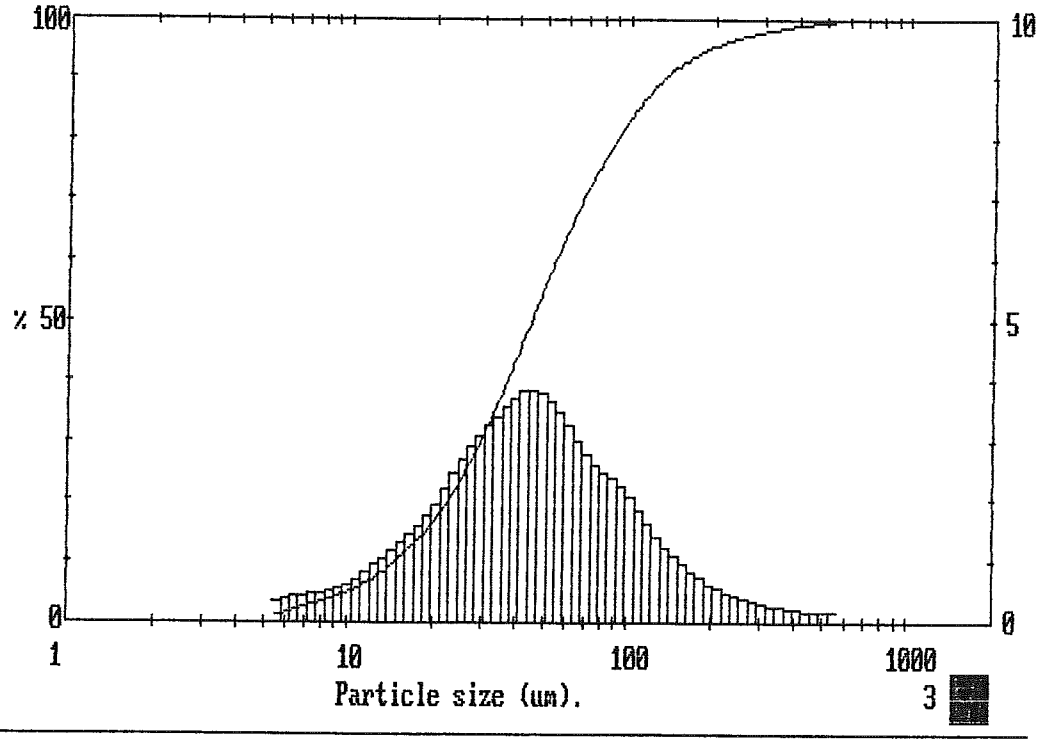

2560 pil lfu1479
Hamilton Harbour Sampling.....Dofasco
August 22,1995 Sample.....C5 - 8

MALVERN Series 2600 SB.09 Master Mode Fri 15 Sep 1995 10:05 am

High Size	Under %	High Size	Under %	High Size	Under %	High Size	Under %	High Size	Under %	High Size	Under %	Span 2.66
564	100	254	96.7	114	84.2	51.3	52.5	23.1	17.7	10.4	4.5	D[4,3] 71.16µm
524	99.8	236	96.1	106	82.1	47.7	48.7	21.4	15.7	9.64	3.9	
488	99.6	219	95.5	98.6	79.8	44.4	45.0	19.9	14.0	8.97	3.4	D[3,2] 31.69µm
454	99.4	204	94.8	91.7	77.4	41.2	41.3	18.5	12.4	8.34	3.0	
422	99.2	190	94.0	85.3	74.8	38.4	37.7	17.2	11.0	7.76	2.6	D[v,0.9] 146.25µm
392	98.9	176	93.0	79.3	72.1	35.7	34.3	16.0	9.7	7.21	2.2	
365	98.6	164	92.0	73.8	69.3	33.2	31.1	14.9	8.5	6.71	1.8	D[v,0.1] 16.35µm
339	98.3	153	90.8	68.6	66.3	30.8	28.0	13.9	7.5	6.24	1.5	
315	98.0	142	89.4	63.8	63.1	28.7	25.2	12.9	6.6	5.80	1.1	
293	97.6	132	87.9	59.3	59.7	26.7	22.5	12.0	5.8			
273	97.2	123	86.1	55.2	56.2	24.8	20.0	11.2	5.1			

Source = :Sample	Beam length = 14.3 mm	Model indp	D[v,0.5] 48.88µm
	Log. Diff. = 2.416		
Focal length = 300 mm	Obscuration = 0.3732	Volume Conc. = 0.0345%	
Presentation = pil	Volume distribution	Sp.S.A 0.1893 m²/cc.	

2560 pil lfu1479
Hamilton Harbour Sampling.....Dofasco
August 22,1995 Sample.....C5 - 10

MALVERN Series 2600 SB.09 Master Mode Fri 15 Sep 1995 10:05 am

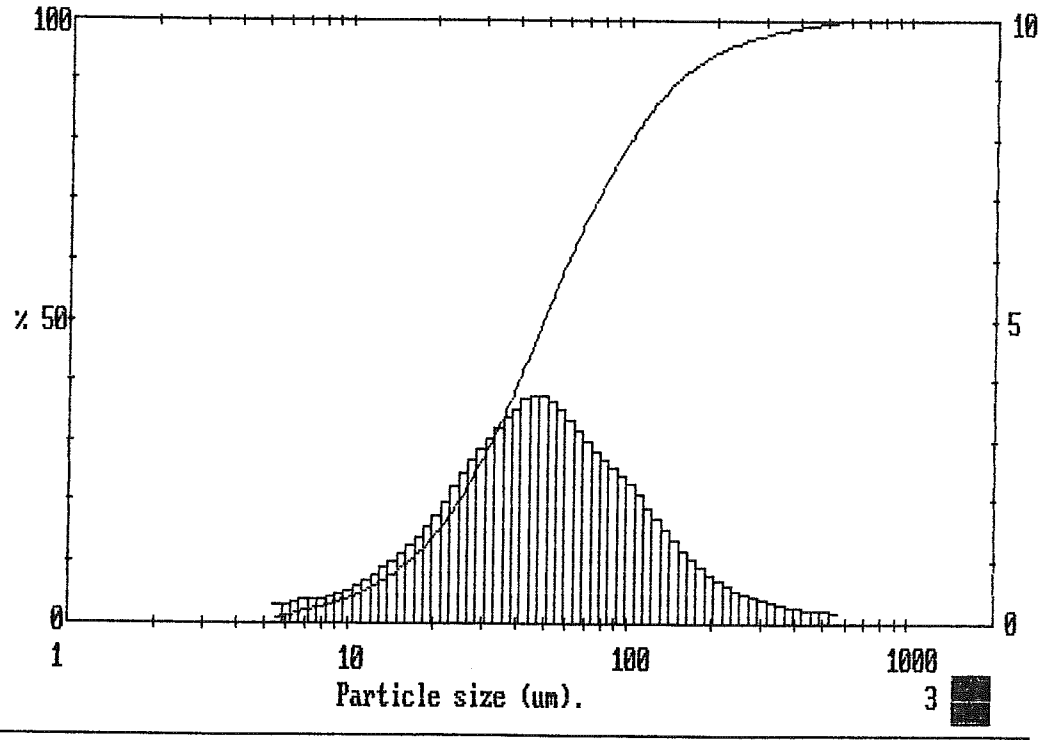

2560 pil lfu1479
Hamilton Harbour Sampling.....Dofasco
August 22,1995 Sample.....C5 - 10

MALVERN Series 2600 SB.09 Master Mode Fri 15 Sep 1995 12:56 pm

High Size	Under %	High Size	Under %	High Size	Under %	High Size	Under %	High Size	Under %	High Size	Under %	Span 4.95
188	100	84.5	97.8	38.0	83.1	17.1	63.8	7.69	40.4	3.46	18.7	D[4,3] 20.22µm
175	100	78.6	96.5	35.4	81.2	15.9	61.4	7.15	38.2	3.21	17.8	
163	100	73.1	95.1	32.9	79.1	14.8	58.9	6.65	35.9	2.99	16.9	D[3,2] 4.83µm
151	100	68.0	93.6	30.6	77.0	13.7	56.3	6.18	33.5	2.78	15.9	
141	100	63.2	92.1	28.4	75.0	12.8	53.9	5.75	31.2	2.59	14.9	D[v,0.9] 56.82µm
131	100	58.8	90.7	26.4	73.3	11.9	51.8	5.35	28.8	2.40	13.8	
122	99.9	54.7	89.3	24.6	71.9	11.1	49.9	4.97	26.7	2.24	12.5	D[v,0.1] 1.97µm
113	99.9	50.8	88.1	22.9	70.5	10.3	48.1	4.62	24.6	2.08	11.1	
105	99.7	47.3	87.0	21.3	69.1	9.56	46.3	4.30	22.8	1.93	9.7	D[v,0.5] 11.09µm
97.8	99.4	44.0	85.8	19.8	67.6	8.89	44.5	4.00	21.2			
90.9	98.8	40.9	84.6	18.4	65.8	8.27	42.5	3.72	19.9			

Source = :Sample
Focal length = 100 mm
Presentation = pil

Beam length = 14.3 mm
Log. Diff. = 1.475
Obscuration = 0.2480
Volume distribution

Model indp
Volume Conc. = 0.0032%
Sp.S.A 1.2430 m²/cc.

2560 pil lfu1479
Hamilton Harbour Sampling .....Dofasco
August 22nd, 1995..... C5 - 10 2 min. sonitated

MALVERN Series 2600 SB.09 Master Mode Fri 15 Sep 1995 12:56 pm

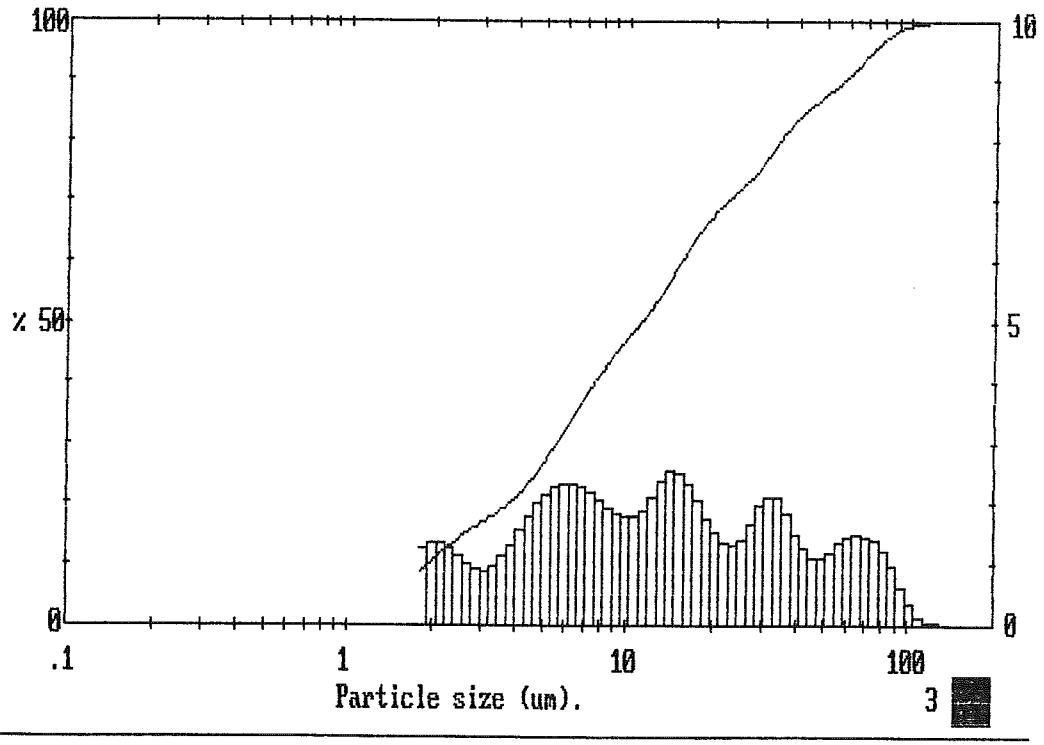

2560 pil lfu1479
Hamilton Harbour Sampling .....Dofasco
August 22nd, 1995..... C5 - 10 2 min. sonitated

MALVERN Series 2600 SB.09 Master Mode Fri 15 Sep 1995 10:09 am

High Size	Under %	High Size	Under %	High Size	Under %	High Size	Under %	High Size	Under %	High Size	Under %	Span 2.92
564	100	254	95.4	114	79.9	51.3	48.1	23.1	16.6	10.4	4.2	D[4,3] 80.07µm
524	99.7	236	94.6	106	77.5	47.7	44.6	21.4	14.8	9.64	3.7	
488	99.5	219	93.7	98.6	75.0	44.4	41.1	19.9	13.1	8.97	3.3	D[3,2] 33.55µm
454	99.2	204	92.7	91.7	72.4	41.2	37.7	18.5	11.7	8.34	2.8	
422	98.9	190	91.6	85.3	69.6	38.4	34.4	17.2	10.3	7.76	2.5	
392	98.6	176	90.4	79.3	66.9	35.7	31.4	16.0	9.1	7.21	2.1	D[v,0.9] 172.87µm
365	98.2	164	89.0	73.8	64.1	33.2	28.5	14.9	8.0	6.71	1.7	
339	97.8	153	87.5	68.6	61.1	30.8	25.7	13.9	7.1	6.24	1.4	
315	97.3	142	85.9	63.8	58.1	28.7	23.2	12.9	6.2	5.80	1.1	D[v,0.1] 16.91µm
293	96.7	132	84.1	59.3	54.9	26.7	20.8	12.0	5.4			
273	96.1	123	82.1	55.2	51.6	24.8	18.6	11.2	4.8			

Source = :Sample	Beam length = 14.3 mm	Model indp	D[v,0.5] 53.36µm
	Log. Diff. = 2.518		
Focal length = 300 mm	Obscuration = 0.3774	Volume Conc. = 0.0371%	
Presentation = pil	Volume distribution	Sp.S.A 0.1788 m²/cc.	

2560 pil lfu1479
Hamilton Harbour Sampling.....Dofasco
August 22,1995 Sample.....C5 - 11

MALVERN Series 2600 SB.09 Master Mode Fri 15 Sep 1995 10:09 am

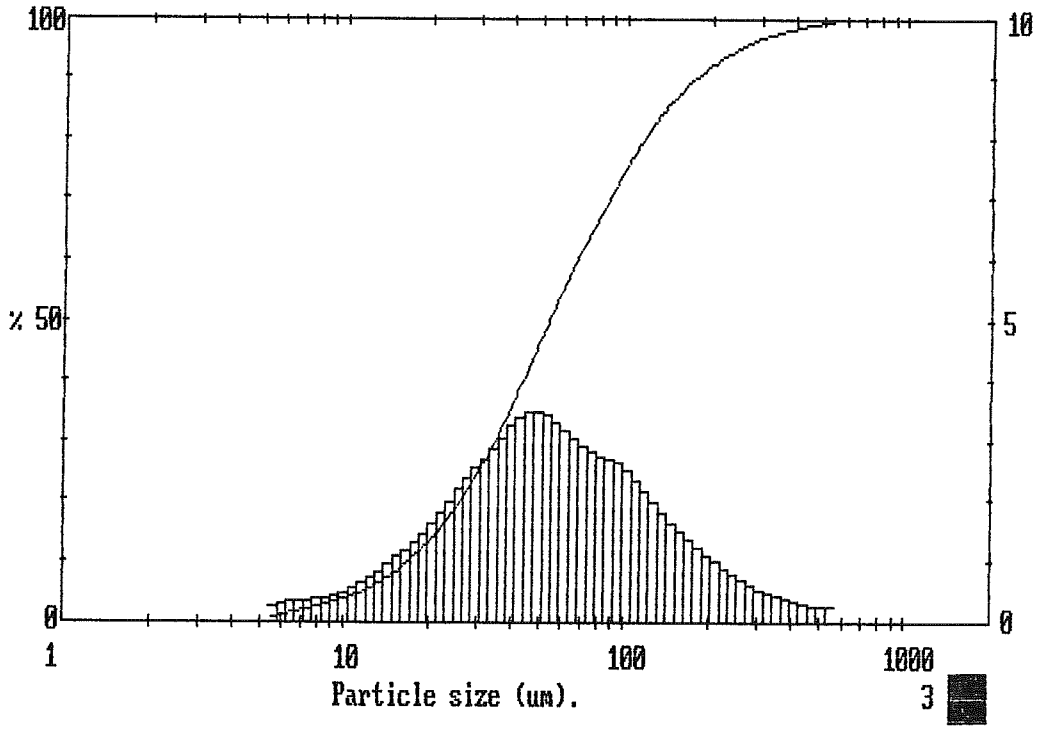

2560 pil lfu1479
Hamilton Harbour Sampling.....Dofasco
August 22,1995 Sample.....C5 - 11

APPENDIX 4

Eroded Aggregate Size vs. Aggregate Settling Velocity, Density and Porosity

Dofasco Settling Experiment
C1-6

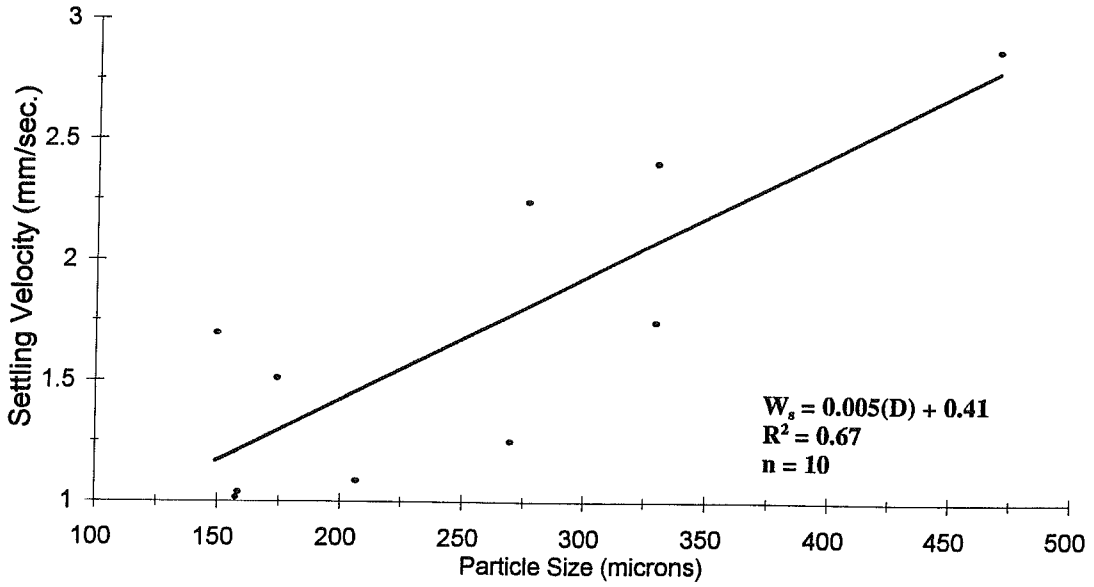

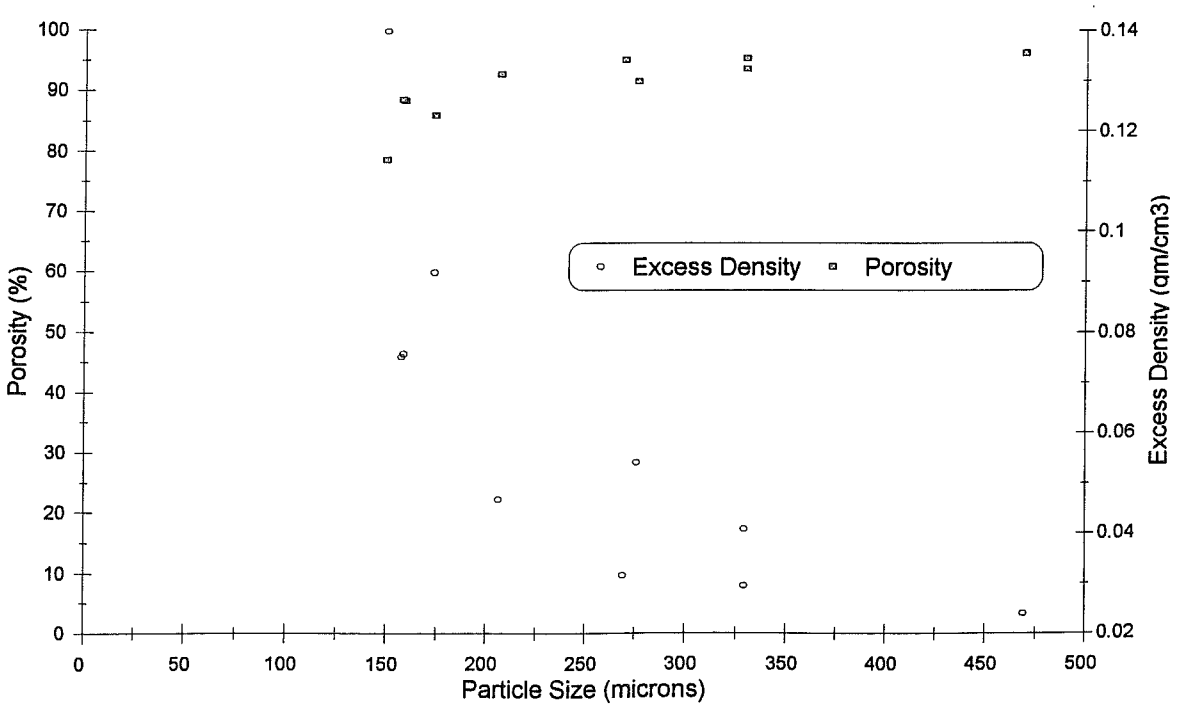

Dofasco Settling Experiment
C1-7

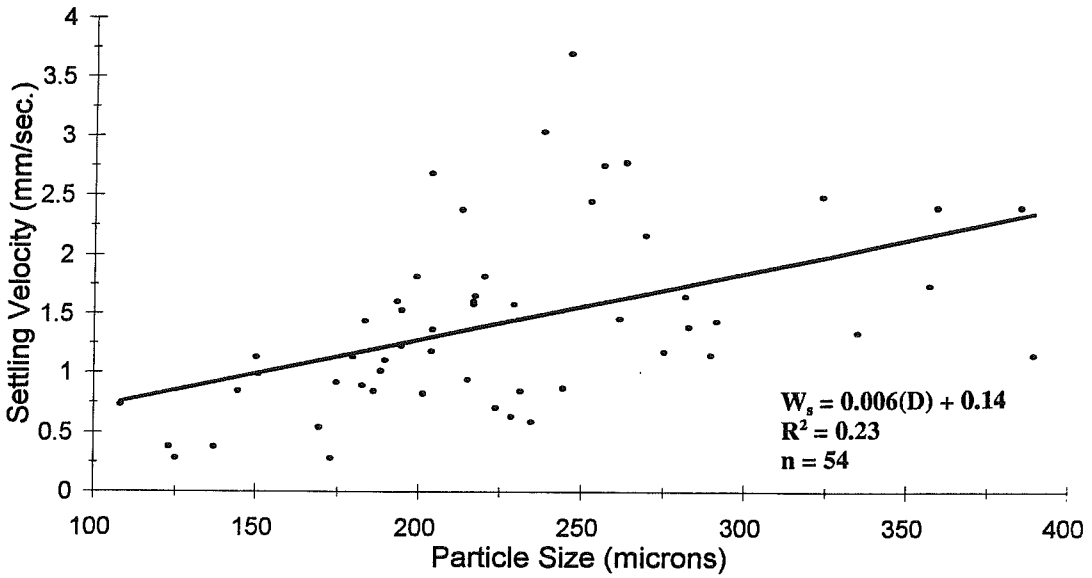

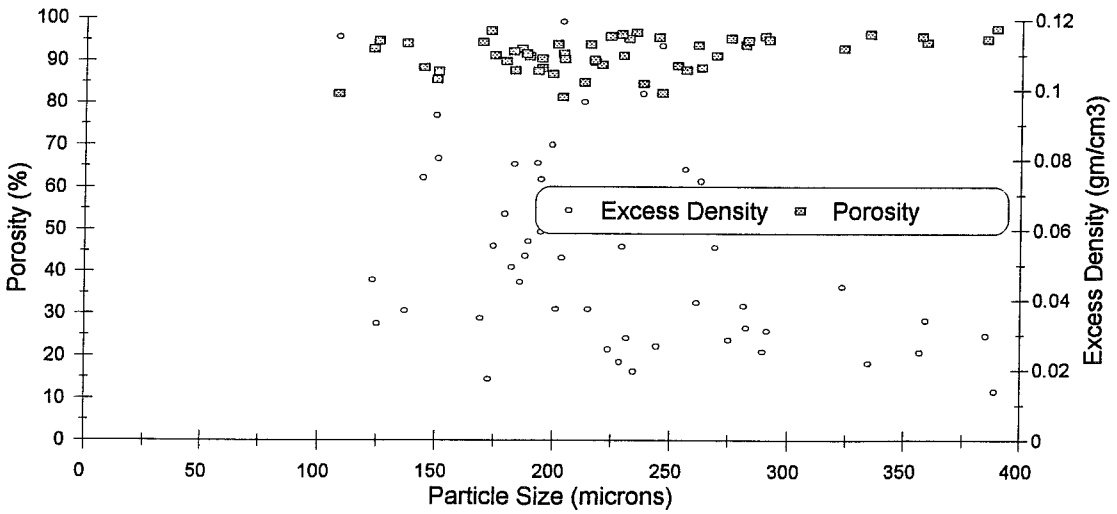

Dofasco Settling Experiment
C1-8

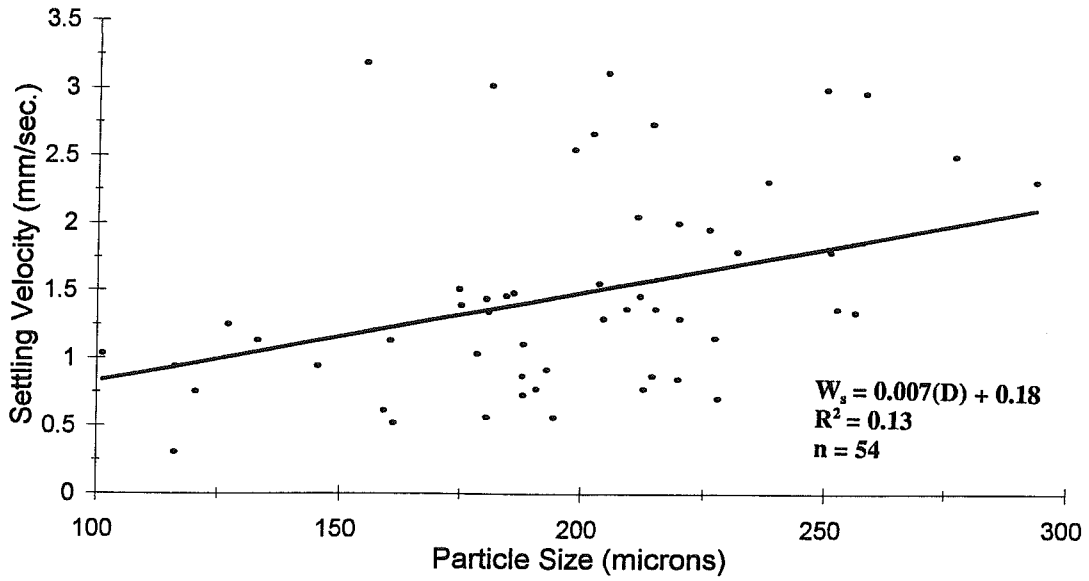

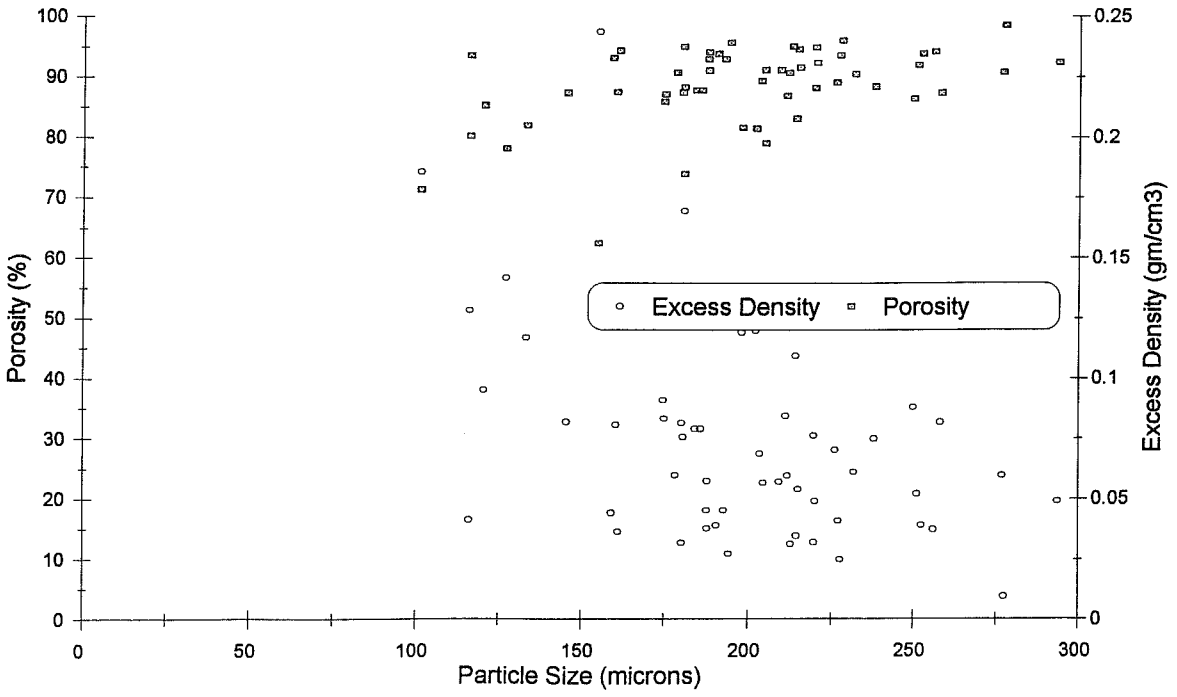

Dofasco Settling Experiment
C1-9

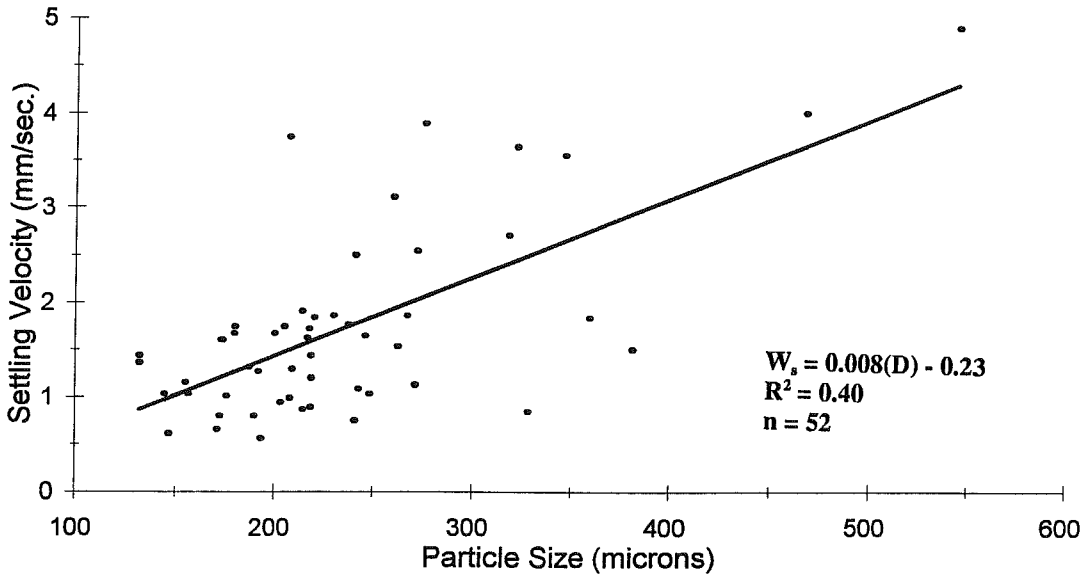

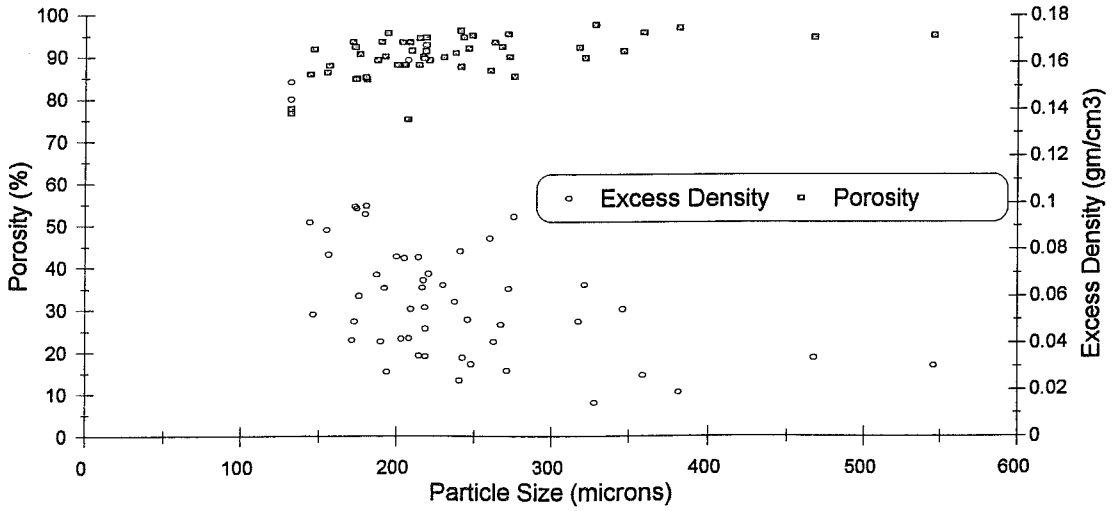

Dofasco Settling Experiment
C1-10

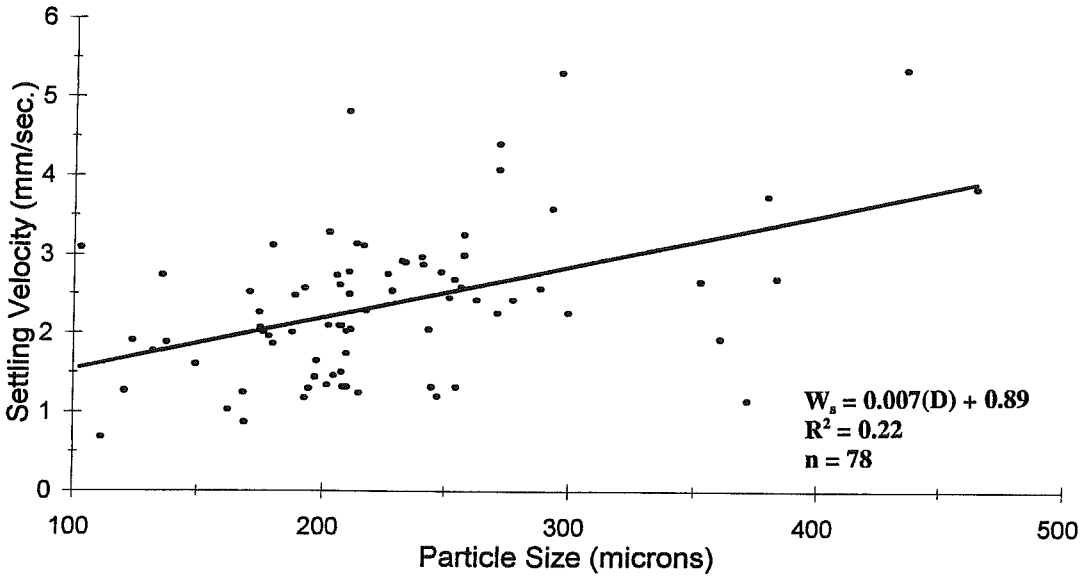

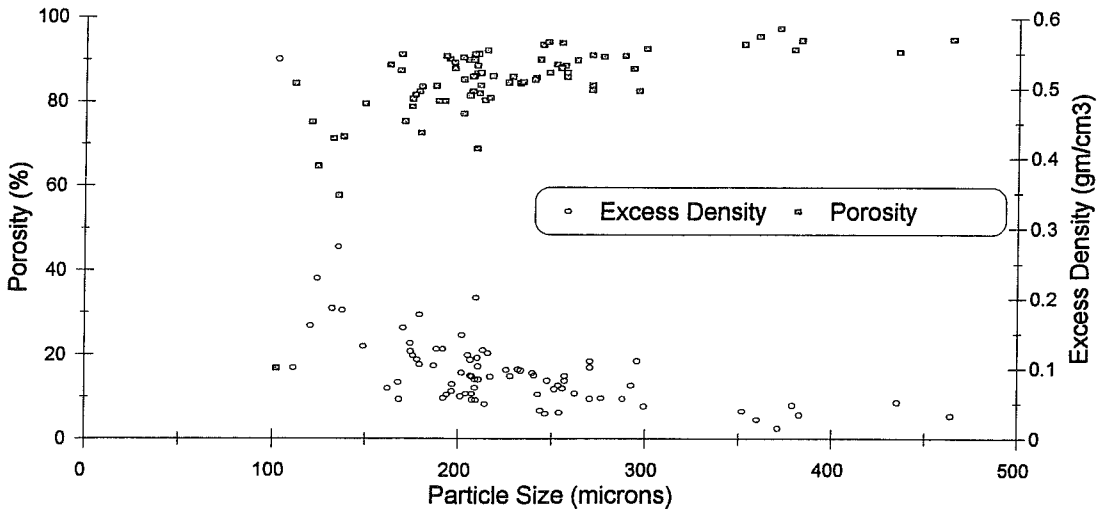

Dofasco Settling Experiment
C1-11

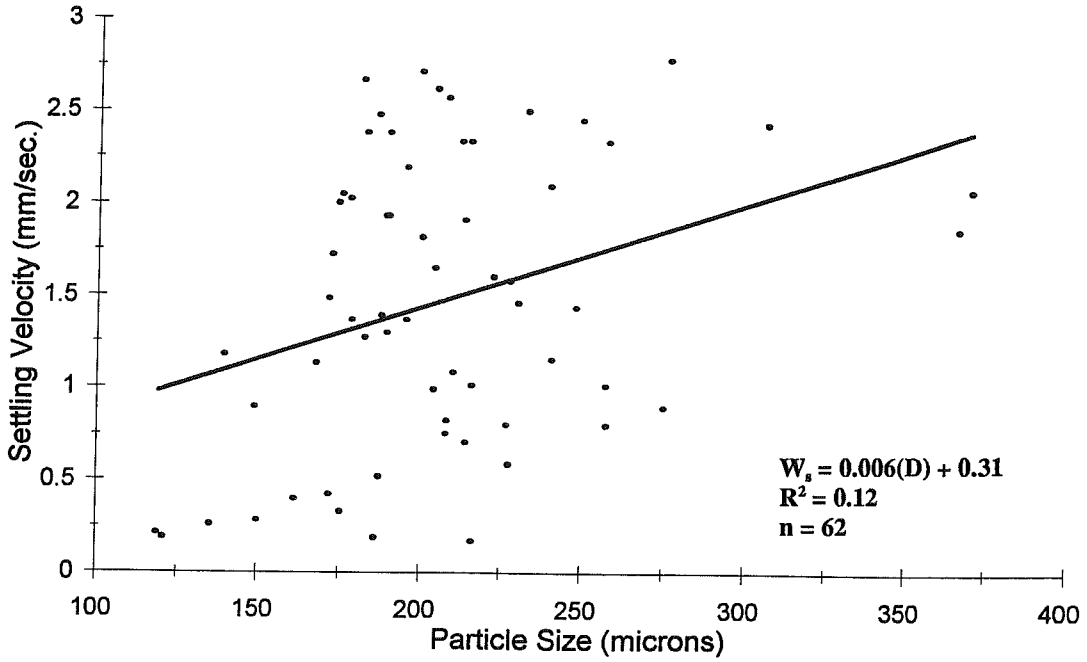

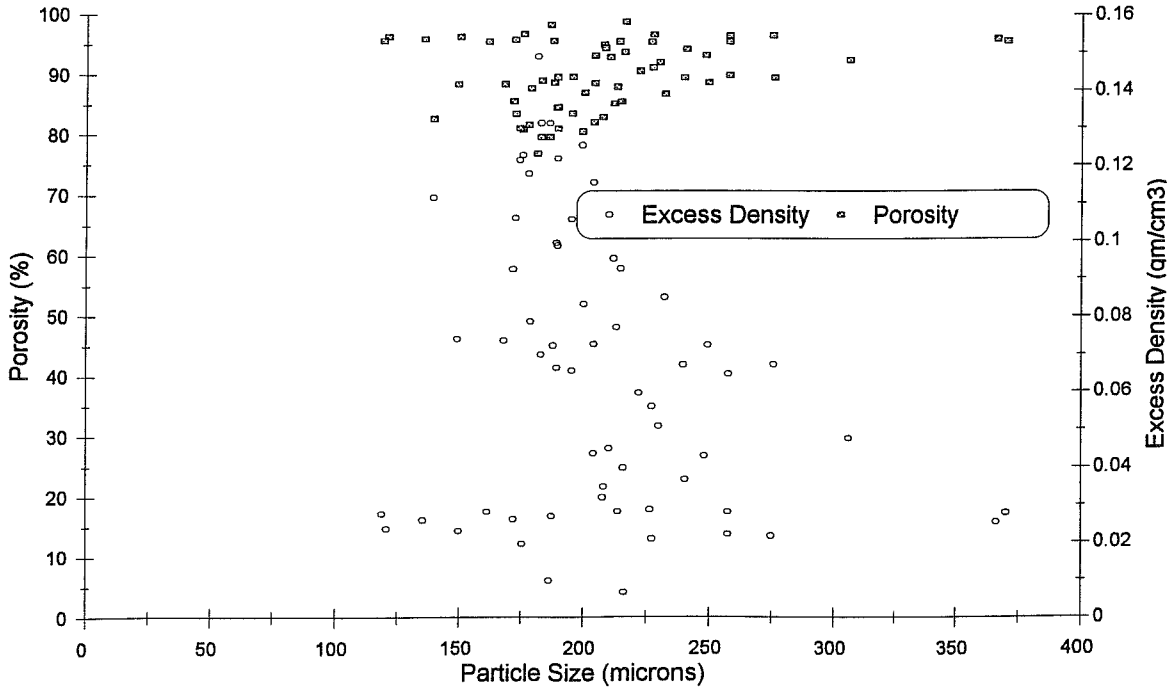

Dofasco Settling Experiment
C1-12

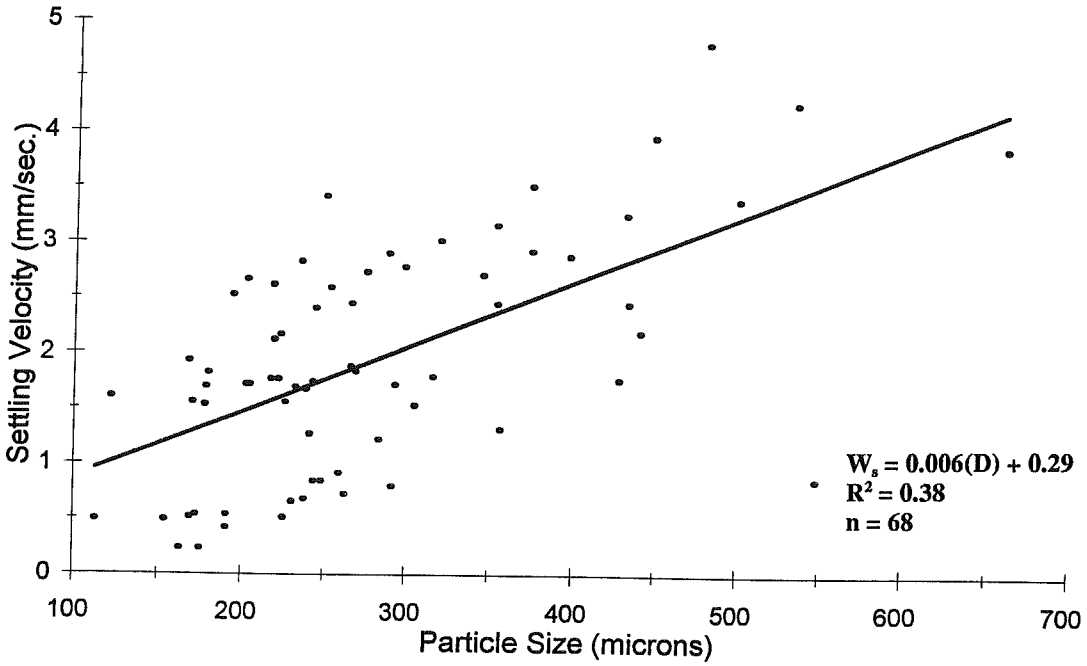

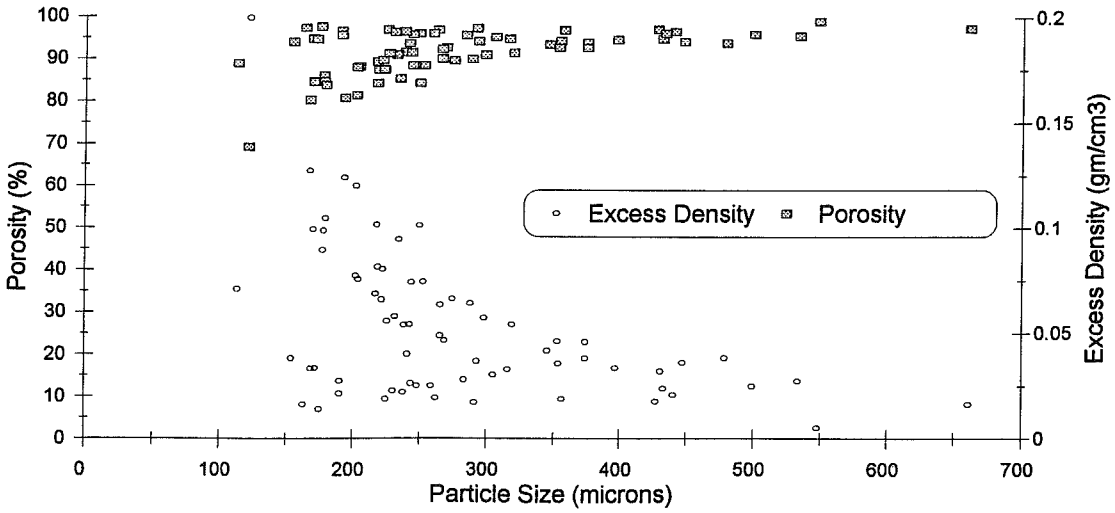

Dofasco Settling Experiment
C3-6

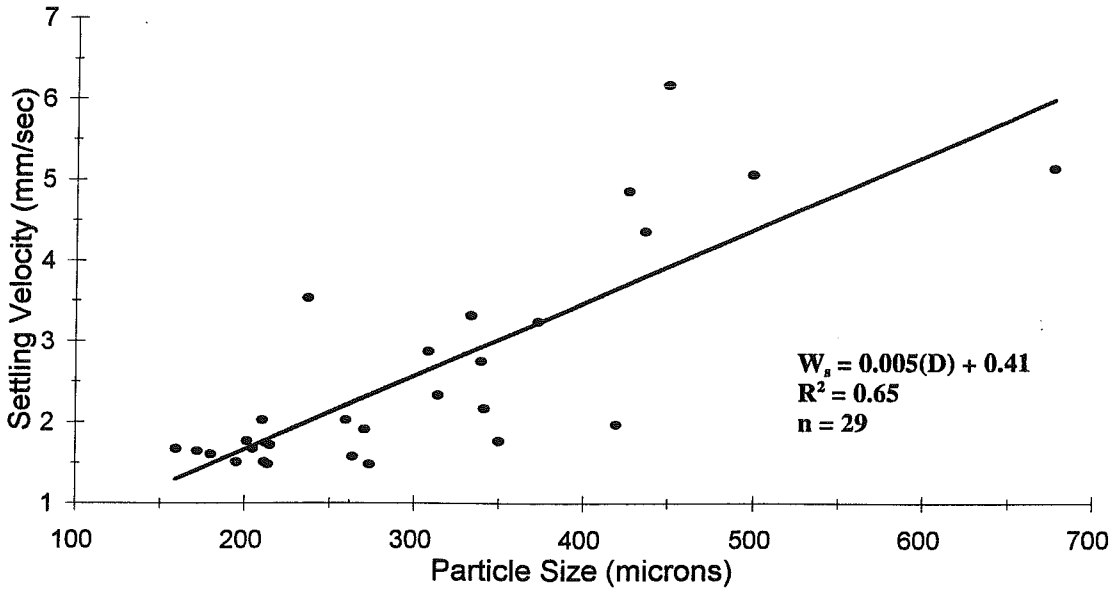

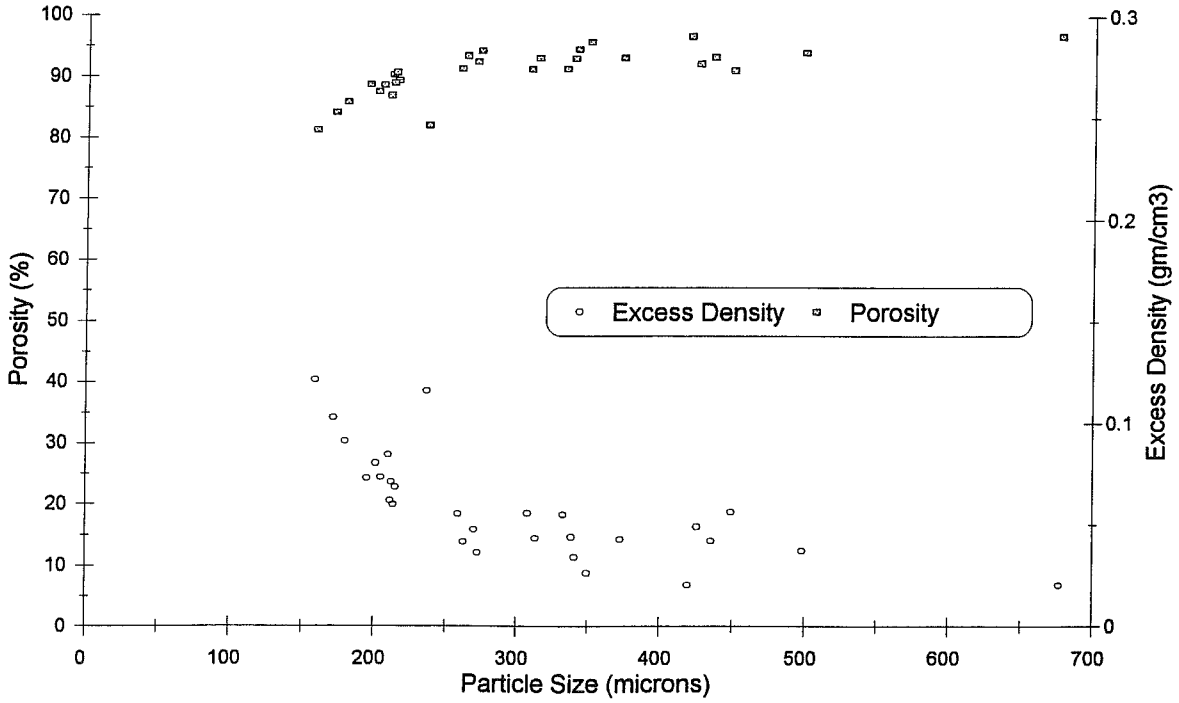

Dofasco Settling Experiment

C3-7

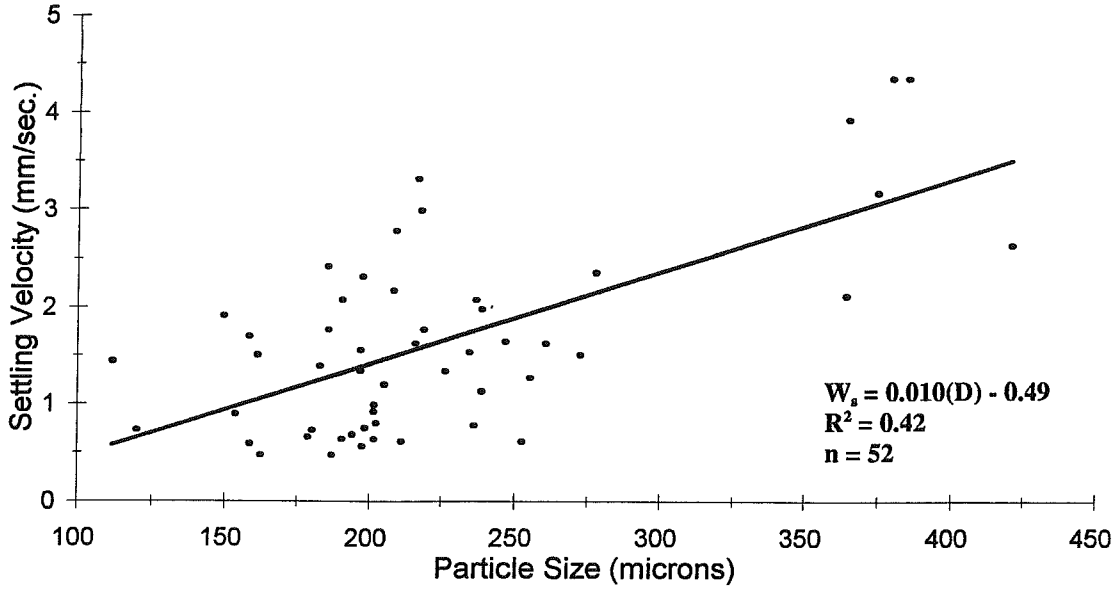

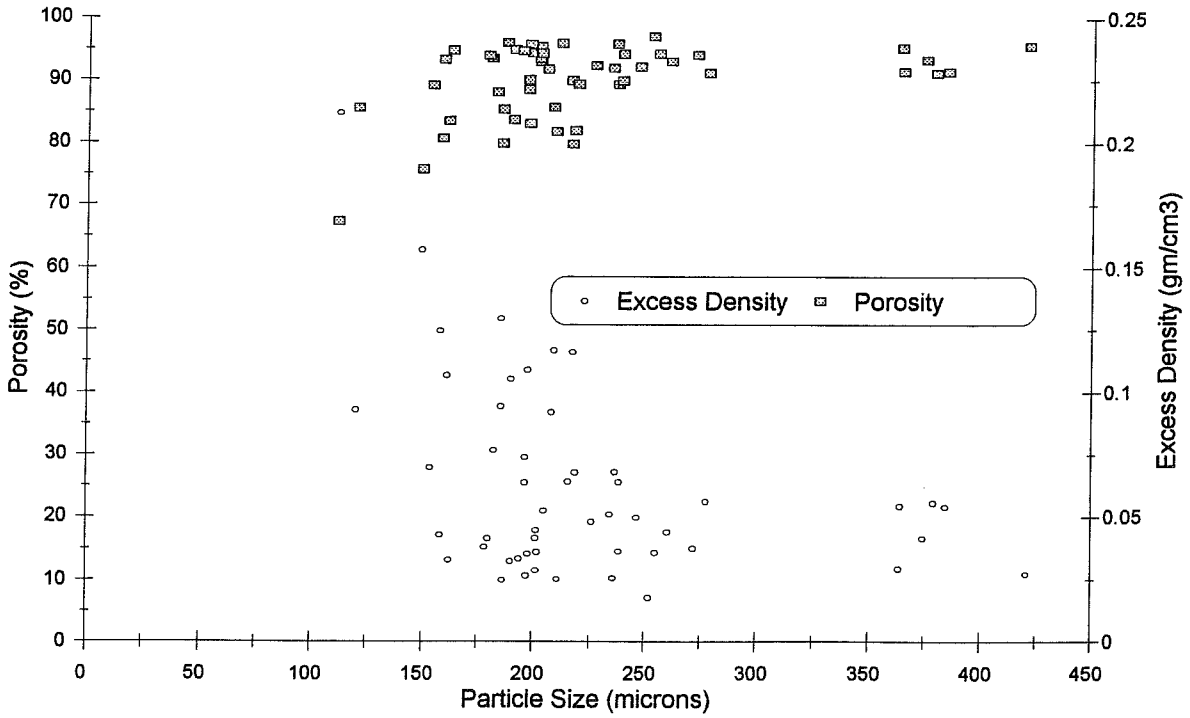

Dofasco Settling Experiment
C3-8

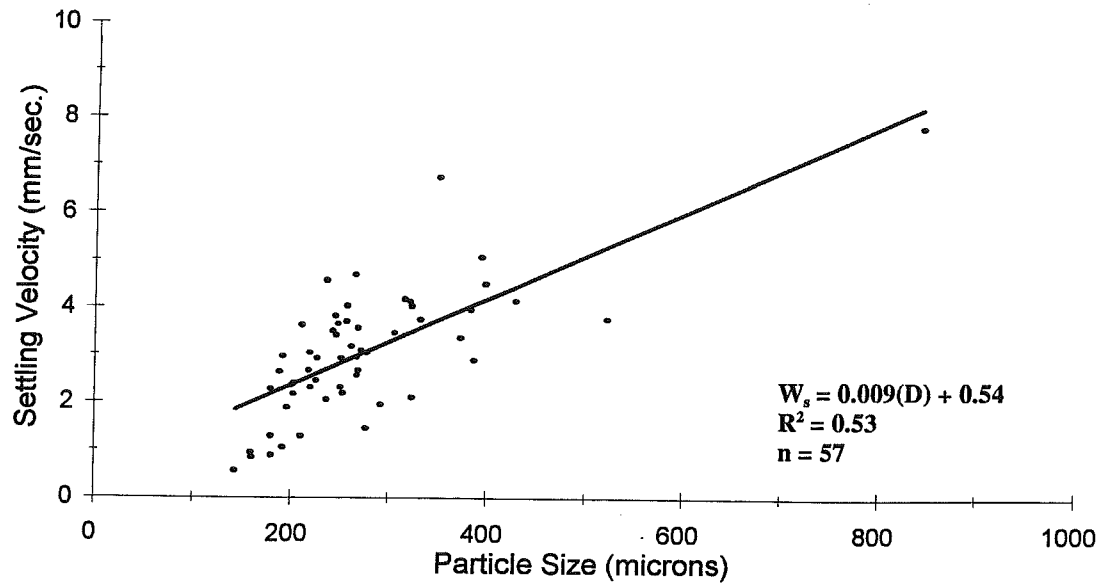

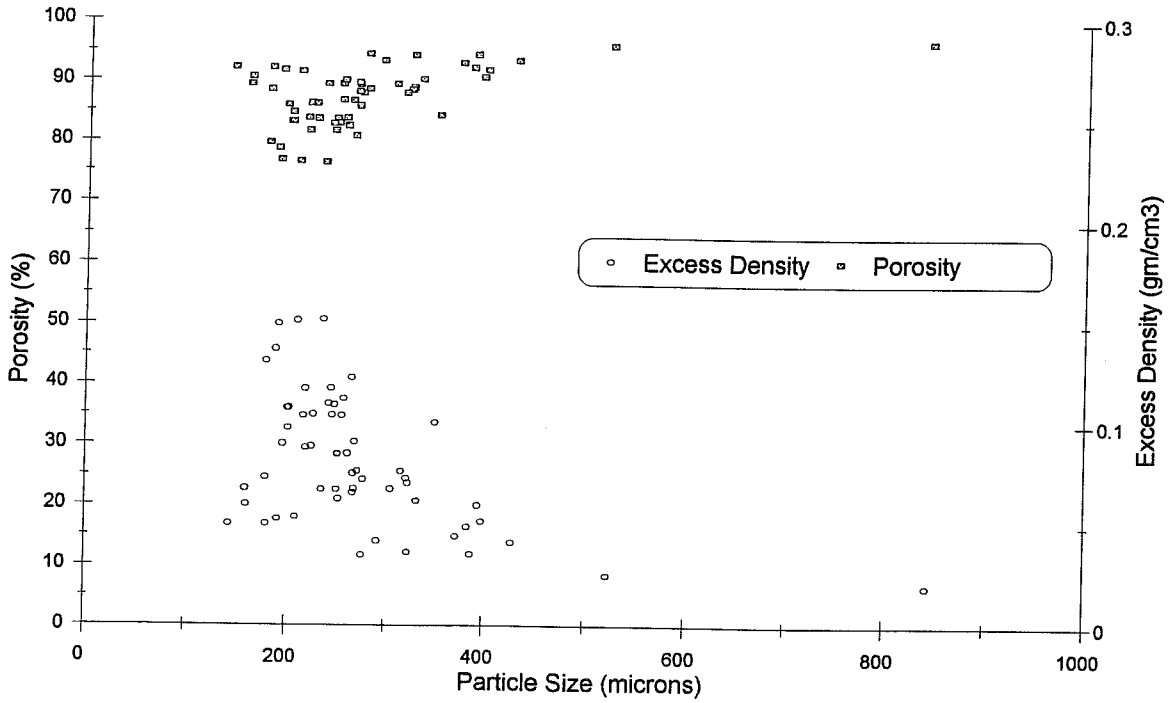

Dofasco Settling Experiment
C3-9

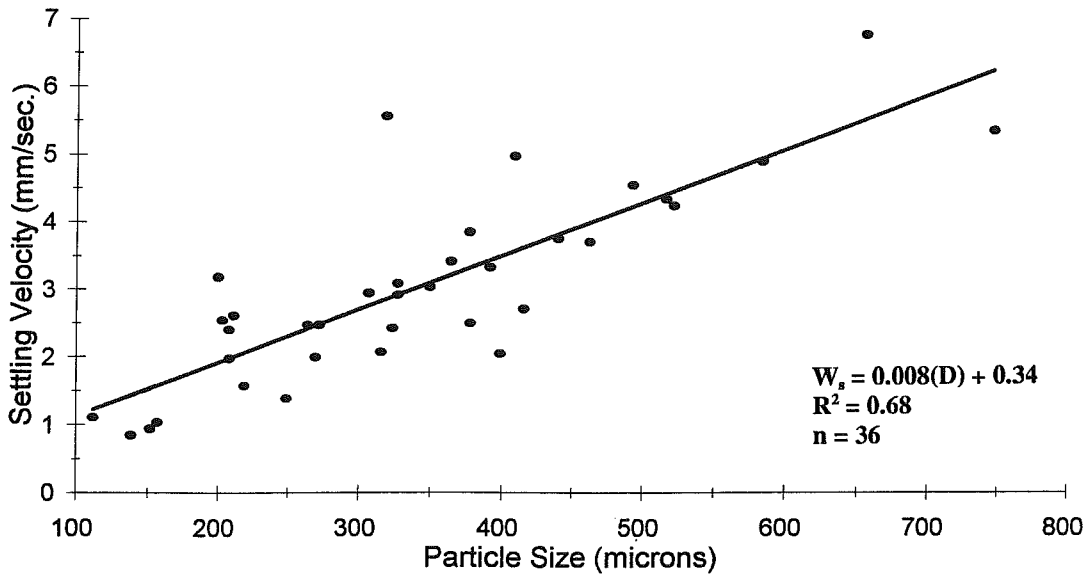

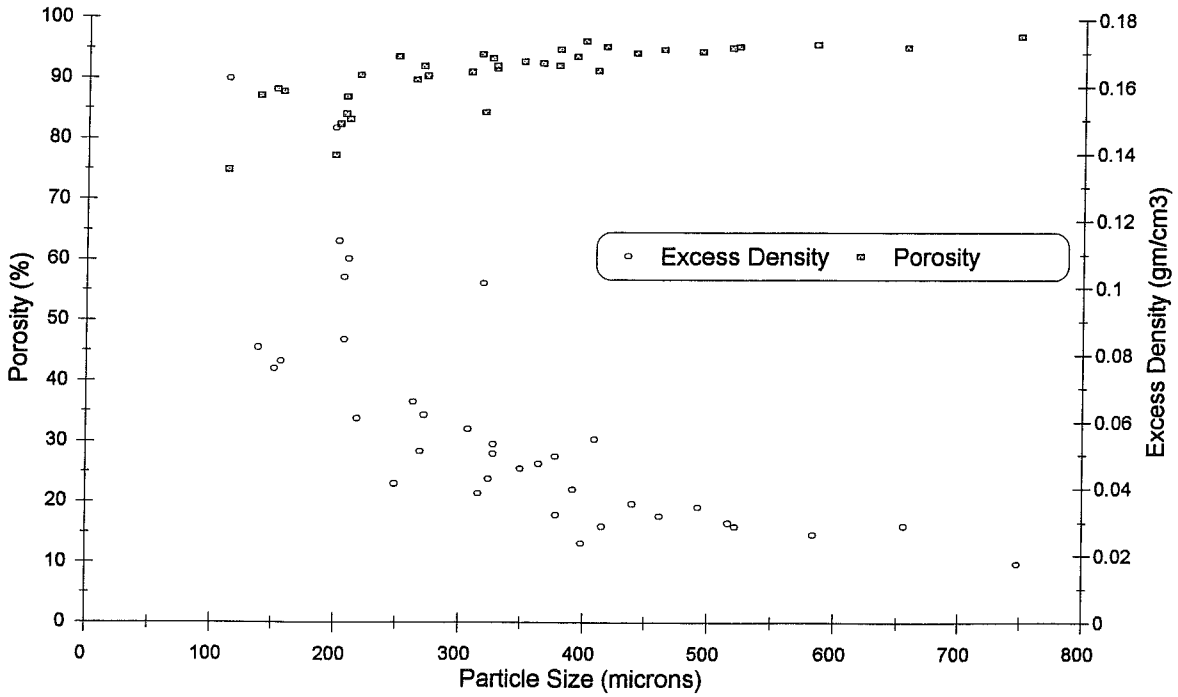

Dofasco Settling Experiment
C3-10

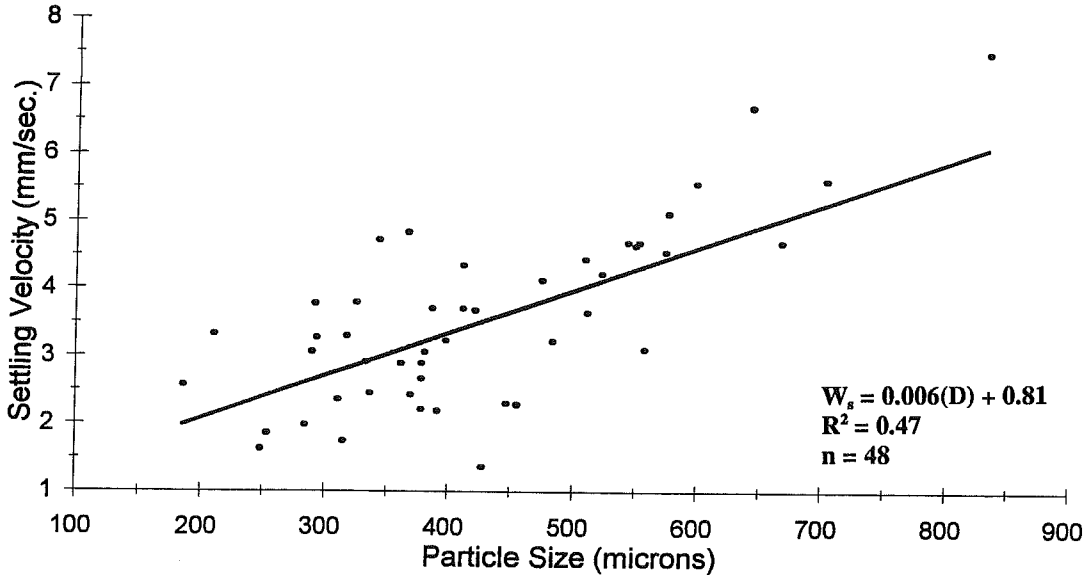

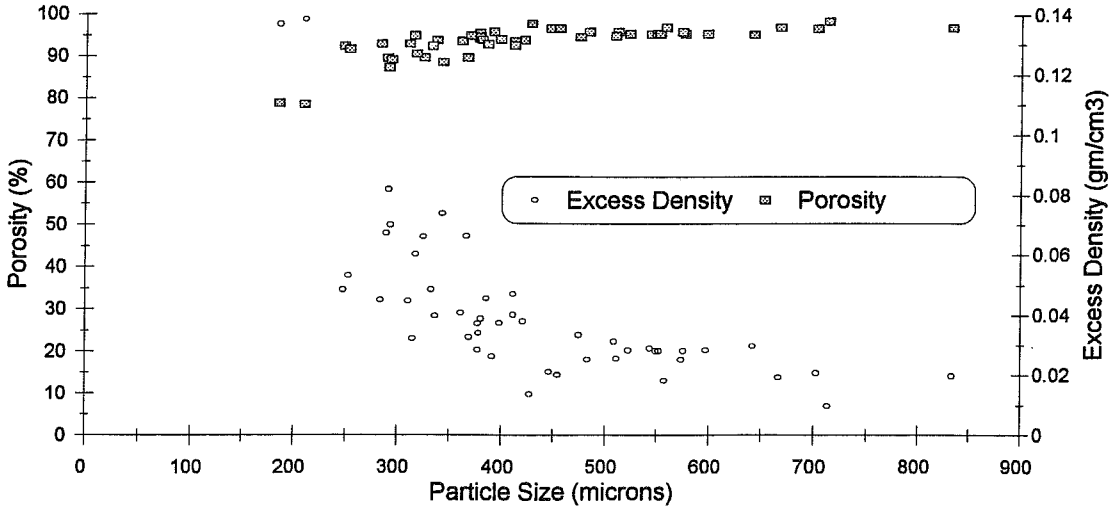

Dofasco Settling Experiment
C3-11

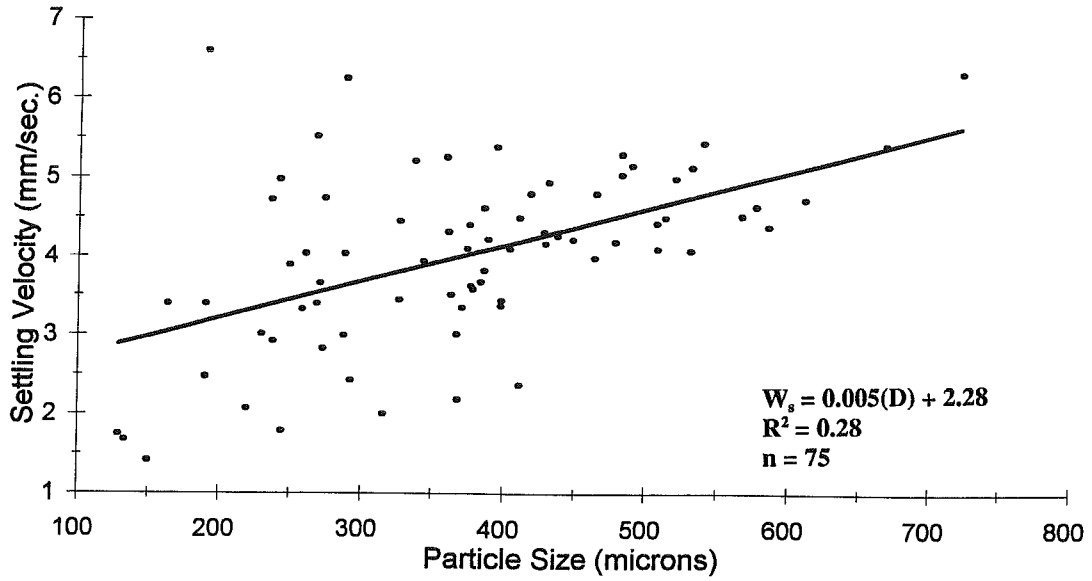

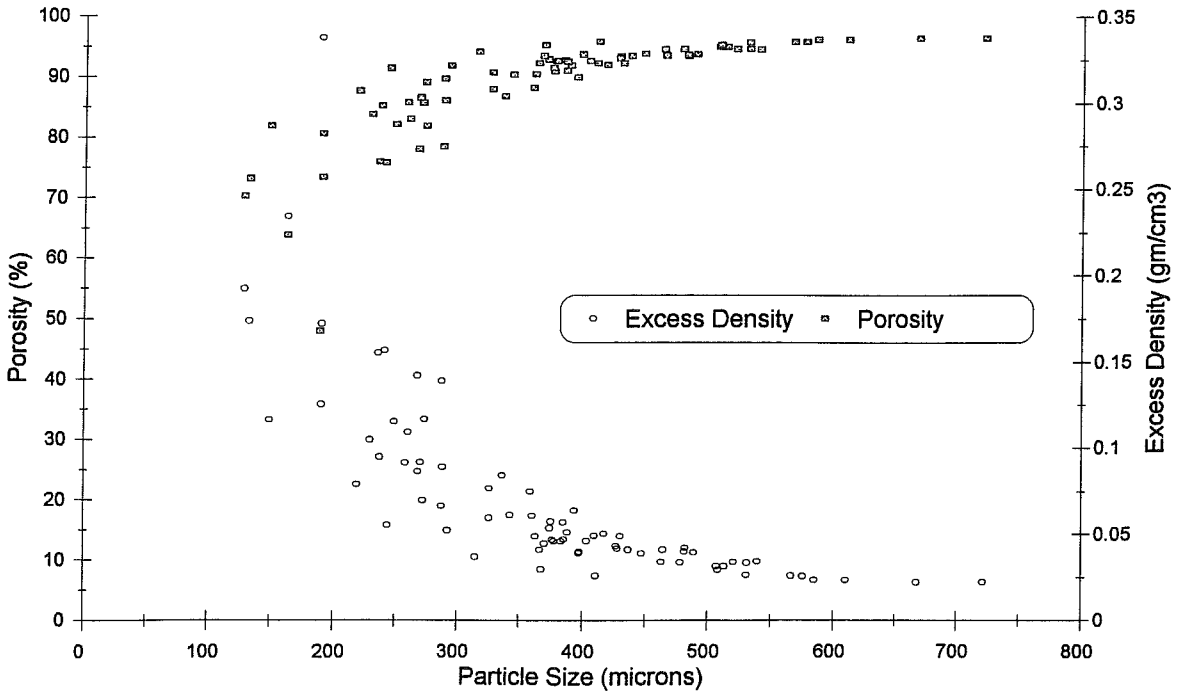

Dofasco Settling Experiment
C5-6

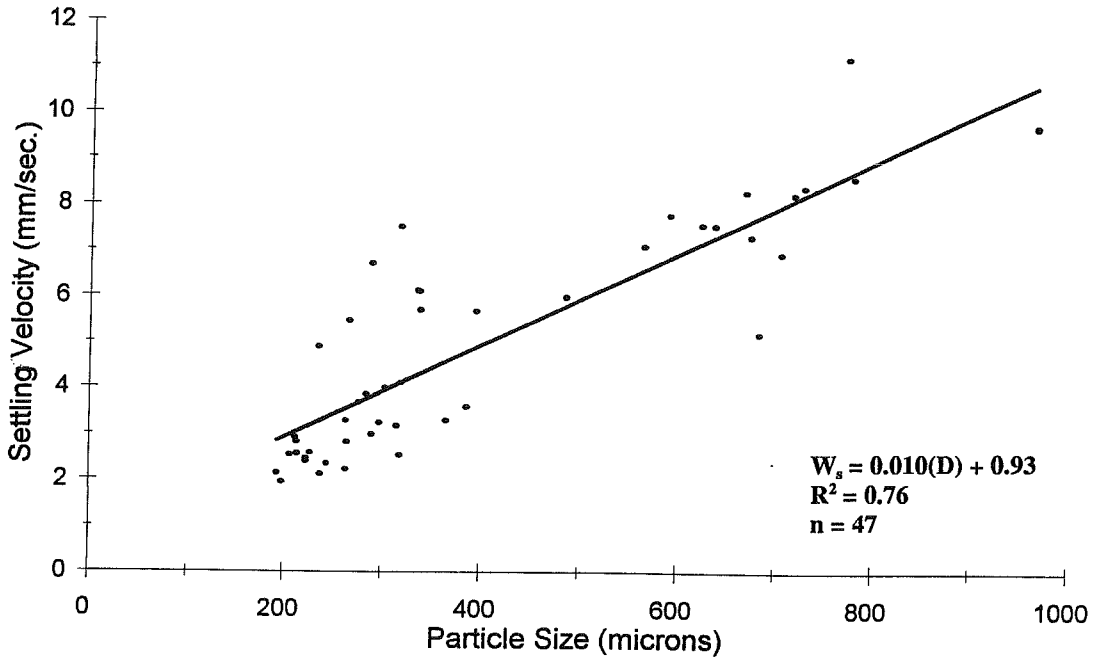

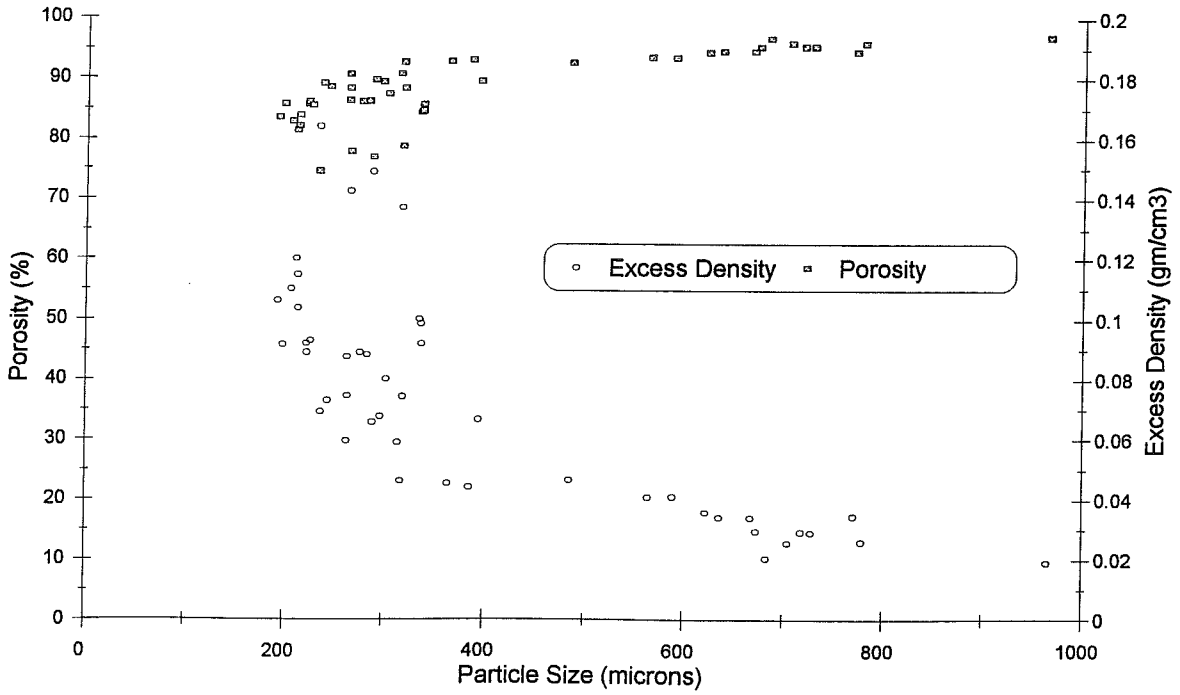

Dofasco Settling Experiment
C5-7

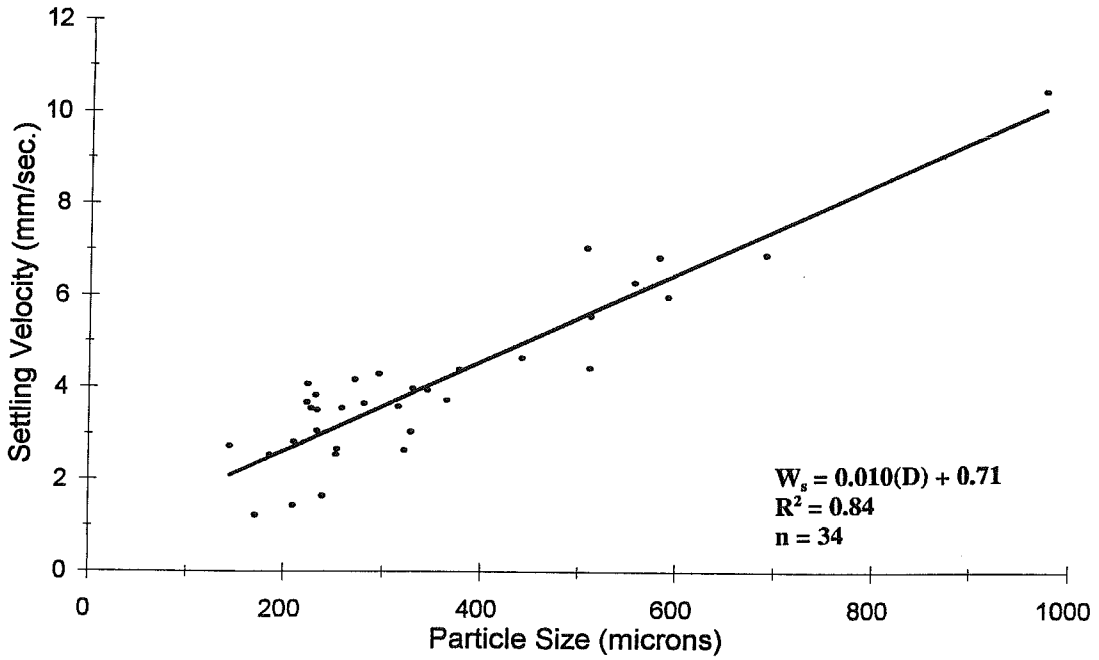

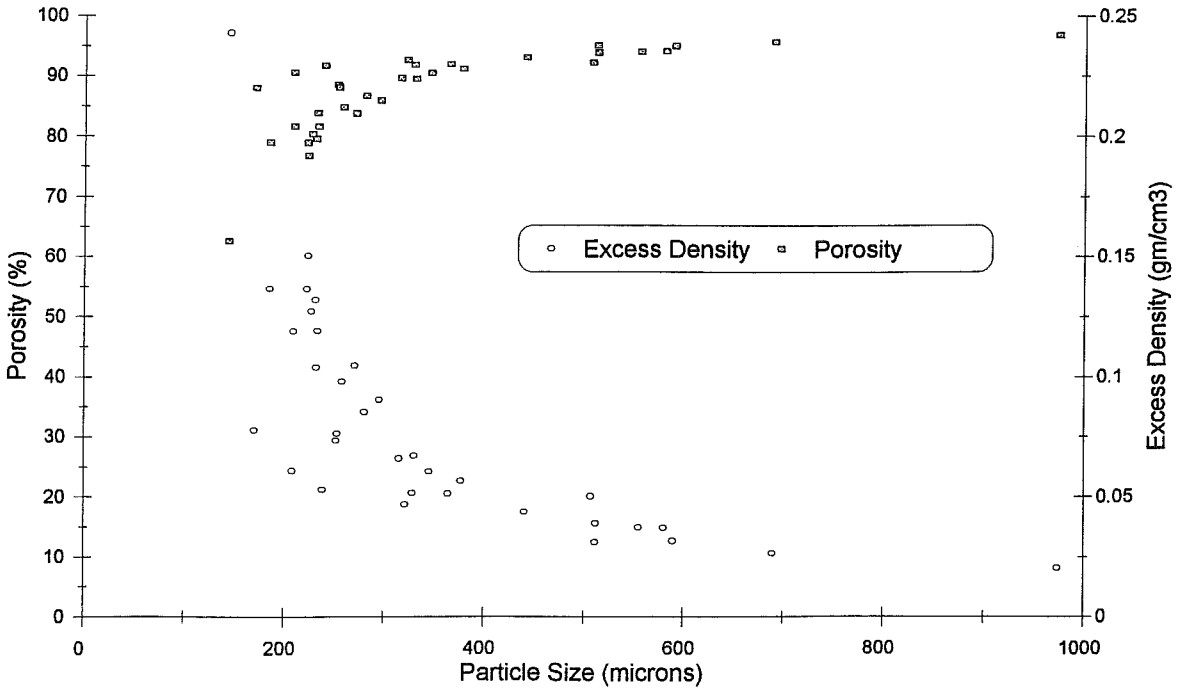

Dofasco Settling Experiment
C5-8

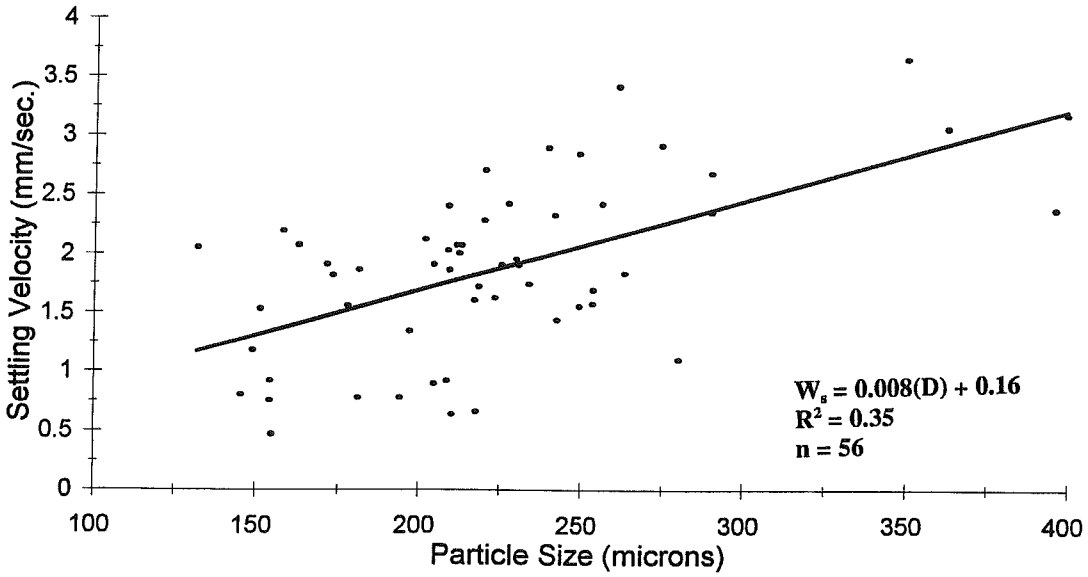

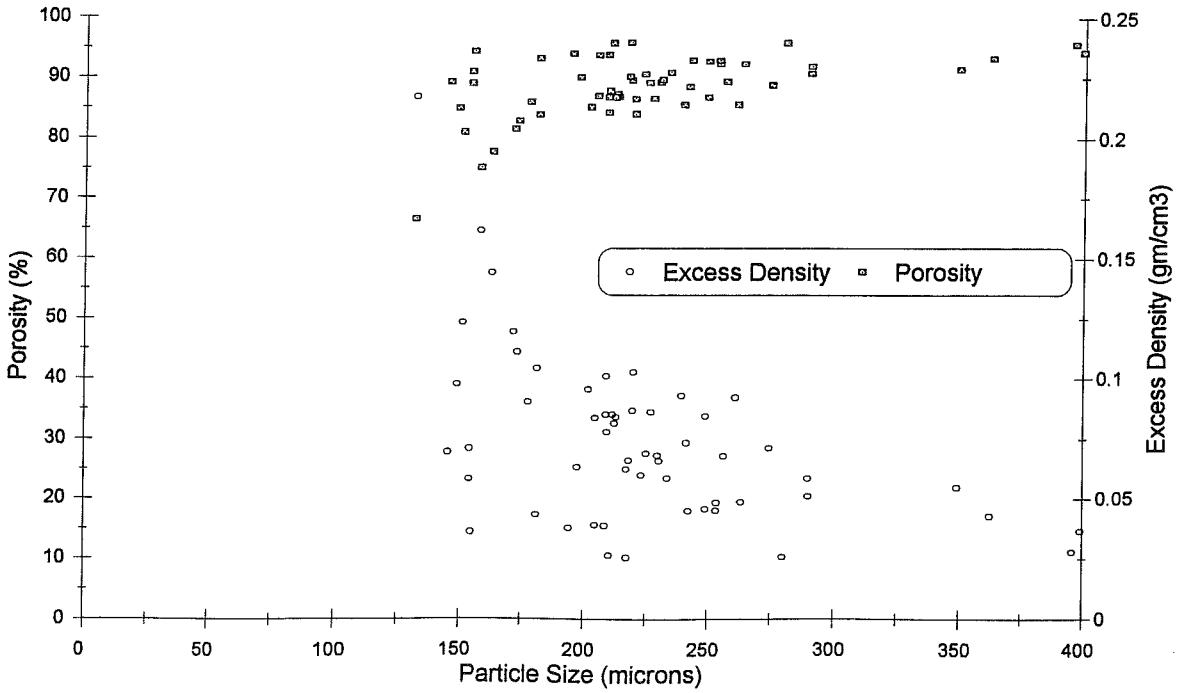

Dofasco Settling Experiment
C5-10

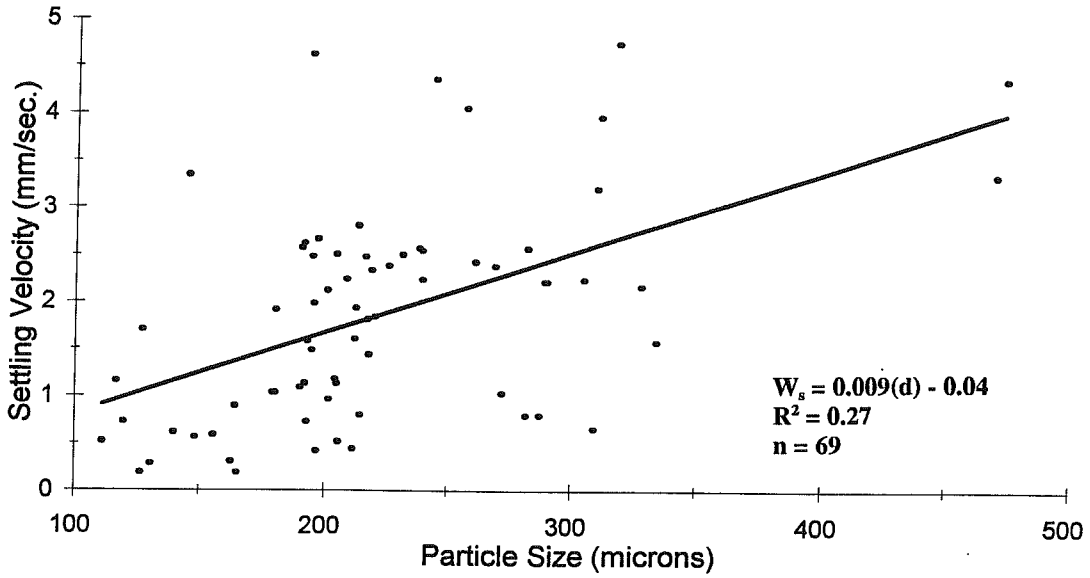

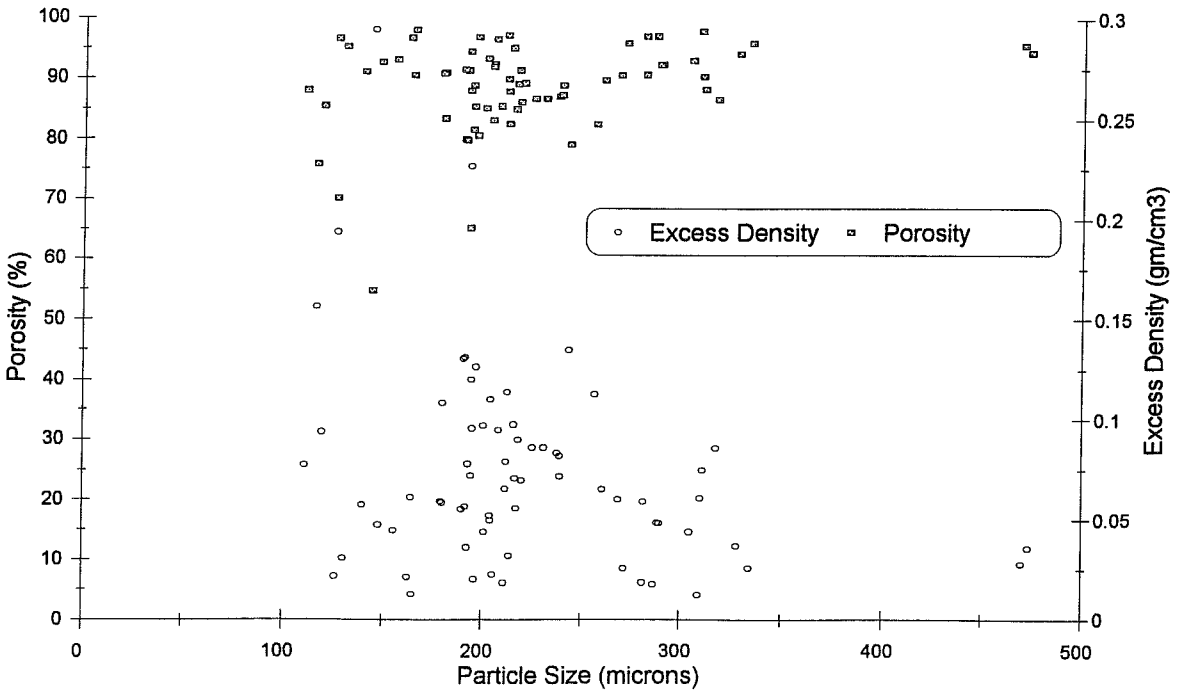

Dofasco Settling Experiment
C5-11

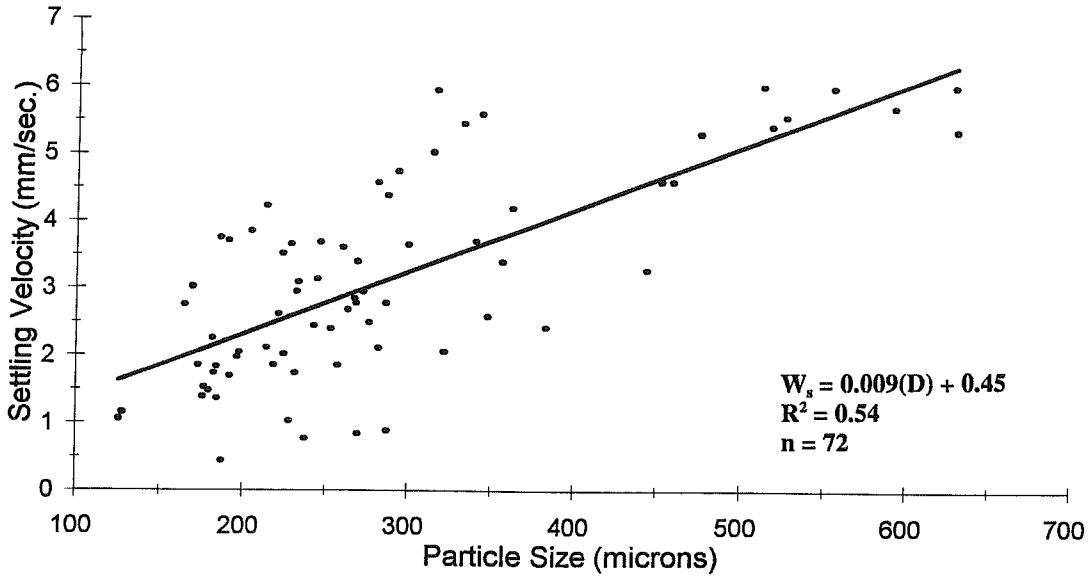

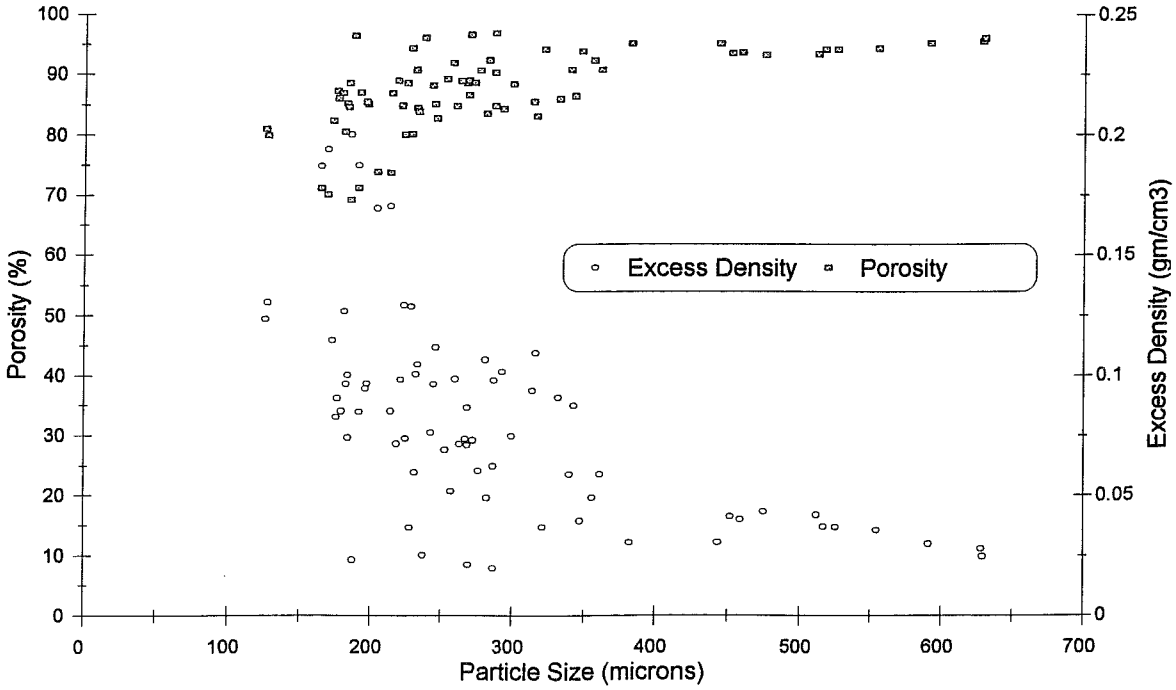

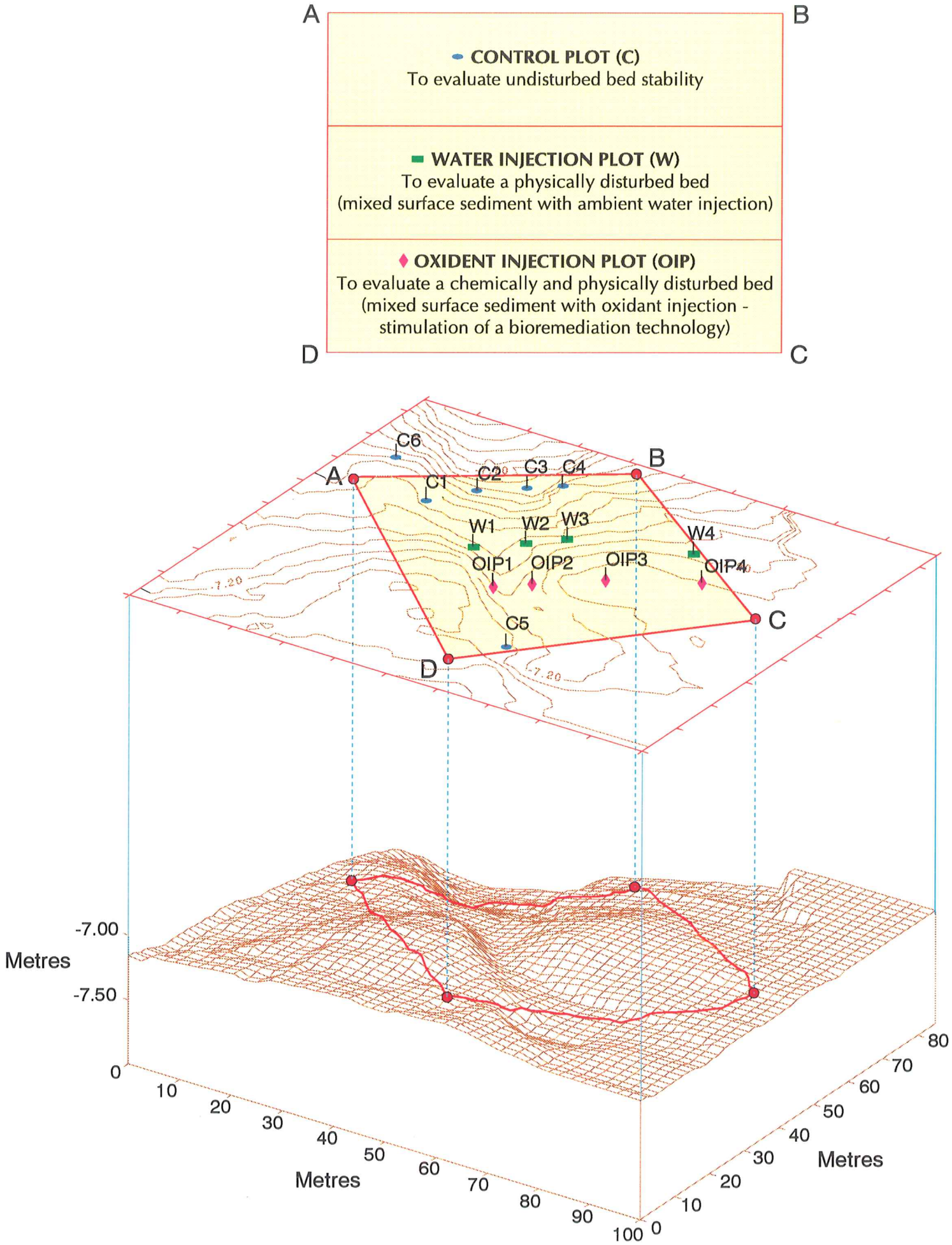
A
B
CONTROL PLOT (C)
To evaluate undisturbed bed stability
WATER INJECTION PLOT (W)
To evaluate a physically disturbed bed
(mixed surface sediment with ambient water injection)
OXIDENT INJECTION PLOT (OIP)
To evaluate a chemically and physically disturbed bed
(mixed surface sediment with oxidant injection -
stimulation of a bioremediation technology)
D
C
C6
C1
C2
C3
C4
W1
W2
W3
W4
OIP1
OIP2
OIP3
OIP4
C5
-7.00
-7.50
Metres
0
10
20
30
40
50
60
70
80
90
100
Metres
0
10
20
30
40
50
60
70
80